Pushing It to the Limit, Advancements in Negishi Couplings

Philip Eckert

Thesis submitted to the University of Ottawa
in partial fulfillment of the requirements for the
Doctorate in Philosophy degree in Chemistry

Department of Chemistry and Biomolecular Sciences
Faculty of Science
University of Ottawa

Abstract

Palladium catalyzed cross-couplings have revolutionized the field of organic synthesis. Using this family of reactions, many different bonds can be formed in a selective manner, include C-C, C-N, C-S and C-O bonds. One reaction included in this family is Negishi cross-coupling, which uses an organozinc reagent as the nucleophilic coupling partner. One aspect of these reactions that has gone largely overlooked is their dependence on inorganic salt additives. In this work, the beneficial, and sometimes harmful, effects of salt additives are investigated. This work realized two new roles for salt additives on Negishi-coupling, the prevention of product inhibition and catalyst deactivation. Throughout these studies, the choice of catalyst is shown to have significant impacts on the yield and selectivity of Negishi coupling reactions. In particular, the use of a chlorine functionalized N-heterocyclic carbene (NHC) ligand is shown to be a critical choice that must be carefully considered. In alkyl-alkyl couplings, this modification was shown to erode the selectivity under certain circumstances. This thesis comes around full circle in the final chapter where insights from mechanistic studies are applied to a commercially relevant cross-coupling. A variety of unnatural amino acids were synthesized using a Negishi coupling as the critical, diversification step. A chlorine functionalized catalyst and salt additive were critical for these couplings, highlighting the importance of studying mechanistic intricacies.

Acknowledgements

I left this section for the end, thinking it would be easy to write. I'm now realizing there is a very long list of people who not only helped me get to this point, but also set me up to achieve my future goals. This section might get much longer than expected…

First and foremost, I must thank my supervisor, Michael Organ. The opportunities and mentorship I received working in your group have been extremely rewarding. It can be difficult trying to remember everything you have done for me over the years. Numerous conferences, scholarships, networking opportunities and incredible colleagues have made my time working under your supervision a pleasure. Looking back on the past 5 years I have no regrets and a lot of that is thanks to you.

Of course, I must thank my thesis committee for the time they have taken over the years to help guide my research. Tom Baker and his extraordinary generosity was crucial in the beginning of my graduate studies. While our lab was still under construction, I was welcomed to Baker's lab. This was an amazing opportunity since I was able to use his experienced team for mentorship since most of our team was still at York. A special thanks go to Chris Godwin, Alex Daniels, and Alex Sicard who were all especially helpful in my first year. I would also like to give Professor Fabien Gagosz and his team a special thank you. I could always count on Fabien having my side during thesis committee meetings and throwing me a few easy questions when Mike and Tom really started grilling me. As well, I could always count on your friendly team any time I had to borrow a chemical or ask them a question about alkyne chemistry. Finally, a special thank you to Professor Jeffrey Manthorpe for his sound advice and input during my committee meetings.

I must acknowledge the numerous colleagues I have had over the years that helped guide my research and general growth. So, in no particular order I must give a huge shoutout to the

following individuals. Colin Diner, maybe one day we'll go snowboarding together again! PA Champagne, when I first met you, I thought Dr. Champagne was the coolest name ever. Now you're Prof. Champagne, you're only getting cooler as the days go on. Vova, you are an absolute wild card. I have learned so much from you both in terms of what to do and more importantly what NOT to do in the lab. Fred, it has been a pleasure watching you learn over the past 4 years. Jee, you and the whole flow team were always the best coworkers I could ask for. As soon as I get a gaming PC we are playing some RS6! Brendon Doyle and Alex Ducharme, I'm going to continue spamming both of you any chemical engineering memes I find. Ali and Sepideh, both of you were huge inspirations for me. I hope the whole family does well in Toronto! Mathieu, thanks for editing this thesis! Kyle and Kumardip who I am handing over my amino acid project to, I have complete faith in you two. I see lots of potential in both of you, and I'm sure you will continue to progress with that project. Please never hesitate to reach out to me with updates or questions! Lastly Dr. Saeed Kashani is sadly not here to read his shoutout, may he rest in peace.

The departmental support staff also require some big thanks. The NMR team works hard keeping our spectacular equipment in working condition and that deserves recognition. Special thanks to Vincent and Peter for all they do. A very big shoutout goes to Glenn Facey, whose course taught me pretty much everything I know about how an NMR spectrometer actually works. NMR spectrometers are no longer a magical black box! Finally, Roxanne Clement was critical to my success as the manager of the high throughput experimentation lab. She was responsible for keeping the GC-FID and GC-MS machines running which was critical to many of my projects. Her tireless effort to continuously improve the HTE lab is greatly appreciated.

Another critical source of support during these 5 years were my friends and family. I must specifically shoutout Maison Greg. At the very beginning of grad school, I moved into a townhouse

with 3 of my best friends and we named it after our leader, Greg. I have so many great memories of all the funny stuff that happened in that house. Various NHL streams, forced memes, and drinking on the roof, it was always a good time at MG. It hasn't even been a year since we left MG and it already feels like a lifetime ago. I could always count on you guys to distract me from the struggles of grad school and am forever grateful for the companionship you all provided.

Lastly, I must thank my immediate family. This could not have been possible without the constant support from my brother and parents. They have always supported and nurtured my love of science. Especially my brother who inspired me to enter grad school. None of this would have been possible without you guys supporting me since day 1.

Oh, and shoutout to my high school chemistry teacher Mr. Joel Bondy and the TV show Breaking Bad, both of which are big reasons why I fell in love with chemistry in the first place.

Publications from this work

Some portions of this thesis appear in the following publications:

Eckert. P.; Sharif, S.; Organ, M. G. *Angew. Chem. Int. Ed.* **2021**, 60, 12224-12241 (*Angew. Chem.* **2021**, 133, 12332-12349). Salt to Taste: The Critical Roles Played by Inorganic Salts in Organozinc Formation and in the Negishi Reaction. (https://doi.org/10.1002/anie.202010917).

Eckert. P.; Organ, M. G. *Chem. Eur. J.* **2020**, 26, 4861-4865. The critical role of LiBr in avoiding catalyst death of Pd-NHC complexes and its impact on cross-coupling. (https://doi.org/10.1002/chem.20200028).

Eckert. P.; Organ, M. G. *Chem. Eur. J.* **2019**, 25, 15751-15754. The Role of LiBr and $ZnBr_2$ on the Coupling of sp^2-Hybridized Oxidative Addition Partners with sp^3-Hybridized Organozincs. (https://doi.org/10.1002/chem.201903931).

Eckert. P.; Organ, M. G. *Chem. Eur. J.* **2022**, (in press). Impact of N-Aryl- and NHC Core-Substituents on the Coupling of Alkylzinc Nucleophiles: Is Bigger always Better? (https://doi.org/10.1002/chem.202200665).

Table of contents

List of abbreviations

BHE	β-Hydride elimination
BINAP	2,2′-Bis(diphenylphosphino)-1,1′-binaphthalene
Boc	*Tert*-butyloxycarbonyl
CSA	Camphorsulphonic acid
12-crown-4	1,4,7,10-Tetraoxacyclododecane
Cy	Cyclohexyl
Dba	Dibenzylideneacetone
DCC	*N,N'*-Dicyclohexylcarbodiimide
Dec	Decane/Decyl
DIBAL	Diisobutylaluminium hydride
DiMeIHept^{Cl}	1,3-Bis(2,6-(2,6)-dimethyliheptphenyl)-4,5-dichloroimidazol-2-ylidene
DFT	Density Functional Theory
DMA	Dimethylacetamide
DMAP	4-Dimethylaminopyridine
DME	1,2 Dimethoxyethane
DMF	Dimethylformamide
DMI	1,3-Dimethyl-2-imidazolidinone
DMSO	Dimethyl sulfoxide
DOSY	Diffusion-ordered spectroscopy
EDC	1-Ethyl-3-(3-dimethylaminopropyl)carbodiimide
ee	Enantiomeric excess
EI	Electron ionization
Equiv.	Equivalents
ESI	Electrospray ionization
Et	Ethyl
Fmoc	Fluorenylmethyloxycarbonyl
GC-FID	Gas chromatography flame ionization detection
GC-MS	Gas chromatography mass spectrometry detection
GPhos	(3-(*Tert*-Butoxy)-2′,6′-diisopropyl-6-methoxy-[1,1′-biphenyl]-2 yl) dicyclohexylphosphane
HPLC	High-performance liquid chromatography
HRMS	High-resolution mass spectrometry
IAd	1,3-Diadamantylimidazol-2-ylidine
iPr_2Zn	Diisopropylzinc
IPr	1,3-Bis(2,6-diisopropylphenyl)imidazole-2-ylidine
IPr^{Cl}	1,3-Bis(2,6-diisopropylphenyl)-4,5-dichloroimidazol-2-ylidene
IPr^{Me}	1,3-Bis(2,6-diisopropylphenyl)-4,5-dimethylimidazol-2-ylidene
IPent	1,3-Bis(2,6-di(3-pentyl)phenyl)imidazole-2-ylidene
IPent^{Cl}	1,3-Bis(2,6-di(3-pentyl)phenyl)-4,5-dichloroimidazol-2-ylidene
IPent^{Me}	1,3-Bis(2,6-di(3-pentyl)phenyl)-4,5-dimethylimidazol-2-ylidene
IHept	1,3-Bis(2,6-di(4-hepty)phenyl)imidazol-2-ylidene
IHept^{Cl}	1,3-Bis(2,6-di(4-hepty)phenyl)-4,5-dichloroimidazol-2-ylidene
IHept^{Me}	1,3-Bis(2,6-di(4-hepty)phenyl)-4,5-dimethylimidazol-2-ylidene
IR	Infrared spectroscopy

IS	Internal standard
KIE	Kinetic isotope effect
Me	Methyl
MMA	Methyl methacrylate
NapIPr	1,3-Bis(2,7-diisopropylnaphthalen-1-yl)-imidazol-2-ylidene
$NapMe_2$	1,3-Bis(2,7-dimethylnaphthalen-1-yl)-imidazol-2-ylidene
NHC	N-heterocyclic carbene
NMP	N-Methyl-2-pyrrolidone
NMR	Nuclear magnetic resonance
OA	Oxidative addition
$Pd(PPh_3)_4$	Tetrakis(triphenylphosphine)palladium(0)
$Pd(dba)_2$	Bis(dibenzylideneacetone)palladium(0)
$Pd_2(dba)_3$	Tris(dibenzylideneacetone)dipalladium(0)
PEPPSI	Pyridine-Enhanced Precatalyst Preparation Stabilization and Initiation
ppm	Parts per million
RE	Reductive elimination
RuPhos	2-Dicyclohexylphosphino-2',6'-diisopropoxybiphenyl
SI	Supporting Information
SIMes	1,3-Bis(2,4,6-trimethylphenyl)imidazolidine-2-ylidene
SIPr	1,3-Bis(2,6-diisopropylphenyl)imidazolidine-2-ylidene
SPhos	2-Dicyclohexylphosphino-2',6'-dimethoxybiphenyl
TBAB	Tetrabutylammonium bromide
TBAC	Tetrabutylammonium chloride
TBAI	Tetrabutylammonium iodide
*t*Bu	*Tert*-butyl
TEP	Tolman electronic parameter
TMEDA	Tetramethylethylenediamine
TMSCl	Trimethylsilyl chloride
THF	Tetrahydrofuran
TLC	Thin-layer chromatography
TM	Transmetallation
TMS	Tetramethylsilane
TS	Transition State

List of figures

List of schemes

List of tables

Chapter 1: Introduction

1.1 Negishi couplings

Palladium catalyzed cross-coupling reactions have become a crucial tool for the assembly of small organic molecules. Using this methodology, the selective coupling of alkyl and aryl halides with a variety of nucleophiles can be achieved under mild conditions.[1,2] These reactions are classified by the type of nucleophile employed, with some of the most common being organoboron reagents (Suzuki-Miyaura coupling),[3] amines (Buchwald-Hartwig couplings)[2] and alkenes (Heck couplings).[4,5] One subfamily of cross-couplings that is renowned for its mild conditions, low toxicity and excellent functional group tolerance are Negishi cross-couplings, which utilize an organozinc nucleophile (Scheme 1).[6] The discovery of palladium catalyzed cross-couplings has revolutionized modern organic synthesis. Indeed, this whole family of reactions are so powerful that in 2010 three pioneers of this field, Ei-ichi Negishi, Richard Heck, and Akira Suzuki were awarded the Nobel prize for their contributions.

Scheme 1: Representative example of a Negishi cross-coupling.

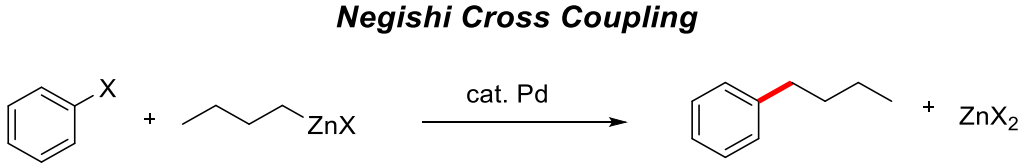

Negishi cross-coupling follows the same general mechanism that nearly all palladium catalyzed cross-coupling reactions follow (Scheme 2). The nomenclature used to describe the different steps in the catalytic cycle are based on changes to the metal centre and its binding environment. To begin, the active palladium (0) catalyst (**1**) oxidatively adds to the electrophilic C-X bond producing intermediate **2**. In this step palladium is oxidized from Pd(0) to Pd(II), giving rise to the name oxidative addition (OA). The species formed at this step is often referred to as the OA intermediate (**2**). From there, the nucleophile (organozinc) exchanges its carbon substituent

for the halide on palladium in a redox neutral step referred to as transmetallation (TM). The Pd(II) centre of the resulting complex (**3**) can be reduced back to Pd(0) by the two carbon groups. This process is called reductive elimination (RE) as it eliminates the cross coupled product (**4**) and reduces Pd(II) to regenerate the active Pd(0) catalyst (**1**). This is the generally accepted mechanism for most palladium catalyzed cross-coupling reactions. However, this mechanism assumes a Pd(0) source to initiate couplings. More stable Pd(II) catalysts (**5**) can also be used, since these palladium salts can often be reduced *in situ*.

Scheme 2: Generalized mechanism for the Negishi cross-coupling reaction.

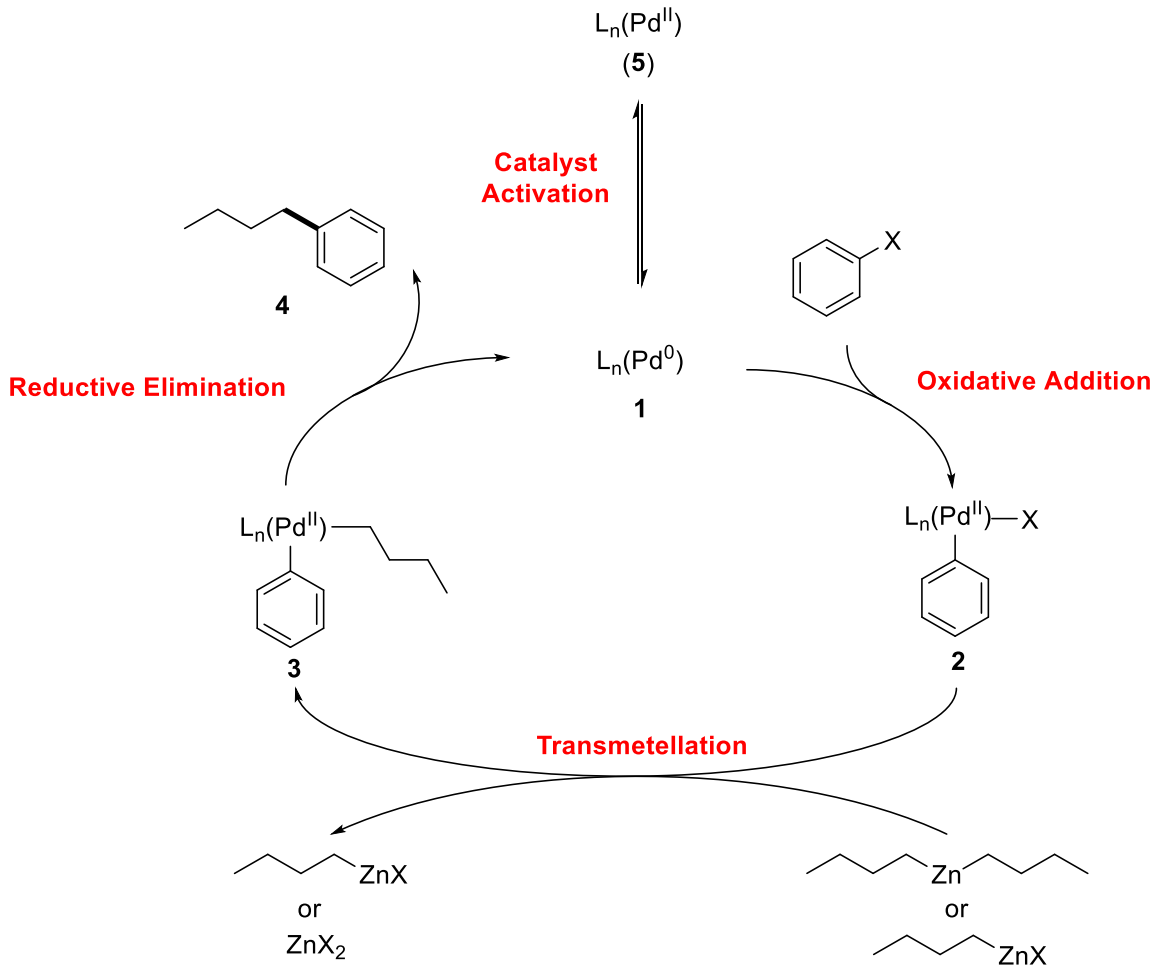

1.1.1 Catalyst activation

The use of air-sensitive reagents poses a significant challenge to organic chemists. While air-sensitive solutions can be stored under an inert atmosphere in bottles equipped with a rubber septum, air-sensitive solids usually require the use of a glovebox. It is for this reason chemists often avoid using air-sensitive Pd(0) catalysts, rather opting for Pd(II) precatalysts. Palladium in its +2 oxidation state is considerably more air and moisture stable, making for a much more user-friendly option. While these complexes are not intermediates on the desired catalytic cycle, in most cases they can be readily reduced *in situ* to their neutral oxidation state.[7–9] Palladium (II) complexes used for this type of catalysis are commonly referred to as precatalysts, since they must first be reduced to Pd(0).

Often, the nucleophile (coupling partner) is capable of reducing the Pd(II) precatalyst. For Negishi cross-coupling reactions, organozinc reagents are known to rapidly reduce palladium (II) precatalysts in most cases.[10] The generally accepted mechanism for catalyst activation in Negishi cross-coupling reactions consist of two TM steps followed by a RE (Scheme 3). The facile reduction of palladium by aryl and alkyl organozinc reagents allows for the substitution of air-sensitive Pd(0) catalysts for more robust Pd(II) precatalysts. Other couplings that use different nucleophiles such as amines, thiols and organoboron reagents are also known to reduce Pd(II) precatalysts *in situ* through analogous pathways.[11–13]

Scheme 3: Mechanism for precatalyst activation in Negishi cross-coupling reactions.

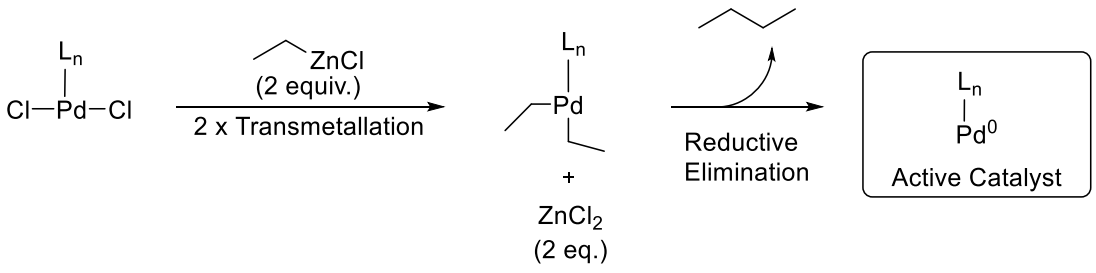

The activation step is not always an easy step. In some cases where a very bulky or electron-deficient organozinc coupling partner is used, the two TM steps can be challenging. In these cases either a Pd(0) catalyst must be used, or a Pd(II) precatalyst can be preactivated prior to introducing the coupling partners. Common activating methods use mild reducing agents such as DIBAL,[10] lithium- or potassium isopropoxide,[14] β-hydrogen-containing amines[14] and even phosphine ligands.[14]

1.1.2. Oxidative Addition (OA)

Following the generation of an active catalyst (or direct addition of an active catalyst) the next step in the catalytic cycle is OA. Since palladium is being oxidized, electron-deficient arenes tend to undergo OA faster than electron-rich ones since the C-X bond is more electrophilic. The choice of halide is also a critical parameter that dictates the rate of OA. The general order of activity for the OA of palladium into carbon halogen bonds is I>Br>Cl>>>F, which is in line with the relative strength of these bonds.[15,16] While iodine is the easiest bond to activate, the liberated iodide anion is a good ligand for palladium, causing potential catalyst poisoning.[17]

The mechanism by which OA takes place varies depending on the nature of the catalyst as well as the hybridization of the carbon electrophile. Oxidative addition of monoligated palladium tends to proceed through a concerted 3-centred transition state (TS) (Scheme 4A).[18–20] Aryl substrates coordinate their pi system to the metal, allowing for a "ring slip" type OA.[21] In contrast, the OA of alkyl halides is often more challenging despite the weaker carbon-halogen bonds,[22] which can be attributed partially to the fact ring slip type OA is impossible without an aryl ring. There are three predominant pathways for OA of alkyl halides; a similar concerted 3-member TS state, an S_N2 type displacement, and radical pathways (Scheme 4B).[18] In 2009, Organ *et al.* modeled the three-step cross-coupling mechanism of a simple alkyl-alkyl coupling, considering

the concerted 3-member transition state.[23] The OA barrier of bromoethane was found to be relatively low with a $\Delta G^{\ddagger}$ of 78.4 or 68.2 kJ/mol depending on the angle of approach.

Scheme 4: Generalized mechanisms for OA of monoligated palladium (0) catalysts with aryl (A) and alkyl (B) halides.

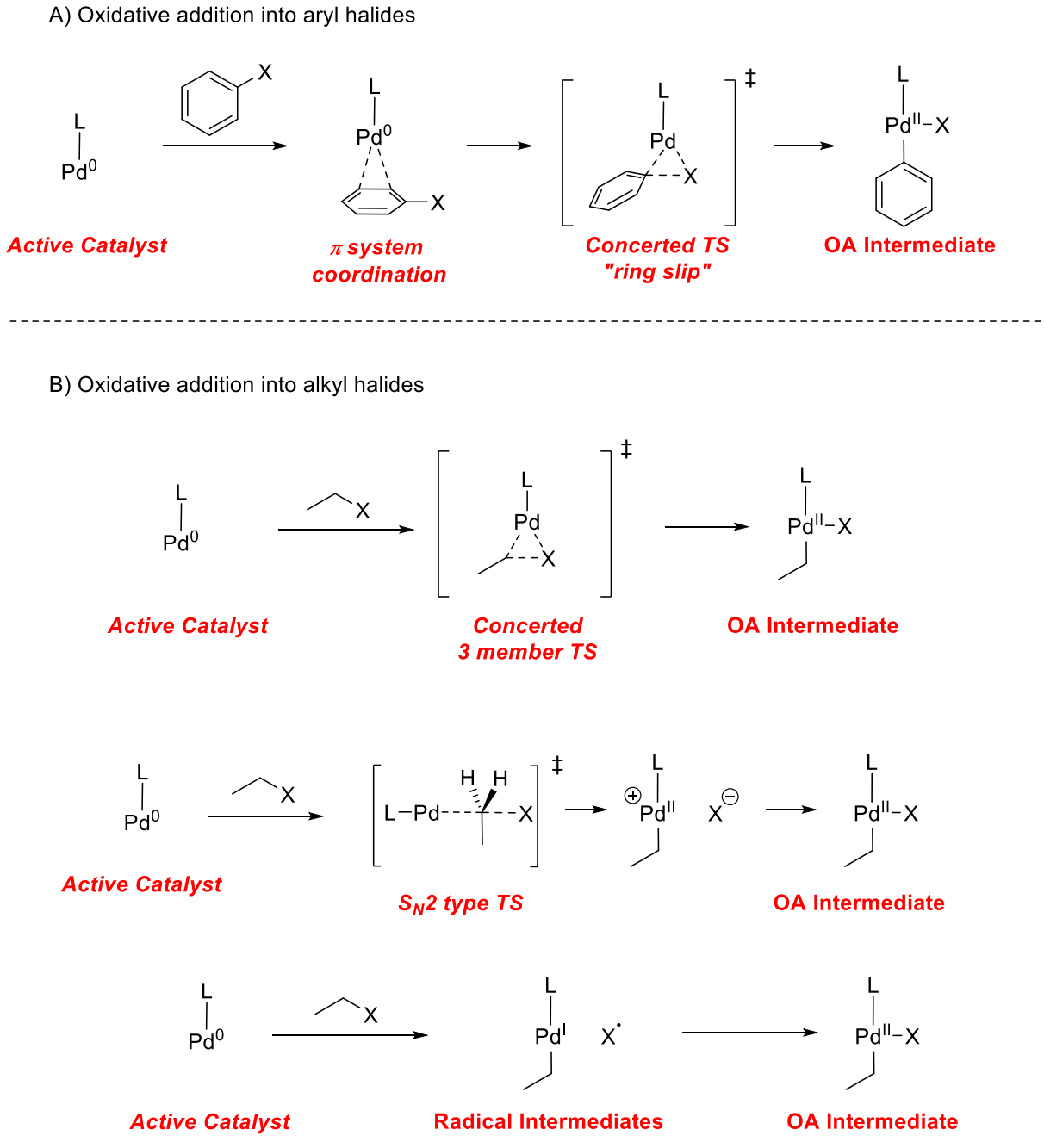

The S_N2 type mechanism dominates in highly polar solvent systems.[18] It has been noted that increased solvent polarity is often necessary for efficient activation of alkyl halides with zinc dust.[24] In 2011 Organ *et al.* showed the selective OA of polyhalogenated alkanes could be carefully controlled by adjusting the solvent polarity (Scheme 5).[25] The coupling of 1-bromo-10-chorodecane (**6**) could be done in an orthogonal manner by using a polar co-solvent, 1,3-Dimethyl-2-imidazolidinone (DMI). Selective activation of the C-Br bond was possible with a 2:1 THF:DMI solvent system. Once this reaction was complete, more DMI can be added to create a 1:2 THF:DMI mixture in which the C-Cl bond could then be activated. Using this methodology, a variety of dihalogenated substrates could be chemoselectively coupled to varying organozinc partners. This dependence on a polar co-solvent supports the proposed S_N2 type mechanism which would benefit from the higher dielectric constant.

Scheme 5: One-pot, orthogonal alkyl–alkyl Negishi cross-coupling reactions that rely on a change in solvent polarity to achieve selective halogen activation.

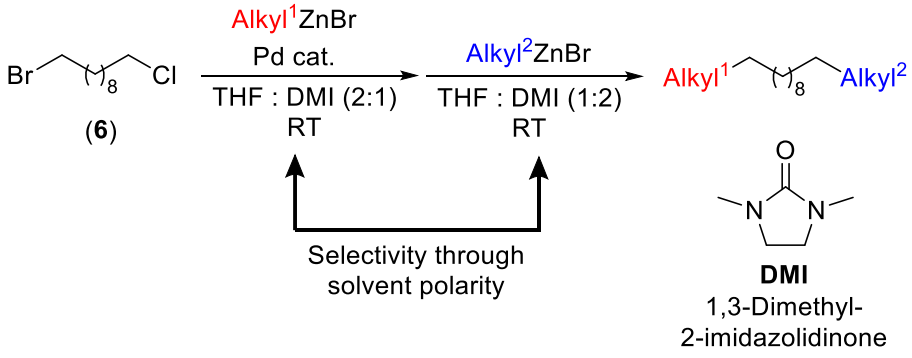

1.1.3. Transmetallation (TM)

It is generally accepted that the OA intermediate (Scheme 2, structure **2**) undergoes substitution with either the mono- or disubstituted organozinc, replacing the halide of the OA intermediate with an R group. The complex following TM (**3**) is referred to as the TM intermediate. Transmetallation is historically one of the most challenging steps to study experimentally, due to

the large number of possible ways in which palladium and zinc species can coordinate and exchange ligands. Further complicating the picture, both the OA intermediate and TM intermediate are challenging to isolate and study. Often highly electron-deficient ligands and substrates must be used to stabilize these intermediates.[26] Furthermore, direct experimental evidence has been reported primarily for bisligated palladium complexes, with no direct experimental studies on the more reactive monoligated catalyst systems.[26–28]

These challenges have led to many DFT studies aimed at revealing the details of this process.[23,26,27,29] One advantage of these studies is the detailed geometric insights that can be derived. Furthermore, more active monoligated palladium catalysts, which are normally very challenging to isolate and study, can be modeled with ease. Most modeled pathways involve first forming a direct Pd-Zn bonding interaction, followed by an exchange of ligands between the two metals. A representative example is shown in Scheme 6 where Aurrecoechea *et. al.* modelled the TM of $MeZnCl(THF)_2$ (**7**) and an OA intermediate ($PdL_2(Vinyl)Br$ ($L=PMe_3$)) (**8**).[30] Transmetallation is initiated by coordination of the organozinc to palladium, with the loss of one solvent molecule coordinated to zinc to form **9**. Loss of the second solvent molecule proceeds through transition state $\mathbf{TS_{9\text{-}10}}$, creating a bridging bromide. Transmetallation takes place through a 4-member transition state ($\mathbf{TS_{10\text{-}11}}$) in which the CH_3 group and bromine are swapped in a concerted manner. In this case, the product (**11**) is not significantly lower in energy than the starting materials (**8** & **7**), implying reversibility of this step. Indeed, this observation is in line with many studies on the often problematic reversibility of TM.[28,31] While the TM may be reversible, the following RE step is almost always irreversible.

Scheme 6: Representative TM step of PdL_2(Vinyl)Br (L=PMe_3) (8) with Zn(Me)ClS_2 (S=THF) (7).

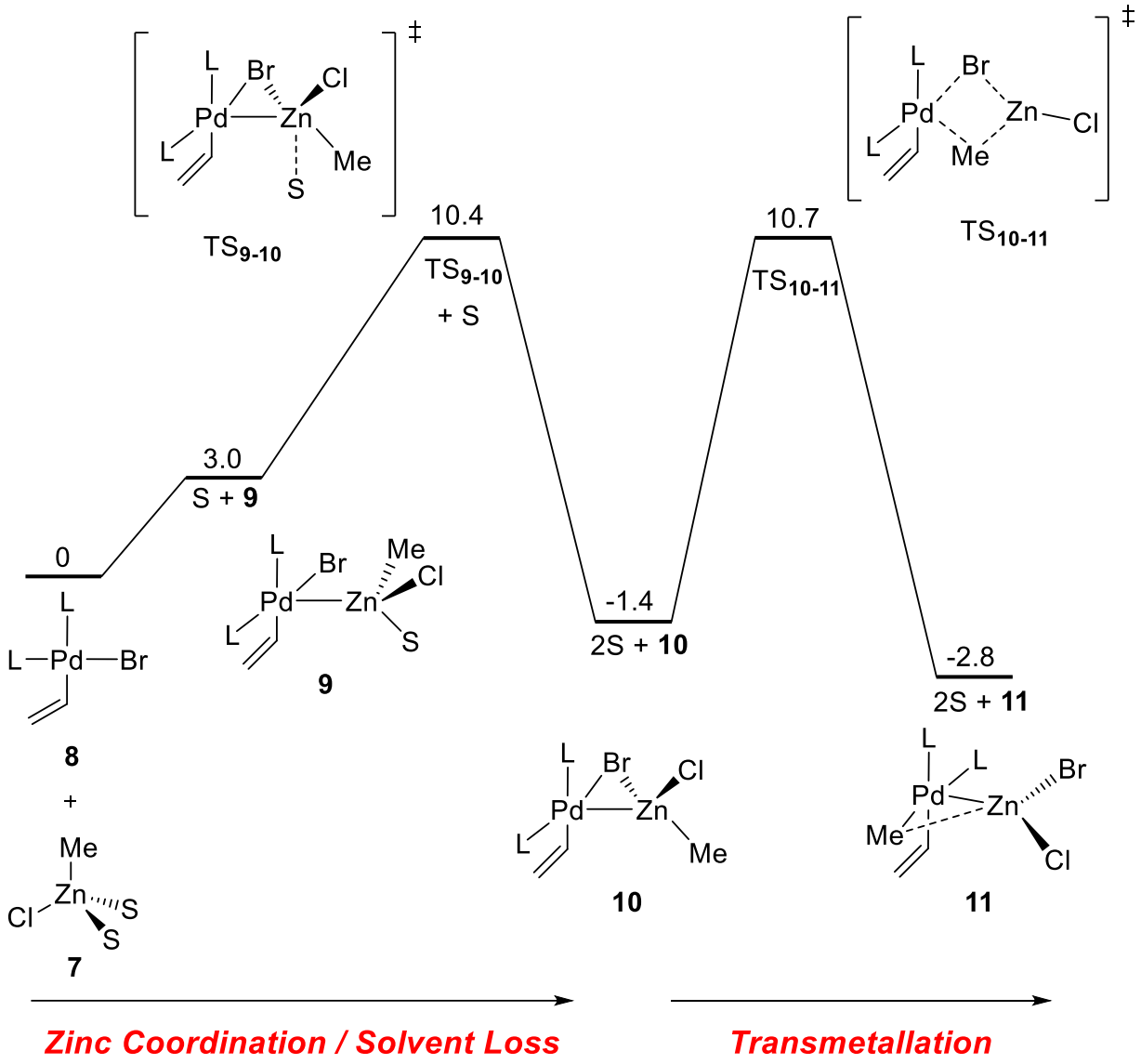

The Gibbs free energies (kcal/mol) of the elementary transformations were computed at the ωB97D/6- 31G*-SDD level in THF.[30]

1.1.4. Reductive Elimination (RE)

The catalytic cycle is completed with the final step, RE. This elementary step can be thought of as the reverse reaction for OA. In this step, palladium is reduced by the two carbon groups, regenerating the active Pd(0) catalyst while a bond forms between the formally oxidized carbon groups. The mechanism for this reaction is analogous to the 3-centre concerted TS seen for

OA (Scheme 7).[32] This final step is often an exothermic process, which acts as the thermodynamic driving force of this reaction due to the strong C-C bond formation. Similar to how electron-rich ligands help facilitate OA, electron-deficient ligands have been shown to promote the RE step. [32,33]

Scheme 7: Representative mechanism of a RE.

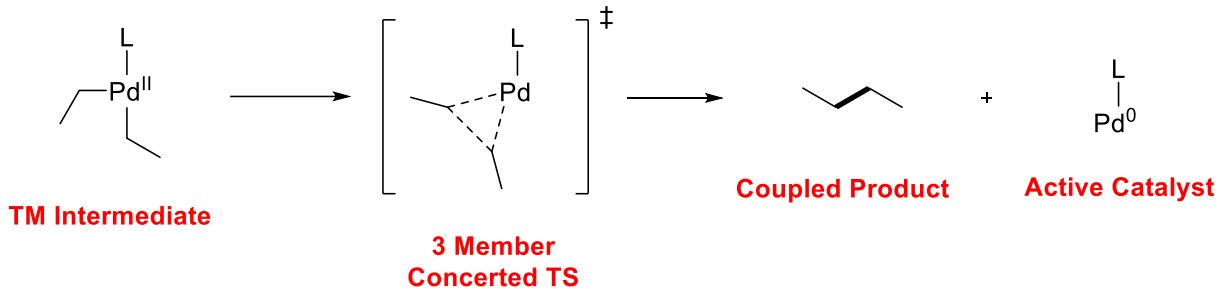

1.2. Byproducts also formed during cross-coupling

While palladium catalyzed cross-coupling has revolutionized the field of organic synthesis, it has notable limitations, which can be caused by a fault with any one of the three fundamental steps. Oxidative addition with poor electrophiles, TM with bulky organozincs and RE of the ancillary ligand(s) are all obvious challenges for this chemistry. In addition to these limitations, some side-reactions erode yield and selectivity of Negishi cross-coupling reactions including β hydride elimination (BHE) and subsequent rearrangements.

1.2.1. β Hydride Elimination (BHE)

One fundamental transformation of palladium complexes that can create problems is BHE. This transformation requires a metal center with a free coordination site and an alkyl ligand bearing β hydrogens (Scheme 8).[34–36] The β hydrogens can form agostic interactions with the palladium centre, leading to the formation of a concerted 4 member TS from which the hydrogen is transferred to palladium as a hydride. This produces a palladium complex with a hydride and the

corresponding ligated alkene. While this step is critical to the success of Heck couplings,[4] and certain cascade reactions,[37] in most other palladium catalyzed coupling reactions it is a problematic competing pathway.[38–40]

Scheme 8: Representative example of a β-hydride elimination (BHE).

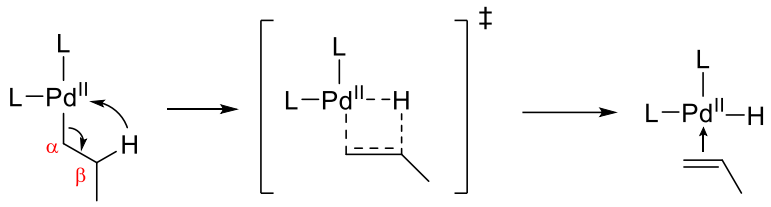

The most challenging subset of cross-coupling reactions are alkyl-alkyl since many stages of the catalytic cycle are susceptible to BHE. A common method for preventing BHE is to use bidentate ligands because they occupy the free coordination site on the metal needed for BHE to occur.[41] This can significantly reduce BHE, although the lower reactivity of bisligated palladium complexes is a limitation when compared to monoligated systems.[42–44]

1.2.2. Rearrangements

β hydride elimination is a reversible transformation, presenting an opportunity for rearrangements to occur. Consider TM intermediate **12** bearing an isopropyl chain (Scheme 9A). Following BHE, a complex with both an alkene and hydride ligand are formed (**13**). The alkene has free rotation and in theory will be distributed across **13** and **14** following a standard Boltzmann distribution. The reverse reaction, migratory insertion (MI) can occur on either substrate, leading to the original branched complex (**12**) or the linear rearranged product (**15**). This side reaction is especially prevalent in cases where there is a thermodynamic driving force favoring the rearranged species. A common example of this are the couplings of secondary alkyl zinc reagents (Scheme 9B), where the rearrangement from a secondary to primary alkyl group is essentially irreversible.[41]

The use of extremely bulky ligands has been shown to help favor RE over these unwanted transformations by disfavoring BHE.[40,45–49]

Scheme 9: Rearrangement pathway for secondary alkyl organozinc reagents.

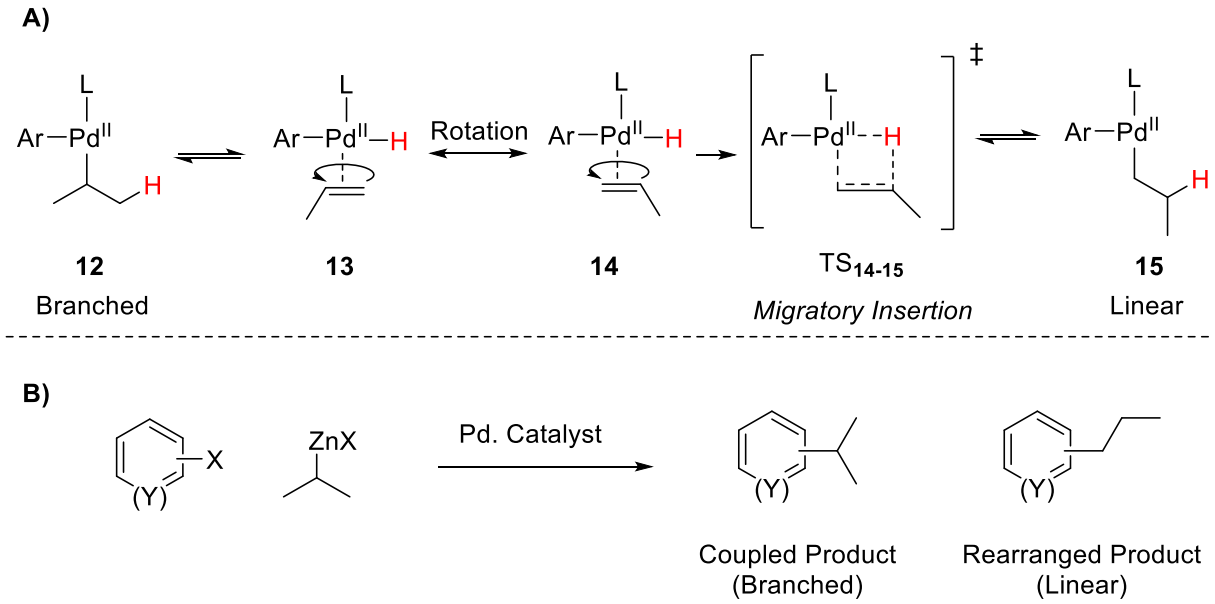

1.3 Catalyst design

Catalyst design has played a crucial role in the general advancement of palladium catalyzed cross-coupling reactions. This field of study has been heavily researched since the initial inception of transition metal catalyzed cross-coupling. Many different scaffolds have been synthesized and successfully employed as ligands for Negishi coupling.[6] Two ligand classes that have proven to be powerful, versatile, and relatively easy to handle are phosphine and N-heterocyclic carbene (NHC) ligands.

1.3.1. Phosphines

Phosphine ligands are based on trivalent phosphorous and rely on its Lewis basic lone pair. Thanks to their strong coordination to metal centres and modularity of the substituents, a plethora of phosphine ligands have been developed for many transformations (Figure 1). A few common

examples include bidentate ligands containing C_2 axial symmetry such as BINAP (**16**), frequently used for asymmetric transformations.[50] The use of extremely bulky phosphines, like tri-*tert*-butylphosphine P(*t*-Bu)$_3$ (**17**), have been shown to favor monoligated palladium species, allowing for remarkably low catalyst loadings.[43,51] Designer ligands from Buchwald *et al.* containing biaryl moieties such as SPhos (**18**) and RuPhos (**19**) have been shown to act as hemilabile chelators through the ancillary aryl system.[52] This hemilability gives the best of both worlds in terms of mono and bisligated palladium catalysts. The tethered aryl system can stabilize important monoligated palladium intermediates without imparting the same overall steric demand of bisphosphine ligands. In recent work from Buchwald, the latest iteration of phosphine ligands, GPhos (**20**) contains an O*t*-Bu substituent in the ortho position of the primary aryl ring which helps improve stability of the most active conformer.[53] This new ligand can be complexed with a palladium source to create a potent catalyst capable of promoting cross-coupling reactions between a variety of sterically hindered primary amines and aryl halides.

Figure 1: Phosphine ligands commonly employed for palladium catalyzed transformations.

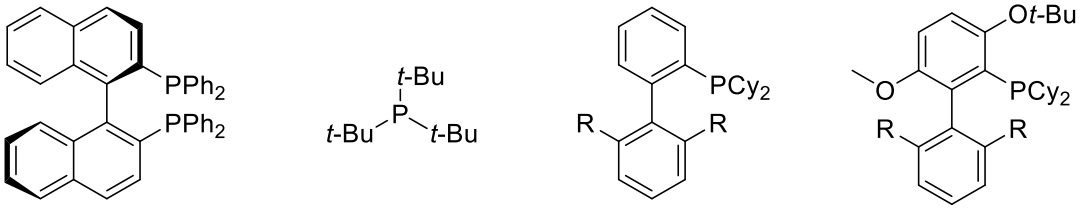

(R) - BINAP (16) **P(*t*-Bu)$_3$ (17)** **SPhos (18)** (R = OMe) **RuPhos (19)** (R = O*i*-Pr) **GPhos (20)** (R = iPr)

Two key parameters that are important to compare when choosing a catalyst are the steric and electronic parameters. Since bulky ligands favor monoligated species, chemists have extensively debated the best method in which to measure, quantify and compare the steric bulk of different ligands. Among the different methods for benchmarking size, the use of Tolman cone

angles is the most widely accepted method.[54,55] In this method, the space a phosphine ligand occupies around the metal center is measured by obtaining the angle of a cone containing the metal at its point, and with edges of the cone touching the van der Waals radii of the outermost atoms of the ligand (Figure 2). The cone angle increases as the size of the substituents on phosphorus grows, thereby creating a method for measuring and comparing the steric bulk of phosphine ligands.

Figure 2: Tolman cone angle diagram and table of selected examples.

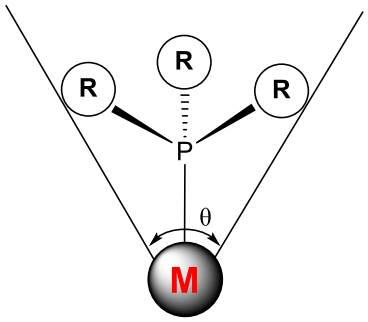

Tolman Cone Angle

R	Cone Angle (θ)
Me	118
Et	132
Ph	145
*t*Bu	182

Tolman did not solely focus on the steric nature of ligands, indeed he also developed a standardized method for comparing the electron donation of different ligands.[56] This method requires the synthesis of $LNi(CO)_3$ complexes, where L is the ligand of concern (Figure 3). This complex can then be analyzed using infrared (IR) spectroscopy to measure the CO bond stretches. Ligands with stronger σ-donation will allow the metal centre to donate more electron density into the Ni-C bond through pi-backbonding. This strengthens the Ni-C bond but weakens the C-O bond, resulting in a lower vibrational frequency for the CO stretch. By comparing the CO stretch of different complexes, the Lewis basicity of a variety of phosphine ligands can be approximated.

Figure 3: Tolman electronic parameter (TEP) diagram and table of selected examples.

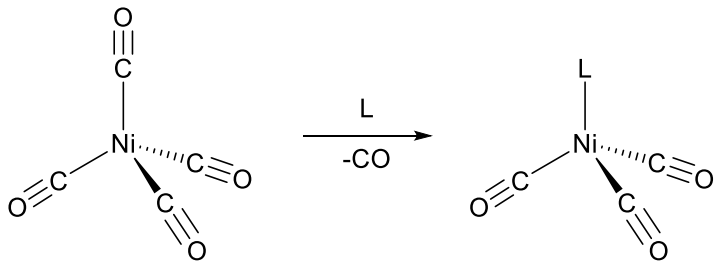

L	v(CO) cm^{-1}
$P(t\text{-}Bu)_3$	2056.1
$P(NMe_2)_3$	2061.9
$P(Me)_3$	2064.1
PPh_3	2068.9
PCl_3	2097.0
PF_3	2110.8

1.3.2. N-Heterocyclic Carbenes (NHC)

The carbon coordinative counterparts to phosphine ligands are NHC ligands (Scheme 10A).[57] Many different NHC scaffolds exist, with the most common motif being an imidazole core. These species are considered persistent carbenes, due to their high stability and prolonged lifetimes. This stability comes from the two nitrogens adjacent to the carbene, which can donate electron density from their lone pairs into the empty p-orbital of the singlet carbene. While the free carbenes have been isolated and characterized, they are usually synthesized and stored as their protonated HX salt forms. These carbenes were first prepared in the 1960s,[58,59] but not used as ligands for palladium catalyzed cross-coupling reactions until 1995.[60] At that time Herrmann *et al.* discovered complexes **21** and **22** could be used as catalysts for Heck couplings (Scheme 10B). This reactivity captured the attention of the catalysis community and since then a large collection of NHC ligands have been synthesized.

Scheme 10: A) Representative synthesis of an NHC from its protonated salt form. B) First use of a Pd-NHC complex as the catalyst for a cross-coupling reaction.[60]

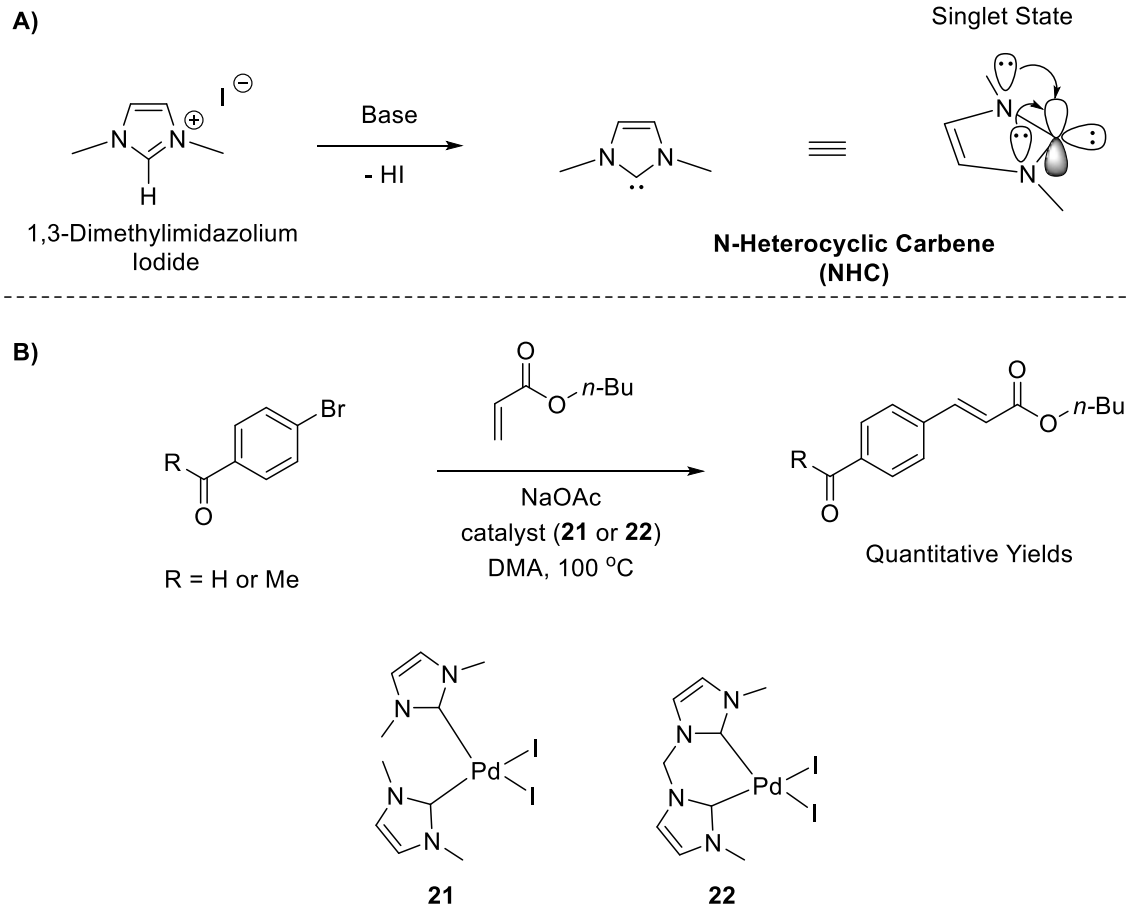

Frequently modified locations are the nitrogen substituents and the backbone of the imidazolium ring (Figure 4). In recent years diortho-substituted aryl groups have proven to be optimal substituents for the nitrogen centres. Two classic, readily available, and highly effective examples are IMes (**23**) and IPr (**24**). In recent years, work by Organ[40,61,62] and Nolan[63–65] have expanded the size of the ortho substituents from iPr all the way up to isononane (**24-27**). Increasing the steric bulk of the N-aryl rings by switching to naphthalene (**28**,**29**)[66,67] and adamantyl (**30**)[59] substituents has also been reported. While many different N-substituents have been developed, this field has not been limited to just these modifications. Numerous modifications to the backbone have been investigated with a few noteworthy examples being the saturation of the alkene to make

SIPr (**31**),[68] as well as substitution with NMe_2 (**32**),[68] methyl (**33**)[68] and chlorine (**34**)[40,46] groups. Furthermore, the use of chiral NHC ligands like IMes* (**35**) and others (**36,37**) have allowed for various asymmetric transformations.[69,70]

Figure 4: Commonly used imidazole based NHC ligands.

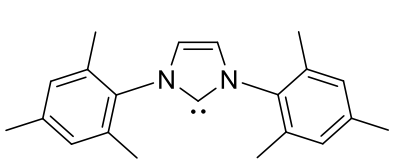

IMes (**23**)

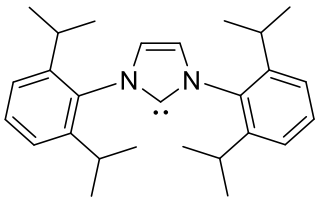

IPr (**24**)

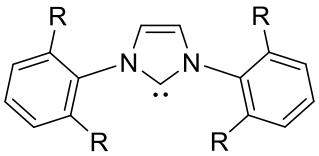

R = IPent (**25**), IHept (**26**), INonane (**27**)

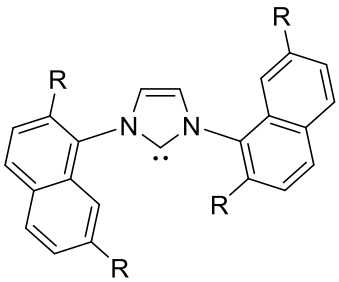

(R = Me) $NapMe_2$ (**28**)
(R = iPr) NapiPr (**29**)

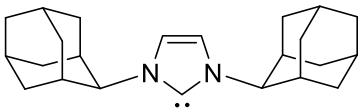

IAd (**30**)

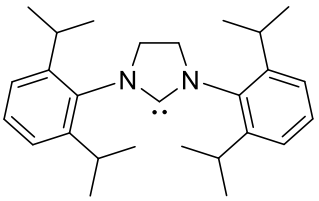

SIPr (**31**)

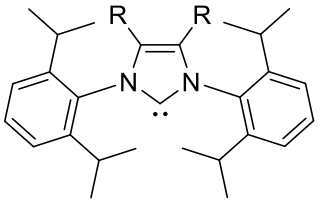

(R = NMe_2) $IPr^{(NMe_2)_2}$ (**32**)
(R = Me) IPr^{Me} (**33**)
(R = Cl) IPr^{Cl} (**34**)

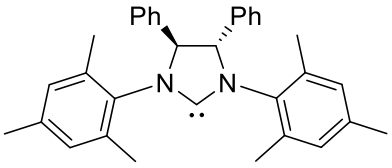

IMes* (**35**)

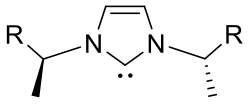

R = Ph (**36**)
R = α-Naphthyl (**37**)

One of the most pronounced advantages of NHC ligands is their remarkable σ-donating capabilities. In 2008 Nolan measured the TEP of a series of NHC and phosphine ligands using a $(L)Ir(CO)_2Cl$ system in which L was a variety of commonly employed phosphine and NHC

ligands.[71] The measured CO stretches revealed the increased σ-donating nature of NHC ligands. The phosphine ligands screened ranged from 2085 – 2072 cm^{-1} while the NHC ligands ranged from 2072 – 2063 cm^{-1} (Figure 5). This significant increase in Lewis basicity was also observed by Crabtree while investigating NHC iridium and rhodium complexes.[72,73] This strong σ-donating nature is believed to be partially responsible for the excellent activity seen in some transition metal-mediated processes, such as OA. The highly electron-rich metal centres created by NHC ligands have allowed for activation of challenging electrophiles such as alkyl chlorides[25] and sterically hindered aryl chlorides.[74]

Figure 5: Nolan's correlation of average ν_{co} values for [(L)Ir(CO)$_2$Cl] complexes with the Tolman electronic parameter (TEP). [71]

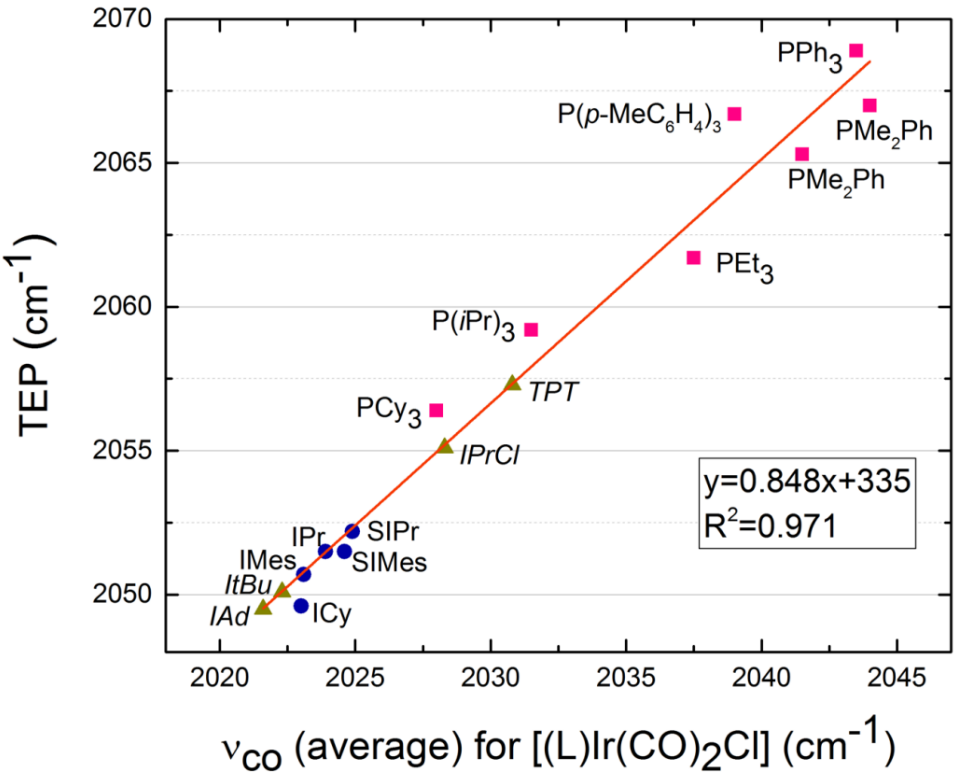

(■) Experimental values for phosphines; (•) Experimental values for NHCs; (▲) Values obtained by linear regression.

An additional factor largely believed to be crucial for the success of NHC ligands is the *directed* bulk provided by ortho substituted N-aryl rings. When considering Tolman's cone angle

method (Figure 2) for quantifying and comparing the steric bulk of phosphines, a key assumption is the steric bulk is spread around the metal centre in a cone shape. This is a reasonable assumption for phosphine ligands considering they are usually sp^3 hybridized with large bulky groups that stick out, away from the lone electron pair. In comparison, NHC ligands have a distinct distribution of the steric bulk around the metal centre. Many studies have used X-Ray crystallography to understand the preferred conformations of these bulky ligands.[59] It is commonly observed that the N-aryl (or alkyl) substituents are pushed towards the metal centre through steric clash with the R groups on the backbone of the imidazole based NHC (Figure 6A). Further complicating the matter, large substituents on the ortho positions have been shown to apply additional steric demands on the metal centre. Considering the many differences between the overall geometry of NHC and phosphine ligands, it was apparent a new method for quantifying and comparing steric bulk was necessary. To this end, Nolan and Cavallo proposed a method for quantifying the steric demand of these ligands by measuring the percentage of a spherical volume around a metal centre that is occupied by the ligand. This measurement is referred to as the percent buried volume ($\%V_{bur}$).[75] This information has been measured and catalogued for many prevalent NHC ligands using [(NHC)Ir$(CO)_2$Cl] complexes (Figure 6B). Very recently, Ogoshi updated this methodology by considering the flexibility of bulky NHC ligands by measuring the change in $\%V_{bur}$ over the course of a transformation using DFT.[76] This provided a new parameter ($\Delta\%V_{bur}$), which essentially measures the flexibility of a ligand. This is an important consideration because bulky ligands have indeed been shown to increase catalyst activity, but the ligands must remain flexible enough to allow the reactants to interact with the metal. This delicate balance between ligand bulk and flexibility is one of the main challenges for chemists in this field.

Figure 6: A) Representative NHC metal complex with accentuated bond angles. B) Diagram of the spherical model used to calculate *%V_{bur}* with a table of comparisons for select NHCs.

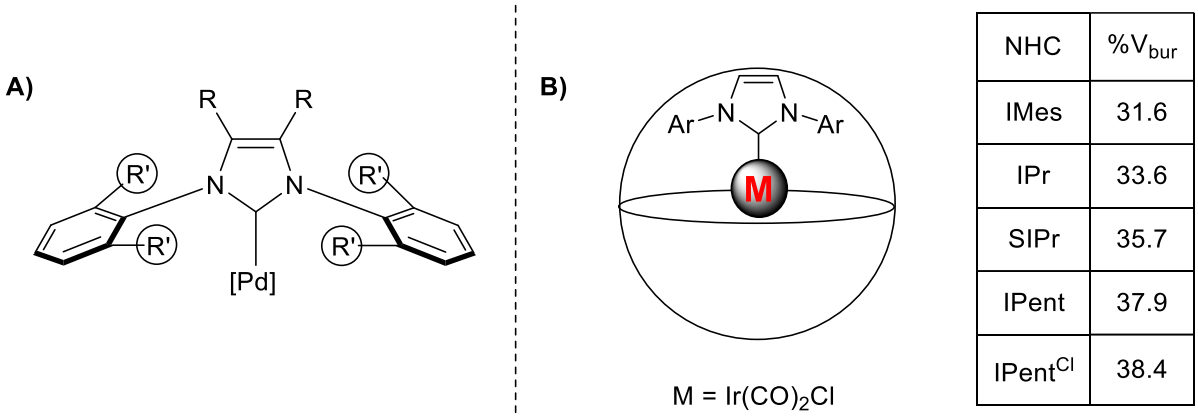

NHC	%V_{bur}
IMes	31.6
IPr	33.6
SIPr	35.7
IPent	37.9
$IPent^{Cl}$	38.4

1.3.3. *Pd-PEPPSI* precatalysts

An important choice chemists face when performing a Negishi coupling is the choice of catalyst. These usually fall into two general classes, those generated *in situ* by complexation of a ligand with a palladium source and pre-ligated palladium complexes. The benefits of the *in-situ* method are the simplicity of not having to isolate a preligated catalyst, ability to choose between the +2 or 0 oxidation state of palladium and easy control of metal to ligand ratio. However, the purity and exact identity of the *in situ* generated catalyst can be questionable. This is especially true for extremely bulky ligands that are challenging to coordinate with palladium.

Considering the high reactivity of Pd-NHC catalysts, but sometimes challenging *in situ* ligation of the NHC,[77,78] pre-formed Pd-NHC complexes have seen an increase in usage. One of the most popular series of Pd-NHC precatalysts are those developed by Organ *et al.*, termed *PEPPSI* (Pyridine Enhanced Precatalyst, Preparation, Stabilization, and Initiation) (Figure 7). This series of precatalysts is defined by their bulky ortho substituents and a pyridine ligand that stabilizes the precatalyst, allowing it to be prepared as an air-stable, free-flowing powder. The pyridine also acts as a "throw-away ligand" upon *in situ* activation that enables rapid precatalyst

initiation and gives rise to its name. The suffix in these catalyst common names refer to the size of the alkyl chain (iPr, iPent, iHept) at the ortho position of the N-Aryl substituents and any backbone modifications, such as the exchange of hydrogen for chlorine or methyl groups, is identified by a superscript at the end of the name i.e. (IPr^{Cl} and IPr^{Me}, respectively). In recent years, some new bulky ligands require a π-cinnamyl group to stabilize the NHC and serve as the throw-away ligand. The complexes are labeled as *(NHC)Pd(cinnamyl)Cl*, the most notable example being *(DiMeIHept^{Cl})Pd(cinnamyl)Cl*.[61,79]

Figure 7: Select examples of *Pd-PEPPSI* precatalysts.

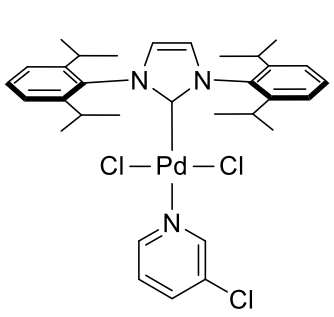

Pd-PEPPSI-IPr

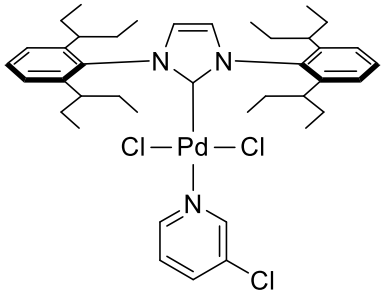

Pd-PEPPSI-IPent

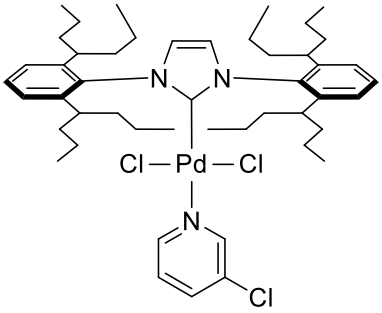

Pd-PEPPSI-IHept

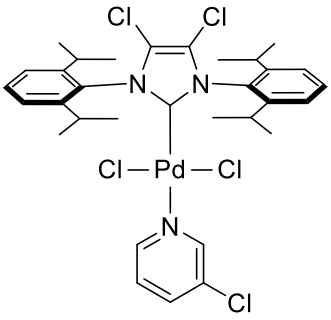

Pd-PEPPSI-IPr^{Cl}

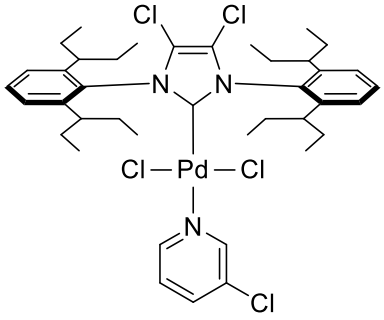

Pd-PEPPSI-IPent^{Cl}

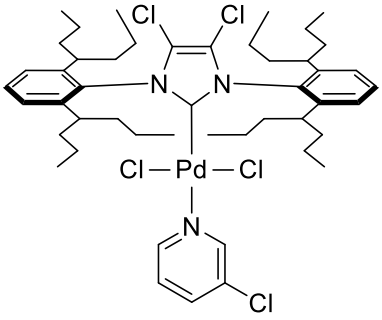

Pd-PEPPSI-IHept^{Cl}

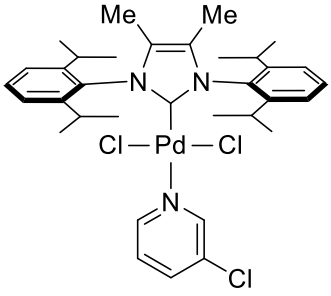

Pd-PEPPSI-IPr^{Me}

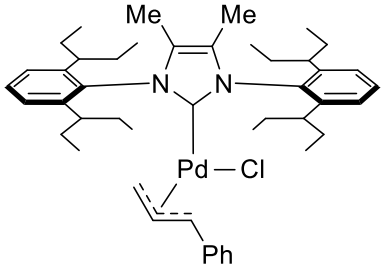

(IPent^{Me})Pd(cinnamyl)Cl

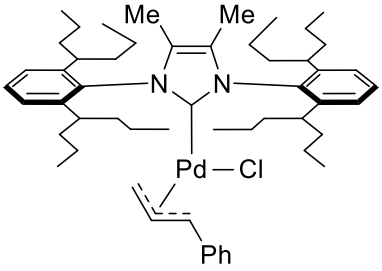

(IHept^{Me})Pd(cinnamyl)Cl

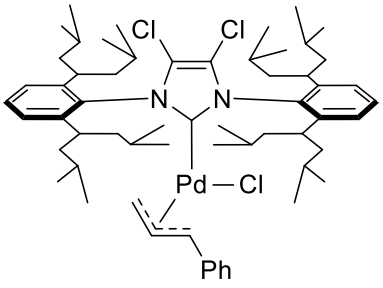

(DiMeIHept^{Cl})Pd(cinnamyl)Cl

There have been many iterations of *Pd-PEPPSI* with significant improvements having come from increasing the steric bulk of the ortho substituents, and installation of chlorine on the imidazole backbone.[46,79–81] Using various 2,6-disubstituted anilines, multiple generations of *Pd-PEPPSI* have been prepared with alkyl chains such as iPent (*n*-pent-3-yl), iHept (*n*-hept-4-yl), and DiMeiHept (2,6-dimethyl-*n*-hept-4-yl). These large chains help place steric bulk closer to the metal centre and to further enhance this effect, the imidazole backbone can be substituted, which pushes the N-Aryl rings and alkyl chains even closer to the metal center. Since the inception of these catalysts, they have successfully catalyzed many challenging Negishi couplings, including the synthesis of tetra-ortho-substituted biaryls (Scheme 11A),[62] alkyl-alkyl couplings (Scheme 11B),[82] and couplings in flow with solid-supported *Pd-PEPPSI* (Scheme 11C).[83] Other notable uses for *Pd-PEPPSI* precatalysts include the selective coupling of challenging amines,[84–86] thiols[13,87] and boronic acids.[88]

Scheme 11: Examples of challenging Negishi couplings successfully catalyzed by *Pd-PEPPSI* catalysts.

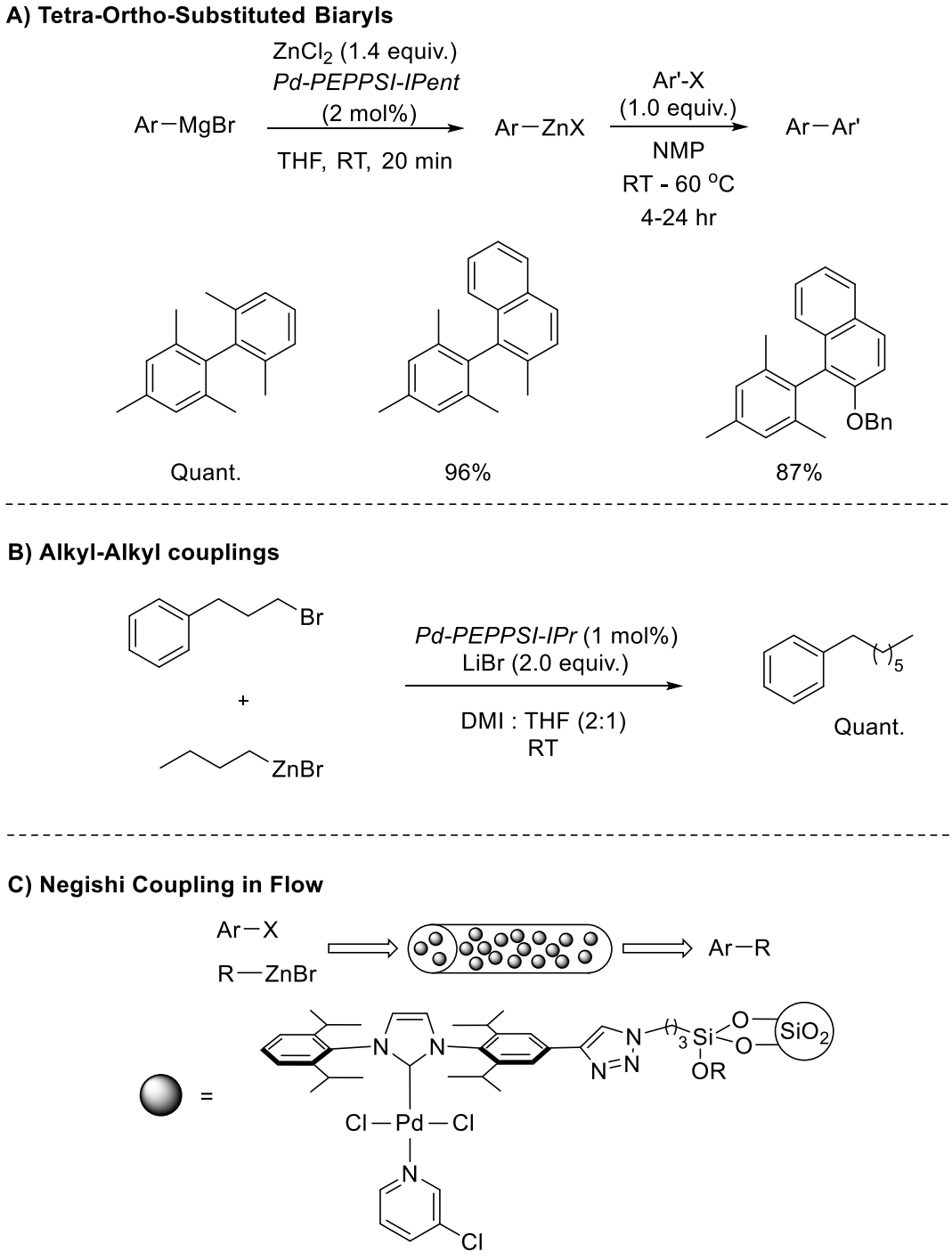

As previously mentioned, a major improvement to the reactivity of *Pd-PEPPSI* was the replacement of hydrogen with chlorine on the imidazolium backbone.[40,46,47,84] One case study

which highlighted the drastic change in selectivity brought about by these chlorines was the coupling of secondary organozincs (Table 1).[40] The coupling of isopropylzinc bromide (**39**) to 3-bromobenzonitrile (**38**) is challenging due to the rearrangement of the alkyl chain. This rearrangement is initiated by BHE at the TM intermediate, followed by rotation about the metal-olefin bond and reinsertion, in a process known as migratory insertion (MI) to give the more thermodynamically favored linear product (**41**) instead of the desired branched product (**40**). This rearrangement presents a weakness for alkyl couplings since the rearranged product can be extremely difficult to prevent. An increase in the steric bulk of the catalyst resulted in higher selectivity for the desired branched isomer (entries 1 and 4). Chlorine modified backbones further increased the selectivity (entries 1 & 4 compared to 2 & 5 respectively). Furthermore, methyl groups on the backbone of *IPr* increased the selectivity (entries 1 & 3). Combining this information, an even bulkier and chlorine functionalized catalyst, *Pd-PEPPSI-IHept*^{Cl}, was created, which was able to produce the branched product only (entry 6). Later, it was shown *Pd-PEPPSI-IHept*^{Cl} can also selectively couple 5-membered heteroaryl halides that are especially challenging since the smaller rings have greater difficulty undergoing reductive elimination and leave more space for β hydride elimination, leading to rearrangement.[47]

Table 1: Effect of catalyst choice on the coupling of 3-bromobenzonitrile (38) with isopropylzinc bromide (39).

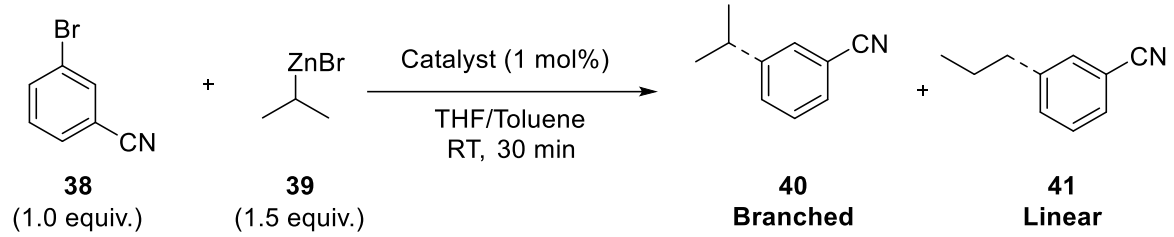

38 (1.0 equiv.) + **39** (1.5 equiv.) → **40** Branched + **41** Linear

Entry	Catalyst	**40** : **41**[a]
1	*Pd-PEPPSI-IPr*	1 : 1
2	*Pd-PEPPSI-IPr*^{Cl}	14.7 : 1
3	*Pd-PEPPSI-IPr*^{Me}	15 : 1
4	*Pd-PEPPSI-IPent*	10 : 1
5	*Pd-PEPPSI-IPent*^{Cl}	56 : 1
6	*Pd-PEPPSI-IHept*^{Cl}	Only Branched

[a] Ratio of branched to linear determined by analyzing the ^{1}H NMR spectrum of the purified product, since the two isomers co-elute.

Upon discovery of these dramatic improvements in selectivity, the source of this beneficial effect was investigated.[47] Considering the precedent for the benefits of larger catalysts, Organ *et. al.* suspected the chlorines were pushing the N-aryl rings down towards the metal and restricting the motion of the alkyl chains. This would cause the alkyl chains to aggregate closer to the metal centre, limiting the space around the metal needed for BHE. These suspicions were supported by modeling the rearrangement pathway with *Pd-PEPPSI-IPr* and *Pd-PEPPSI-IPr*^{Cl} using DFT (Scheme 12).[46] Both catalysts displayed similar barriers for RE leading to the branched product (**TS**$_{42\text{-}47}$). The barriers to BHE showed a significant difference between the two catalysts, with *Pd-PEPPSI-IPr*^{Cl} possessing a barrier higher than *Pd-PEPPSI-IPr* (15.3 versus 13.0 kcal/mol respectively, **TS**$_{42\text{-}43}$). Furthermore, the rearranged intermediate (**45**) was confirmed to be the more

favorable metal-alkyl isomer, lower in energy than the branched intermediate (**42**) by -1.7 and -1.9 kcal/mol for the two catalysts.

Scheme 12: DFT potential energy surface for RE versus BHE with *Pd-PEPPSI-IPr* and *Pd-PEPPSI-IPr^{Cl}*.

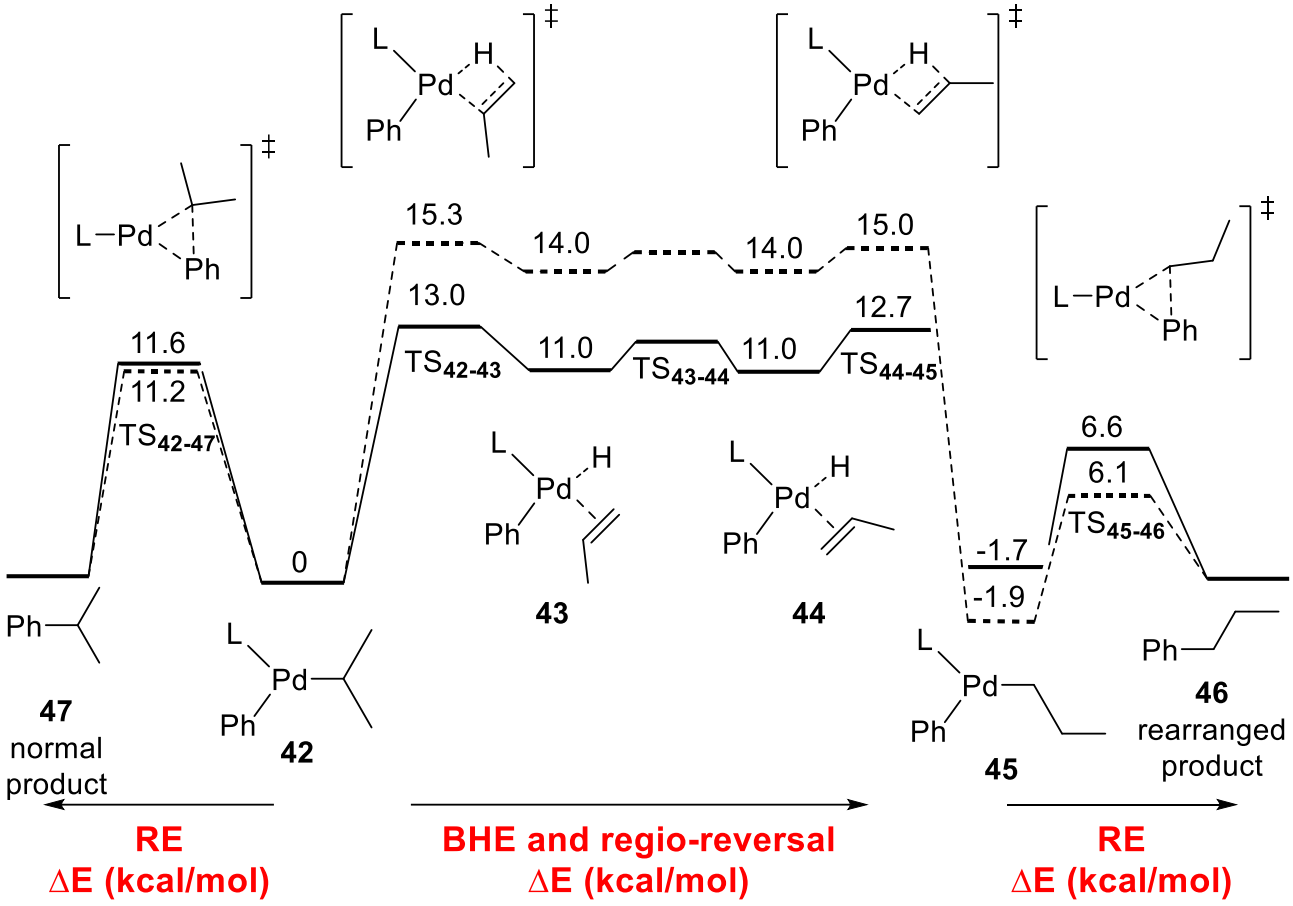

The Gibbs free energies (kcal/mol) of the elementary transformations were computed at the B3LYP level with LANL2TZ(F) on Pd and 6-31G* on the remaining atoms for the case of L = *IPr* (—) and *IPr^{Cl}* (••••).[46]

In this report, TEP values were calculated for the NHC ligands studied using the ν_{CO} of the corresponding (NHC)IrCl(CO)$_2$ complexes (Table 2). As expected, a general trend was observed where an increase in carbonyl stretch was seen with increasing electron withdrawing backbone modifications. Interestingly, the selectivity of *Pd-PEPPSI-IPr^{Me}* and *Pd-PEPPSI-IPr^{Cl}* were comparable but their TEP were different (entry 2 and 3). Based on these results, and the

observations that the larger *IPent* and *IHept* ligands gave better selectivity (Table 1), it was concluded the effect imposed by the NHC backbone groups is primarily steric.

Table 2: TEP analysis of (NHC)IrCl(CO)$_2$ complexes.

Entry	NHC	V_{CO} (CH_2Cl_2, cm^{-1})	V_{CO} (average)	TEP (cm^{-1})
1	*IPr*	2066.8, 1981.0	2023.9	2051.5
2	*IPr*^{Me}	2064.5, 1978.2	2021.3	2049.3
3	*IPr*^{Cl}	2071.4, 1985.1	2028.3	2054.0
4	*IPent*	2064.7, 1978.6	2021.7	2049.6
5	*IPent*^{Cl}	2069.3, 1982.2	2025.8	2053.0

1.4 Salt effects in Negishi coupling

One important aspect of Negishi coupling is the strong dependence on salt additives, which was overlooked since the discovery of the reaction because most methods for synthesizing organozinc reagents generate stoichiometric salt byproducts or benefit from the direct addition of salt (Scheme 13A-D). Synthetic protocols such as metathesis of organolithium and Grignard reagents with zinc salts (Scheme 13A)[89–93] and the use of Rieke zinc (Scheme 13B)[94] generate stoichiometric salt byproducts, the composition of which depends on the choice of reagents. The use of inexpensive, readily available zinc powder for direct insertion into C-X bonds is of great interest for synthetic applications. Unfortunately, zinc powder on its own is not capable of C-X bond insertion, possibly due to the stable zinc oxide protective layer on the metal surface. Knochel developed a robust protocol for the preparation of organozinc reagents by preactivating zinc dust with TMSCl and 1,2-dibromoethane along with 1–2 equivalents of LiCl, which aided activation of more challenging C-X bonds (Scheme 13C).[95] Huo's protocol is one of the few commonly

employed techniques that does not require salt, nor generate salt byproducts (Scheme 13D).[24] In this protocol the organozinc is prepared by direct insertion of zinc dust into C-X bonds. This method is similar to Grignard formation in that iodine is used to activate the surface of the metal, but one important distinction is the need for a very polar solvent (e.g., DMA or DMI). For simplicity's sake, freshly prepared organozinc solutions are usually titrated, then used as-is.

Scheme 13: Commonly employed techniques for the preparation of organozinc reagents, such as a) metathesis,[89–93] b) the Rieke zinc protocol,[94] c) the Knochel protocol,[95] and d) the Huo protocol.[24]

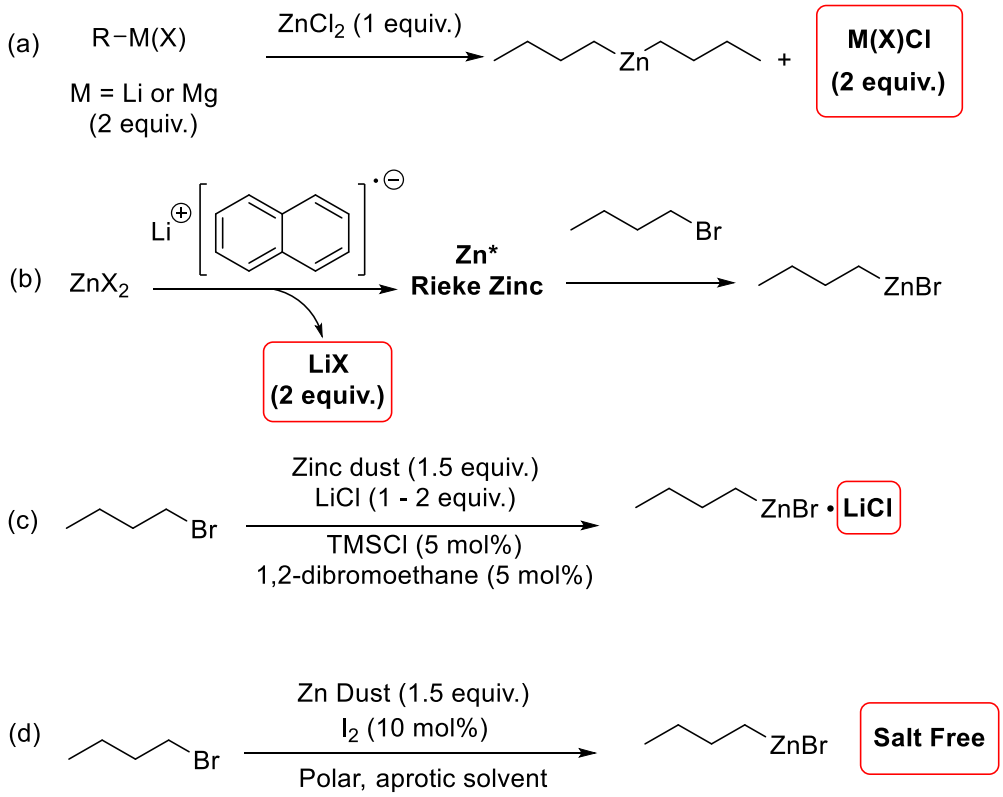

1.4.1 Early evidence of salt effects in Pd catalyzed cross-coupling

One of the earliest reports of salt additives affecting the outcome of a palladium catalyzed cross-coupling came from Stille in 1986[96] who observed that LiCl was crucial for the successful coupling of alkenyl triflates (**48**) with tributyl(vinyl)tin (**49**) (Table 3). When this coupling was performed in the absence of LiCl only trace amounts of product were produced (entry 1). In

comparison, the same coupling produced a yield of 71% with 0.6 equivalent of LiCl (entry 2). Increasing the LiCl loading to 1.1 or 3.0 equivalents gave nearly quantitative yields of **50** (entries 3 & 4).

Table 3: Influence of LiCl on the cross-coupling of vinyl triflate, 48, and vinyltributylstannane, 49.[a]

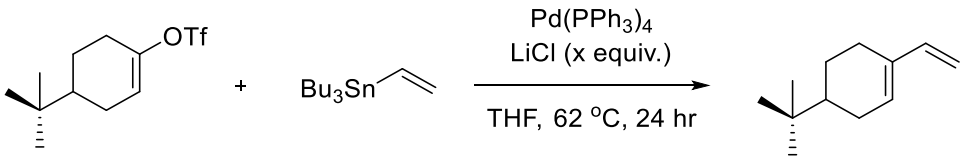

48 (1.0 equiv.) **49** (1.2 equiv.) **50**

Entry	$Pd(PPh_3)_4$ (mol%)	LiCl (equiv.)	Yield of **50** (%) [b]
1	1.97	0	<10
2	2.07	0.6	71
3	2.04	1.1	>95
4	1.98	3.0	>95

The authors discovered the palladium catalyst was irreversibly degrading in the absence of LiCl. Oxidative addition of $Pd(PPh_3)_4$ into alkenyl triflate **48** was successful in the presence of LiCl, producing OA intermediate **51** but failed without the additive (Scheme 14). The salt-free attempts produced a brown solution with a new singlet at 22.9 ppm in the ^{31}P NMR. The authors were unable to identify this new compound, but showed it was incapable of catalyzing the coupling of **48** and **49**. It was suggested that LiCl coordinates to palladium, forming electron-rich choloropalladium(0) anions $[L_nPdCl]^-$, which then undergo OA. Even though this report was not able to pinpoint the exact role of salt in keeping the catalyst alive, the findings are still applicable

to other palladium catalyzed cross-coupling reactions. Smooth OA and ensuring catalyst survival are crucial tasks in nearly all palladium catalyzed cross-couplings.

Scheme 14: Effect of LiCl additive on the OA of $Pd(PPh_3)_4$ into alkenyl triflate 48.

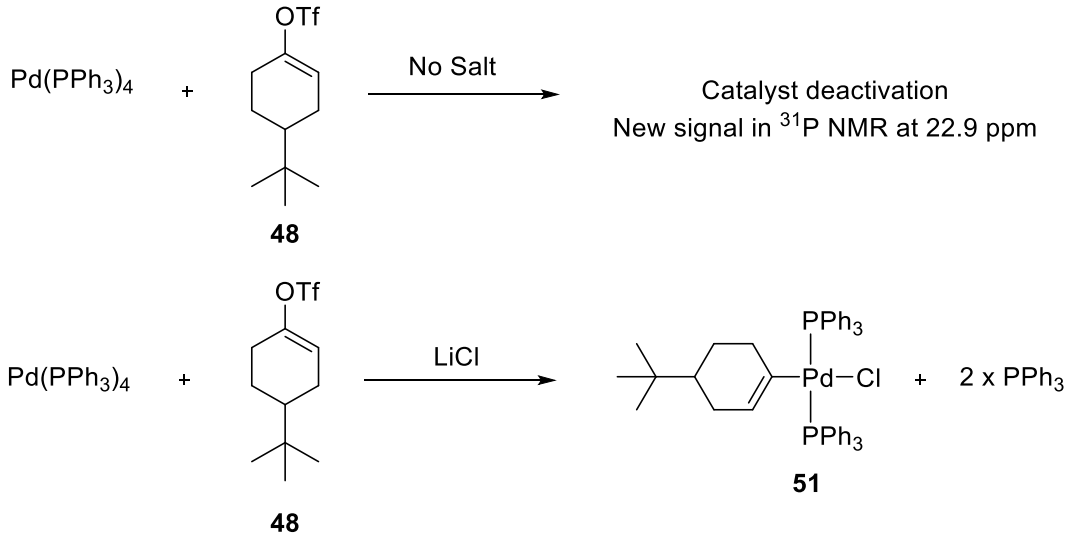

1.4.1 Evidence of salt effects in Negishi cross-coupling

Stille's observations on these salt effects were largely overlooked until 2006 when Organ *et al.* discovered a notable salt dependency in an alkyl-alkyl Negishi coupling while testing the capabilities of *Pd-PEPPSI-IPr* precatalyst.[82] Two organozinc preparations that should have generated identical organozinc reagents yielded drastically different results when used in the same coupling (Table 4). In this work, the same alkylzinc (**53**) prepared using Rieke's protocol,[94] which generates 2.0 equivalents of LiBr *in situ*, produced quantitative conversion (entry 1) while the organozinc prepared from Huo's protocol[24] (salt-free) did not provide any of the cross-coupled product (entry 2). It was proposed that LiBr, produced as a byproduct of Rieke's protocol, was responsible for the observed reactivity. This hypothesis was confirmed by adding 2.0 equivalents of LiBr to the salt-free reagent, resulting in full conversion of **52** to **54** (entry 3).

Table 4: First discovery of a salt effect in Negishi coupling.

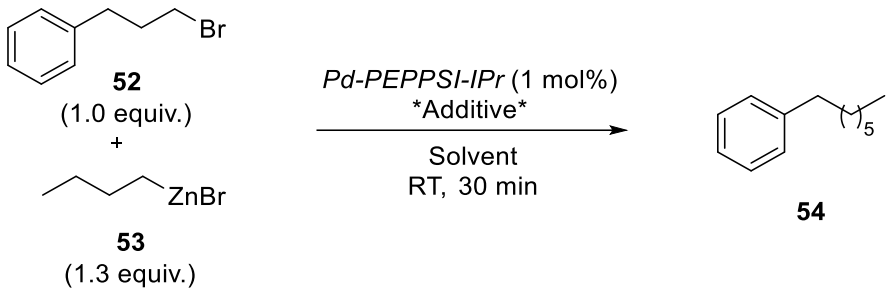

Entry	Solvent	*n*-BuZnBr (**53**) source	Additive	Yield of **54** (%)
1	THF:NMP, 2:1	Rieke's protocol[94]	-	Quant.
2	THF:DMI, 2:1	Huo's protocol[24]	-	0
3	THF:DMI, 2:1	Huo's protocol[24]	LiBr (2 equiv.)	Quant.

1.4.2 Alkyl-alkyl couplings (higher order zincates)

To shed more light on the exact role of such salts in the alkyl-alkyl Negishi reaction, the researchers carried out an additive study where a variety of organic and inorganic salts were evaluated (Table 5, entries 3–9).[97] The additives containing bromine were generally more effective than those containing chlorine or iodine, while the counterion did not seem to play a significant role, aside from ensuring solubility. To this end, when 12-crown-4, a known chelator for Li^+, was used, coupling still proceeded without interruption (Table 5, entry 10). These observations established that it was the anion (i.e., the halide) in the added salt that was essential for the cross-coupling reaction.

Table 5: Effect of *n*-BuZnBr (53) formation method and additives on the Negishi cross-coupling of 52 and 53 catalyzed by *Pd-PEPPSI-IPr*.

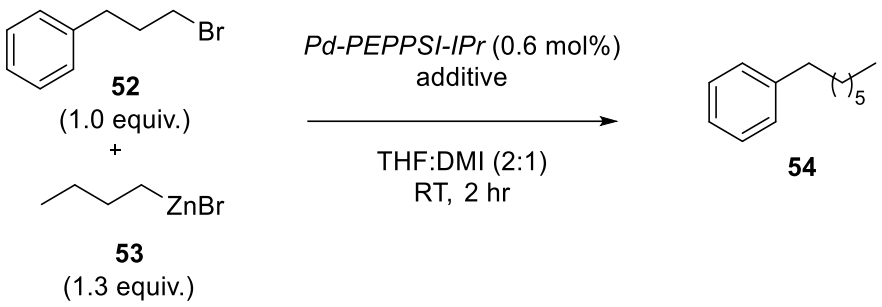

Entry	*n*-BuZnBr (**53**) Source	Additive (2.0 equiv.)	Conversion to **54** (%)
1	Rieke's protocol[94]	none	Quant.
2	Huo's protocol[24]	none	0
3	Huo's protocol[24]	LiCl/Br	Quant.
4	Huo's protocol[24]	LiI	5
5	Huo's protocol[24]	$MgBr_2$	92
6	Huo's protocol[24]	$MgCl_2$	15
7	Huo's protocol[24]	TBAB	79
8	Huo's protocol[24]	TBAC	34
9	Huo's protocol[24]	TBAI	2
10	Huo's protocol[24]	LiBr + 12-crown-4	84

[a] TBAB = tetra-*n*butylammonium bromide; TBAC = tetra-*n*butylammonium chloride; TBAI = tetra-*n*butylammonium iodide.

To determine the amount of LiBr required for coupling to occur, a titration experiment was performed in which a salt-free solution of *n*-BuZnBr was coupled with **52** in the presence of increasing amounts of LiBr (Figure 8). No coupling was observed until approximately 1.0 equivalent of LiBr (with respect to organozinc) was added. Once one full equivalent of LiBr was introduced, a steep increase in conversion occurred with each successive addition of 0.1 equivalent of LiBr, achieving quantitative conversion after 1.4 equivalents. The fact that a super-

stoichiometric amount of LiBr was required for the initiation of the reaction led the researchers to postulate that higher-order zincates of type ($2Li^+$) $RZnBr_3^{2-}$ are the active transmetallating species. Further supporting evidence was obtained by a second titration in which increasing amounts of $ZnBr_2$ were added to the reaction containing 2.0 equivalents of LiBr (Figure 8). It was thought $ZnBr_2$ would sequester LiBr from the solution, preventing the formation of higher-order zincates. The observed decrease in yield supports the idea that $ZnBr_2$ was sequestering LiBr, which in turn lowers the concentration of active transmetallating species. Upon addition of 1.0 equivalent of $ZnBr_2$ coupling shut down completely.

Figure 8: Double titration study of alkyl-alkyl coupling between 52 and *n*-BuZnBr (53).

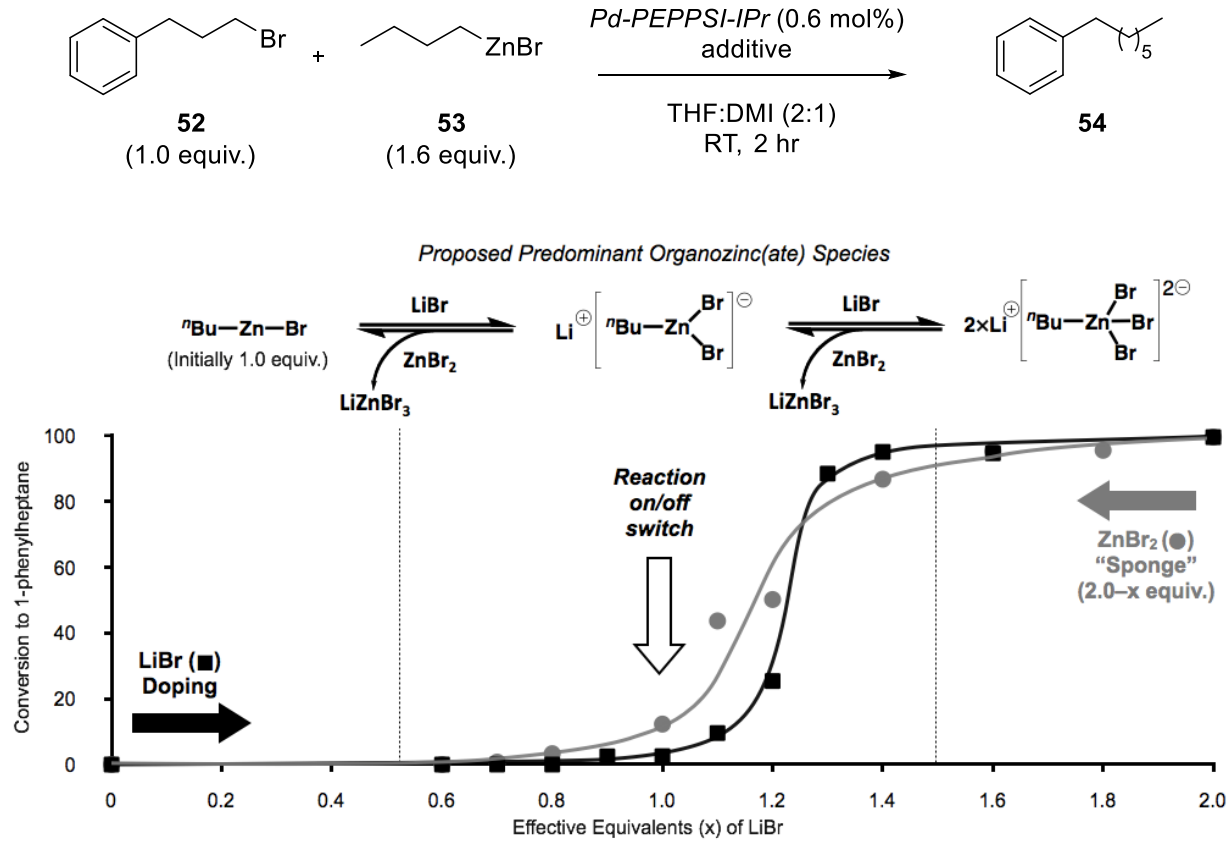

The first titration (■) uses increasing stoichiometries of LiBr (x equiv.) in the cross-coupling of **52** (1.0 equiv.) with *n*-BuZnBr (**53**)

(1.6 equiv.) catalyzed by *Pd-PEPPSI-IPr* (0.6 mol%). In the second titration (•), increasing amounts of $ZnBr_2$ (2.0-x equiv.) were added to the same reaction with 2.0 equiv. of LiBr present.

Related to this work, Koszinowski and Böhrer analyzed THF solutions of organozinc(ate) species formed by LiCl-mediated zinc insertion[98] or metathesis between organolithium compounds and $ZnCl_2$[99] using anion-mode electrospray ionization (ESI) mass spectrometry. Mononuclear $ZnCl_3^-$, Zn(*n*-Bu)Cl_2^- species and polynuclear Zn_2(*n*-Bu)Cl_4^-, $LiZn_2$(*n*-Bu)$_2Cl_4^-$ species were detected in significant quantities, alongside smaller amounts of $LiZnCl_4^-$ and LiZn(*n*-Bu)Cl_3^- (Figure 9).[98] These ESI studies also revealed that the nature of the halide present in the zincate complexes has a profound effect on the aggregation state of organozinc reagents. For example, mononuclear zincates are dominant with alkyl bromides and iodides, while many polynuclear zincates are formed with chlorides.

Figure 9: Anion-mode ESI mass spectrum of a 10 mM solution of Li *n*-Bu/$ZnCl_2$ in THF.

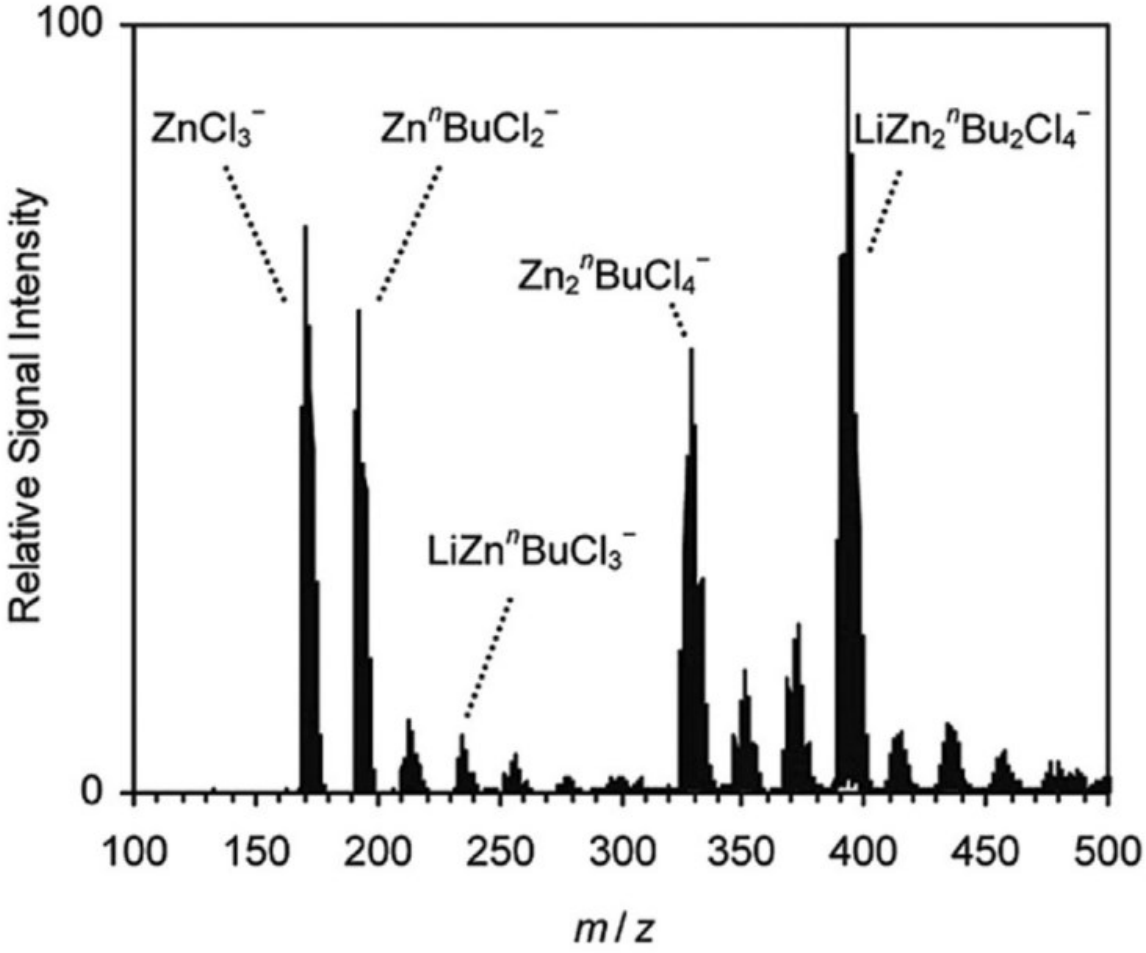

Later in 2011, Organ *et al.* employed mass spectrometry in combination with NMR spectroscopy to identify and characterize the higher-order zincate species that were believed to be involved in alkyl-alkyl Negishi coupling.[100] To do so, solutions of *n*-BuZnBr with increasing amounts of LiBr in THF, DMI or NMP (or combination of these solvents) were prepared and analyzed using ESI mass spectrometry. Only various solvent and Li^+ adducts were observed in positive-ion mode, however negative-ion mode confirmed the presence of *n*-$BuZnBr_2^-$ and $ZnBr_3^-$ as the dominant species. By increasing the amount of LiBr from 0 to 1.5 equivalents the ratio of *n*-$BuZnBr_2^-$ to $ZnBr_3^-$ changed from *circa* 1:8 (Figure 10A) to 5:1 (Figure 10E).

Figure 10: Mass spectra showing the change in ratio of *n*-BuZnBr$_2^-$ toZnBr$_3^-$ ion intensities as a function of LiBr loading.

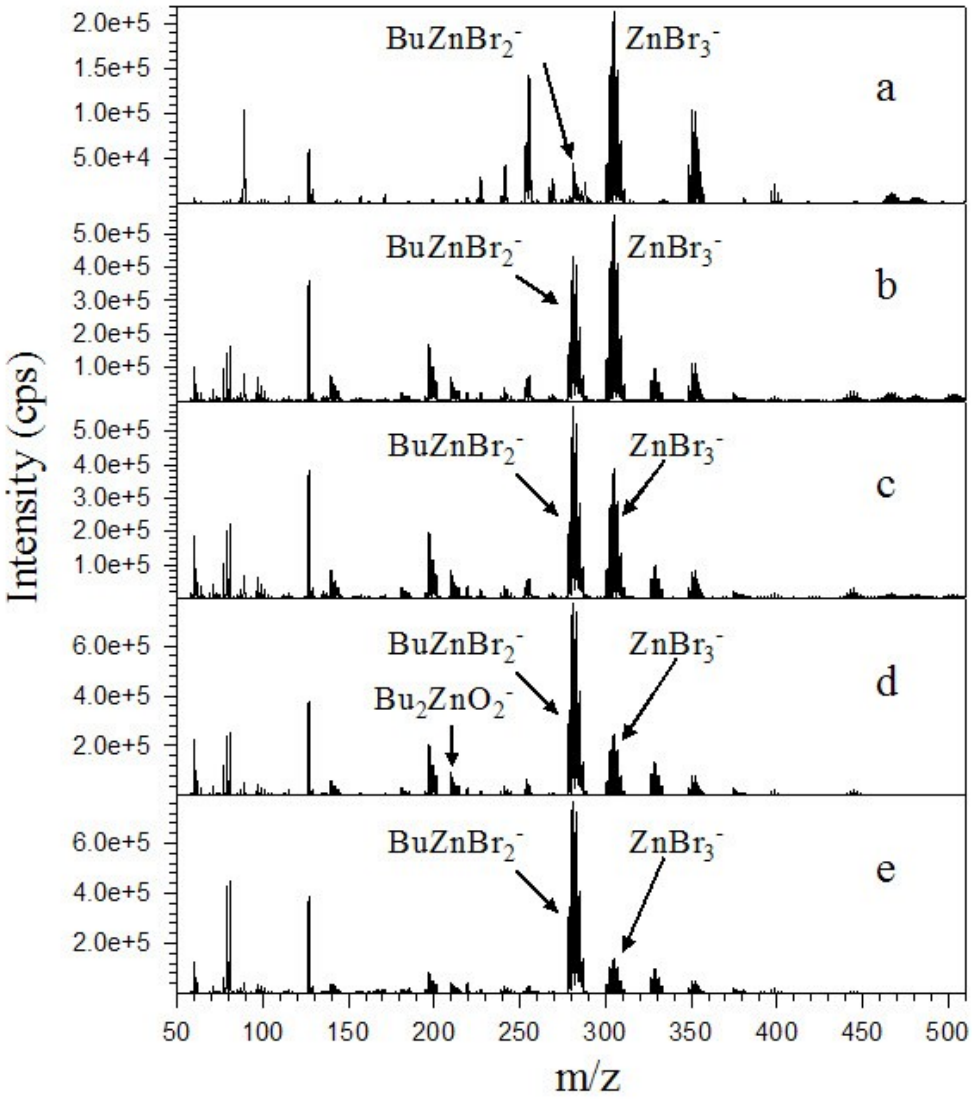

The data were collected with *n*-BuZnBr (**51**) in DMI solvent with the following equiv. of LiBr added: a) 0; b) 0.5; c) 0.75; d) 1.0; and e) 1.5.

According to Organ's previous study,[97] no coupling occurs unless a minimum of 1.0 equivalent of LiBr is added to the reaction mixture (Figure 8). However, significant quantities of *n*-BuZnBr$_2^-$ were detected after addition of only 0.5 equivalent of LiBr (Figure 10b). This finding suggested the mono-anionic "ate" species, analogous to the purported active transmetallating organoborates in Suzuki–Miyaura couplings,[101,102] are not the active transmetallating species in

alkyl Negishi coupling. At this loading of LiBr, the higher-order zincates (n-$BuZnBr_3^{2-}$) would not be expected to exist until all the lower-energy n-$BuZnBr_2^-$ would be first populated. When the loading of LiBr eclipses 1.0 equivalent, the coupling now becomes catalytic in Br^- because each turnover of the catalytic cycle liberates one bromide ion from **52**. This is perhaps also important in keeping the electrophilic zinc bromide coordinatively saturated to eliminate its disruptive effects on coupling. By increasing the LiBr loading to 1.5 equivalents, trace amounts of n-$BuZnBr_3Li^-$ could be detected (not shown in Figure 10, see original manuscript), which was concurrent with the commencement of coupling.[100]

An opportunity to study the role of higher-order zincates in Negishi coupling was provided when Clyburne's group developed an approach to isolable higher-order zincate **55**.[103] Initially, **55** was prepared *in situ* and coupled with **52** using *Pd-PEPPSI-IPr* precatalyst but no conversion was observed (Table 6, entry 1).[104] There was concern that the phosphonium cation could be interfering with catalysis, so PPh_4Br was substituted with n-Bu_4NBr (TBAB) and the reaction did proceed, albeit with incomplete conversion (Table 6, entry 2). The presence of competing byproducts including dehalogenation (**58**), elimination (**59**), and homo-coupling (**60**) prompted Organ *et al.* to use *Pd-PEPPSI-IPent*, which was known to be a more active catalyst. With *Pd-PEPPSI-IPent*, the reaction proceeded to completion and no byproducts were detected (Table 6, entry 3). The most telling result was obtained when this coupling was successfully repeated in pure THF (Table 6, entry 4). Up until that point, all alkyl-alkyl Negishi couplings reported by Organ[25,39,82,97] and others[105,106] required highly polar co-solvents, such as DMI, to proceed, consistent with the formation of a higher-order zincate. In Table 6, the alkylzincate(s) form(s) under conditions that do not permit a Schlenk equilibrium to establish. That is, each catalytic cycle liberates a bromide ion from **52**, which sequesters the $ZnBr_3$ byproduct, leading to coordinatively saturated $ZnBr_4^{2-}$.

Table 6: Effects of salt additives on the coupling of 52 with various ethylzinc derivatives.

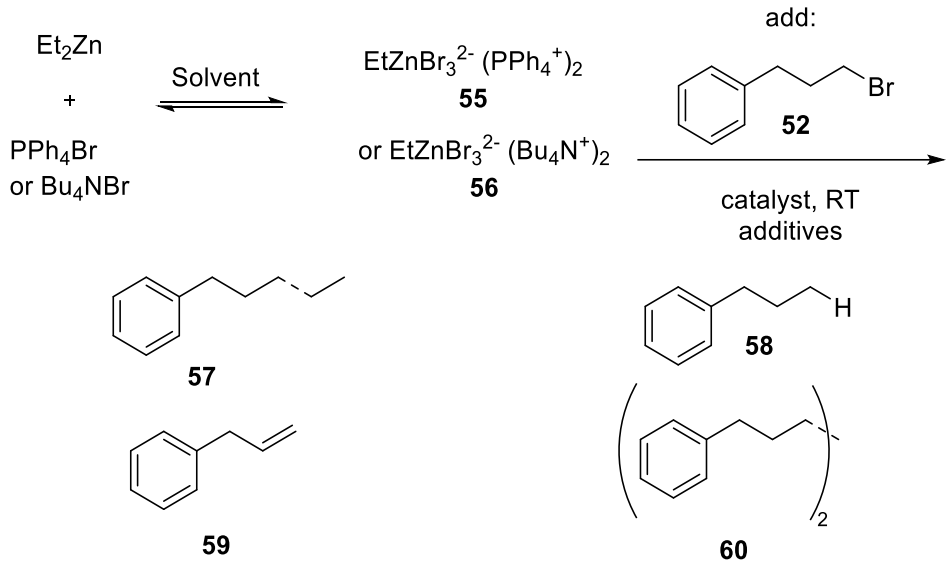

Entry	Zincate	Solvent	Catalyst (%)	Ratio **52:57:58:59:60**
1	**55**	THF/DMI (2:1)	*Pd-PEPPSI-IPr* (4)	no reaction
2	**56**	THF/DMI (2:1)	*Pd-PEPPSI-IPr* (4)	1:3:3:3:0
3	**56**	THF/DMI (2:1)	*Pd-PEPPSI-IPent* (4)	0:1:0:0:0
4	**56**	THF	*Pd-PEPPSI-IPent* (4)	<0.1:1:0:0:0

1.4.3 Aryl-aryl couplings (solvent polarity)

The above studies on salt effects focused on alkyl organozinc nucleophiles, with the main contributing factor believed to be formation of higher order zincates. Following these initial discoveries, the effect of salt additives on arylzinc species was studied. In 2014, Organ *et al.* showed that the increase in solvent polarity caused by the addition of salt additives or polar co-solvents was critical for biaryl couplings.[107]

For Negishi cross-coupling, one of the most common solvents is THF for several reasons. First, it is a reliable solvent for the preparation of organozinc solutions, which are often used as is, and it is generally compatible with most palladium catalysis. While THF is the most common solvent choice, many other solvent combinations are often employed to aid in solubility of substrates and adjust reactivity. Common co-solvents used for Negishi couplings include toluene, DMF, DMI, NMP, and other aprotic solvents. Regardless of the choice of solvent, one physical change brought about by the addition of salt is an increase in the dielectric constant (ε) of the solvent medium. This is believed to be the source of the beneficial salt effects observed in aryl-aryl couplings catalyzed by NHC-Pd complexes.

Aryl zinc halide (ArZnX) reagents are often generated by TM of the corresponding Grignard reagent with 0.5–1.0 equivalent of ZnX_2, generating either the mono- or diaryl zinc species in solution, along with the corresponding MgX_2 byproduct. A series of experiments were performed to investigate the role of MgX_2 in the coupling of PhZnX (**62**) and 2-bromoanisole (**63**). PhZnX was generated from equal amounts of Grignard reagent **61** and $ZnCl_2$ in THF, generating a stoichiometric amount of MgX_2 as a byproduct (Scheme 15A). This solution of **62** was then combined with **63** and *Pd-PEPPSI-IPent* producing biaryl product **64** quantitatively. When the magnesium salts were removed, minor amounts of **64** where produced (Scheme 15B), but reactivity was restored when 1.0 equivalent of $MgCl_2$ (Scheme 15C) or a polar co-solvent was added (Scheme 15D). The researchers proposed that PhZnX forms highly stabilized aggregates that are too poorly nucleophilic to undergo TM, similar to the observations made by Marder and Lei who discovered that organozinc compounds prepared from the Grignard reagent were far more active than those prepared from organolithium species.[108] With a salt additive or polar co-solvent,

the increase in solvent polarity helps break up these aggregates, leading to an increase in the nucleophilicity of PhZnX, thereby facilitating TM.

Scheme 15: Effect of magnesium salts and solvent polarity on the cross-coupling of PhZnX (62) with 2-bromoanisole (63) using *Pd-PEPPSI-IPent*.

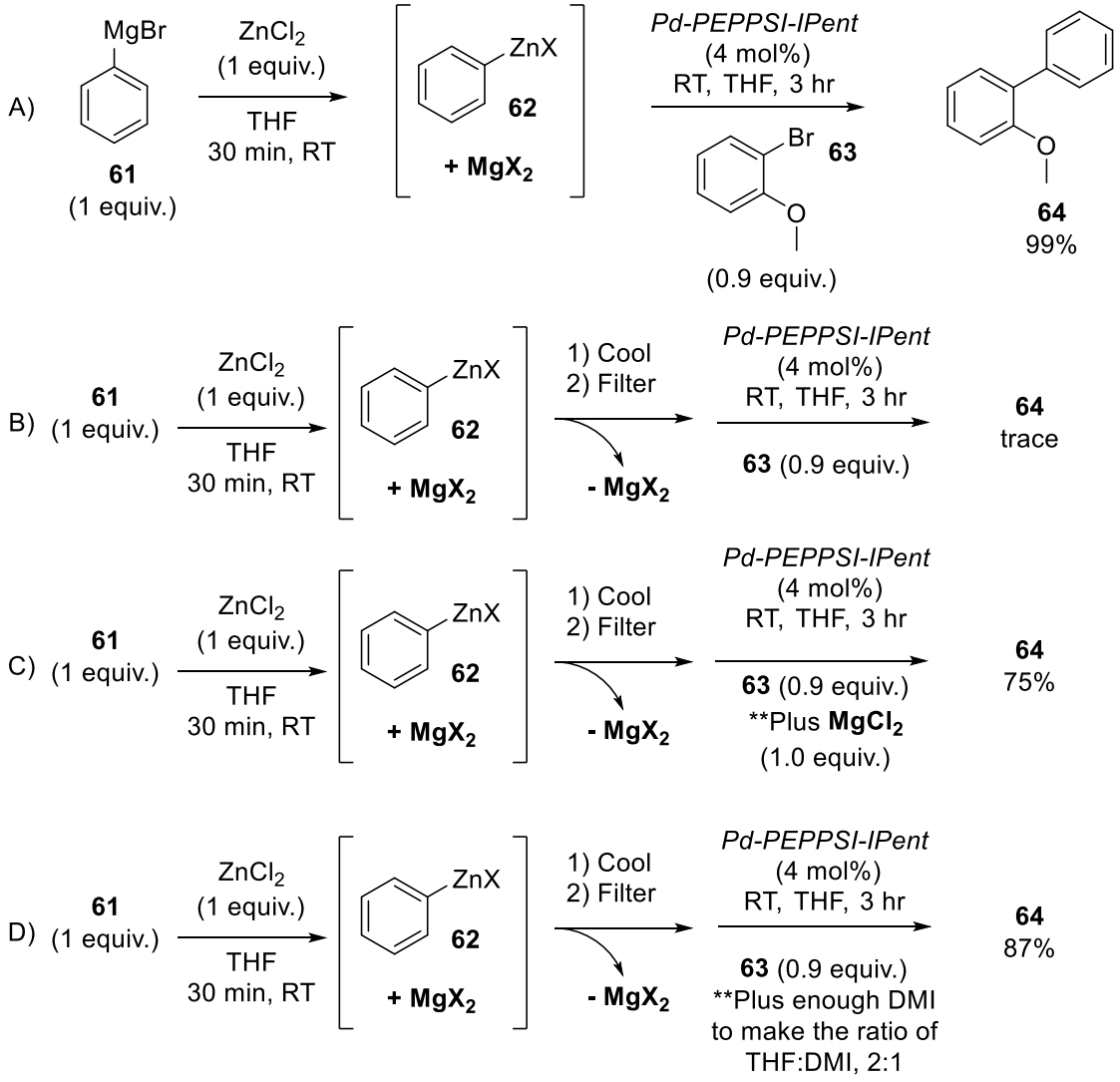

In comparison, diphenylzinc (Ph_2Zn, **65**) did not display the same polarity dependence. Diaryl zinc compounds are inherently more reactive than ArZnX, due to the decreased electron richness of the latter caused by the halogen ligand. When a 1:1 ratio of **65**/**63** was employed, quantitative yield was achieved; however, when a 1:2 ratio was employed, only 47% of **64** was

seen (Table 7, entries 1 vs. 2). Presuming that Ar_2Zn readily transferred the first aryl group, a ratio of 1:2 suggests that the remaining ArZnX, the byproduct of the first TM, does not undergo TM nor does it enter into a Schlenk equilibrium to produce additional Ar_2Zn that can further react. This slow TM of ArZnBr is believed to be the bottleneck that halts the reaction below 50% conversion (Table 7, entry 2). When LiBr or $ZnBr_2$ was added to the couplings, high yields were restored (Table 7, entries 3 and 4). The fact that $ZnBr_2$ helps this reaction is noteworthy because it is one of the rare cases where ZnX_2 salts do not harm Negishi coupling, which seems to support a role for the salt of increasing polarity of the medium and not a direct interaction with the nucleophile. In support of this hypothesis, a similar increase in yield was observed when DMI was used as cosolvent (Table 7, entry 5) with no additional salt. Both results can be explained by the increase in solvent polarity that helps facilitate TM of PhZnX.

Table 7: Effects of salts and solvent polarity on the cross-coupling of diphenylzinc (Ph_2Zn, 65) with 2-bromoanisole (63).

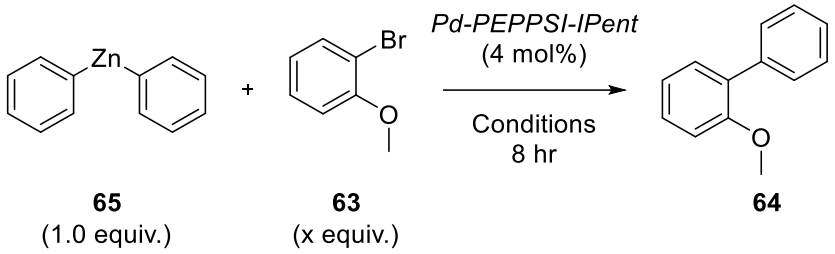

65 (1.0 equiv.) **63** (x equiv.) **64**

Entry	**63** (equiv.)	Solvent	Additives	Yield of **64** (%)
1	0.95	THF	-	98%
2	1.9	THF	-	47%
3	1.9	THF	LiBr (1.0)	87%
4	1.9	THF	$ZnBr_2$ (1.0)	90%
5	1.9	THF:DMI 2:1	-	80%

1.4.3 Aryl-alkyl couplings

Prior to the work in this thesis, the only report on the role of salt additives in aryl-alkyl couplings came from Koszinowski *et al.* in 2015.[109] When aryl iodide **66** was coupled to salt-free *n*-BuZnBr (**53**) using a Pd-phosphine catalyst, a similar dependence on LiBr additives was immediately observed (Figure 11). In the absence of salt, only trace amounts of the coupled product were produced (Figure 11A). The addition of either 4.0 or 8.0 equivalents of LiBr was necessary to achieve full conversion. When this coupling was carried out with 4.0 equivalents of $ZnBr_2$ the reaction was significantly slower and suffered a large decrease in yield (Figure 11B). Consistent with Organ's proposal, the authors concluded $ZnBr_2$ was sequestering the critical LiBr needed for coupling to occur. Worth noting is the varying potency of these inhibitory effects. With a Pd-NHC catalyst, only 1.0 equivalent of $ZnBr_2$ was required to significantly disrupt coupling

(Figure 8), whereas Pd-phosphine systems can achieve moderate coupling with 4.0 equivalents of $ZnBr_2$ present (Figure 11B). Even though the two systems show different levels of susceptibility towards $ZnBr_2$, there was a consensus that this was caused by zinc salts sequestering crucial LiX additives.

Figure 11: Time profile of the coupling between aryl iodide 66 and *n*-BuZnBr (53) with different salt additives.

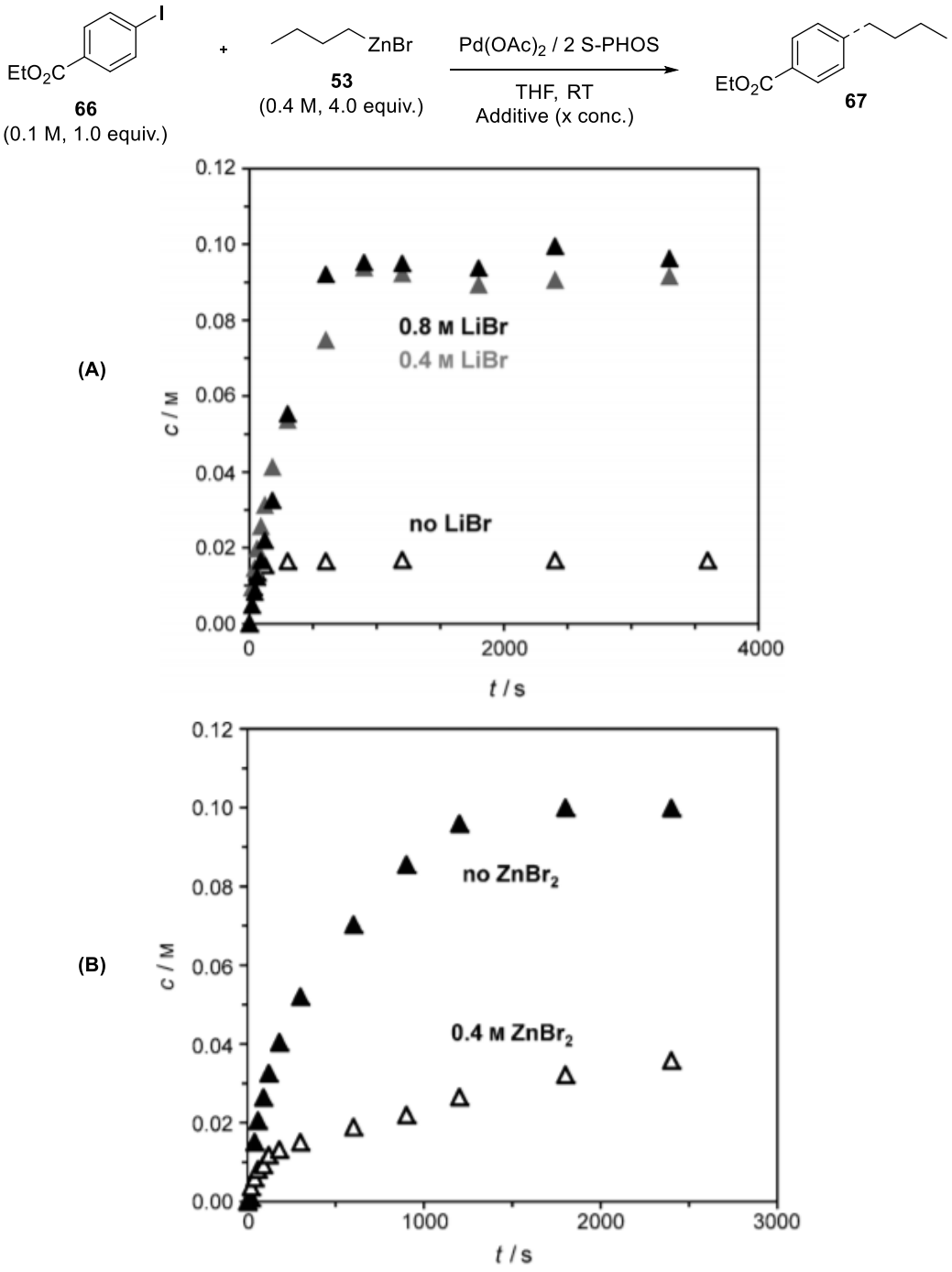

a) Time profile of coupling with no LiBr, 0.4M LiBr and 0.8M LiBr. b) Time profile of successful coupling conditions with and without $ZnBr_2$ (0.4 M).[109]

In a separate experiment, the coupling was initiated in the absence of LiBr and allowed to proceed for approximately 40 min before adding LiBr (Figure 12A). While the addition of the LiBr did revive the reaction, full reactivity was not restored. This suggested the palladium catalyst was decomposing, and salts such as LiBr prevent deactivation or revive deactivated catalyst. The researchers suspected palladium was forming colloidal aggregates based on the commonly observed colour change from bright yellow (or red) to black upon initiation of the reaction. The authors also noted the precatalyst solutions changed colour from yellow to red, but at a slower rate when LiBr is present.

Figure 12: Time profile of the coupling between aryl iodide 66 and *n*-BuZnBr (53) using different procedures.

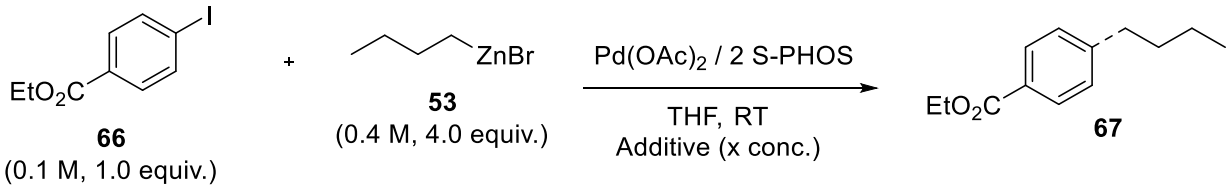

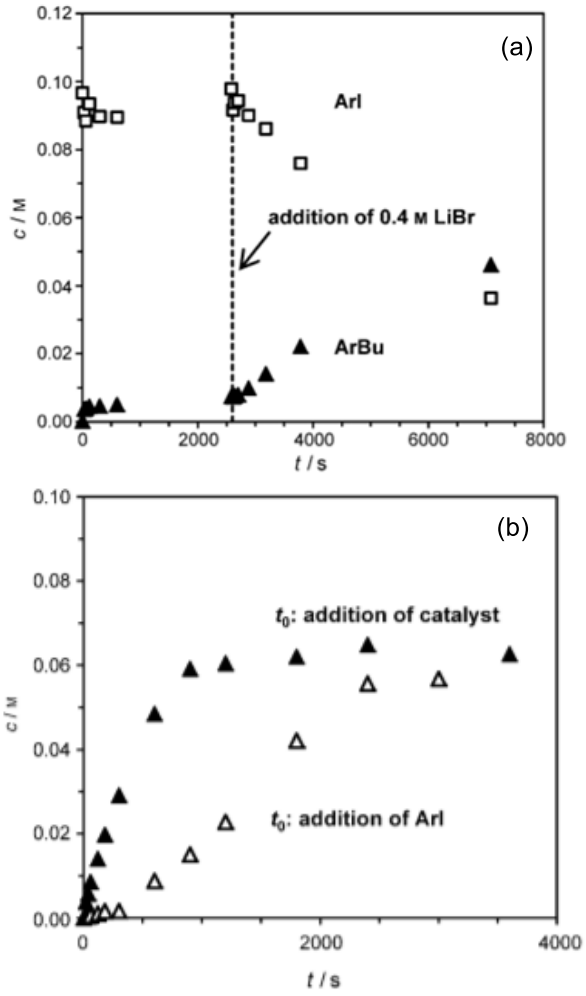

a) The reaction did not proceed to a significant extent before LiBr (0.40 m) was added. b) Either **66** (△) or the catalyst (▲) was added last to initiate the reaction.

Studying the order in which the reagents are combined provided Koszinowski with further evidence of catalyst poisoning. In Figure 12B the coupling of **66** and *n*-BuZnBr (**53**) was initiated by the addition of either the precatalyst solution or the electrophile (**66**). Under standard conditions, the precatalyst solution was added last to initiate the reaction. In one experiment the

aryl iodide **66** was added last to initiate the reaction, meaning the Pd(II) precatalyst was first incubated with the organozinc. This presumably formed $L_nPd(0)$ *in situ* before the aryl iodide was added 5–10 min later. Palladium(0) species are almost always air and moisture sensitive, requiring a strictly inert atmosphere to prepare and handle them. Producing these species *in situ* with no electrophile to quench them could create optimal conditions for the formation of palladium aggregates. This would explain the different kinetic profiles seen in Figure 12B, which the authors noted were mildly inconsistent. Three different runs were reported with poor overlap between all three trials, one representative trial is shown in Figure 12B. This irreproducibility is problematic, but not surprising considering the unstable nature of Pd(0) species. Furthermore, palladium aggregates are already known to be catalytically active to varying extents.[110] This varying reactivity likely explains the observed irreproducibility.

One plausible source of catalyst failure in Koszinowski's study was discovered using mass spectrometry. When a 1:2 solution of $Pd(OAc)_2$ /S-PHOS was immediately analyzed using positive mode ESI MS, the base peak was identified as a dimer with the formula $L_2Pd_2(PCy_2)^+$. This hinted at ligand degradation via cleavage of the P-Ar bond on S-PHOS (**18**). When the same solution was analyzed 90 min later the intensity of this peak grew. The same solution with LiBr added (5.0 equivalents with respect to palladium) showed the same $L_2Pd_2(PCy_2)^+$ cation, but this time as a minor peak with $L_2Pd_2Br^+$ as the base peak. The decrease in signal intensity for the $L_2Pd_2(PCy_2)^+$ peak in the presence of LiBr supports the idea that LiBr is involved in preventing ligand degradation.

1.5 Plan of study

Significant progress has been made in uncovering the diverse roles of salt additives in Negishi coupling and the benefits of using organozincs prepared in the presence of salts. It has

been established that simple lithium salts, in particular LiCl and LiBr, are generally beneficial additives. However, not all salt additives show these improvements, and some even harm these reactions (i.e., $ZnBr_2$). To realize the wider use of the Negishi coupling reaction, a more comprehensive understanding of these salt effects is critical.

With Pd-NHC catalyzed aryl-aryl and alkyl-alkyl couplings well understood, the last piece of the puzzle left to investigate is aryl-alkyl couplings. These couplings are a hybrid between the two already well studied cases. In these couplings, an aryl halide is usually coupled with an alkyl organozinc so only one intermediate on the catalytic cycle (i.e. the TM intermediate) is capable of undergoing BHE. These reactions will have aspects similar to aryl-aryl couplings in the sense that an aryl-Pd intermediate will be the electrophile. However, most roles for salt additives are centred around adjusting the reactivity of the organozinc. This means the formation of higher order zincates should be thoroughly investigated while also considering other potential factors, such as the change of solvent polarity.

Initial plans included a substrate scope in which aryl bromides with different functional groups will be coupled to a simple alkylzinc reagent, both with and without salt additives. This will firstly confirm whether or not there is a salt effect in this class of couplings, as well as provide clues for what step(s) in the catalytic cycle are being affected. It is expected that electron deficient aryl bromides will undergo coupling with ease, since they are inherently activated. Electron withdrawing groups create a more electrophilic C-Br bond and the resulting OA intermediate should be more susceptible to TM due to the more electrophilic Pd(II) centre. In comparison, electron rich aryl bromides will likely struggle to undergo both OA and TM due to their low electrophilicity. These trials are expected to see a significant salt effect based on the previous work on higher-order zincates. The increased nucleophilicity of the organozinc could help overcome a

higher barrier to TM. These preliminary studies should provide fundamental information on aryl-alkyl coupling, such as under what conditions salt improves these couplings and provide clues as to which step is determining. With this information future experiments can be developed to further probe the role of salt on aryl-alkyl couplings.

Chapter 2: The role of LiBr and $ZnBr_2$ on the coupling of sp^2-hybridized oxidative addition partners with sp^3-hybridized organozincs

2.1 Effect of LiBr on couplings with monoalkylzinc species

In the initial experiments, salt-free *n*-BuZnBr was prepared using the Huo protocol[24] and treated with a series of aryl bromides (Table 8). Whereas alkylzinc reagents experienced zero coupling with alkyl electrophiles until at least 1.0 equivalent of LiBr was present, bromobenzene could be coupled to 60% conversion without any LiBr added (Table 8, entry 5). As a control, the Pd catalyst was omitted from the transformations in Table 8. Only **68a** containing a nitro group showed background conversion when no Pd was used (~30% conversion). When electron-poor electrophiles were examined, all gave excellent conversion without LiBr, which improved slightly in some cases (Table 8, entries 1–5). In the case of electron-donating groups, conversion without salt was low (Table 8, entry 6) or nonexistent (Table 8, entry 7), yet when LiBr was added a significant increase in conversion was observed in all cases.

Table 8: Negishi coupling of *n*-BuZnBr (53) with aryl bromides (68a-g) with, and without, LiBr.

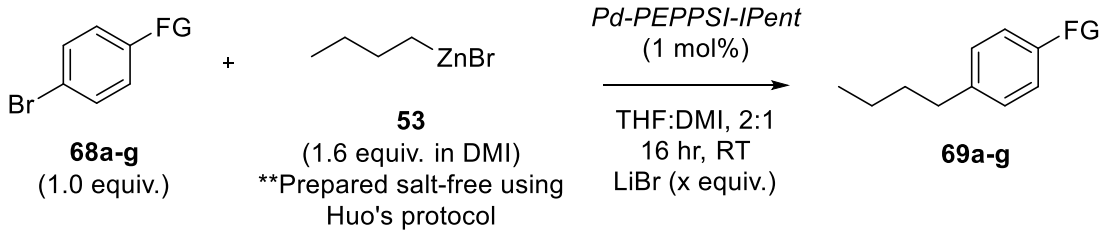

Entry (compound)	FG	% conv. (No LiBr)[a]	%conv. (3.2 equiv. LiBr)[a]
1 (**68a**)	NO_2	93	98
2 (**68b**)	CHO	88	90
3 (**68c**)	$COCH_3$	82	86
4 (**68d**)	CO_2Me	96	92
5 (**68e**)	H	60	72
6 (**68f**)	OCH_3	28	65
7 (**68g**)	$N(CH_3)_2$	trace	25

[a] Percent conversion was determined by ^{1}H NMR spectroscopy using 1,3,5-trimethoxybenzene as an internal standard. Experiments were carried out in duplicate, and the average result is reported.

2.2 Effect of salts on couplings with dialkylzinc species

If an argument can be made that the LiBr is enhancing the nucleophilicity of the organozinc reagent through the formation of higher order zincates, and this is why there is such a stark increase in conversion in entries 5–7 in Table 8, a similarly dramatic increase in conversion should also be expected by simply constructing a more electron-rich organozinc reagent. Indeed, when *n*-Bu_2Zn (**70**, freshly distilled to remove any salts) reacts with **68g**, a poorly reactive OA partner, under similar conditions to those used in Table 8, 50% conversion was attained without any LiBr (Table 9, Series 1, entry a). Interestingly, now adding any amount of LiBr (0.3–1.2 equivalent, Table 9,

Series 1, entries b–e) did not further increase conversion. Even 3.2 equivalents of this salt made no difference (Table 9, Series 1, entries f).

Table 9: Impact of LiBr and $ZnBr_2$ on Negishi coupling using *n*-Bu_2Zn (70) and 4-bromo-*N,N*-dimethylaniline (68g).[a]

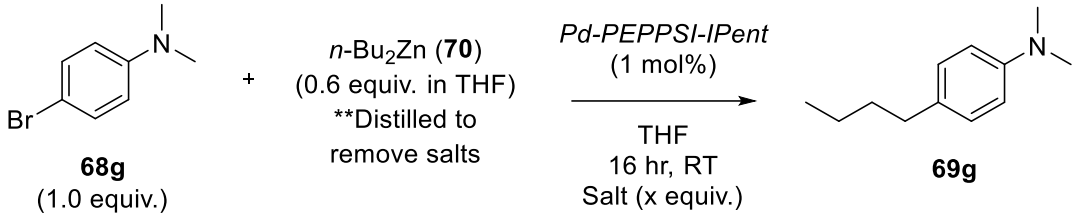

Entry (equiv. of salt employed)

Series	Salt	a (0)	b (0.3)	c (0.6)	d (0.9)	e (1.2)	f (3.2)
1	LiBr	50[b]	50	49	52	50	43
2	$ZnBr_2$	50[b]	39	20	13	10	-

[a] Percent conversion to **68g** was determined by ^1H NMR spectroscopy using 1,3,5-trimethoxybenzene as an internal standard. Experiments were carried out in duplicate, and the average result is reported. [b] Under otherwise identical reaction conditions, 1.0 equivalent of *n*-Bu_2Zn led to 55% conversion.

Since both butyl groups could be transferred there could / should have been full conversion to **69g** with only 0.6 equivalent of *n*-Bu_2Zn. This raised the question as to whether the Schlenk equilibrium was active under these coupling conditions. That is, without LiBr, *n*-BuZnBr may not be active enough to couple with a deactivated OA partner (e.g., Table 8, entry 7), and *n*-Bu_2Zn is not forming in these runs and therefore no coupling takes place. Conversely, if only *n*-Bu_2Zn is able to react in the absence of LiBr, once consumed there is nothing left to undergo coupling, thus the reactions halt near 50% conversion. When the amount of *n*-Bu_2Zn was increased to 1.0 equivalent, there was only +5% increase in conversion (Table 9, footnote [b]). This implies that the reaction stalls when poorly reactive OA partners, such as **68g**, are employed.

The impact of $ZnBr_2$ on the coupling of *n*-Bu_2Zn was next evaluated. Interestingly, whereas adding LiBr had no major effect on *n*-Bu_2Zn, when $ZnBr_2$ was added in increasing amounts, coupling was proportionally reduced (Table 9, Series 2, entry a vs. entries b–e). There are two proposed explanations for this result. The increasing amounts of $ZnBr_2$ could allow the Schlenk equilibrium to become active and more *n*-BuZnBr forms which cannot undergo coupling with such a deactivated electrophile and conversion plummets. Alternatively, $ZnBr_2$ is certainly more Lewis acidic than LiBr and can bind to the reduced Pd(0) strongly enough following RE to poison it in an off-cycle resting state.[23,81,111]

In the case of *n*-Bu_2Zn, neither LiBr nor $ZnBr_2$, natural byproducts of making the organometallic species and the coupling, respectively, seem to help the transformation. Structurally and functionally, these two salts are quite different. LiBr has significant Lewis basic behaviour through the halide as a consequence of a looser ion pair with the low electronegativity lithium (c=0.98).[112] Conversely, the more electronegative zinc (c=1.6) creates a tighter metal-halide bond and the Lewis acidic properties of zinc dominate for the salt as a whole.

We wondered if LiBr and $ZnBr_2$, might interact in some way to exert either a positive or negative influence over the coupling (Table 10). With no LiBr added, the increasingly negative impact of the exogenous $ZnBr_2$ is apparent as conversion drops from 39% to 13% as the amount of this salt is increased from 0.3 to 0.9 equivalent (Table 10, Series 1–3, entry a). Strikingly, when equimolar or slightly higher amounts of LiBr were added to the reaction mixtures containing $ZnBr_2$, cross-coupling was restored to the level seen with no salt at all (Table 10, Series 1–3, entries d and e compared with Table 9, entry a).

Table 10: Impact of adding LiBr and $ZnBr_2$ together on Negishi coupling using *n*-Bu_2Zn (70) with 4-bromo-*N,N*-dimethylaniline (68g).[a]

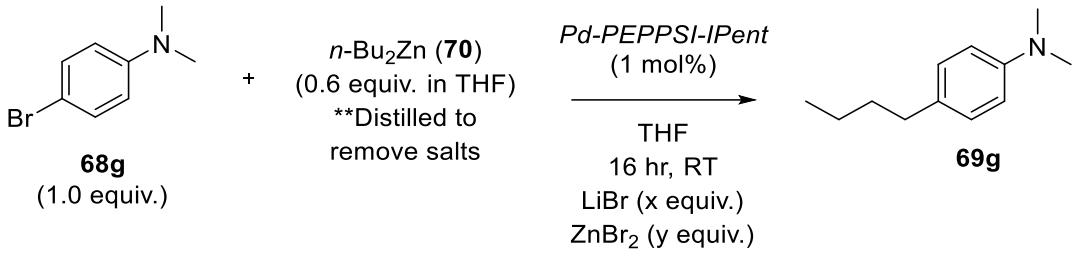

Series ($ZnBr_2$ equiv. used)	Entry (LiBr equiv. used) a (0)	b (0.3)	c (0.6)	d (0.9)	e (1.2)
1 (0.3)	39	49	48	52	61
2 (0.6)	20	37	38	46	49
3 (0.9)	13	23	30	36	44

[a] Percent conversion was determined by ^1H NMR spectroscopy using 1,3,5-trimethoxybenzene as an internal standard. Experiments were carried out in duplicate, and the average result is reported.

That LiBr failed to improve conversion of the dialkylzinc nucleophile in the absence of $ZnBr_2$, but so profoundly increased conversion when $ZnBr_2$ was present, suggests that the most important interaction of LiBr is not with *n*-Bu_2Zn, which may be different in the case of *n*-BuZnBr, but rather with $ZnBr_2$. It is proposed that the Lewis basic bromide ion coordinates to $ZnBr_2$ to form $LiZnBr_3$ and/or possibly Li_2ZnBr_4. This mitigates the Lewis acidic zinc by strong coordinative saturation of the metal centre. If this situation is operative, it could be possible to incorporate catalyst design elements to aid in circumventing poisoning.

2.3 Effect of backbone modification on couplings with dialkylzinc species

Installing chlorines on the backbone of *Pd-PEPPSI-IPent* to produce *Pd-PEPPSI-IPent*^{Cl} has been shown to profoundly accelerate the rate of cross-coupling in general.[14,84,85,113] The

dramatic improvements in these reactions were attributed to electronic and steric influences of the chlorines. NHC ligands are among the strongest σ-donors making the metal centre quite electron-rich.[71] While this is beneficial for OA, it makes TM and RE more difficult. It also renders the metal more susceptible to Lewis acids, such as $ZnBr_2$. Chlorines on the NHC backbone reduce the Lewis basic nature of Pd(0), thereby making it less susceptible to poisoning. When *Pd-PEPPSI-IPent*^{Cl} was substituted for *Pd-PEPPSI-IPent* consumption of **68g** was now quantitative with 80% conversion to **69g** (Table 11, entry a), up from 50% with *Pd-PEPPSI-IPent* (Table 9, Series 1, entry a). Consistent with the developing hypothesis above, when $ZnBr_2$ was added in increasing amounts (Table 11, entries b–d) conversion to **69g** slightly decreased whereas when the same amounts of this salt were added to the reaction with **68g**, conversion dropped by a factor of four (Table 9, Series 2).

Table 11: Influence of NHC backbone modifications on the negative impacts of $ZnBr_2$ in the Negishi coupling of *n*-Bu_2Zn (70) with 4-bromo-*N*,*N*-dimethylaniline (68g).[a]

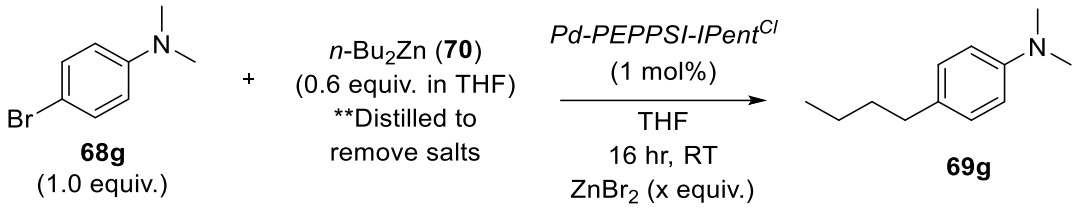

Entry ($ZnBr_2$ equiv. used)	a (0)	b (0.3)	c (0.6)	d (0.9)
	80	77	69	60

[a] Percent conversion was determined by ^{1}H NMR spectroscopy using 1,3,5-trimethoxybenzene as an internal standard. Experiments were carried out in duplicate, and the average result is reported.

2.4 Conclusion

These results have shown that LiBr has a profound effect on the coupling of alkylzinc halide nucleophiles with deactivated (electron-rich) aryl OA partners, but its role is less

important with activated (electron-deficient) ones. It is proposed that in this case, like with alkyl OA partners that Organ *et al.* have investigated in the past,[97,100,114] the alkyl zincates are again forming in the presence of LiBr which are necessary to help drive TM. If the aryl halide is electron-poor, the Pd metal centre becomes more electron-deficient, which helps drive TM forward, making the LiBr much less important.

Dialkylzincs, which are known to be much more nucleophilic than mono alkylzinc species, might be expected to undergo TM more readily with deactivated (electron-rich) OA partners. Indeed, this was observed; whereas **68g** did not react at all with *n*-BuZnBr (**53**), it reacted to 50% conversion with *n*-Bu_2Zn (**70**). Interestingly, the addition of LiBr had zero impact on conversion but when $ZnBr_2$ was added to the reaction of **68g** with *n*-Bu_2Zn (**70**), coupling plummeted. However, the addition of LiBr, which on its own had no impact, restored full coupling in the presence of $ZnBr_2$ to levels seen when no salt was present at all.

The fact that *n*-Bu_2Zn couplings see no benefit upon the addition of LiBr but show dramatic improvement when $ZnBr_2$ is in the mixture points to a different, or at least an additional, important role. It is thought that this role is to coordinatively saturate $ZnBr_2$, a Lewis acid that can bind to the electron-rich NHC-Pd(0) centre, thereby slowing catalyst deactivation. Since these zinc salts are a natural byproduct of these types of couplings, the term product inhibition is used to describe this effect. In support of this, when the catalyst was modified with two chlorines on the backbone of the NHC ring, coupling dramatically increased (still in the absence of any LiBr). One could argue that the chlorines withdraw electron density away from Pd(0) making it less basic. Additionally, there is now an increased steric presence in the coordination sphere of the metal as repulsion between the chlorines and N-aryl substituents on the NHC force these two rings toward

the Pd metal centre. Together these two effects disfavour binding to $ZnBr_2$, thus avoiding the formation of off-cycle resting states.

2.5 Further developments

The results from this experimental study were published in September of 2019.[115] Two months earlier, in July of 2019, Pidko *et al.* reported a theoretical DFT study on the formation of intermetallic Pd-Zn species and their involvement in inhibition pathways.[116] The authors used the TPSSD3/DZP level of theory to examine the binding strength of ZnX_2S_2 (S = THF, X = Cl, Br, I) to the $L_2M(0)$ active catalyst, as well as several isomerizations (Scheme 16). Both nickel and palladium were studied with a trialkyl (PMe_3) and a triaryl (PPh_3) phosphine ligand.

Scheme 16: Possible transformations of $[Ni(PR_3)_2]$ and $[Pd[PR_3)_2]$ (71) in THF involving ZnX_2 and PhX.

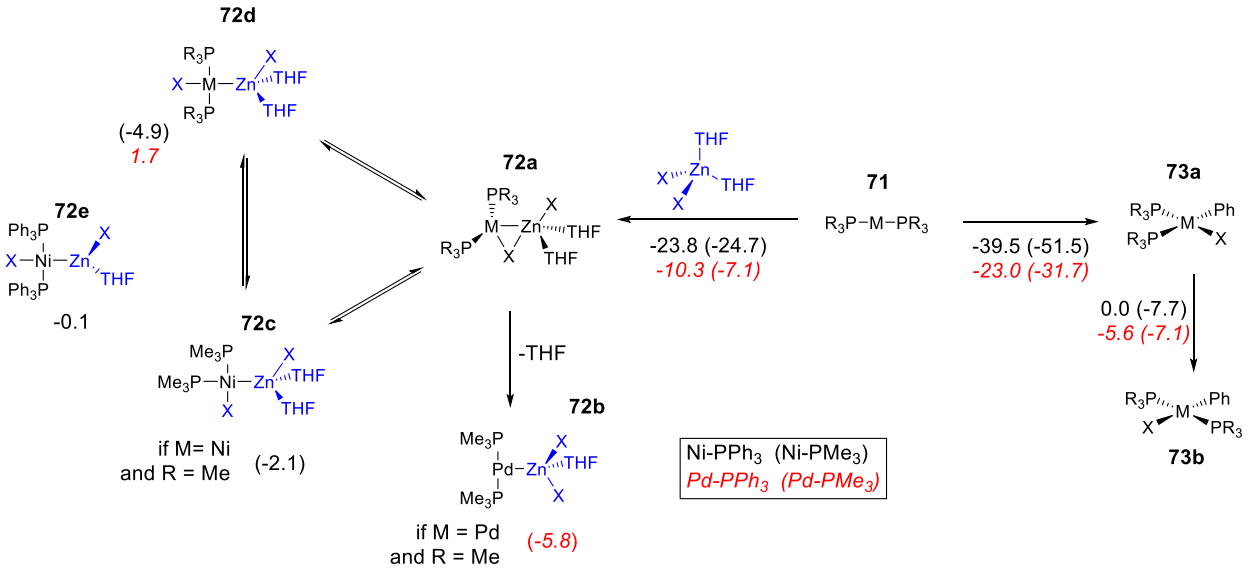

The Gibbs free energies (kcal/mol) of the elementary transformations were computed at the ωB97-3c level of theory for the case of X=I and are listed under the corresponding arrows. Select Gibbs free energies (ΔG) of the 72a→72b–e transformations are shown below the corresponding structures. ΔG values in Ni systems are given in regular typeface while ΔG values in Pd systems are in red, italic typeface. PPh_3 values are presented without parentheses and PMe_3 values are presented in parentheses. For X=Cl, see SI of original manuscript.

The binding of ZnI_2S_2 (where S = THF) to all combinations of metal and phosphine ligand was exergonic (**71→72a**). Furthermore, various transformations of **72a** to form more stable

complexes were investigated, exposing many other off-cycle intermediates that were even lower in energy (**72b–e**). These inhibitory pathways were compared to OA, representing productive coupling. Oxidative addition to form the cis product **73a** followed by isomerization to the trans product **73b** was found to be exergonic for all metal and ligand combinations. However, no transition states for OA were reported, making it difficult to appreciate how far uphill the catalyst must go in order to get back on cycle once **72a–e** forms. Nonetheless, these results paint a picture of an $L_2M(0)$ catalyst that is in a dynamic competition between OA and reversible product binding/inhibition.

In addition to the binding affinity of zinc salts to the $L_2M(0)$ intermediate, the $L_2M(II)$ OA intermediates (**73a,b**) were investigated to see if they were susceptible to $ZnBr_2$ coordination (Scheme 17). In comparison to the active M^0 catalyst (**71**), the OA intermediate (**73a,b**) is now M(II) and coordinatively saturated, meaning the most favorable structures did not involve any direct palladium-zinc interactions. Rather, zinc formed a bridging complex (**74a,b**) with the halide on **73a,b**. These interactions were also favorable but not as strong as the previously discussed M(0) interactions. As with the M(0) interactions, the binding affinity of zinc salts was compared to productive coupling. For this intermediate, productive coupling was the complexation of an organozinc reagent ($EtZnXS_2$) to form a pre-transmetallation complex (**75a,b**). This binding interaction was favorable for nearly all the metal/ligand combinations but was still weaker than the ZnX_2S_2 interactions, suggesting this intermediate is also susceptible to inhibition by the zinc salt. The authors acknowledged this pathway is likely not as significant since the organozinc is typically used in excess and ZnX_2 byproducts build up over time. The M(II) interactions were also repeated using a truncated NHC ligand (1,3-diisopropylimidazol-2-ylidene) to represent commonly employed NHC ligands. The same trend was seen where the interactions between

$L_2M(II)PhX$ and ZnX_2S_2 were slightly stronger than $EtZnXS_2$. The authors did not report anything regarding the binding affinity of zinc salts to the NHC-M(0) intermediate.

Scheme 17: Competitive binding of $[(THF)_2ZnX_2]$ and $[(THF)_2EtZnX]$ to cis-$[L_2PhM^{(II)}X]$ (73a) and trans-$[L_2PhM^{(II)}X]$ (73b), M=Ni or Pd, L=PMe_3 or PPh_3.

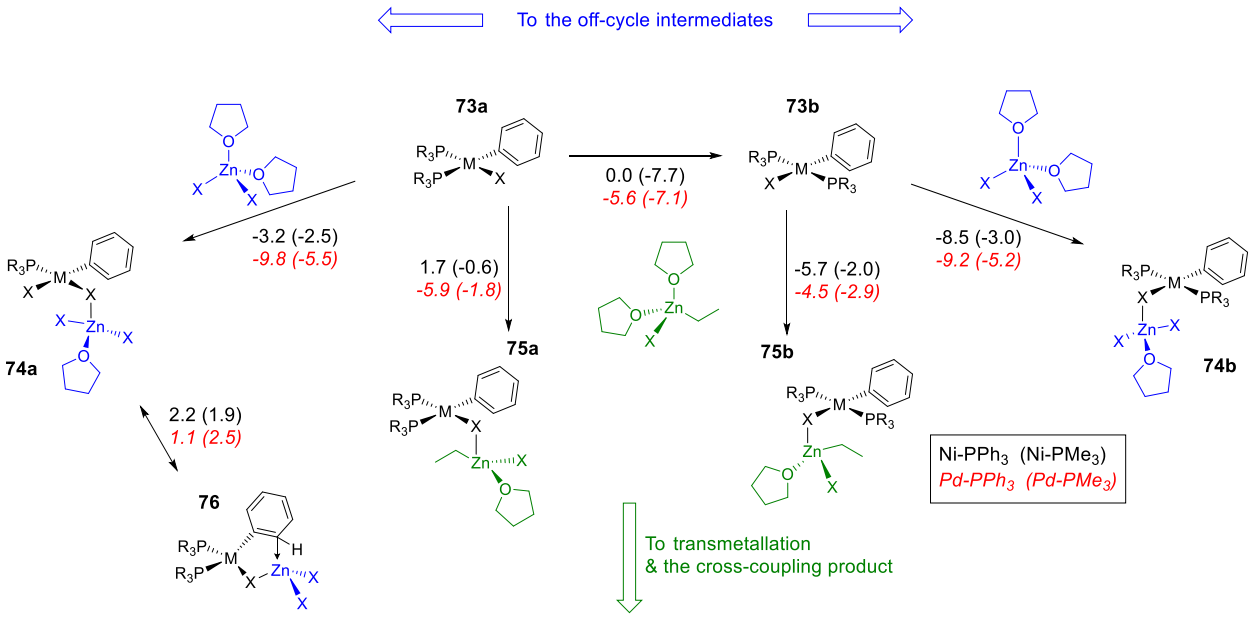

The elementary reaction free energies (kcal/mol) were computed at the ωB97-3c level of theory for the case of X=I and are given under the corresponding arrows. ΔG values in Ni systems are given in regular typeface while ΔG values in Pd systems are in red, italic typeface. PPh_3 values are presented without parentheses and PMe_3 values are in parentheses. For X=Cl, see SI of original manuscript.

While Pidko's study has pointed out the harm in these Pd-Zn interactions, other DFT studies have shown them to be crucial to the success of some Negishi couplings. In 2012 Aurrecoechea *et al.* investigated cooperative Pd-Zn interactions during Negishi coupling.[30] The authors modeled the entire catalytic cycle using DFT, specifically looking at the different ways in which Pd-Zn interactions affect the barriers of the three fundamental steps (OA, TM, RE). It was discovered that these bimetallic Pd–Zn interactions were detrimental to OA but helped favor RE by relief of steric crowding around the metal centre. Indeed, the results from this study remind us that Pd-Zn interactions are critical to the success of Negishi coupling, even if at times they are inhibitory. Based on the results from this chapter, readers can better plan and execute Negishi

cross-coupling reactions by being mindful of the harmful effects excess zinc salts pose, and how to counteract them with LiBr.

Chapter 3: The critical role of LiBr in avoiding catalyst death and its impact on cross-coupling

3.1 Initial discovery of catalyst deactivation

Similar to the observations made by Kosinowksi *et al.*,[109] a stark color change from bright yellow to dark black was seen for nearly all the Negishi couplings performed in Chapter 2. This drastic color change seemed to be slower in the reactions employing LiBr. Based on these observations, catalyst deactivation to form palladium aggregates was suspected, warranting an investigation into the lifetime and activity of *Pd-PEPPSI* precatalysts.

When activated (electron-poor) OA partner methyl 4-bromobenzoate (**68d**) was reacted with *n*-Bu_2Zn (**70**) in the presence of *Pd-PEPPSI-IPent*, the reaction proceeded to full conversion (Table 12, entry 1). In fact, the reaction was so rapid it was complete in under 5 minutes (entry 2). Conversely, when deactivated (electron-rich) OA partner (4-bromo-*N,N*-dimethylaniline, **68g**) was reacted under the same conditions the reaction never proceeded beyond ~50% conversion (entry 4).

Table 12: Coupling of electron-poor (i.e., activated) and -rich (i.e., deactivated) aryl bromides 68d and 68g, respectively, to *n*-Bu_2Zn (70).

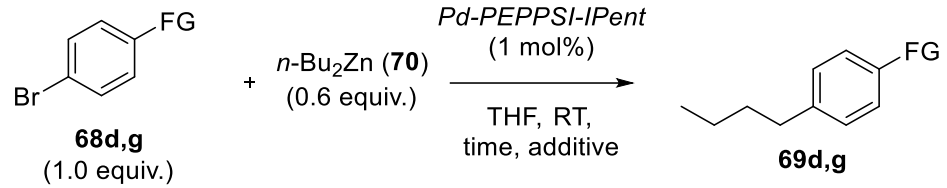

Entry	FG	time	Additive	% conv to **69**
1	CO_2Me (**68d**)	24 hr	-	95
2	CO_2Me(**68d**)	5 min	-	95
3	CO_2Me(**68d**)	5 min	LiBr (2 equiv.)	95
4	$N(CH_3)_2$(**68g**)	24 hr	-	49
5	$N(CH_3)_2$(**68g**)	24 hr	LiBr (2 equiv.)	50

[a] All experiments were conducted in duplicate, and the average conversion is reported.

Since there were concerns about the catalyst lifetime, the activity of the used catalyst was tested by continued additions of coupling partners to the initial reaction mixture (Scheme 18, entry 1). Strikingly, when additional portions of **68d** were added to the mixture after just 10 min., there was essentially no additional coupling of the newly added electrophile. This implied that despite the extremely rapid kinetics, the catalyst was undergoing irreversible deactivation along the way.

Scheme 18: Sequential coupling of aryl bromide 68d and *n*-Bu_2Zn (70) with, and without, additive.

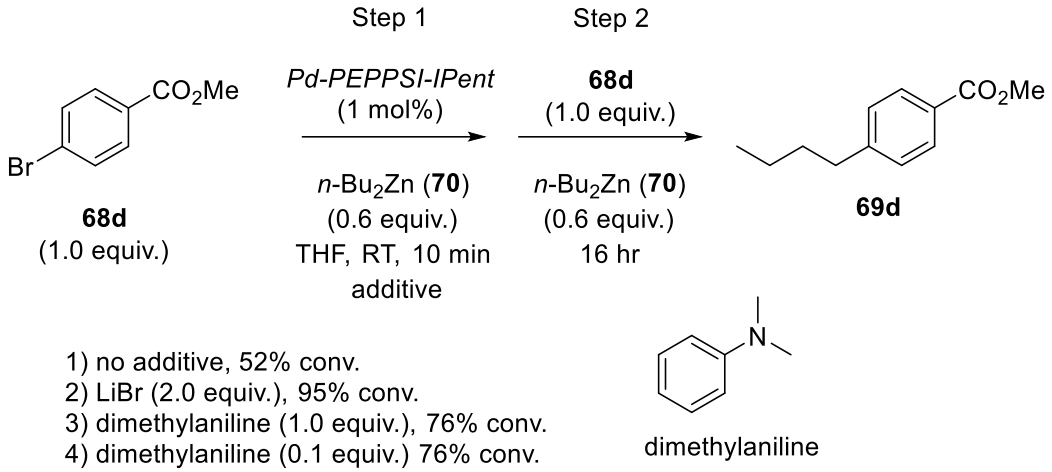

[a] Percent conversion is based on 2 equiv of **68d** reacting to provide 2 equiv of **69d** for full conversion, i.e., both steps together. All experiments were conducted in duplicate, and the average conversion is reported.

Even more perplexing, **68d** was added to the coupling of **68g** after it had taken place to the extent that it normally does after 10 min (~50%), significant conversion of the new coupling partner (**68d**) to **69d** (~60%) now takes place (Scheme 19, entry 1). This suggests that something harmful is happening to the catalyst in the coupling of an activated electrophile (**68d**), which happens to a much smaller extent (if at all) when the deactivated OA partner **68g** is present.

As previously discussed in chapter 2, the standard couplings of **68g** and **68d** with *n*-Bu_2Zn never showed much improvement upon addition of LiBr. The coupling of ester **68d** is nearly quantitative either way (Table 12, entries 1-3), and the aniline **68g** showed no improvement (Table 12 entries 4 and 5). When LiBr was added to the sequential coupling of **68g** followed by **68d**, no improvement in conversion was observed (Scheme 19, entry 2 vs. 1). In sharp contrast, when salt was added to the sequential coupling of just **68d**, now the additional equivalent of **68d** was fully coupled (Scheme 18, entry 2 vs. entry 1).

Scheme 19: Sequential coupling of aniline 68d followed by ester 68g with *n*-Bu_2Zn with, and without, LiBr.

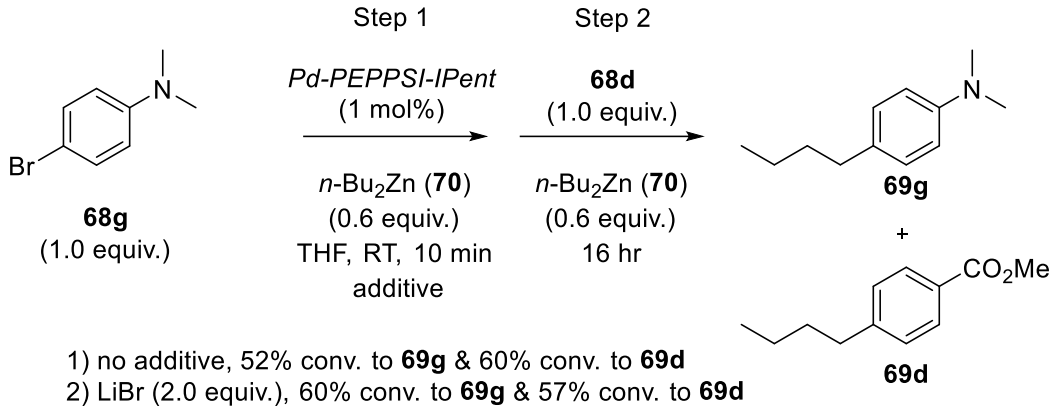

[a] Percent conversion is based on 1.0 equiv of **68g** reacting to provide 1.0 equiv of **69g** for full conversion, and 1.0 equiv of **68d** reacting to provide 1.0 equiv of **69d** for full conversion. All experiments were conducted in duplicate, and the average yield is reported.

These observations suggest that LiBr is acting to protect the catalyst during couplings with **68d**, but it is not necessary for improving catalyst performance in the coupling of **68g**. This implies the electron-rich aniline is somehow able to stabilize the activated form(s) of *Pd-PEPPSI-IPent* within the catalytic cycle, or in a resting state, and in doing so prevents the pathway responsible for its irreversible decomposition. One reasonable explanation is that the aniline nitrogen coordinates to palladium on and off during catalysis, and this plays an essential role in preventing actions by the metal that lead to untoward consequences.

To examine this theory, 1.0 equivalent of dimethylaniline was added to the sequential reaction of **68d** resulting in a dramatic increase in the coupling of the second equivalent of **68d** (Scheme 18, entry 3 vs. 1). The interaction between dimethylaniline and Pd must be strong for when the amount of aniline is reduced 10-fold, the enhanced catalytic performance was identical (entry 4 vs. 3). These experiments therefore suggest a critical role for LiBr in protecting the catalyst from degradation.

3.2 Byproducts of catalyst degradation

With confirmation of catalyst degradation, the byproducts of these harmful pathways were searched for. Careful isolation by silica gel chromatography of spent reaction mixtures provided two separate salts, **77** and **78**, which are byproducts of *Pd-PEPPSI-IPent* and presumed to be the endpoints of catalyst death (Figure 13).

Figure 13: Byproducts arising from degradation of *Pd-PEPPSI-IPent*.

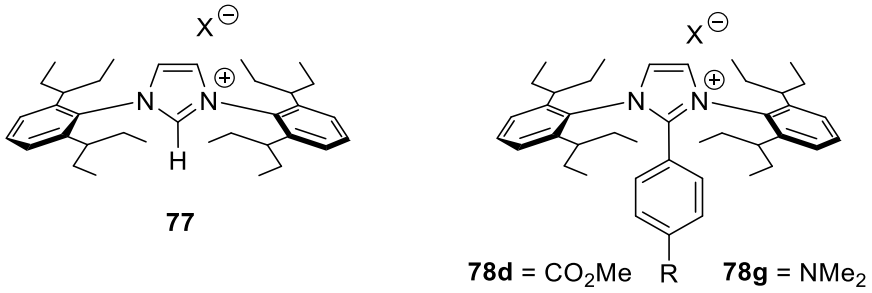

One question was if the protonated NHC salt **77** was forming *in situ*, or if the free carbene, produced by simple ligand dissociation form Pd, was being protonated during the work up. It is believed (*vide infra*) that imidazolium byproduct **77** forms in the catalytic cycle from BHE and RE of butyl-Pd complex **80** (Scheme 20).[117] Conversely, it is believed the aryl-NHC byproduct **78** forms from RE of OA intermediate **79**.[117,118] It is important to remember these mechanisms must take into account how LiBr, dimethylaniline, and the aniline substrates and/or products prevent these irreversible catalyst death events from occurring.

Scheme 20: Proposed catalytic cycle to account for the formation of the imidazolium (77) and aryl-imidazolium (78) byproducts derived from their corresponding Pd-NHC complexes (80 and 79, respectively).

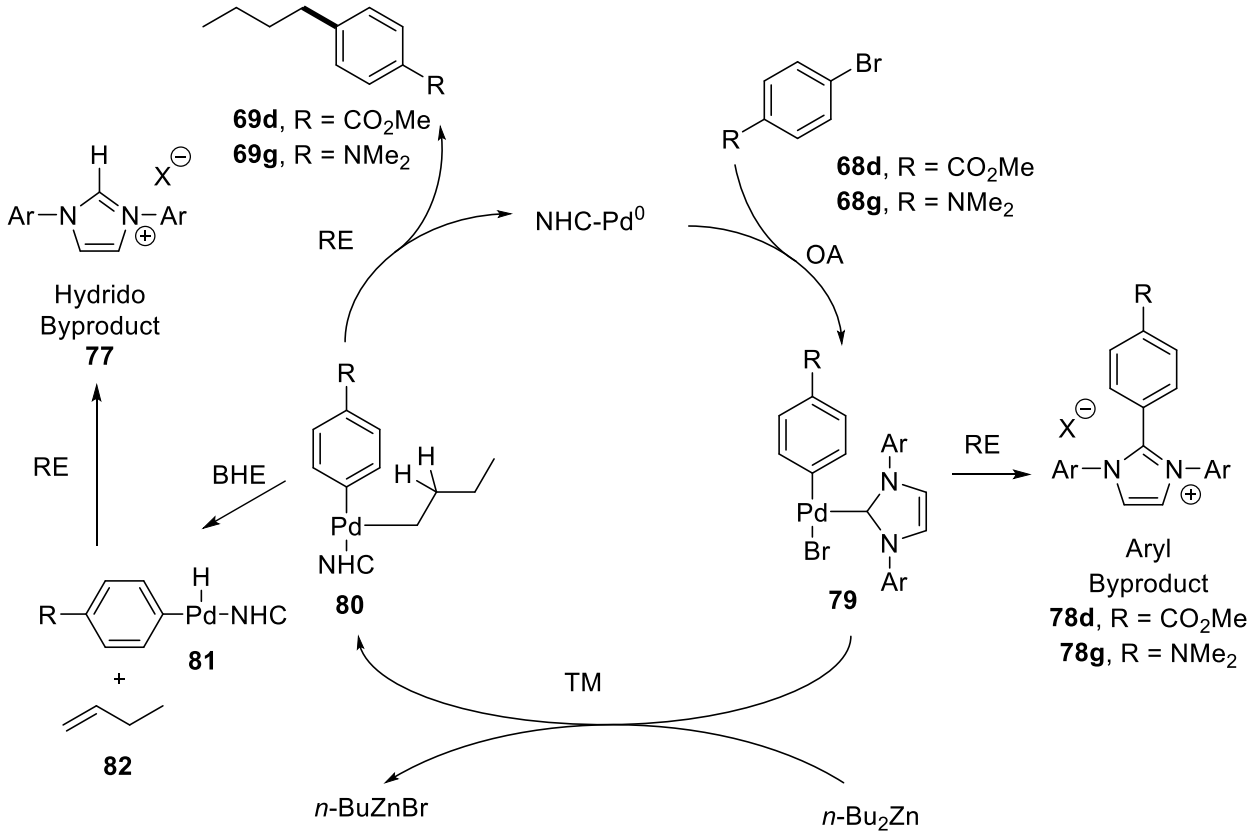

To examine this, the impact that LiBr has on the presence, and the ratio, of byproducts **77** and **78** was assessed (Table 13). To accomplish this both the scale of the reactions and catalyst loading had to be doubled, giving a 4-fold increase in the total amount of NHC byproducts. This produced enough material to isolate and characterize, without deviating too far from the established results. When the electron-rich (deactivated) OA partner **68g** was treated with a slight excess of *n*-Bu_2Zn the ratio of imidazolium - (**77**) to aryl- (**78g**) byproduct was 2.3:1. Importantly, this ratio sharply inverted (1:2.3) when LiBr was present (Table 13, entry 1 vs. 2). Strikingly, **68d** was substituted for **68g**, which now is a highly activated OA partner, only imidazolium byproduct **77** formed without LiBr (entry 3). These results illustrate that the nature of catalyst death (i.e., **77** vs. **78**) is indeed influenced by the presence of salt.

Table 13: Impact of LiBr and number of equivalents of *n*-Bu_2Zn on the formation of imidazolium byproduct (77) and aryl-imidazolium byproduct (78).

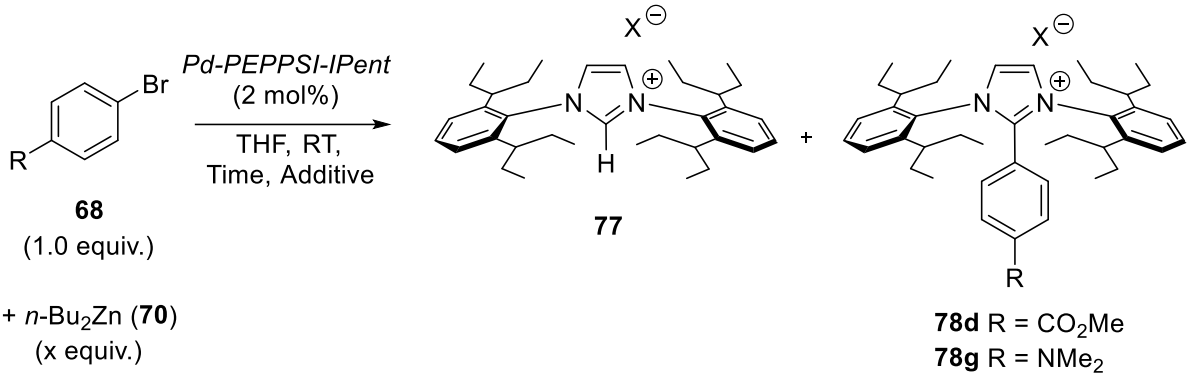

Entry	*n*-Bu_2Zn equiv.	Time (hr)	Additive	Imidazolium byproduct (**77**)[a]	Aryl byproduct (**78**)[a]
1 (**68g**)	0.6	16	-	2.3	1
2(**68g**)	0.6	16	LiBr (2 equiv.)	1	2.3
3(**68d**)	0.6	16	-	1	0
4(**68d**)	0.45	1	-	1	2.3
5(**68d**)	0.45	1	LiBr (2 equiv.)	0	1
6(**68d**)	0.45	1	$ZnBr_2$ (1 equiv.)	1	2.3

[a] The ratio of **77** to **78,** obtained by ^{1}H NMR of the crude product, is provided in these columns. All experiments were conducted in duplicate, and the average yield is reported

We can rationalize the above outcomes by suggesting that bromide ion (from the salt additive) coordinatively saturates the TM intermediate (**80**), thereby driving RE to the desired product (**69**) and slowing the BHE necessary to deliver the imidazolium byproduct (**77**). Clearly, this BHE pathway is much faster than the RE process that takes **77** to aryl-imidazolium byproduct **78** because without the salt, BHE dominates. In support of this theory, when *n*-Bu_2Zn was made the limiting reagent, now the limiting reagent and, without salt, the ratio of **77**:**78d** inverted from 1:0 to 1:2.3 (entry 4 vs. 3). This can be rationalized as the extra catalyst from the higher loading

making it to the end of the reaction and getting captured by the excess OA partner (**68d**) to form **79**. This intermediate is eventually converted to the aryl-imidazolium byproduct **78d** since no organozinc remains to proceed through TM. Interestingly, when LiBr was added to these conditions (entry 5), BHE could be completely suppressed thereby eliminating the formation of **77** altogether. When $ZnBr_2$ was tested, there was no effect (entry 6). These results support the notion that RE of **79** (to give **78**) is relatively slow and mostly happens when there is no *n*-Bu_2Zn left with which to react, or an electron-rich OA partner is used. This leaves BHE from complexes such as **80** as the primary culprit in the loss of catalyst activity in the cross-coupling of alkyl nucleophiles.

3.3 Effect of slowing or eliminating BHE on catalyst lifetime

It is possible to imagine that the catalyst death occurring in Table 12 could be curtailed with reagents that do not have β hydrides. It was believed that if BHE could be significantly slowed, if not halted completely, by a primary kinetic isotope effect (KIE) associated with the β-deuterated analogue of *n*-Bu_2Zn. Consistent with the above hypothesis, the yield of the cross-coupling of per-deuterated *n*-Bu_2Zn-d_{18} (**70'**) was significantly increased over its protio counterpart (Scheme 21). The crude reaction mixture contained primarily coupled product **69g'**, trace starting **68g**, and some deuterio-reduced product (**83**) illustrating that BHE was not entirely shut down.

Scheme 21: The use of per-deuterated *n*-Bu_2Zn-D_{18} (70') to examine its effect on BHE from TM intermediate 80.[a]

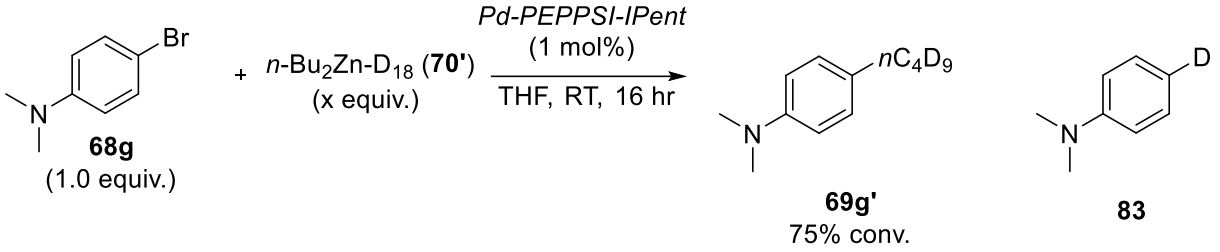

[a] All experiments were conducted in duplicate, and the average yield is reported.

To push this concept to its limit bis-neopentylzinc (**84**), which has no β hydrides, was prepared and subjected to a sequential coupling experiment (Scheme 22 and Scheme 18). Despite the profound hindrance associated with nucleophile **84**, full conversion of both equivalents of **68d** now occurred without the need for any salt additives. Furthermore, couplings with this reagent did not display the characteristic color change from bright yellow to black that nearly all other Negishi couplings displayed. These findings further implicate BHE as the primary cause of catalyst death.

Scheme 22: Sequential reaction of bis-neopentylzinc (84) with 68d with *Pd-PEPPSI-IPent* in the absence of LiBr.

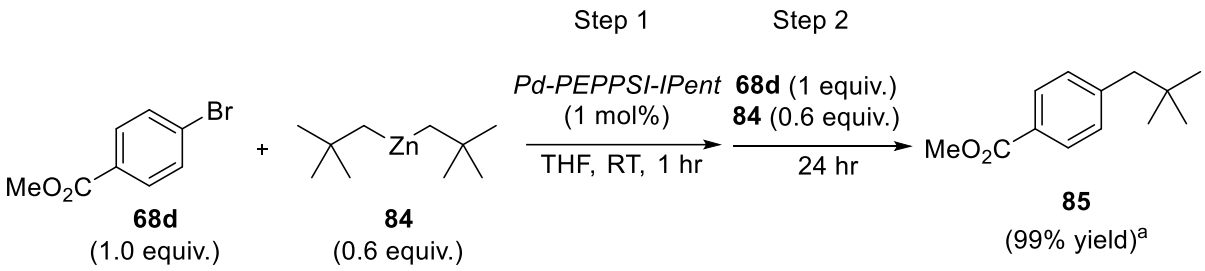

[a] Percent yield is based on 2 equiv of **68d** reacting to provide 2 equiv of **85** for full conversion. All experiments were conducted in duplicate, and the average yield is reported.

3.4 Conclusion

We have demonstrated that BHE is the primary cause of catalyst death in the coupling of alkyl nucleophiles with aryl electrophiles using Pd-NHC catalysts. There are a number of factors

that impact the rate at which decomposition by this pathway occurs. Electron-rich OA partners such as **68g** (and their associated cross-coupled products, e.g., **69g**) possessing coordinating functionality curtail BHE, by coordinating to the metal center of the RE intermediate (e.g., **80**). Conversely, electron-poor substrates (e.g., **68d**) cross-couple very rapidly and neither they, nor their corresponding products (e.g., **69d**) can coordinate suitably well with **80**, and catalyst decomposition to imidazolium byproduct (**77**) is rapid. This makes the catalyst shorter-lived, which is why there is zero coupling if additional substrates are added to the reaction mixture after the initial coupling takes place (Scheme 18 entry 1). That **68g** and/or **69g** help stave off BHE is supported by the fact that the coupling of **68d** takes place to a significant extent when it is added to the coupling mixture comprised initially from **68g** after it has reacted as much as it is capable. Related to this, catalytic amounts of dimethylaniline can be added to the coupling of **68d** and when more **68d** is added, the reaction continues to completion (Scheme 18 entry 4).

In addition to the positive impact that LiBr has on the coupling of alkyl nucleophiles within the catalytic cycle,[97,114] it plays a clear role in keeping the catalyst out of undesirable resting states. Seemingly related to the role proposed above for aniline derivatives, bromide ion, a very good ligand for Pd,[119] can help keep the metal centre coordinately saturated and prevent it from undergoing BHE. Consistent with the above developing hypotheses, transformations involving alkyl substrates that are incapable of readily undergoing BHE (e.g., **70'**) see improved catalyst lifetimes and activity. Removing all β hydrides all together (e.g., **84**) eliminates BHE completely, leading to much higher turn-over numbers for the catalyst.

BHE is not the only hurdle Pd-NHC complexes face in these cross-coupling procedures. The aryl-imidazolium byproduct **78** represents a minor pathway leading to catalyst deactivation. RE from OA intermediate **79**, rather than TM with the nucleophile to provide **80**, gives rise to aryl-

imidazolium byproduct **78**. Based on these results, electron-rich OA partners undergo this RE faster than electron-deficient partners. This is likely due to the electron donating group helping to drive the reduction of Pd(II) to Pd(0). It cannot be concluded that the bromide ion coordinating to **79** slows down the RE process that delivers **78**, but the presence of LiBr certainly does not prohibit **78** from forming. What is known is that the presence of the bromide ion directs catalyst death away from the dominant BHE pathway, leaving RE of **79** (to give **78**) as the primary catalyst deactivation mechanism.

Chapter 4: Benchmarking the electronic effects of chlorine bearing NHC ligands

4.1 Effect of chlorine modified NHC ligands on alkyl-alkyl couplings

The role of salt additives on alkyl-alkyl Negishi couplings has already been well documented.[97,114] These studies were performed around the same time as the initial discovery of the beneficial effects of chlorine substituents on the core of NHC ligands.[46,85] Considering the impact *Pd-PEPPSI IPent*^{Cl} had on aryl-alkyl couplings as shown in chapters 2 and 3, it would seem likely that NHC ligands with chlorine backbones would have an impact on alkyl-alkyl couplings. To address these effects, all available versions of *Pd-PEPPSI,* including isopropyl, iPent (3-(*n*)pentyl) and iHept (4-(*n*)heptyl) with, and without chlorine backbones were screened for their ability to catalyze the coupling between *n*-Bu_2Zn (**70**) and a simple alkyl bromide (**52**). In most studies from Organ *et al.*, the larger and chlorine modified versions outperform their counterparts. In alkyl-alkyl Negishi couplings, chlorine substituted NHC ligands were harmful at times. The first 3 catalysts (*Pd-PEPPSI-IPr, Pd-PEPPSI-IPr*^{Cl} and *Pd-PEPPSI-IPent*) were successful at producing hexylbenzene (**54**) with minimal elimination (**86**) and dehalogenation (**87**). Furthermore, *Pd-PEPPSI-IHept* was also able to produce moderate amounts of the coupled product **54**. The larger catalysts were clearly capable of performing this reaction, but introduction of the chlorine backbone produced primarily the elimination byproduct **86** (*Pd-PEPPSI-IPent* and *Pd-PEPPSI-IHept* compared to *Pd-PEPPSI-IPent*^{Cl} and *Pd-PEPPSI-IHept*^{Cl}, respectively). This was intriguing since it was unclear if this was due to a steric or electronic effect. Considering that *Pd-PEPPSI-IHept* was still able to achieve modest yields while *Pd-PEPPSI-IHept*^{Cl} was almost entirely incompetent suggested sterics was likely not a contributing factor. In contrast, *Pd-PEPPSI-IPr* and *Pd-PEPPSI-IPr*^{Cl} were both effective, but *Pd-PEPPSI-IPr*^{Cl} displayed a slightly higher selectivity, which contradicts the trend seen in the larger catalysts. It is unusual that large, chlorine modified NHC ligands lowered selectivity, given the numerous times they showed

improvements in other similar applications. [40,46,47,84] Elucidating the source of these undesirable effects could help design future generations of *Pd-PEPPSI* precatalysts.

Figure 14: Effect of catalyst size and chlorine substitution on alkyl-alkyl couplings.[a]

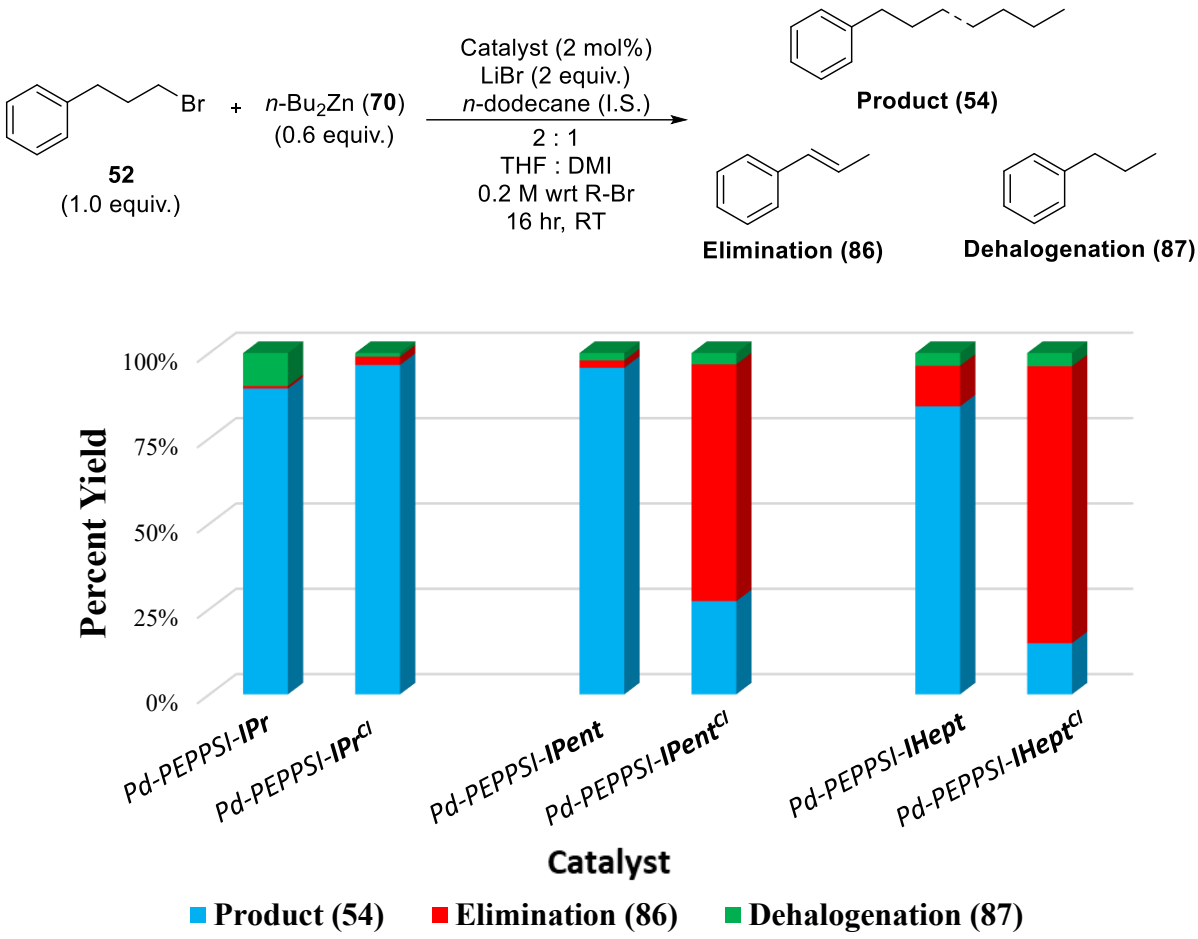

[a] All reactions performed in duplicate, average of two reported. Yield determined using GC-FID with calibration curves.

4.2 Determining the source of BHE

The initial discovery that large, chlorine modified NHC ligands were a poor choice for alkyl-alkyl couplings was unexpected and raised many questions. Before tackling these queries, it was important to confirm the source of the major elimination product **86**. Two control tests were performed to determine the source of this unwanted pathway. First, a control test with no palladium catalyst ruled out E2 elimination followed by palladium catalyzed isomerization (Scheme 23). The

full recovery of starting alkyl bromide (**52**) confirmed that the formation of the elimination byproduct (**86**) is Pd catalyzed.

Scheme 23: Control test used to determine the source of BHE.[a]

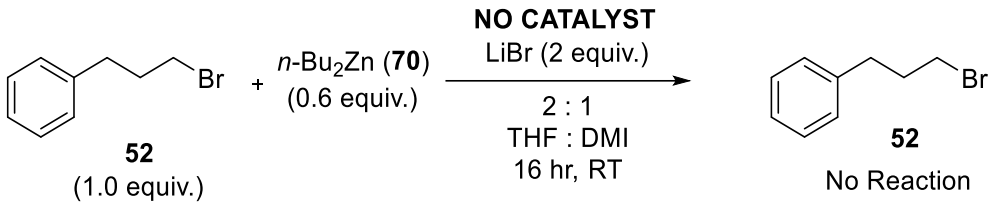

[a] All reactions performed in duplicate, average of the two trials is reported.

The second test was able to pinpoint which step on the catalytic cycle was undergoing BHE. It is possible for both the OA intermediate **88** and the TM intermediate **90** to undergo BHE under alkyl-alkyl coupling conditions (Scheme 24). If the OA intermediate undergoes BHE, it can only produce **89**, which could lead to elimination product **86**. The TM intermediate **90** has two possible BHE pathways, producing either **91** or **86**. As a result, the detection of both these alkenes can be used to determine the source of BHE. Unfortunately, the use of GC-FID to analyze these couplings makes it challenging to detect butene isomers due to their low boiling point. To address this problem, *n*-Bu_2Zn was substituted with a longer chain analogue (decyl) so its elimination byproducts could be easily detected using GC-FID. The detection of decene isomers would be indicative of BHE occurring at the TM intermediate (**90**), while the lack of these artifacts would suggest the OA intermediate (**88**) is the source of BHE.

Scheme 24: Mechanism for the formation of potential elimination byproducts.

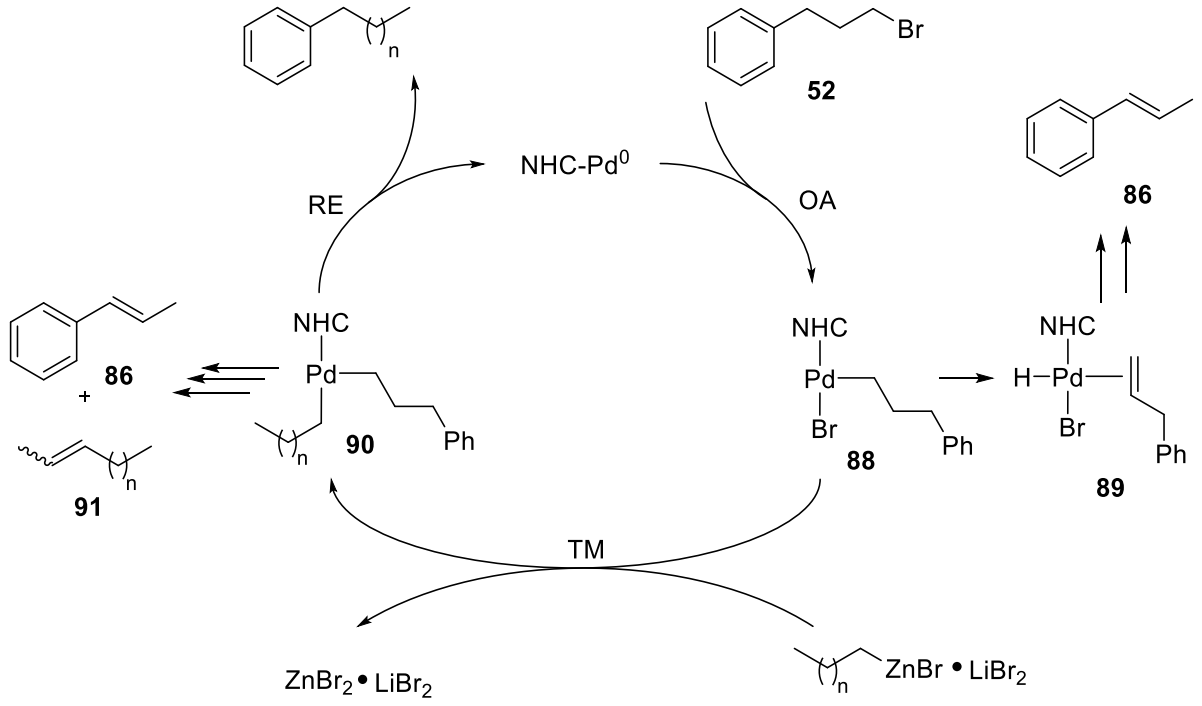

Decylzinc bromide (**92**) was prepared salt-free in DMI using Huo's[24] protocol and coupled with **52** using the unsuccessful catalysts (*Pd-PEPPSI-IPent*^{Cl} and *Pd-PEPPSI-IHept*^{Cl}, Table 14). The results from these couplings suggest that the OA intermediate is the primary source of **86,** based on the trace amounts of decenes detected. Nearly all the organozinc was converted to decane, which is likely formed by neutralizing the HBr that is produced, and thus turning over the Pd(II) catalyst. One important caveat from this experiment is the switch from dialkyl to monoalkylzinc reagent since the analogous dec_2Zn could not be distilled under vacuum like *n*-Bu_2Zn. It is already well established that the monoalkyl organozinc reagents are less reactive and likely contain some amount of $ZnBr_2$ as a result of the Schlenk equilibrium. To compensate for this, the couplings were repeated with a larger dose of LiBr (3 equivalent) resulting in similar amounts of **86** being formed (entries 3 and 4). Considering these couplings are already known to work under these conditions with monoalkyl-zinc reagents and *Pd-PEPPSI-IPr*,[25,39,97,104] it can be concluded that large catalysts

with chlorine functionalized backbones cause BHE to occur at the OA intermediate (**88**). With the source of BHE identified, it was possible to investigate the extent to which electronic and steric interactions from the NHC ligand impact formation of **86**.

Table 14: Alkyl-alkyl couplings with decylzinc bromide (92) and 3-bromo-1-phenyl propane (52).[a]

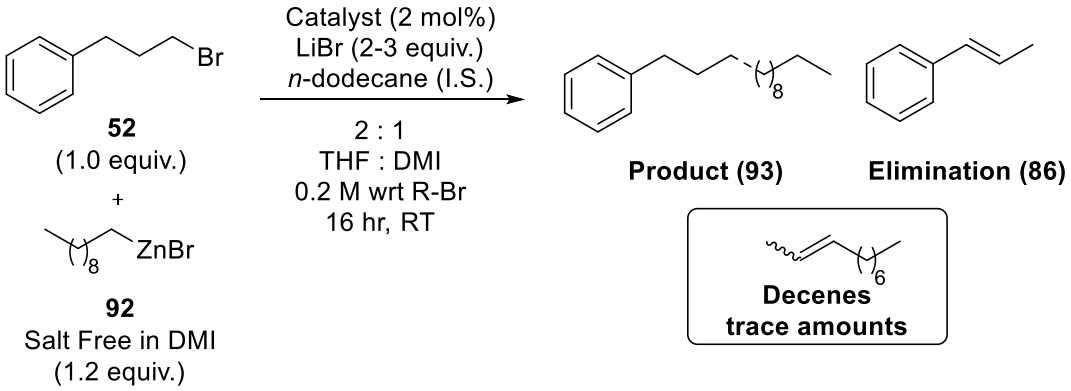

Entry	Catalyst	LiBr equiv.	Yield of **86**
1	*Pd-PEPPSI-IPent*^{Cl}	2.0	89%
2	*Pd-PEPPSI-IHept*^{Cl}	2.0	97%
3	*Pd-PEPPSI-IPent*^{Cl}	3.0	90%
4	*Pd-PEPPSI-IHept*^{Cl}	3.0	93%

[a] All reactions performed in duplicate, average of the two trials is reported. Yield of **86** determined using GC-FID with calibration curves. All reactions saw trace amounts of decene isomers by GC-MS.

4.3 Comparing chlorine and methyl functionalized NHCs

In previous studies, a useful method for determining the electronic and steric contributions was to compare chlorine substituted NHCs to their methyl counterparts.[40,47] Methyl groups on the backbone have a similar size to chlorine, but act as electron donating groups. Making these comparisons was possible for *Pd-PEPPSI-IPr*^{Cl} but the methylated versions of *Pd-PEPPSI-IPent* and *Pd-PEPPSI-IHept* have yet to be synthesized. To find the root cause of this chlorine effect,

the methylated versions of *Pd-PEPPSI-IPent* and *Pd-PEPPSI-IHept* were prepared so they could be compared to their chlorine counterparts. The synthesis of *Pd-PEPPSI-IPr*^{Me} was trivial, with literature procedures readily used to prepare the precatalyst.[40] In comparison, *Pd-PEPPSI-IPent*^{Me} and *Pd-PEPPSI-IHept*^{Me} could not be synthesized using the conditions used for their chlorine counterparts.

The 2,6-dialkyl anilines (**94**) could be prepared according to literature procedures,[74] but the bis-condensation onto 2,3-butadione was problematic (Scheme 25). With 2,6-diisopropylaniline the condensation was trivial, providing nearly quantitative yield of the bisimine. With larger anilines, the first condensation goes smoothly, producing monoimine **97**, but condensation of the second aniline is very slow. Refluxing with toluene in a Dean-Stark apparatus was challenging due to the extreme temperatures and insulation needed to effectively carry over the toluene vapors. Furthermore, 2,3-butadione could carry over if the mono condensation product is not first formed at lower temperatures. To avoid these harsh conditions, the biscondensation was performed in DCM with an excess of the 2,6-dialkylaniline (**95**) and magnesium sulfate to help push the reaction to completion by sequestering the water produced. Column chromatography was then used to separate the bisimine (**96**) and the remaining aniline (**95**) and monoimine (**97**) could be recovered and submitted to further condensations. Cyclization to form NHC salts **98** using previously reported conditions proceeded with adequate yields and crystallization from the EtOAc used for the liquid-liquid extraction conveniently provided the NHC salt in high purity.[74] Unfortunately, conventional ligation attempts of NHC salts **98** to palladium to form *Pd-PEPPSI* analogs were unsuccessful. Multiple attempts under previously reported conditions used for the chlorine functionalized analogs failed, producing only palladium black and recovered NHC salt. To get around this hurdle, the methylated NHCs were ligated to palladium-(π-cinnamyl)-chloride dimer

to give *(NHC)Pd(cinnamyl)chloride* complexes (**99**). The switch to cinnamyl chloride complexes was not ideal due to the difference in the stabilizing ligand employed. However, the selectivity of the reaction should not be affected since both the pyridine[120] and cinnamyl[121,122] ligands are known to readily generate active NHC-Pd(0) species.

Scheme 25: Synthesis of methylated *(NHC)Pd(cinnamyl)chloride* complexes.

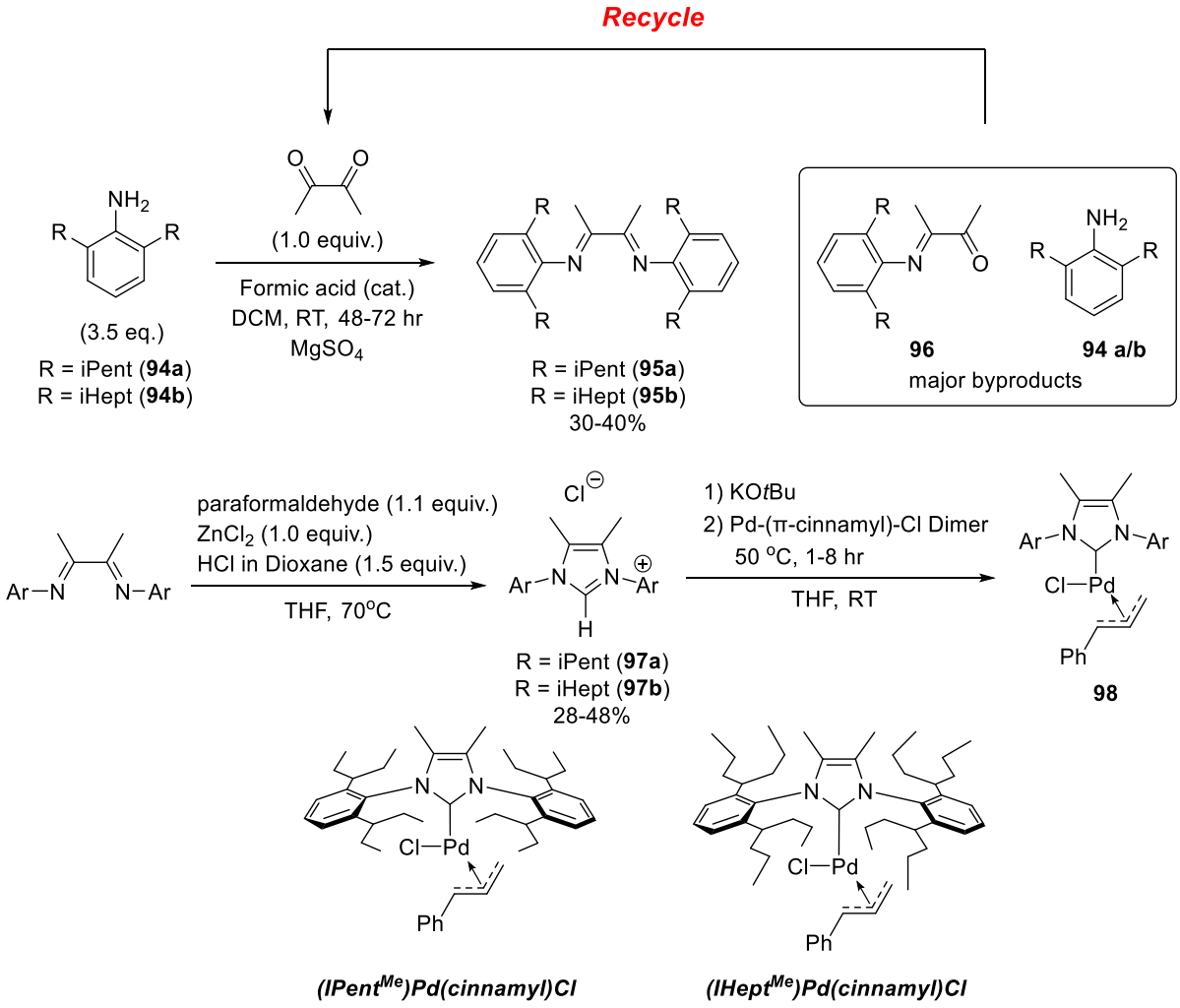

These cinnamyl-based catalysts were found to require cold storage conditions as the bright yellow powders degraded into brown clumpy solids after sitting approximately 3 months at ambient temperature in a well-maintained glovebox. The identity of the byproducts and source of this degradation was not investigated, but based on visual appearances it appeared

(IPent^{Me})Pd(cinnamyl)Cl degraded faster than *(IHept^{Me})Pd(cinnamyl)Cl*. This was unexpected since the larger *(DiMeIHept^{Cl})Pd(cinnamyl)chloride* complex (Figure 7) is known to be indefinitely air stable at ambient temperatures.[79] These observations highlight the importance of pyridine as a stabilizing throw away ligand.

With the methylated precatalysts in hand, their performance in the alkyl-alkyl coupling of interest was tested. Surprisingly, the results mirrored those of the chlorine functionalized catalysts (Figure 15). The smaller NHC ligands with iPr chains all provided relatively high yields of the coupled product **54**, with minimal side products. The catalysts with larger alkyl chains produced similar yields of the elimination byproduct **86** for both the methyl and chlorine modified ligands (*Pd-PEPPSI-IPent^{Cl}* and *Pd-PEPPSI-IHept^{Cl}* compared to *(IPent^{Me})Pd(cinnamyl)Cl* and *(IHept^{Me})Pd(cinnamyl)Cl* respectively). These results also continue the trend in which the NHC ligands with large iHept chains produce more elimination product than those bearing iPent and iPr chains, suggesting sterics cause the change in reactivity seen in chlorine functionalized NHC ligands.

Figure 15: Effect of methyl functionalized NHC ligands on alkyl-alkyl couplings.[a]

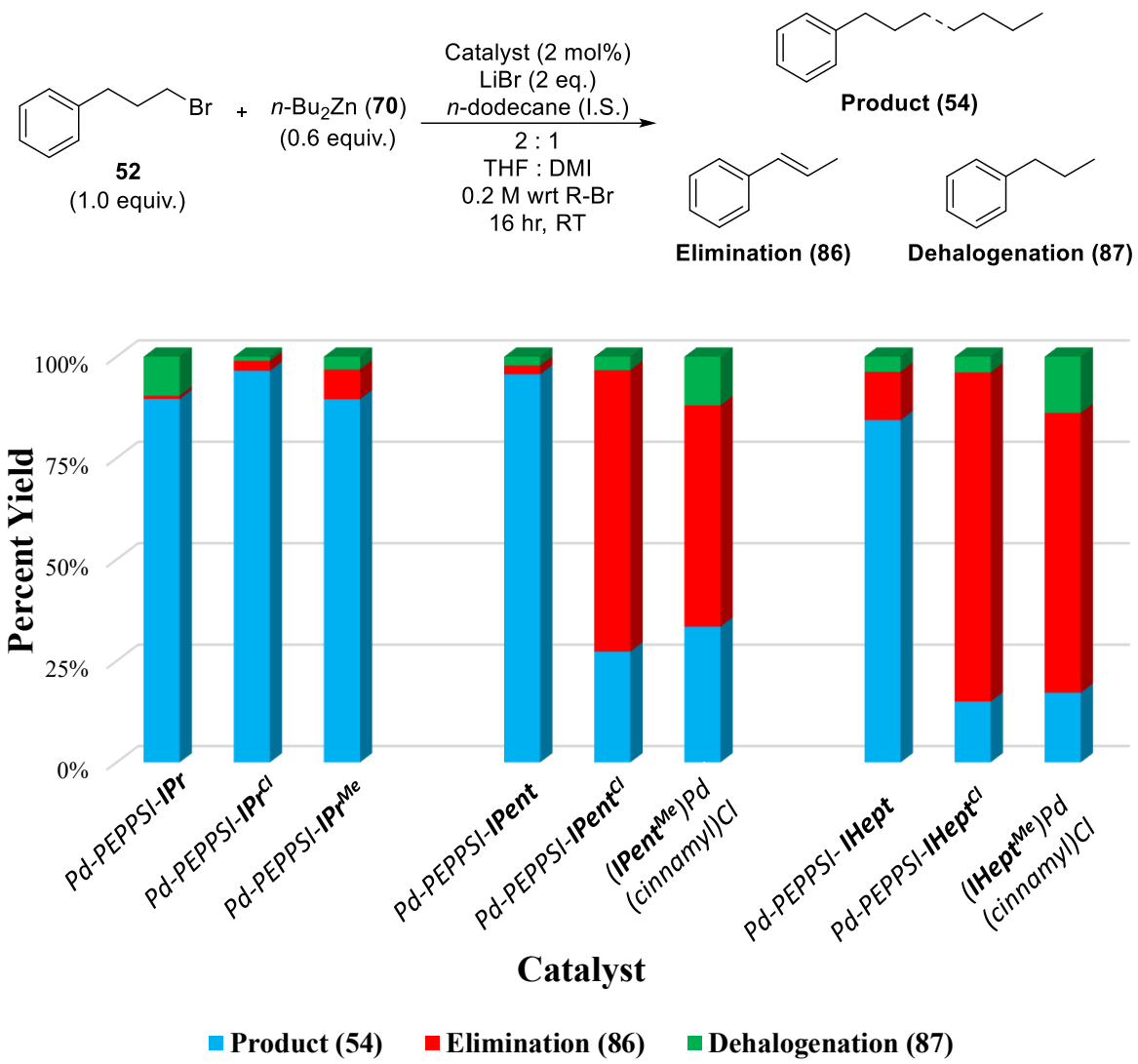

[a] All reactions performed in duplicate, average of two reported. Yield determined using GC-FID with calibration curves.

The increased selectivity for product **54** vs elimination (**86**) can be rationalized by considering the approach an organozinc reagent must take for a successful TM to occur. The OA intermediate can undergo two different pathways, TM with the organozinc or BHE followed by isomerization to the highly stable elimination product **86** (Scheme 26). In this case, productive coupling (TM) is bimolecular while BHE is unimolecular, making it a challenging competition. As alkyl chains on the N-aryl NHC rings become larger, the coordination sphere around palladium becomes progressively more hindered, making TM with organozinc reagents increasingly

challenging. This is problematic since the longer the OA intermediate waits to undergo TM, the more time it has to undergo BHE and produce **86**. Adding to this problem, large backbone modifications restrict the motion of the alkyl chains, mitigating their 'flexible steric bulk',[57] making it harder for them to free up space around palladium for the organozinc approach

Scheme 26: Effect of ligand size on alkyl-alkyl couplings, resulting in the selectivity between BHE and TM.

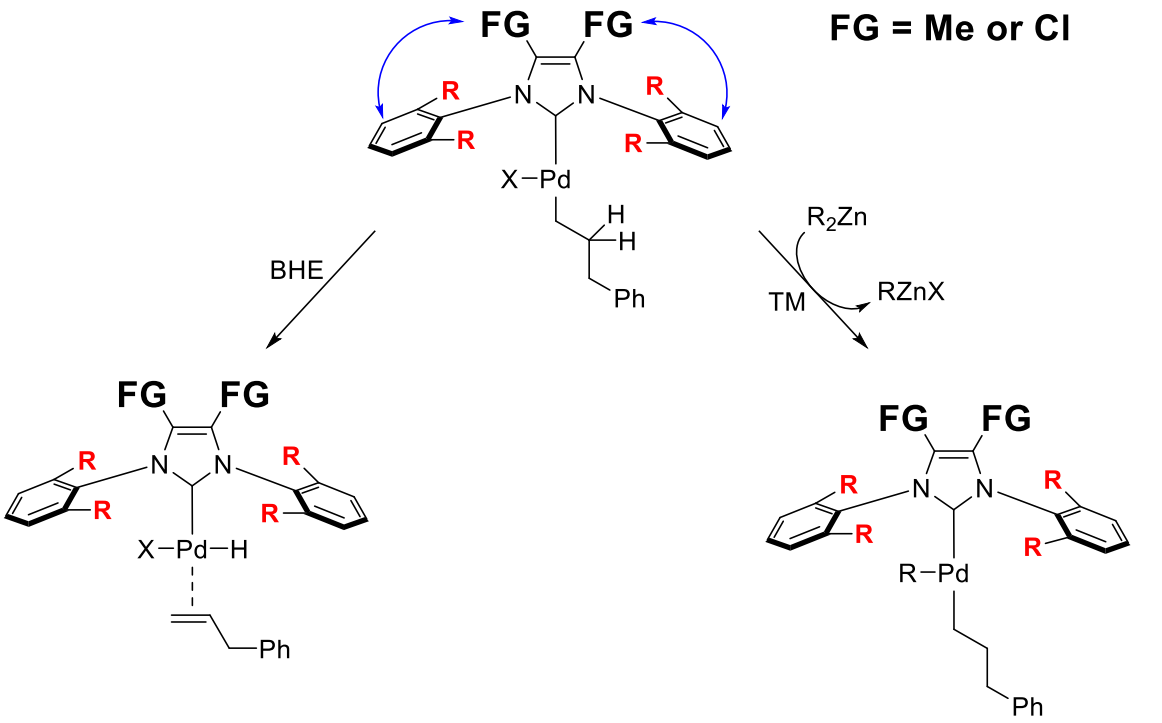

This delicate balance between TM and BHE is in line with the increase in elimination byproduct seen with backbone modification on NHC ligands with iPent and iHept chains, but not iPr (Figure 15). Since the isopropyl chain is the smallest in this series, it is the least capable of shielding the palladium centre, even with backbone modifications. This explains why *Pd-PEPPSI-IPr*^{Cl} and *Pd-PEPPSI-IPr*^{Me} both displayed similar selectivity to *Pd-PEPPSI-IPr* (Figure 15). Further supporting this theory, higher selectivity was seen when the couplings with the ineffective

catalysts were repeated with a higher loading of the organozinc (Figure 16). By doubling the concentration of the organozinc, the balance between TM and BHE is skewed towards TM, resulting in higher conversion to the coupled product. Indeed, the *IPent* and *IHept* NHC ligands saw an improvement in the yield of **54** no matter the backbone modification. Again, the difference between the methyl and chlorine NHC core substituent is minimal, and a slightly higher yield was achieved with the smaller *IPent* based NHC ligands. However, the yield of these reactions still fails to match those of the *IPr* based ligands at half the organozinc loading. These findings further display the superiority of small, *IPr* based ligands for alkyl-alkyl couplings.

Figure 16: Effect of *n*-Bu_2Zn loading on alkyl-alkyl couplings.[a]

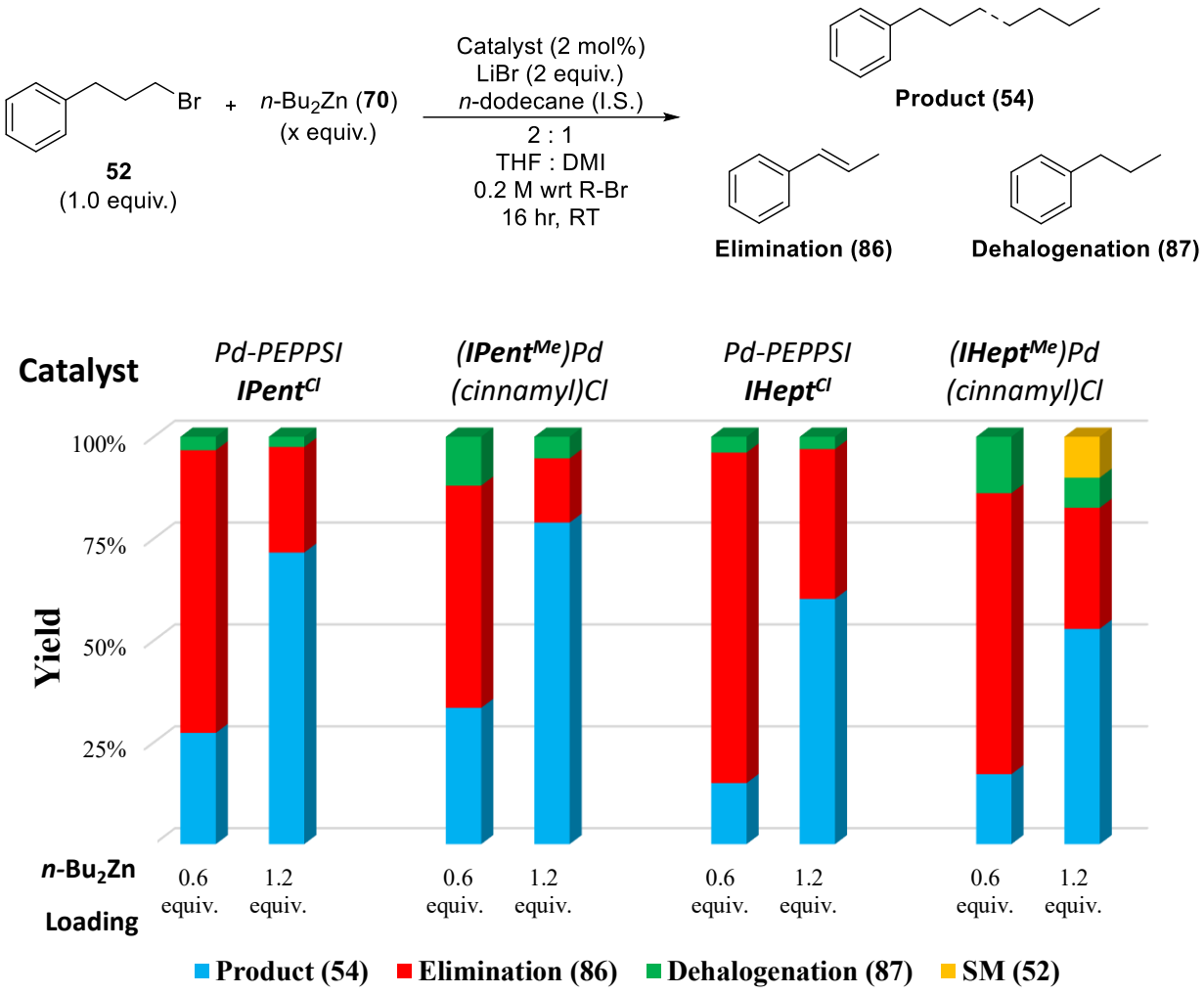

[a] All reactions performed in duplicate, average of two reported. Yield determined using GC-FID with calibration curves.

Even though this new chlorine effect was mostly caused by steric influences, it was still believed there remained an undiscovered electronic contribution. Analysis of the kinetic profiles of the successful catalysts provided further insights. First, the size of the alkyl chains was compared by monitoring the same reaction with *Pd-PEPPSI-IPr*, *Pd-PEPPSI-IPent* and *Pd-PEPPSI-IHept* (Figure 17A). Consistent with the developing hypothesis, the larger catalysts had slower kinetics. This decrease in reaction rate can be reasonably explained by slower kinetics for both OA and TM based on the steric hindrance introduced by large alkyl chains. It is important to

note that this steric hindrance reduced the overall rate of the reaction, but ultimately still produced the coupled product in reasonably high yields. More interesting was the comparison between *Pd-PEPPSI-IPr* and its modified analogues (Figure 17B). An electronic trend becomes quickly apparent, in which reaction rates improved with increasingly electron withdrawing ligands (IPr^{Cl} > *IPr* > IPr^{Me}). Since the isopropyl chains are too short to be effectively pushed towards the palladium centre, and the methyl and chlorine modified backbones displayed significantly different activity, these observations are believed to be caused by electronic factors.

Figure 17: Kinetic profiles for the coupling of 52 and *n*-Bu_2Zn catalyzed by different versions of Pd-NHC complexes.[a]

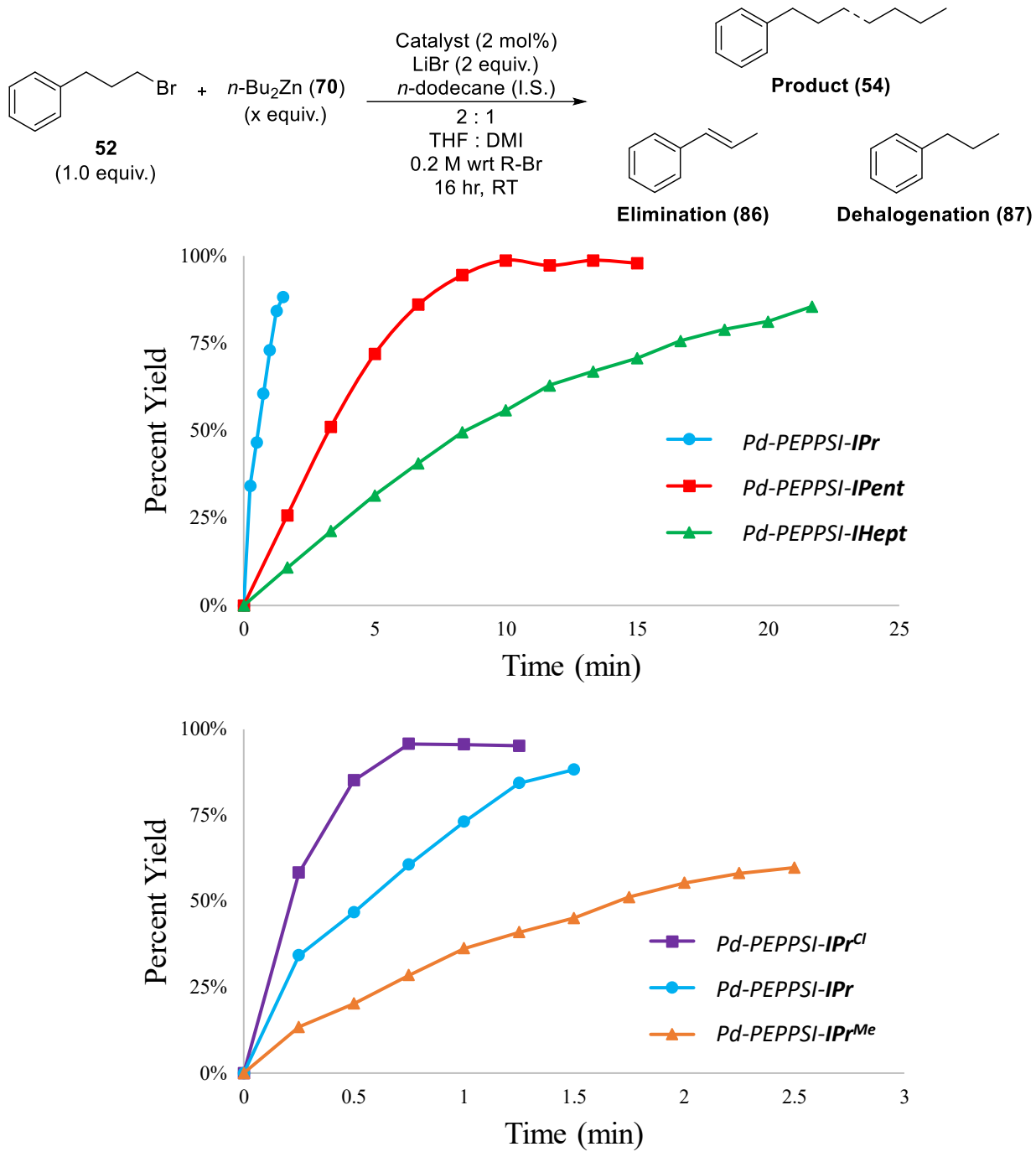

[a] Yields determined using GC-FID with calibration curves.

A change in σ-donating ability of the NHC is likely lowering the barrier(s) to one or more of the three fundamental steps of the catalytic cycle. OA seems unlikely to be the step that is

enhanced since it usually relies on an electron-rich Pd(0) centre. Chlorine substituted imidazoles have been reported to increase the rate of RE as previously discussed with secondary alkylzinc couplings (Table 1).[40] However, the control tests with decylzinc bromide (Table 14) suggested RE is very rapid and identified the OA intermediate as the source of elimination product. With these considerations, it seems the chlorine groups are enhancing the rate of TM by increasing the electrophilicity of the OA intermediate. This increase in electrophilicity would help drive TM, increasing the observed rate of reaction (Figure 17B) and suppressing the formation of the elimination byproduct **86** (Figure 15) by shortening the lifetime of the OA intermediate. While installing chlorines on the backbone probably enhances the electrophilicity of larger catalysts like *Pd-PEPPSI-IPent*^{Cl} and *Pd-PEPPSI-IHept*^{Cl}, the extremely bulky alkyl chains block the approach of the nucleophile and instead favor BHE producing **86** (Scheme 26). For this reason, large, chlorine bearing catalysts should be avoided for alkyl-alkyl couplings and reserved for couplings of OA partners that do not contain β hydrogens.

4.4 Revisiting Negishi coupling with secondary organozincs

With the revelations from the alkyl-alkyl couplings reported above and the new methylated NHC-Pd catalyst in hand, the coupling of secondary alkylzinc reagents was revisited since they are the original case study that highlighted the selectivity of large, chlorine functionalized NHC ligands.[47] It is well understood that larger catalysts gave better selectivity for the desired product over the rearranged product. Comparisons between *Pd-PEPPSI-IHept* and *Pd-PEPPSI-IHept*^{Cl} have already been made,[40,47] but at that time the only catalyst that had a methylated version available for comparison was *Pd-PEPPSI-IPr*. Without the comparison of *Pd-PEPPSI-IHept*^{Cl} to its methylated counterpart, it is not clear if electronic changes were also enhancing RE. It could be purely steric in nature, but the combination of steric hindrance and a more electron-deficient

palladium centre would facilitate RE, meaning that both steric and electronic effects are operative leading to enhanced selectivity.

Couplings were performed with diisopropylzinc (iPr_2Zn) and a series of 5-membered heteroaromatic bromides, known to be especially problematic for these couplings since they tend to produce the rearranged, linear product (Table 15). All reactions proceeded with full consumption of aryl bromide (**99**), with varying degrees of selectivity. The general trend seen for all heteroaryl bromides tested was an increase in selectivity (i.e., the RE product (branched) vs the MI product (linear)) when the backbone is substituted with methyl or chlorine. This is consistent with the steric clash induced by the large groups on the backbone thereby preventing access to the requisite conformation necessary for BHE. When comparing the two modifications, *Pd-PEPPSI-IHept^{Cl}* consistently provided better selectivity than *(IHept^{Me})Pd(cinnamyl)Cl*. This further supports the arguments that a combination of both steric and electronic influences contributes to the increased selectivity of chlorine bearing catalysts. Both modifications apply similar steric pressure on the alkyl chains, but chlorines take it one step further by providing an electronic driving force in parallel that helps drive RE.

Table 15: Comparison of *Pd-PEPPSI-IHept* and its analogs in the coupling of iPr_2Zn (100) and various 5-member ring heteroaromatic bromides (99).[a]

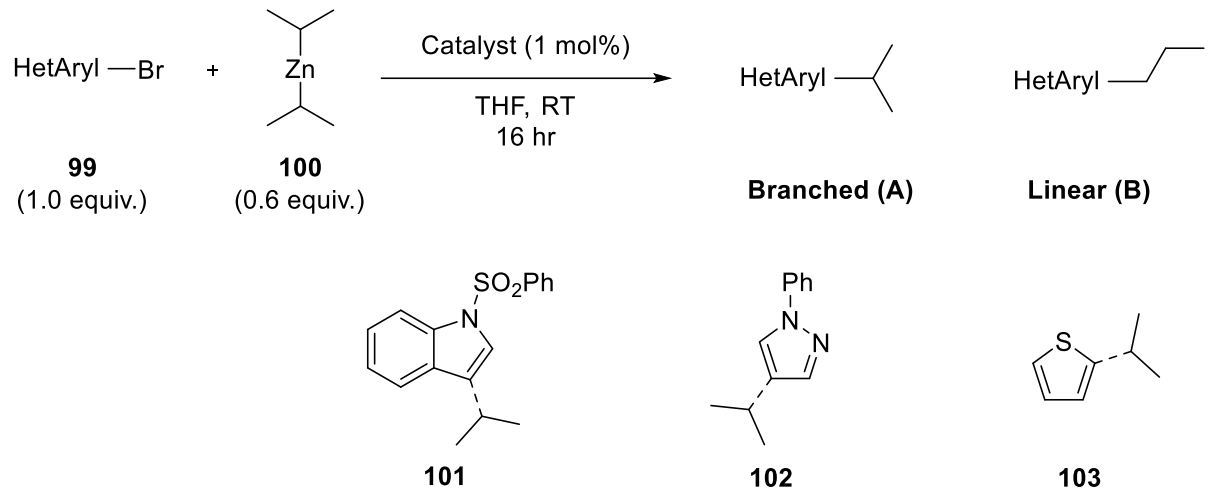

Catalyst	**101A** : **101B**	**102A** : **102B**	**103A** : **103B**
*Pd-PEPPSI-**IHept***	1 : 1	1 : 3	1 : 8
***IHept**^{Me}Pd(cinnamyl)Cl*	7 : 1	1.5 : 1	1 : 1
*Pd-PEPPSI-**IHept**^{Cl}*	13 : 1	3.3 : 1	2.3 : 1

[a] Ratio of branched to linear determined by analyzing the ^{1}H NMR spectrum of the purified product, since the two isomers co-elute.

4.5 Conclusion and outlook

The results from this chapter further highlight the intricate balance between the steric and electronic changes brought about by modification of the backbone of NHC ligands. Through a combination of catalyst screening and kinetic profiling, it could be concluded that chlorine backbone modifications help drive both TM and RE. Both steps are believed to be enhanced by a more electrophilic palladium centre. RE is also enhanced by a combination of this change in σ-donating ability and the increase in steric pressure on the palladium centre. However, these benefits come with an important caveat, that backbone modifications severely restrict the motion of the

larger alkyl chains such as *IPent* and *IHept*. For alkyl-alkyl couplings this is a fatal flaw since large, chlorine bearing ligands block the approach of the organozinc and end up favoring BHE.

In another study, the ratio of rearranged to branched product in secondary alkylzinc couplings was examined. Unlike the alkyl-alkyl couplings, now BHE can only occur at the TM intermediate. Again, a combination of steric and electronic influences is responsible for the enhanced selectivity of *Pd-PEPPSI-IHept^{Cl}* under these conditions. The methylated analog *(IHept^{Me})Pd(cinnamyl)Cl* had selectivity that was consistently between the smaller *Pd-PEPPSI-IHept* and more electron withdrawing *Pd-PEPPSI-IHept^{Cl}*. From these findings it was clear that chlorines on the backbone helped by both restricting the motion of the alkyl chains and creating a more electron-deficient palladium centre, which increases the rate of RE leading to less isomerized product in these couplings.

Future reaction optimizations can benefit from the considerations investigated in this chapter. Based on the trends seen, chemists can carefully choose the right variation of *Pd-PEPPSI* for their desired coupling. Couplings of alkyl organozinc reagents with challenging TM and RE steps can be enhanced with chlorine substituted NHC ligands, while couplings that are susceptible to BHE at the OA intermediate should only be conducted with small *IPr* based catalysts. While the newly synthesized methyl series of catalysts never outperformed the chlorine substituted catalysts, they nonetheless found application in reactions with challenging electrophiles. For the activation of strong C-X bonds, an electron-rich catalyst such as *(IHept^{Me})Pd(cinnamyl)Cl* might find utility. Finally, future unexpected results from large chlorine bearing NHCs can be compared with the newly synthesised methylated *(NHC^{Me})Pd(cinnamyl)Cl* catalysts to aid in mechanistic studies.

Chapter 5: Negishi coupling of α-methyl amino acids

5.1 Background

Proteins are large, complex biomolecules that perform many crucial roles in the body. They are responsible for the structure, function, and regulation of the body's internal processes. Peptides are generally considered smaller versions of proteins, both consisting of amino acids bound in a linear fashion to create biopolymers. These chains fold up on themselves into various conformations that ultimately give rise to their functionality. The first example of a peptide being used as a medication was the use of insulin to treat type 1 diabetes. This landmark discovery highlighted many of the benefits of peptide-based drugs including high potency, high selectivity and low toxicity. All these benefits derive from the fact that peptides are the machinery already used and recognized by nature. Using peptides, very potent therapies can be developed that have the capability of binding biological targets in ways small molecule drugs cannot. Furthermore, these drugs often have very low toxicity since they are eventually broken down into amino acids.

While these benefits are great for patient care, there are many challenges associated with peptide-based drugs including low oral bioavailability,[123] short half-lives[124] and costly production.[125] Low oral bioavailability is a result of the extremely acidic environment in the stomach which is incompatible with peptides, thus limiting the delivery of these drugs to injection. Another drawback is the immune system's extraordinary ability to rapidly detect and destroy foreign biomolecules. Once the immune system detects foreign peptides, it deploys specialized enzymes called proteases that hydrolyze the amide backbone, releasing the free amino acids in a process called proteolysis.[126] Finally, the large and complex nature of peptides makes their chemical synthesis challenging. Advances have been made in this field, with solid phase synthesis (SPP) proving to be an effective method for circumventing the poor solubility of peptides during stepwise syntheses.[127] Peptide synthesizers are now capable of preparing peptides comprised of

more than 200 amino acids.[128] However, the iterative stepwise synthesis still slows drug discovery campaigns in which rigorous structure activity relations (SAR) studies become time intensive.

Since the average half-life of peptide-based drugs is about 30 minutes *in vivo*, a major goal for this field is the extension of these lifetimes.[124] Unnatural amino acids have been investigated for their ability to enhance peptide half-lives. Usually, the goal of these modifications is to modify the amide bond, or its surroundings, to make it less likely to be recognized by natural proteases. This is a delicate balancing act because the peptides must be modified enough to evade detection and hydrolysis, but not so much that biological activity/recognition is lost. One effective modification reported by Horne *et al.* was methylation of the peptide backbone (Scheme 27).[129] In this study, the authors investigated four different modifications and their effect on stability towards proteolysis. Methylation of the alpha carbon (**C_α-Me**) and inversion of the R group (**D-α**) proved to be the most effective at slowing proteolysis, while N-methylation (**N-Me-α**) and β amino acids (**β**) had mild to modest increases in half lives. The results from this study suggest the incorporation of α-methylated amino acids into peptides at strategic positions could significantly improve their metabolic stability.

Scheme 27: Representative example of proteolysis and the unnatural residues used by Horne *et al.* to slow proteolysis.[129]

Proteolysis

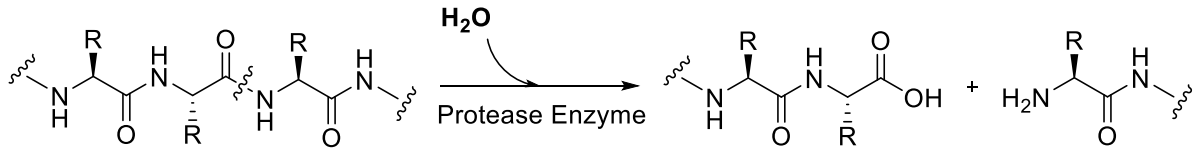

Unnatural residues examined

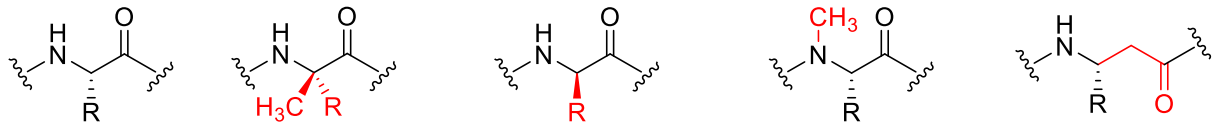

Natural **C_α-Me** **D-α** **N-Me-α** **β**

To the best of our knowledge, few methods exist for the preparation of α-methylated amino acids and these are lengthy synthetic approaches that lack the ability to diversify the R group.[130–132] This lack of literature precedence limits the implementation of these unnatural amino acids in peptide-based drug discovery programs. It was envisioned an amino acid scaffold (**104**) could be prepared with the α-methyl backbone, protecting groups on the two ends, and a CH_2X group for the sidechain (Scheme 28). With this amino acid template, Negishi coupling (and other Pd catalyzed cross-coupling reactions) could be performed either using this template as the electrophile (Scheme 28A) or as the nucleophile (Scheme 28B). This would allow for the R group to be installed last, simplifying the development of a library of amino acids containing this backbone modification. While these couplings will be especially difficult due to the steric bulk surround the C-X bond, it was believed that the *Pd-PEPPSI* series of precatalysts would be capable of performing these couplings.

Scheme 28: Electrophilic (A) and nucleophilic (B) approach to Negishi coupling with amino acid template 107.

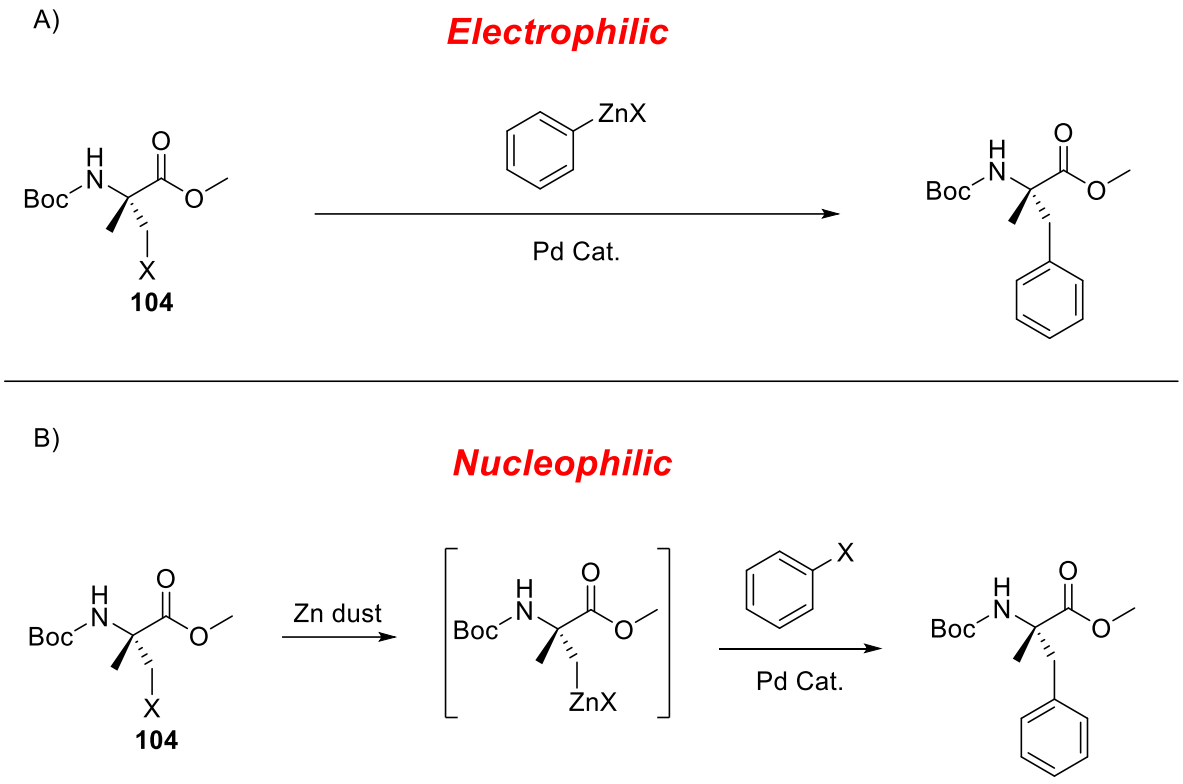

Fortunately, the conversion of non-methylated analogs to the corresponding organozinc reagents and subsequent couplings have been well documented.[133–139] One problem that commonly plagues these couplings is β elimination of the N-Boc group. A study from Jackson *et al.* examined the zinc insertion step and subsequent decomposition of the non-methylated version of **104** using NMR spectroscopy.[140] They noted this organozinc reagent (**105**) undergoes β elimination in THF, releasing the eliminated ester and Boc-NH_2 (Scheme 29). By comparing the ^{13}C and ^{1}H NMR spectra of **105**, the authors concluded the carbamate coordination to zinc is predominant in THF. This is corroborated by experiments conducted in DMF that produced good yields of the organozinc. It is for this reason the zinc insertion and subsequent couplings are usually performed in DMF. Using this protocol, the authors employed **105** in Negishi couplings with various acyl

chlorides, achieving yields of 20-59%. Further developments from Jackson *et al.* have shown that swapping the Boc protecting group for trifluoroacetamide greatly slows the rate of β elimination.[141]

Scheme 29: Predominant structures of organozinc 108 and decomposition pathway *via* β elimination.

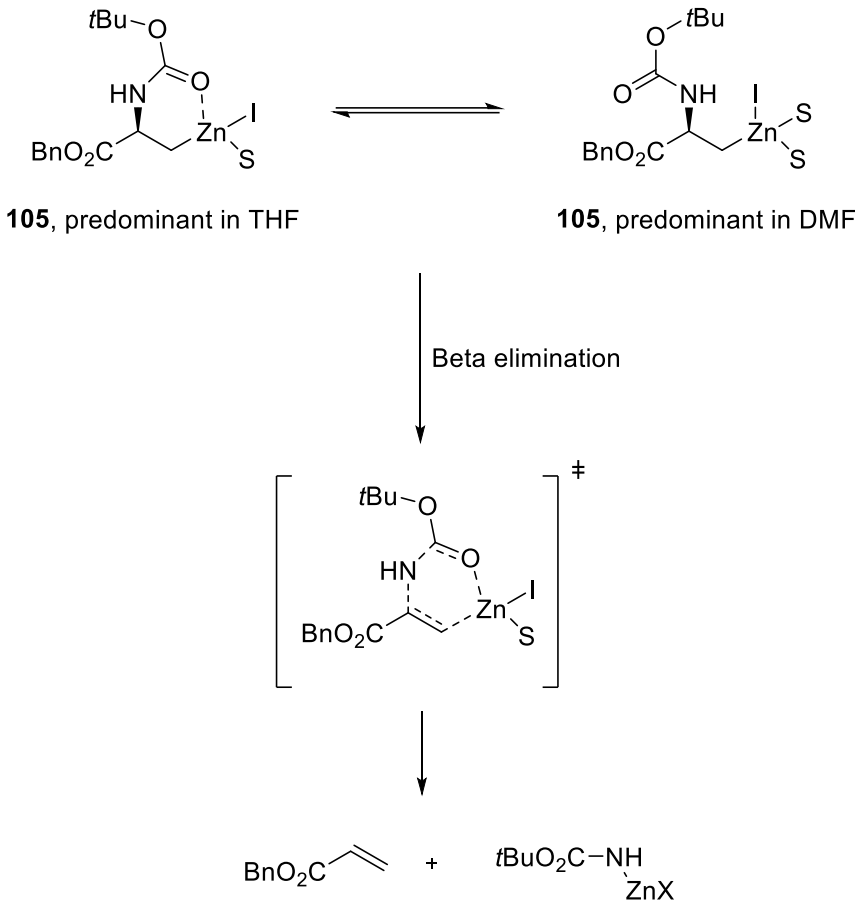

In 2010 Jackson *et al.* published improved conditions for the Negishi coupling of **105** with various aryl halides (Scheme 30). [135] DMF was again the solvent of choice due to the stability of the organozinc species. Various palladium sources and phosphine ligands were tested for the subsequent Negishi coupling, and $Pd_2(dba)_3$ and SPhos (2:1) proved to be the most efficient catalyst system. The general procedure began with the zinc insertion step, treating **106** with 3 equivalents of zinc dust that had been preactivated with I_2 in DMF. A solution of $Pd_2(dba)_3$, SPhos, and aryl halide were added directly to the mixture without removing the remaining zinc powder.

The resulting slurry was stirred either at room temperature for aryl iodides or 50 °C for aryl bromides. Using this technique, a wide range of aryl halides could be coupled to produce new, unnatural amino acids (**107**).

Scheme 30: Improved Negishi coupling conditions for 106.[135]

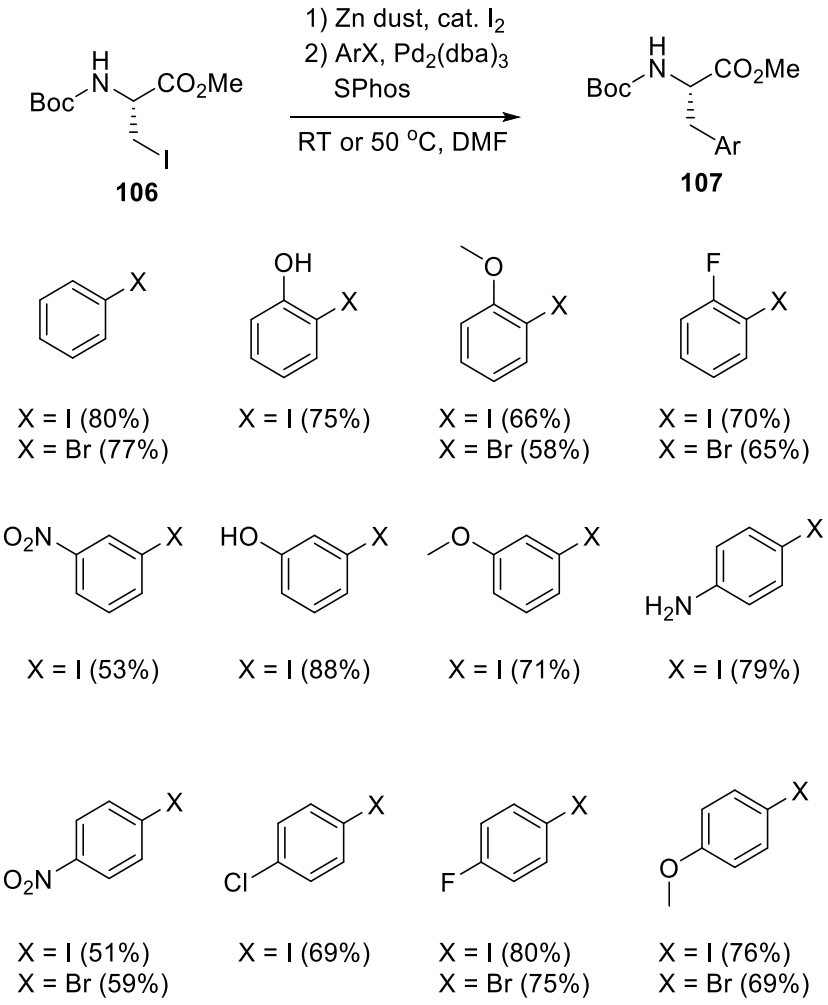

5.2 Plan of study

The goal of this project is to make α-methylated amino acids more readily available, the progress of which can be measured by a few key milestones, the first of which is the synthesis of the α-methylated amino acid template (Scheme 31). Initial reaction development on racemic template **108** will save time and once the Negishi coupling of this amino acid is optimized, a

substrate scope and a route to the enantiopure amino acid template (**104**) can be prepared. With this methodology, some of the challenges associated with the discovery, production, stability, and bioavailability of peptide-based therapeutics can be addressed.

Scheme 31: Key milestone accomplishments for this project.

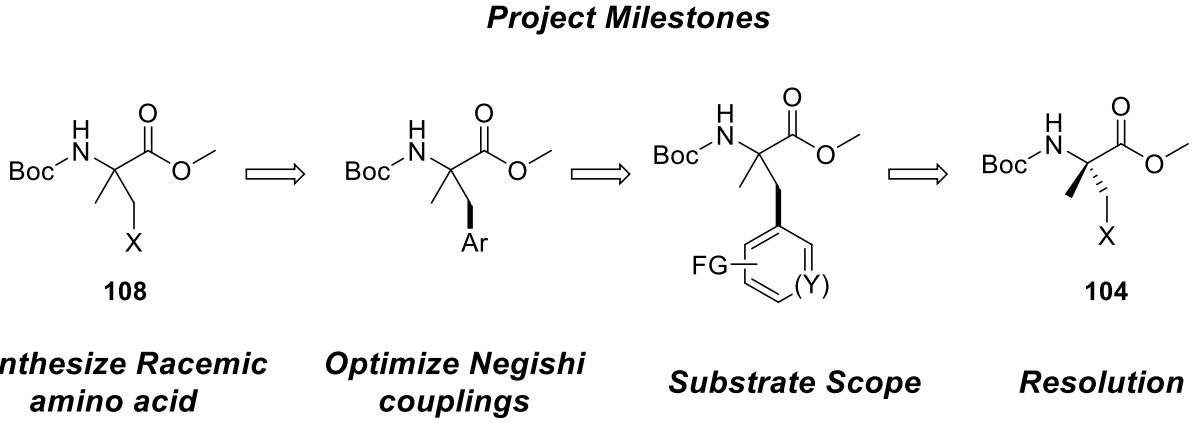

5.3 Synthesis of racemic amino acid template

The first task was the synthesis of a racemic amino acid bearing the α-methylated backbone and a CH_2X group. One straightforward method would be the protection of α-methyl serine followed by Appel halogenation of the alcohol. Unfortunately, this halogenation reaction is known to be ineffective, likely due to the steric bulk surrounding the alcohol.[142] Instead, our synthetic route began with the preparation of racemic α-methyl-serine (**110**)[143] followed by installation of the N-Boc protecting group to give **111** (Scheme 32).[144] To install the halogen, a method developed by Olma *et al.* was employed where the acid is first cyclized to give **112**[142] followed by treatment with MgX_2 (X = Cl, Br) to open the lactone and install the halogen in the desired position (**113**).[145] Initially Olma *et al.* performed this reaction with $MgCl_2$ and $MgBr_2$ to install chlorine or bromine respectively, and it was discovered this methodology also worked with MgI_2 to produce the corresponding iodide (**113b**). The only step that had no literature precedence was the final step in

which the carboxylic acid is protected as a methyl ester. Due to the acid sensitive Boc group, Fischer esterification was ruled out. Treatment with iodomethane and base produced trace amounts of **108**. Esterification using a carbodiimide coupling agent (DCC or EDC) along with catalytic 4-dimethylaminopyridine (DMAP) provided the final amino acid template **108** in reasonable yields. EDC was the optimal coupling agent due to the challenges associated with filtering the byproduct arising from DCC. The urea byproduct from EDC (*N*-[3-(dimethylamino)propyl]-*N*′-ethyl-urea) was washed away readily with acid, while the DCC urea byproduct (*N,N*′-Dicyclohexylurea) produced extremely fine solids that were difficult to filter. With this synthetic scheme, **108a** and **108b** could be prepared on a multigram scale, using column chromatography only for the purification of the final product.

Scheme 32: Synthesis of racemic amino acid template 108.

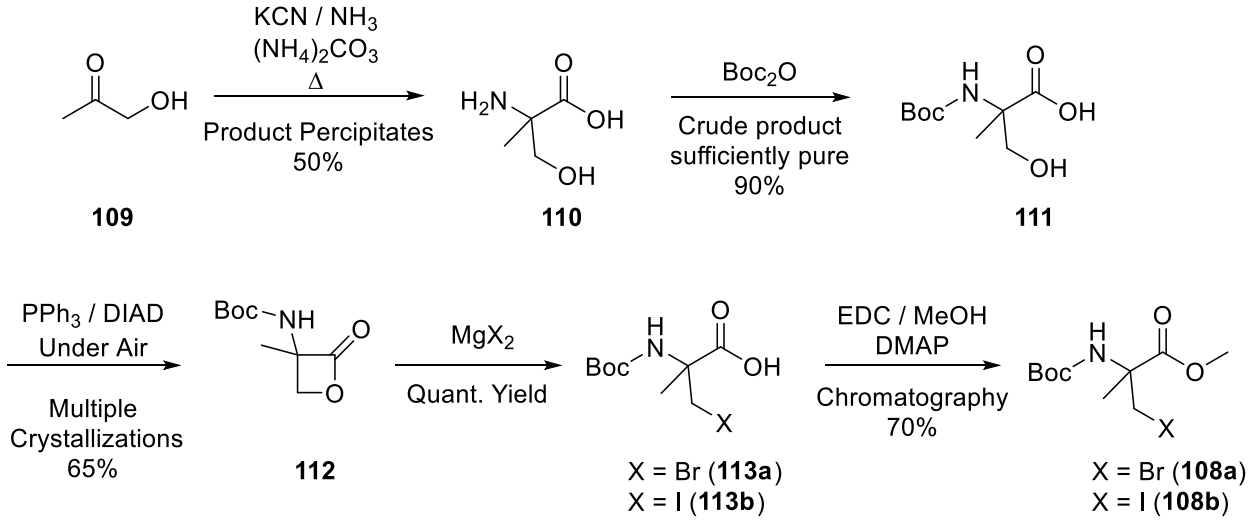

5.4 Optimizing Negishi coupling

With the halogenated amino acid template in hand, multiple attempts were made to perform Negishi couplings of **108a** with a variety of alkyl and aryl organozincs, derived from different precursors. The choice to use a variety of precursors for these organozinc reagents was based on

the previous work on salt effects (Chapters 1-3). These couplings were performed under previously established conditions, with a variety of catalysts and salt additives. Unfortunately, none of these couplings were successful and a range of unwanted byproducts were observed by GC-MS (Scheme 33A). One unexpected byproduct was aziridine ring **114** and control reactions without any catalyst still led to significant **114** (Scheme 33B) illustrating that the inherent basic conditions were responsible for the side product. Performing these couplings with ZnI_2 and MgI_2 additives in an attempt to reopen the ring *in situ* were unsuccessful. Furthermore, the iodo analog (**108b**) was not investigated for these couplings since the weaker C-X bond would likely undergo cyclization even faster than **108a**.

Scheme 33: A) Failed attempts at coupling 108a with various organozinc reagents. B) Proposed mechanism to account for the formation of aziridine byproduct 114.

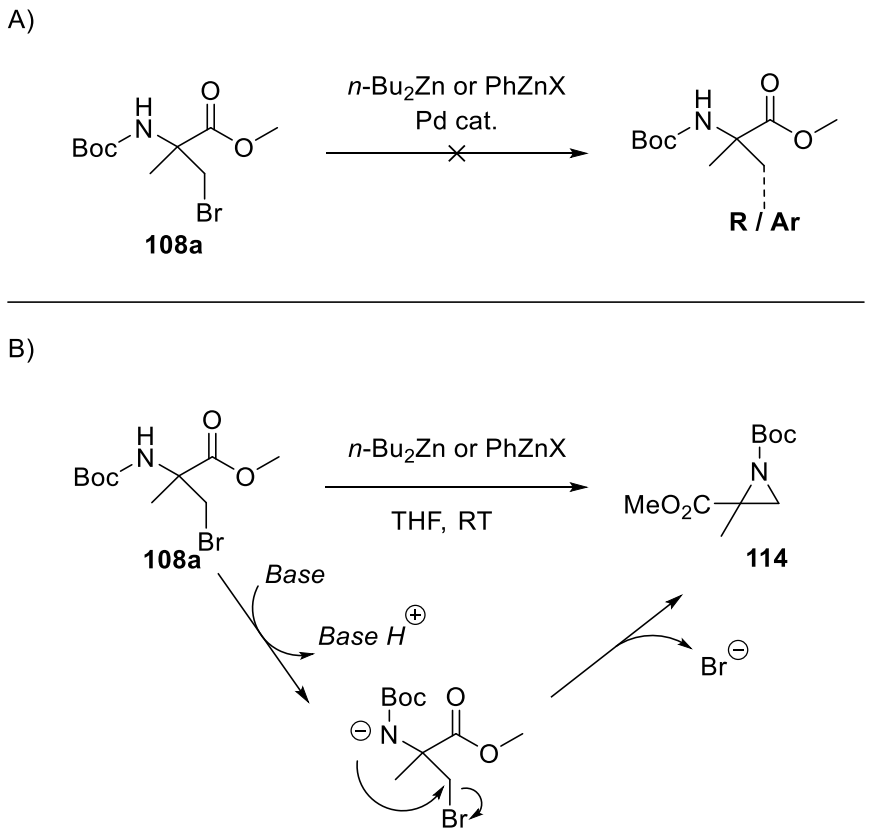

After ruling out use of **108a** as the electrophile, the conversion of **108** to its corresponding organozinc and subsequent use in Negishi coupling was investigated. Initial optimization was performed with brominated template **108a** with no success. It was discovered the C-Br bond was indeed activated by zinc dust preactivated with I_2 in polar solvents such as DMF, DMI and NMP at slightly elevated temperature (40-50 ^oC). While these temperatures are regularly used to synthesize "standard" aromatic and alkyl organozinc reagents, this organozinc undergoes β elimination at these temperatures, releasing methyl methacrylate (MMA) and tert-butylcarbamate (Boc-NH_2). This was not surprising considering the non-methylated analogs are well known to undergo this type of decomposition (Scheme 29).[140] Swapping the bromine (**108a**) for iodine (**108b**) provided a much more active C-X bond that readily reacted at room temperature in just a few minutes. Various conditions were tested to determine the optimal solvent and additive combination needed for efficient activation of the C-I bond (Table 16). DMF was the optimal solvent, consistently producing a 78% yield of the organozinc **115** (entry 1 vs 3 and 4), while the presence of salt had no impact on organozinc formation (entry 2).

Table 16: Optimization of zinc insertion step to form organozinc 115.[a]

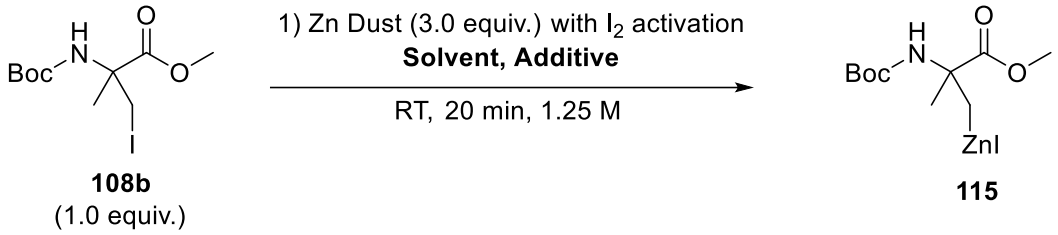

108b
(1.0 equiv.)

115

Entry	Solvent	Additive	Yield of **115**[a]
1	DMF	-	78%
2	DMF	LiCl (2 equiv.)	78%
3	DMI	-	49%
4	NMP	-	56%

[a] Yields determined using ^{1}H NMR spectroscopic analysis of the reaction mixtures and 1,3,5-trimethoxybenzne as an internal standard. Average of two trials.

With the zinc insertion optimized, Negishi couplings with **115** could be attempted. Employing 4-bromomethylbenzoate (**68g**) as the electrophile, since it was known to be active, a variety of *Pd-PEPPSI* precatalysts were screened, along with a variety of salt additives at various temperatures. Unfortunately, initial attempts failed to produce any coupled product and destruction of the organozinc through β elimination, especially upon heating, was the only side reaction. Finally, after an exhaustive catalyst and additive screening, the first successful coupling was achieved after preactivating the catalyst and leaving the reaction overnight at room temperature (Scheme 34). This trial produced a 40% yield of the desired product and confirmed these Negishi couplings were indeed possible with Pd-NHC complexes, albeit at a slow rate.

Scheme 34: First successful coupling with a Pd-NHC complex.

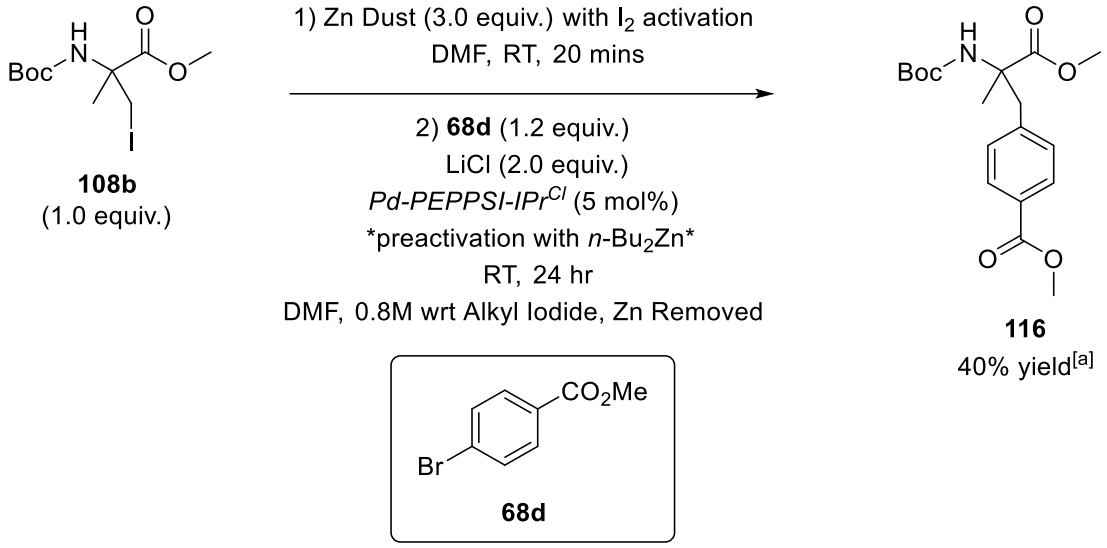

[a] Isolated yield.

With this first hit, optimization could begin to try and increase the efficiency of this transformation (Table 17). A duplicate trial revealed mildly inconsistent yields (entry 1). This capriciousness could be caused by unreacted organozinc remaining after 24 hrs as evident by ^{1}H NMR analysis. Extending the reaction time to 72 hr produced more consistent results (entry 2). A control test in which LiCl was excluded produced no observable product (entry 3), reinforcing the importance of the salt effects discussed in chapters 2 and 3. Substituting *Pd-PEPPSI-IPr* for *Pd-PEPPSI-IPr^{Cl}* produced similar yields of **116** (entry 4). Finally, the preactivation step was shown to be unnecessary with *Pd-PEPPSI-IPr^{Cl}* when the same coupling produced similar yields without a preactivation step (entry 5).

Table 17: Optimization of Negishi coupling of 108b with 68d.

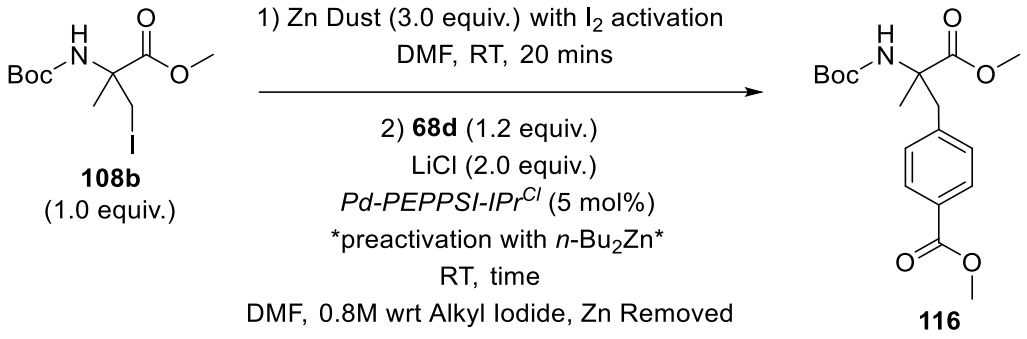

Entry	Time	Conditions	Yield of **116**
1	24 hr	As written above	40-60%
2	72 hr	Longer time	53%
3	72 hr	No LiCl	NR
4	72 hr	*Pd-PEPPSI-IPr* instead of *Pd-PEPPSI-IPr^{Cl}*	45%
5	72 hr	No preactivation	58%

[a] Isolated yields. Average of two trials unless otherwise specified.

With a better understanding of the optimal reaction conditions, other *Pd-PEPPSI* precatalysts were screened. The established coupling conditions were performed with a variety of precatalysts both with and without a preactivation step (Table 18). Unsurprisingly, the most successful couplings used catalysts with lower steric hindrance (*Pd-PEPPSI-IPr*, *Pd-PEPPSI-IPr^{Me}* and *Pd-PEPPSI-IPr^{Cl}*, entries 1-3). This is critical since the larger catalysts will likely hinder the approach of the organozinc. With a less hindered catalyst, both the preactivation and TM steps should be easier. This hypothesis was confirmed when all couplings with larger precatalysts failed (entries 4-7).

Table 18: Catalyst screening for the Negishi coupling between template 108b and 68d.[a]

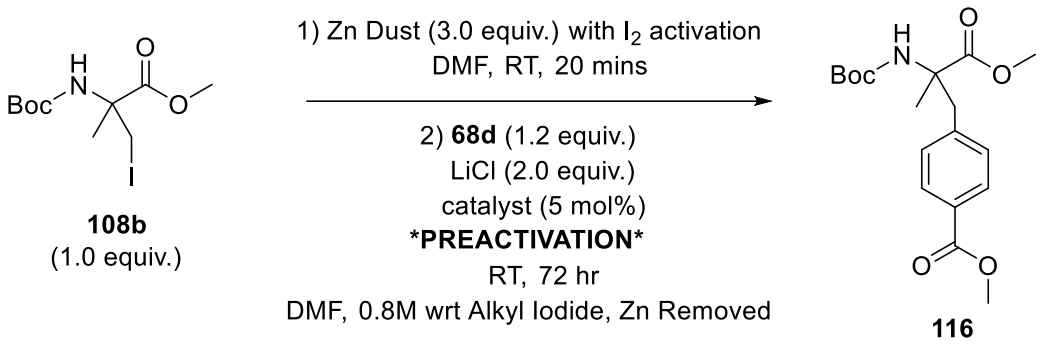

Entry	Precatalyst	No Preactivation[a]	Preactivated[a][b]
1	*Pd-PEPPSI-IPr*	Trace	45%
2	*Pd-PEPPSI-IPr*^{Me}	18%	26%
3	*Pd-PEPPSI-IPr*^{Cl}	58%	53%
4	*Pd-PEPPSI-IPent*	Trace	Trace
5	*Pd-PEPPSI-IPent*^{Cl}	Trace	Trace
6	*Pd-PEPPSI-IHept*	Trace	Trace
7	*Pd-PEPPSI-IHept*^{Cl}	Trace	Trace

[a] Isolated yields. Average of two trials. Trace yields judged by ^{1}H NMR spectroscopy of reaction mixture. [b] Preactivation was performed by first stirring the catalyst, LiCl, Ar-Br and DMF with a few drops of *n*-Bu_2Zn prior to adding the organozinc (**115**).

Under both conditions, the highest yield of **116** was observed with *Pd-PEPPSI-IPr*^{Cl}, making it the catalyst of choice moving forward though it was still unclear what made *IPr*^{Cl} the optimal ligand. Looking closer at the trials using smaller ligands (entries 1-3) an interesting trend appears. Both *Pd-PEPPSI-IPr* and *Pd-PEPPSI-IPr*^{Me} showed significant improvements when preactivated (entries 1 & 2), while *Pd-PEPPSI-IPr*^{Cl} had a slight decrease in yield when preactivated (entry 3). This result was unexpected since the preactivation seemed to benefit *IPr* and *IPr*^{Me}. In addition, less of the organozinc is used as a sacrificial reductant, leaving more available for the desired transformation. Furthermore, *Pd-PEPPSI-IPr*^{Cl} was the only Pd-NHC

complex that was capable of being activated by the bulky organozincs. These differences could once again be explained through a combination of steric and electronic effects arising from the chlorine functionalized backbone. When comparing the preactivated trials of all the *IPr* variants (entries 1-3, preactivated), a trend is seen where an increase in electron donation from the NHC leads to lower yields. This is in line with the results from Chapter 4, where NHC ligands with chlorine substituted backbones helped drive the challenging TM step. Due to the large steric bulk of the organozinc, it is reasonable to believe the TM step is rate limiting in this reaction. Using a chlorine bearing NHC ligands helps increase the electrophilicity of the OA intermediate, leading to higher yields. However, the trials with no preactivation show a different trend where only *Pd-PEPPSI-IPr*^{Cl} can efficiently enter the catalytic cycle (entry 3), while *Pd-PEPPSI-IPr*^{Me} shows some reactivity (entry 2) and *Pd-PEPPSI-IPr* gives no reaction (entry 1). This could be rationalized by the large groups on the backbone helping push the pyridine ring away, likely an essential step for preactivation. This would explain why *Pd-PEPPSI-IPr*^{Me} shows some potential, but the increase in yield upon preactivation still suggests not all of the catalyst is being activated by **115**. The chlorine functionalized precatalyst *Pd-PEPPSI-IPr*^{Cl} likely has both steric and electronic driving forces that work together to get it on cycle and encourage TM.

One aspect of these couplings that differs from all the other Negishi coupling in this thesis was the disregard for the excess Zn^0 remaining after the insertion step. Normally after forming an organozinc reagent from zinc powder, the residual zinc is allowed to settle to the bottom of the flask, and the solutions are carefully collected with a syringe and needle without disturbing the solids. However, the zinc dust is often left in the reaction solution when performing couplings with the non-methylated amino acid.[133–135,146] The zinc dust is seemingly inert to the coupling conditions and left in out of convenience. Up until now, the excess zinc was removed by letting it

settle before carefully collecting the supernatant by syringe. It is possible the zinc dust could act as a reducing agent and help the precatalysts enter the active cycle. The established conditions were tested under similar conditions except all reagents were added to the same vial, resulting in a slurry of zinc dust (Table 19). It was immediately obvious that zinc dust was incapable of reducing the palladium precatalyst under these conditions. The zinc dust lowered the yield of the functional catalysts (*Pd-PEPPSI-IPr*^{Cl} and *Pd-PEPPSI-IPr*^{Me} entries 1 & 2) and failed to activate *Pd-PEPPSI-IPr* (entry 3). Based on these results, excess zinc dust was removed in further trials.

Table 19: Negishi coupling of 108b and 68d performed with and without excess zinc dust.[a]

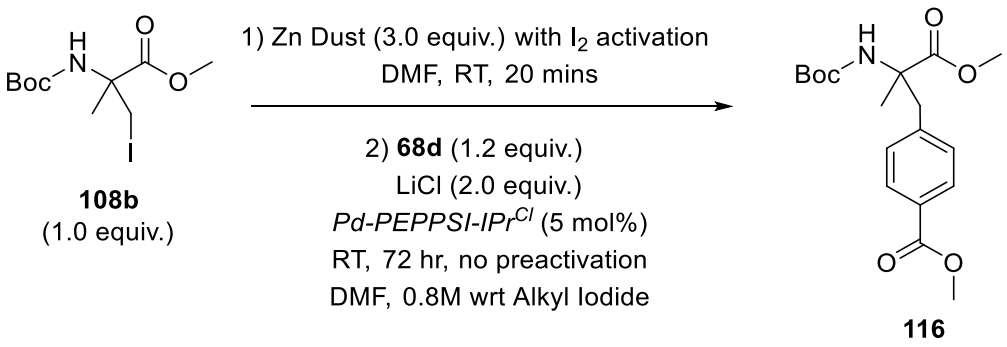

Entry	Precatalyst	Zn Slurry	Zn Removed
1	*Pd-PEPPSI-IPr*^{Cl}	52%	58%
2	*Pd-PEPPSI-IPr*^{Me}	Trace	18%
3	*Pd-PEPPSI-IPr*	Trace	Trace

[a] Isolated yields, average of two trials. Trace yields judged by ^{1}H NMR of reaction mixture

The catalyst loading was varied to see how low it could go in an effort to make this methodology more applicable to large-scale production. Performing the established couplings with decreasing catalyst loadings severely decreased the yields (Table 20, entries 1-3). Dropping the catalyst loading from 5 mol% down to 2.5 mol% lowered the yield to 18%, and 1 mol% produced

only trace amounts of **116**. Considering this was a model reaction with an activated electrophile, it was clear the catalyst loading could not be lowered any further.

Table 20: Catalyst loading and additive optimization for the coupling of 108b and 68d.[a]

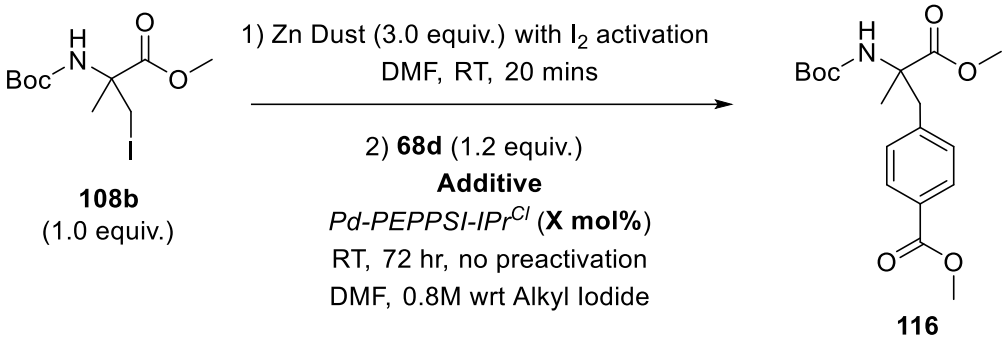

Entry	Additive	Precatalyst loading	Yield of **116**
1	LiCl (2 equiv.)	5 mol%	58%
2	LiCl (2 equiv.)	2.5 mol%	18%
3	LiCl (2 equiv.)	1.0 mol%	NR
4	LiBr (2 equiv.)	5 mol%	Trace
5	$MgCl_2$(2 equiv.)	5 mol%	Trace
6	NaI (2 equiv.)	5 mol%	NR

[a] Isolated yields, average of two trials. Trace yields judged by ^{1}H NMR spectroscopy of the reaction mixture

Lastly, the choice of salt additive was investigated. It was already made clear that LiCl was crucial for these couplings (Table 17, entry 3). Various salt additives were tested including LiBr, $MgCl_2$ and NaI, all of which failed to produce results similar to that of LiCl (Table 20, entry 1 compared to entries 4-6). The decrease in yield upon switching to LiBr was confusing, since in all previous studies on the salt effect, LiBr and LiCl displayed very similar reactivity.[97,104,107,114] Magnesium salts such as $MgCl_2$ were only beneficial to aryl-aryl couplings, owing to the increase in solvent polarity.[107] This salt additive showed no reactivity, which is not surprising considering

the reaction is already conducted in a very polar solvent. Finally, the I_2 used to activate the zinc dust led us to attempt the reaction using NaI, but this salt had poor solubility in DMF, and no reaction was observed. These results showed there was something unique about LiCl which allows this reaction to proceed.

To decipher the role of LiCl the ^{1}H NMR spectra of organozinc **115** in the presence of the salt additives was collected. Solutions of **115** were prepared and dosed with the additives of interest. These solutions were then analyzed using ^{1}H NMR spectroscopy, calibrating the axis on the upfield CH_3 signal of the solvent (Figure 18). These results provided some insights into what was unique about LiCl versus all the other additives tested. All samples with salt additives showed a general upfield shift for the two C-H signals alpha to the zinc atom. This suggested the formation of higher order zincates as previously reported by Organ *et al.* (chapter 1).[97,114] As halides coordinate to the zinc centre, they form anionic zincates. These zincates are electron rich and push the alpha C-H protons upfield, indicating an increase in the nucleophilicity of the organozinc which helps drive the TM step forward. This increase in reactivity can be compared by examining how far upfield the alpha proton signals are shifted in comparison to a salt-free sample. When considering the shifts for the different salt additives, it becomes clear why LiCl is far superior to LiBr. The latter had the smallest shift while LiCl had the largest upfield shift. It would seem the choice of halogen is critical since $MgCl_2$ and LiCl both had larger shifts than LiBr. These results point to a previously established role of salt additives, the formation of higher order zincates. Tetramethylethylenediamine (TMEDA), a common bidentate chelator was also tested, showing a surprising downfield shift of the alpha proton signals (see SI). These findings confirmed that LiCl was the best salt additive for these couplings.

Figure 18: ^{1}H NMR spectra of organozinc 115 in DMF with various salt additives.

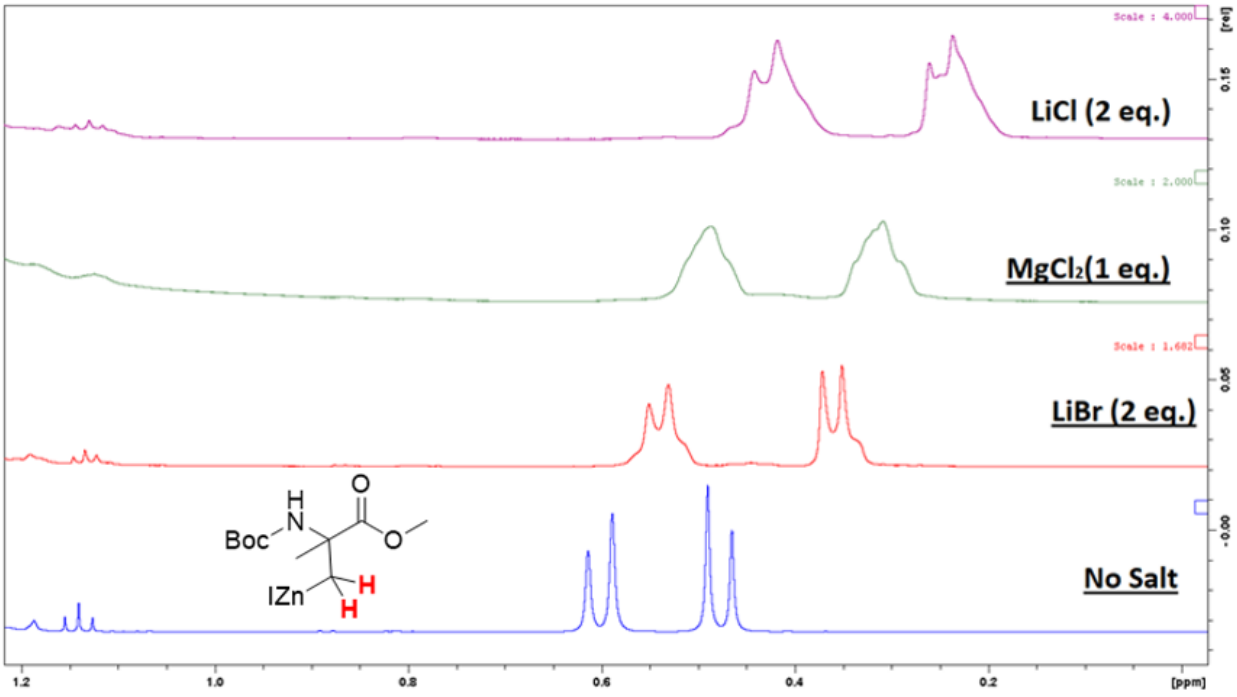

5.5 Substrate scope

Until this point, the only coupling partner used for couplings with **108b** was 4-bromomethylbenzoate (**68d**). This substrate served its purpose as an easy electrophile to activate, with minimal steric hindrance. It was important to test the optimized conditions on more challenging substrates that more closely resemble those that are likely to be employed in drug discovery. A handful of heteroaryl halide coupling partners were tested. These are substrates that are more likely to be incorporated into pharmaceuticals, but more challenging for palladium catalysis due to unwanted interference from the Lewis basic functional groups.[80] Not surprisingly, the yield of these couplings decreased when these new electrophiles were employed (Scheme 35). Various pyridine derivatives were tested, with disappointing and sometimes inconsistent results. The coupling was inconsistent with 2-iodopyridine, producing between 38-58% of the coupled product **117**, while 3-iodopyridine produced none of the desired coupled product (**121**).

Regioselective activation of a polyhalogenated pyridine was attained with **118**, albeit with low and inconsistent yields. Performing the reaction at a higher temperature with a preactivation step produced no significant increase in coupling. The analogous reaction with a polyhalogenated pyrimidine **119** failed entirely, potentially due to the bromine/iodine combination or the switch from pyridine to pyrimidine. Finally, the most challenging coupling partner, iodouracil (**120**), was also incapable of participating in the coupling. From these preliminary results it is clear this methodology requires further optimization for coupling of such challenging electrophiles.

Scheme 35: Substrate scope for the coupling of 108b.

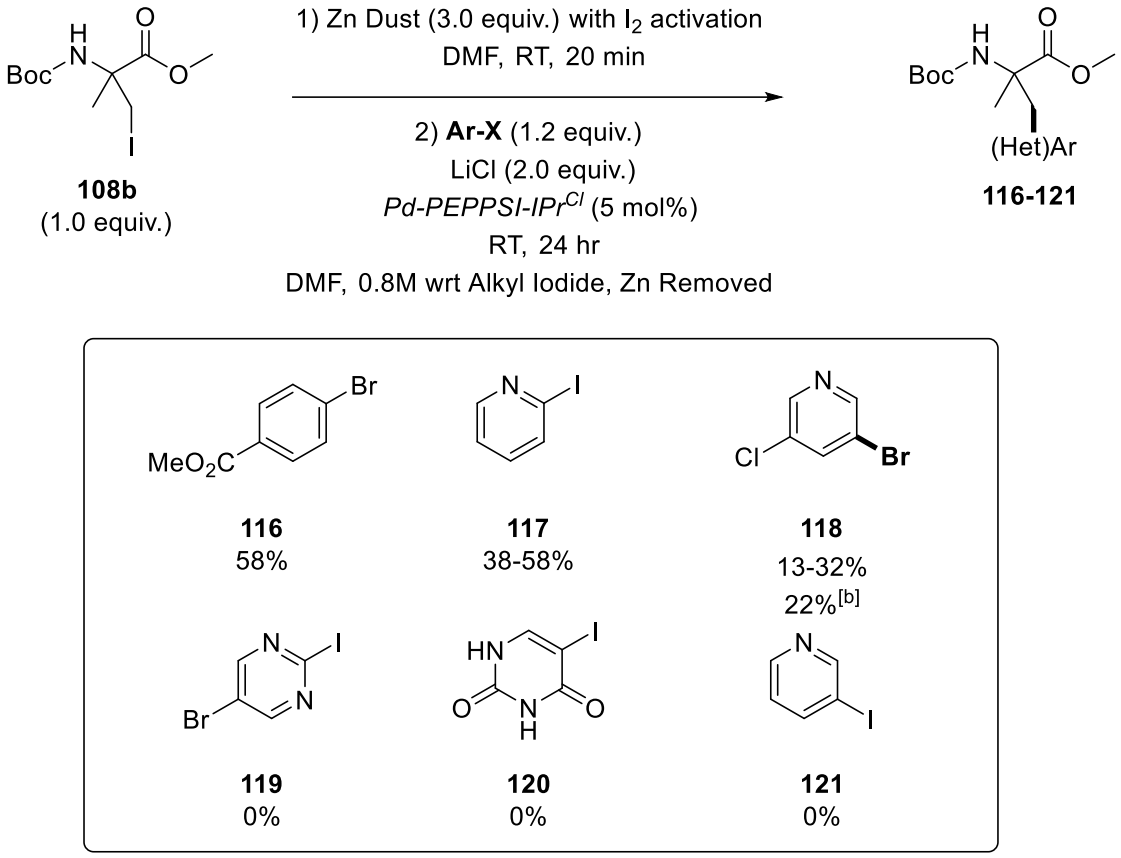

[a] Reactions performed in duplicate. Average of two trials, unless otherwise specified. Isolated yield is reported. [b] Catalyst was preactivated with *n*-Bu_2Zn and the reaction mixture was heated at 50 °C for 3 hr.

5.6 Synthesis of chiral amino acid template

With the zinc insertion and Negishi steps nearly optimized, it was important to prepare an enantiopure amino acid template. Both lactone **112** and N-Boc-α-methyl serine **111** are commercially available as enantiopure intermediates; however, they are very expensive, making the large-scale preparation of the final amino acid template with these intermediates impractical. A chiral resolution was chosen for the sake of keeping the synthesis short and easily scalable. While chiral resolutions lead to the loss of at least half the material, for initial drug discovery efforts this is acceptable. In fact, having access to both enantiomers in one preparation actually benefits drug discovery campaigns. Furthermore, there was already a reliable procedure reported

for the chiral resolution of a closely related derivative of α-methyl serine using an inexpensive and readily available resolving agent.

The first step of the racemic amino acid synthesis was taken from a report by GSK on a scale up campaign for GSK1842799, an API being investigated for its ability to treat transplant rejection and autoimmune diseases.[143] The authors could prepare racemic α-methyl serine (**110**) on kilogram scales, with the only purification being precipitation with acetone as a counter solvent (Scheme 36). From there, a Fischer esterification protected the carboxylic acid as a methyl ester. This produced a crude oil which could be resolved using (1S)-(+)-Camphorsulfonic acid (CAS), producing salt **122** with diastereomeric excesses (de%) of up to 95%. The only drawback of this method is the need to install a methyl ester prior to the resolution since our synthetic sequence requires the free carboxylic acid for the cyclization step. Ultimately, this introduced three new steps (esterification, resolution and saponification) to the synthetic sequence in order to set the stereocenter. Fortunately, the esterification and resolution proceeded smoothly and could deliver 30-40g of diastereomeric salt **122** with de% of 94%. Once the ester derivative was resolved, it could be hydrolyzed under basic conditions to regenerate the now chiral a α-methyl serine (**123**) and release the resolving agent. From there, the final chiral amino acid template could be prepared using the same procedures for the racemic material. Surprisingly, the final chiral amino acid **127** was an oil while the racemic template **108b** was a solid. With the chiral amino acid template in hand, it was possible to confirm the optimized conditions worked on the enantiopure amino acid. Indeed, when subjected to the optimized zinc insertion and Negishi coupling conditions, a yield of 55% was achieved of the coupled product (**128**).

Scheme 36: Synthesis of chiral amino acid template 127 and use in a Negishi coupling.

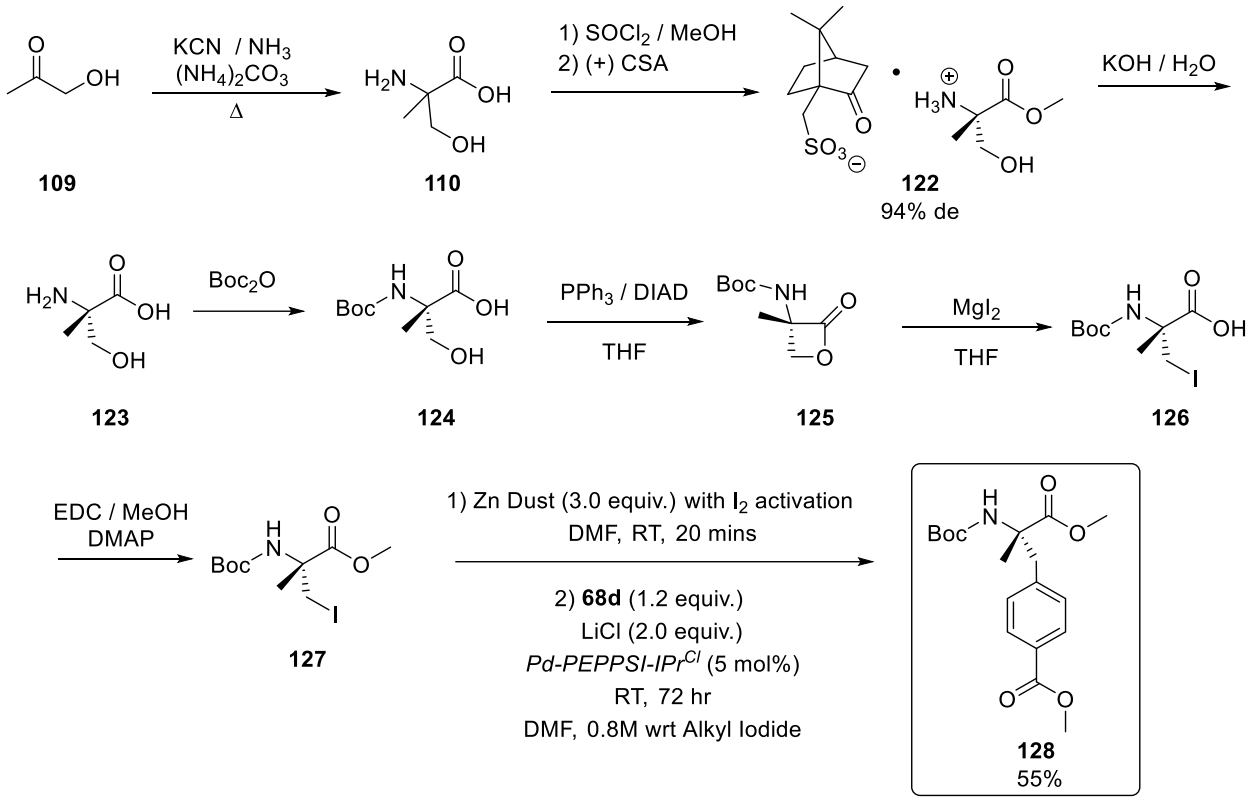

5.7 Conclusion and outlook

The work conducted so far has laid the groundwork for this project. Initial work centred around preparing and optimizing the Negishi coupling of a racemic α-methyl amino acid template. By using the racemic amino acid, the synthesis was expedited so time could be spent on the challenging Negishi coupling. With help from literature reports on metallating analogous non-methylated amino acids DMF was established as the ideal solvent for converting the template amino acid to its corresponding organozinc. After optimization, it was determined that the subsequent Negishi coupling worked best using *Pd-PEPPSI-IPr*^{Cl} in DMF with LiCl additive. With these conditions the bulky nucleophile could be coupled with various aryl and heteroaryl halides. Finally, the enantioenriched amino acid was synthesized to provide a template that can be used for peptide synthesis.

There remains a great deal of work to further develop this methodology and achieve its final objectives. With the findings so far, there are now many new routes open to continue this project. One end goal near completion is the generation of a large library of amino acids bearing this α-methyl group. To realize this goal, the coupling should be further optimized to allow for a broader substrate scope. Furthermore, the chemistry must be scaled up as couplings to this point have only been performed on 0.25 mmol scales, thus production of the template will similarly need to be scaled.

Once the Negishi reactions are mastered, this chemistry can be migrated to short peptides. This would further enhance its use in drug discovery campaigns and give credence to the importance of studying the intricacies of palladium catalysis. However, this endeavor is complicated by the choice of protecting group. Initially this chemistry was conducted with a N-Boc and methyl ester protecting groups. N-Boc was chosen for its versatility, ease of installation and removal, and resistance to the basicity of an organozinc. These properties made Boc protecting group a wise choice for the coupling of individual amino acids, but for peptide synthesis, F-moc protecting groups are dominant. This is because the conditions used to cleave it are much milder than those needed for Boc groups. Furthermore, many biorelevant modifications such as glycosylation and phosphorylation are incompatible with the strong acidic conditions needed to cleave Boc groups.[147] For these reasons, future work will need to investigate the use of different protecting groups. This will entail the synthesis of different versions of the amino acid template with different protecting groups, and the incorporation of these residues in short peptides. Once these peptides are prepared, work can begin on performing Negishi couplings with peptides.

Finally, one last avenue for this project is the preparation of other α-methylated templates. Current efforts in the Organ lab are focused on extending the CH_2X group to longer chains. This

will allow for even larger libraries of unnatural amino acids bearing these α-methyl groups. Currently, Kyle Passley, a PhD candidate within our group, is working on preparing an analog of **127** bearing a CH_2CH_2X sidechain. With the longer chain it might be possible to switch from iodine to bromine or even chlorine. With the steric bulk further away from the C-X bond, the TM should be easier. Furthermore, with the N-Boc group an extra carbon away, the β elimination pathway should be shut down. This will make Negishi coupling with this template much easier since heating would now become an option, if necessary. Indeed, this new compound could provide a new route to a wide range of unnatural amino acids.

Chapter 6: Conclusions and outlook

The work from the final amino acid project highlights the importance of the previous chapters, and ultimately brings this thesis around full circle. This thesis began with the study of salt additives on Negishi coupling in aryl (electrophile)-alkyl (nucleophile) couplings. During this time, two new roles for salt in these couplings were discovered. Product inhibition by the ZnX_2 harmed the reaction but this could be circumvented using LiBr, which is believed to sequester the ZnX_2. The second overlapping role was prolonging the catalyst lifetime.

Another aspect of the aryl-alkyl couplings discovered was the beneficial effects of chlorine modified NHC ligands, inherently resisting product inhibition and prolonging catalyst lifetimes. This chlorine effect was investigated on alkyl-alkyl couplings to see if there were similar trends. The delicate balance between steric and electronic effects were benchmarked by preparing the new methylated catalysts (*IPent^{Me})Pd(cinnamyl)Cl* and (*IHept^{Me})Pd(cinnamyl)Cl*. The results from this case study showed that chlorine bearing NHCs both restrict the motion of the alkyl chains and provide an electronic driving force that enhances both TM and RE.

In the final chapter, the knowledge and experience from the previous chapters was applied to an industrial collaboration. The Negishi coupling of an α-methylated amino acid was accomplished through the development of optimized reaction conditions that included a salt additive (LiCl) which was likely forming higher order zincates. The other critical aspect was the use of *Pd-PEPPSI-IPr^{Cl}* as a catalyst. The small, chlorine bearing catalyst helped address the challenging TM step by offering a less sterically hindered approach for the bulky organozinc and providing an extra electronic driving force to help drive TM (and RE). This final chapter truly exemplifies the importance of studying the mechanistic intricacies of these reactions. The salt effect was initially discovered serendipitously by curiosity driven research and has since turned

into a corner stone of our group's research. Considering the depth and complexity of this field there is certainly a plethora of interesting details that remain to be discovered.

Chapter 7: Supplemental information (by chapter)

7.1 General experimental

All experiments were conducted under an atmosphere of dry nitrogen in oven or flame dried glassware using standard Schlenk techniques unless noted otherwise. Glovebox manipulations were performed in an MBraun Unilab glove-box under an atmosphere of dry nitrogen. All reagents were purchased from Sigma-Aldrich, Oakwood chemicals, or Alfa Aesar and were used without further purification, unless noted otherwise. Unless otherwise specified, precatalysts were provided by Total Synthesis Ltd., Toronto, Canada. All reaction vials (20 mL disposable scintillation vials) were purchased from VWR. Analytical thin layer chromatography (TLC) was performed on EMD 60 F254 pre-coated aluminum plates and spots were visualized with UV light (254 nm). Column chromatography purifications were carried out using the flash technique on ZEOprep 60 silica gel (40 - 63 μm) unless noted otherwise. NMR spectra were recorded on a Bruker 400 AVANCE II, Bruker 500 AVANCE III or Bruker 600 AVANCE III spectrometer. NMR spectra using non deuterated solvents were performed using proton gradient shimming. DMI (1,3-dimethyl-2-imidazolidinone) was referenced to tetramethylsilane (TMS) in order to set its chemical shift. Percent conversion determined by ^{1}H NMR spectroscopy used 1,3,5-trimethoxybenzene as the internal standard. The chemical shifts for ^{1}H NMR spectra are given in parts per million (ppm) referenced to the residual proton signal of the non-deuterated solvent; coupling constants are expressed in Hertz (Hz). ^{13}C NMR spectra were referenced to the carbon signal(s) of the solvent. The following abbreviations are used to describe peak multiplicities: s = singlet, d = doublet, t = triplet, q = quartet, m = multiplet. GC-FID analysis was performed on a Agilent 6850 Series II instrument. High resolution mass spectrometry (HRMS) analysis was performed by the John L. Holmes Mass Spectrometry Facility at the University of Ottawa.

7.2 Supporting info for chapter 2

Synthesis of *n*-BuZnBr (53)[24]

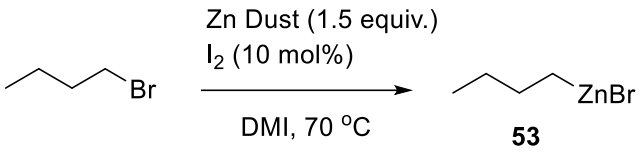

Procedure adapted from literature.[24] In a glovebox, a 100 mL round bottom flask was charged with a stir bar, zinc dust (1.0 g, 15 mMol, previously dried under high vacuum at 100 °C) and iodine (127 mg, 0.5 mMol). The flask was sealed with a rubber septum and moved out of the glovebox. Dry 1,3-dimethyl-2-imidazolidinone (DMI, 10 mL) and 1-bromobutane (1.1 mL, 10 mMol) were added by syringe. The flask was then placed in an oil bath preheated to 70 °C and the mixture stirred vigorously for 12 hr after which it was allowed to cool to room temperature. The resulting solution of *n*-BuZnBr was then titrated using Knochel's method.[148]

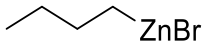

n-Butyl Zinc Bromide (**53**) ^{1}H NMR (DMI, 300 MHz) δ 1.26 (m, 2H), 1.06 (m, 2H), 0.61 (t, *J* = 7.3Hz, 3H), 0.05 (t, *J* = 7.8Hz, 2H) ppm.

Synthesis of *n*-Bu_2Zn (70)[149]

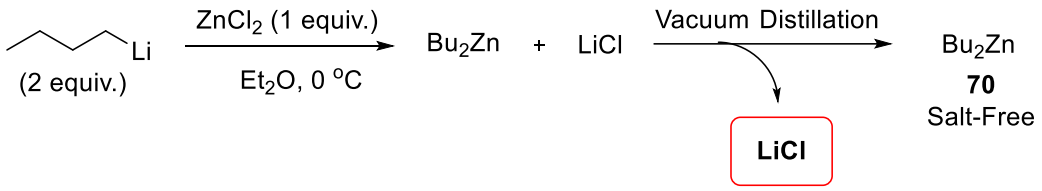

In a glovebox, a 100 mL round bottom flask was charged with a stir bar and dry free flowing zinc chloride (3.407 g, 25 mMol). The flask was sealed with a rubber septum and moved out of the

glovebox. Dry, inhibitor-free diethyl ether (24 mL) was added by syringe. The solution was stirred vigorously for approximately 30 min. or until the zinc chloride was fully dispersed. The flask was then placed in an ice bath and n-Butyllithium added drop-wise over 20 min. (20 mL of a 2.5 M solution in hexanes, 50 mMol). The reaction was then removed from the ice bath and allowed to warm to room temperature while stirring. After 60 min. stirring was stopped and the LiCl solid allowed to settle to the bottom of the flask. While the salt settles, a short path distillation apparatus was assembled with a 100 mL boiling flask containing a stir bar, a 50 mL receiving flask, and a rubber septum used to seal the thermometer joint. This apparatus was then evacuated and purged with nitrogen (3X). The supernatant in the first reaction flask was carefully collected using a 24 mL syringe and a long needle. The distillation apparatus was put under positive pressure of nitrogen and the rubber septum was removed. The supernatant was then added to the boiling flask by threading the long needle through the thermometer joint and into the boiling flask. The rubber septum was placed back into the thermometer joint and the boiling flask was placed in an oil bath and stirred at 40 °C. The solvent mixture (diethyl ether/hexanes) was removed under a gentle vacuum until only the crude *n*-Bu_2Zn was left (pale yellow oil). The vacuum was reduced to 500 mTorr and the receiving flask was placed in a liquid nitrogen bath. The neat *n*-Bu_2Zn was vacuum transferred until only a small amount of cloudy oil remained in the boiling flask. The apparatus was removed from the oil/liquid nitrogen baths and purged with nitrogen. The receiving flask was removed from the distillation apparatus and quickly sealed with a new rubber septum. This flask was immediately placed back in the liquid nitrogen bath and evacuated/purged with nitrogen (3X) using a needle and syringe connected to a Schlenk line. The flask was removed from the liquid nitrogen bath and 12 mL of dry THF was slowly added. The flask was allowed to warm to room temperature and the resulting solution was titrated using Knochel's method.[148] The remaining

contents of the boiling flask were slowly and carefully quenched by drop-wise addition of isopropanol, followed by water.

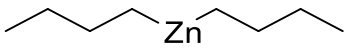

Di-n-Butyl Zinc (**70**) ^{1}H NMR (THF, 500 MHz) δ 1.47 (m, 4H), 1.24 (m, 4H), 0.83 (t, *J* = 7.3 Hz, 6H), 0.11 (t, *J* = 7.8 Hz, 4H) ppm.

General coupling procedure A (coupling of *n*-BuZnBr 53)

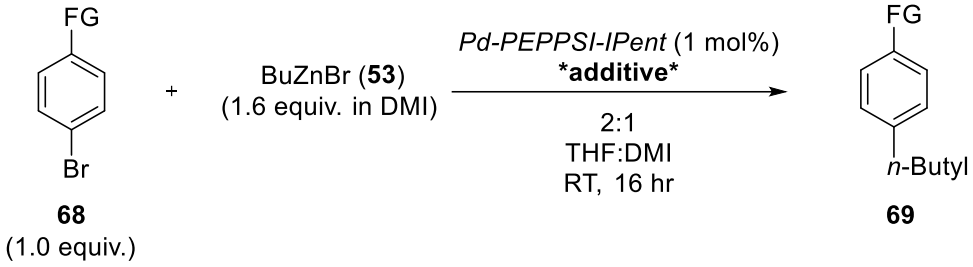

In a glove box, a 20 mL disposable scintillation vial was charged with a small stir bar, aryl bromide (0.4 mMol), *Pd-PEPPSI-IPent* (3 mg, 0.004 mMol) and any necessary additives (e.g. LiBr 69 mg, 0.8 mMol). Dry THF was added (twice the volume of the DMI organozinc solution required, e.g. 2.1 mL) and the solution stirred until everything dissolved. The solution of *n*-BuZnBr in DMI (1.05 mL of a 0.6 M solution, 0.64 mMol) was added by syringe. The vial was capped and the solution stirred for 16 h after which it was passed through a pad of dry silica. This plug was flushed with 20 mL of 10% ethyl acetate in hexanes and the resulting eluent washed (3X) with brine. The organic phase was dried over anhydrous sodium sulphate, filtered and concentrated under vacuum. Percent conversion was determined by ^{1}H NMR spectroscopy using 1,3,5-trimethoxybenzene as the internal standard. In a standard experiment, a precisely weighed amount of 1,3,5-trimethoxybenzene (20-30 mg) was added to the crude reaction mixture. The entire mixture was dissolved in $CDCl_3$ (*ca*. 2 mL) and analyzed using ^{1}H NMR spectroscopy. The percent conversion

to the coupled product, byproducts and remaining starting material was quantified by comparing the integrations to the aromatic signal from the internal standard. A representative ^{1}H NMR spectrum is shown below.

Figure 19 Example of a ^{1}H NMR spectra of the crude product with 1,3,5-trimethoxybenzene as an internal standard.

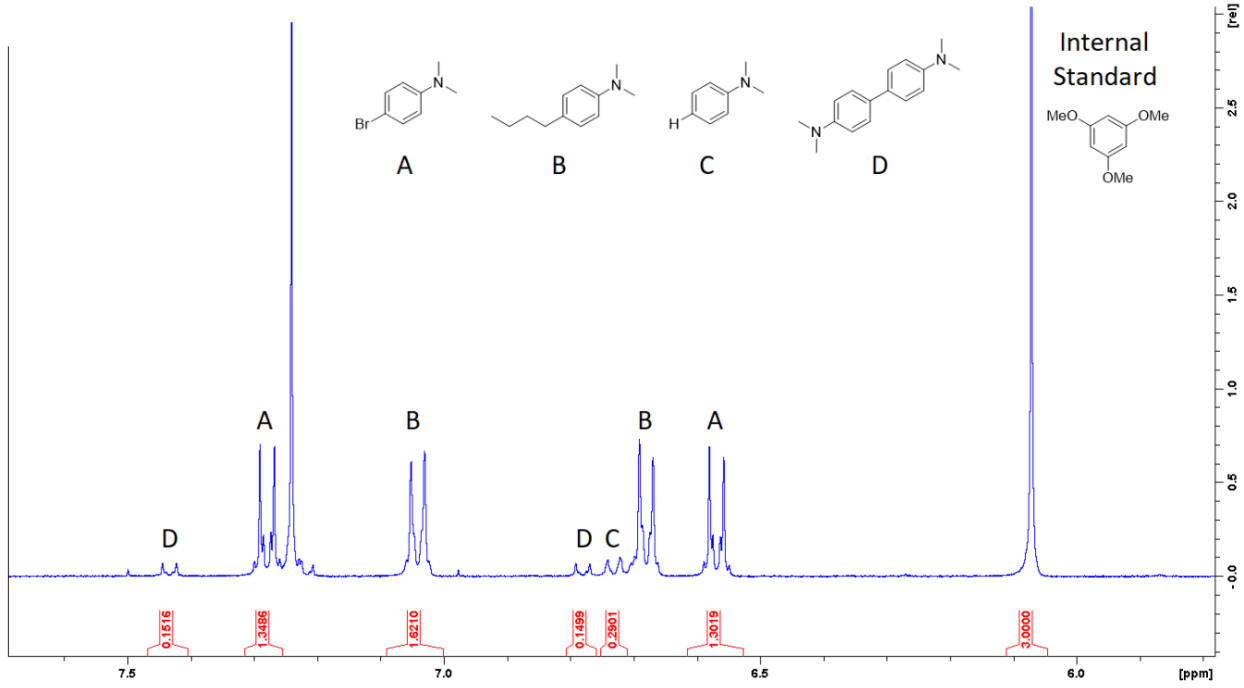

General coupling procedure B (coupling of *n*-Bu_2Zn 70)

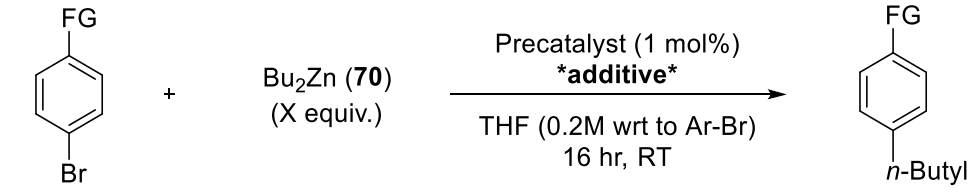

68
(1.0 equiv.)

69

In a glove box, a 20 mL disposable scintillation vial was charged with a small stir bar, aryl bromide (0.4 mMol), *Pd-PEPPSI-IPent* (3.2 mg, 0.004 mMol) or *Pd-PEPPSI-IPent*^{Cl} (3.4 mg, 0.004

mMol) and any necessary additives (e.g., LiBr 69 mg, 0.8 mMol). Dry THF was added so that the final volume was 2 mL after the *n*-Bu_2Zn solution was added (e.g., 1.7 mL). This solution was stirred until everything dissolved. *n*-Bu_2Zn in THF was added by syringe (e.g., 0.30 mL of a 1.25 M solution, 0.24 mMol). The vial was capped, and the mixture was stirred for 16 h after which it was passed through a pad of dry silica gel. This plug was flushed with 20 mL of 10% ethyl acetate in hexanes and the combined eluent was washed (3X) with brine. The resultant organic phase was dried over anhydrous sodium sulphate, filtered, and the solvent was removed under vacuum to give the crude product, which was then purified via flash chromatography. Alternatively, the percent conversion was determined by ^{1}H NMR spectroscopy using 1,3,5-trimethoxybenzene as an internal standard.

Spectral data

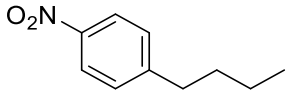

1-*n*-Butyl-4-nitrobenzene (**69a**) Following General Coupling Procedure A, the title compound was isolated as a yellow oil. ^{1}H NMR (500 MHz, $CDCl_3$) δ 8.11 (d, *J* = 8.8 Hz, 2H), 7.30 (d, *J* = 8.8 Hz, 2H), 2.69 (t, *J* = 7.7 Hz, 2H), 1.61 (m, 2H), 1.34 (m, 2H), 0.92 (t, *J* = 7.3 Hz, 3H) ppm; ^{13}C NMR (125 MHz, $CDCl_3$) δ 150.8, 146.3, 129.2, 123.6, 35.6, 33.1, 22.3, 13.8 ppm; HRMS (EI) calculated for $C_{10}H_{13}NO_2^+$, 179.0946; found 179.0929. The spectral data are consistent with those reported in the literature.[150]

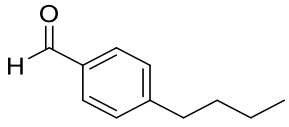

4-*n*-Butylbenzaldehyde (**69b**) Following General Coupling Procedure A, the title compound was isolated as a clear oil. ^{1}H NMR (400 MHz, $CDCl_3$) δ 9.95 (s, 1H), 7.77 (d, *J* = 8.2 Hz, 2H), 7.32 (d, *J* = 8.0 Hz, 2H), 2.67 (t, *J* = 7.8 z, 2H), 1.61 (m, 2H), 1.34 (m, 2H), 0.91 (t, *J* = 7.3Hz, 3H) ppm; ^{13}C NMR (100 MHz, $CDCl_3$) δ 192.0, 150.5, 134.4, 129.9, 129.1, 35.9, 33.2, 22.3, 13.9 ppm; HRMS (EI) calculated for $C_{11}H_{14}O^{+}$, 162.1045; found 162.1026. The spectral data are consistent with those reported in the literature.[151]

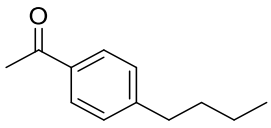

4-*n*-Butylacetophenone (**69c**) Following General Coupling Procedure A, the title compound was isolated as a clear oil. ^{1}H NMR (500 MHz, $CDCl_3$) δ 7.86 (d, *J* = 8.4 Hz, 2H), 7.25 (d, *J* = 8.4 Hz, 2H), 2.65 (t, *J* = 7.7 Hz, 2H), 2.56 (s, 3H), 1.60 (m, 2H), 1.34 (m, 2H), 0.91 (t, *J* = 7.4 Hz, 3H) ppm; ^{13}C NMR (125 MHz, $CDCl_3$) δ 197.9, 148.8, 134.9, 128.6, 128.5, 35.7, 33.3, 26.6, 22.3, 13.9 ppm; HRMS (EI) calculated for $C_{12}H_{16}O^{+}$, 176.1201; found 176.1191. The spectral data are consistent with those reported in the literature.[151]

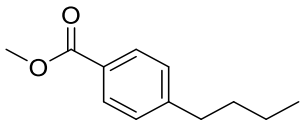

Methyl 4-*n*-Butylbenzoate (**69d**) Following General Coupling Procedure A, the title compound was isolated as a clear oil. ^{1}H NMR (400 MHz, $CDCl_3$) δ 7.93 (d, *J* = 8.3 Hz, 2H), 7.22 (d, *J* = 8.4 Hz, 2H), 3.88 (s, 3H), 2.64 (t, *J* = 7.8 Hz, 2H), 1.59 (m, 2H), 1.33 (m, 2H), 0.91 (t, *J* = 7.3 Hz, 3H) ppm; ^{13}C NMR (100 MHz, $CDCl_3$) δ 167.2, 148.5, 129.6, 128.4, 127.6, 51.9, 35.7, 33.3, 22.3, 13.9 ppm; HRMS (EI) calculated for $C_{12}H_{16}O_2^{+}$, 192.1122, found 192.1150. The spectral data are consistent with those reported in the literature.[152]

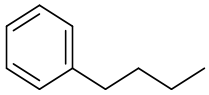

n-ButylBenzene (**69e**) Following General Coupling Procedure A, the title compound was isolated as a clear oil. ^{1}H NMR (400 MHz, $CDCl_3$) δ 7.28-7.22 (m, 2H), 7.18-7.12 (m, 3H), 2.59 (t, *J* = 7.7 Hz, 2H), 1.58 (m, 2H), 1.34 (m, 2H), 0.91 (t, *J* = 7.5 Hz, 3H) ppm; ^{13}C NMR (100 MHz, $CDCl_3$) δ 142.9, 128.4, 128.2, 125.5, 35.7, 33.7, 22.4, 13.9 ppm. The spectral data are consistent with those reported in the literature.[153]

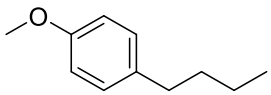

4-n-Butylanisole (**69f**) Following general coupling procedure A, the title compound was isolated as a clear oil. ^{1}H NMR (500 MHz, $CDCl_3$) δ 7.13 (d, *J* = 8.8 Hz, 2H), 6.87 (d, *J* = 8.8 Hz, 2H), 3.83 (s, 3H), 2.60 (t, *J* = 7.7 Hz, 2H), 1.61 (m, 2H), 1.39 (m, 2H), 0.97 (t, *J* = 7.4Hz, 3H) ppm; ^{13}C NMR (125 MHz, $CDCl_3$) δ 157.6, 135.1, 129.3, 113.7, 55.3, 34.8, 33.9, 22.3, 14.0 ppm; HRMS (EI) calculated for $C_{11}H_{16}O^{+}$, 164.1201; found 164.1204. The spectral data are consistent with those reported in the literature.[152]

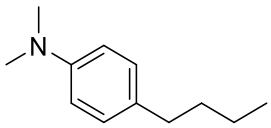

4-n-Butyl-*N,N*-dimethylaniline (**69g**) Following General Coupling Procedure A, the title compound was isolated as a clear oil. ^{1}H NMR (400 MHz, $CDCl_3$) δ 7.05 (d, *J* = 8.7 Hz, 2H), 6.69 (d, *J* = 8.6 Hz, 2H), 2.90 (s, 6H), 2.51 (t, *J* = 7.7 Hz, 2H), 1.55 (m, 2H), 1.34 (m, 2H), 0.91 (t, *J* = 7.3Hz, 3H) ppm;^{13}C NMR (100 MHz, $CDCl_3$) δ 148.9, 131.4, 129.0, 113.1, 41.0, 34.6, 34.0, 22.4,

14.0 ppm; HRMS (EI) calculated for $C_{12}H_{19}N^{+}$, 177.1517; found 177.1518. The spectral data are consistent with those reported in the literature.[152]

7.3 Supporting info for chapter 3

General synthesis of *n*-Bu_2Zn D_{18} (70') and bis-neopentylzinc (84)

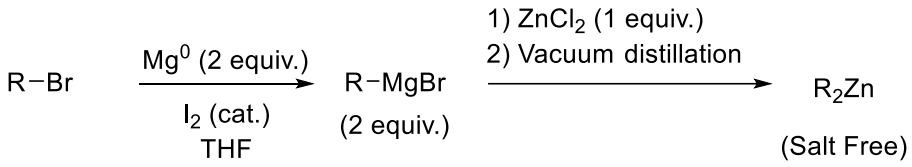

In a glovebox, a 250 mL round bottom flask was charged with a stir bar, Mg turnings (2.43 g, 100 mMol), and iodine (approximately 15 mg). The flask was sealed with a reflux condenser affixed with a rubber septum at the top. This was moved out of the glovebox and dry THF (50 mL) was added through the septa using a 60 mL syringe equipped with a long needle. The Mg turnings were stirred for 15 min, or until most of the black color in solution dissipated after which the alkyl bromide (50 mMol) was added dropwise while gently warming the flask with a heat gun. Once the reaction initiated (as indicated by a mild exotherm and the loss of color from the iodine) the heat gun was turned off and the rest of the alkyl bromide was added dropwise at a rate fast enough to maintain a gentle reflux. After addition of the alkyl bromide was complete, the reaction was stirred for 30 min. The final solution was titrated using Knochel's method[148] after which it was transferred to another 250 mL flask already under Nitrogen using a 60 mL syringe while making sure to note the volume of solution. This flask was then brought into a glovebox and zinc chloride (0.5 equivalent with respect to the Grignard) was added to the vigorously stirred solution. After stirring for 1 hr the flask was put in a freezer to induce precipitation. After the salts settled to the bottom

of the flask (approximately 1 hr) the supernatant was purified using the same vacuum transfer method previously described in the synthesis of n-Bu_2Zn.

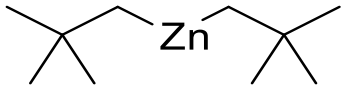

Bis-neo-Pentyl Zinc (**84**) ^{1}H NMR (THF, 500 MHz) δ 0.97 (s, 18H), 0.35 (s, 4H) ppm. The spectral data are consistent with those reported in the literature.[154]

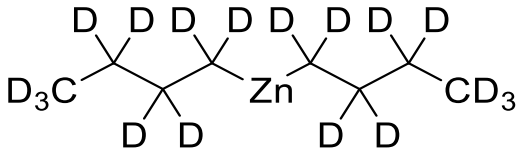

n-Bu_2Zn d_{18} (**70'**) ^{13}C NMR (THF, 500 MHz) δ 15.9, 18.1, 26.2, 31.9 ppm. The spectral data are consistent with those reported in the literature.

General procedure C (sequential addition experiments)

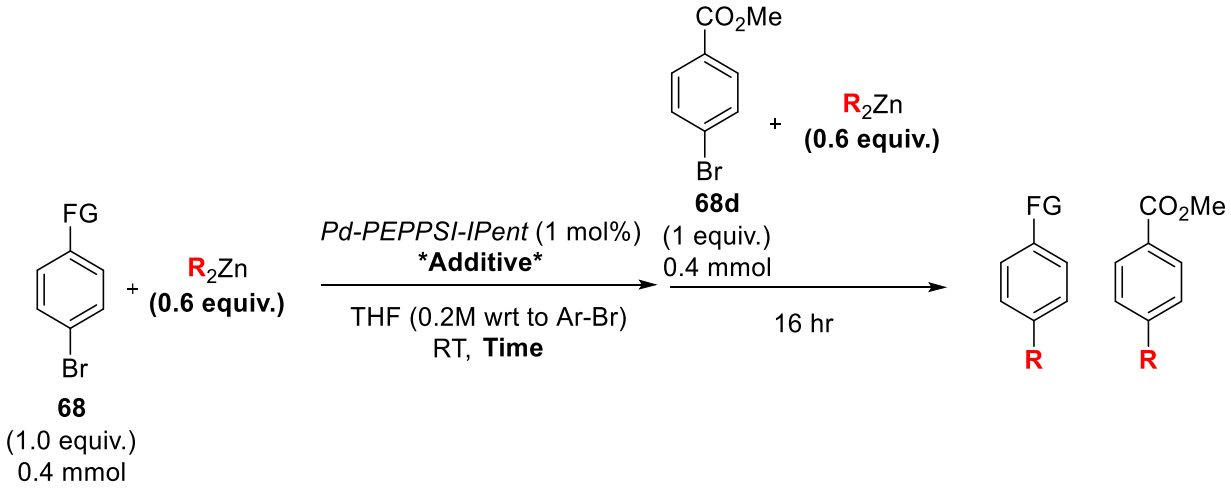

In a glove box, a 20 mL scintillation vial was charged with a small stir bar, aryl bromide (0.4 mmol), Pd- *Pd-PEPPSI-IPent* (3.2 mg, 0.004 mmol) and any additives (e.g., LiBr 69 mg, 0.8 mmol). A separate vial was also charged with methyl 4-bromobenzoate (86 mg, 0.4 mmol). Dry

THF was added to bring the final volume to 2 mL after the first organozinc (R_2Zn) addition (e.g., 1.7mL). The resultant solution was stirred until everything after which the organozinc solution (R_2Zn) was added in one shot by syringe (e.g., 0.30 mL of a 1.25 M *n*-Bu_2Zn solution, 0.24 mMol). The reaction was stirred for the desired amount of time after which the methyl 4-bromobenzoate in the separate vial was quickly dissolved in an aliquot of the organozinc solution (e.g., 0.30 mL of a 1.25 M *n*-Bu_2Zn solution, 0.24 mMol). The resultant solution was then transferred to the first vial using a 1 mL syringe and the reaction mixture was stirred for 16 h before quenching on a pad of dry silica. This plug was flushed with a solution of 10% ethyl acetate in hexanes (20 mL). The resultant organic wash was extracted (3X) with brine and the organic phase was dried over sodium sulphate, filtered, and concentrated under vacuum to give the crude product which was then purified via flash chromatography or analyzed with ^1H NMR spectroscopy using the previously detailed protocol.

General procedure D (isolating catalyst byproducts)

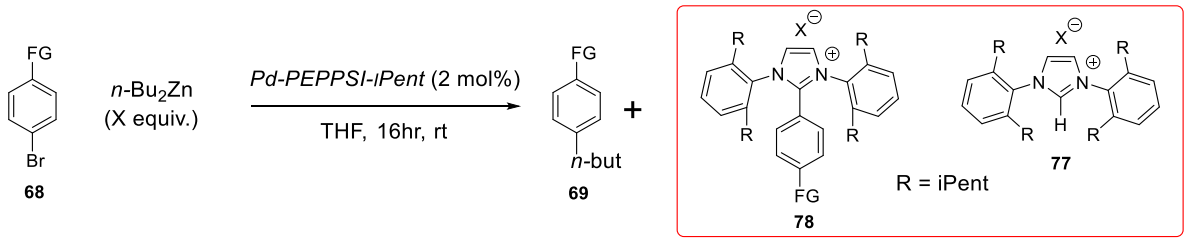

General coupling procedure A was used with the following modifications, the reaction scale was doubled and the precatalyst loading was increased from 1 to 2 mol% (12.0 mg of *Pd-PEPPSI-IPent*, 0.016 mMol). The reaction was quenched on a pad of dry silica and flushed with a solution of 10% ethyl acetate in hexanes (20 mL). The receiving flask was exchanged for a new empty flask, and the plug was flushed subsequently with a solution of 10% methanol in DCM. The resultant MeOH/DCM mixture was concentrated under reduced pressure to give the crude catalyst

byproducts, which were then purified by flash chromatography on a glass pipette column to afford the catalyst byproducts (0 → 1% MeOH in DCM).

Spectral data

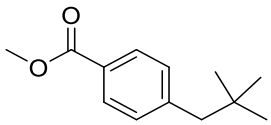

Methyl 4-Neopentylbenzoate (**85**) Follow general coupling procedure A, the title compound was isolated as a clear oil. ^{1}H NMR (500 MHz, $CDCl_3$) δ 7.92 (d, *J* = 8.4 Hz, 2H), 7.17 (d, *J* = 8.4 Hz, 2H), 3.89 (s, 3H), 2.53 (s, 2H), 0.89 (s, 9H); ^{13}C NMR (125 MHz, $CDCl_3$) δ 167.3, 145.4, 130.5, 129.0, 127.8, 52.0, 50.2, 31.9, 29.4; HRMS (EI) calculated for $C_{13}H_{18}O_2^+$, 206.1307; found 206.1286. The spectral data are consistent with those reported in the literature.[155]

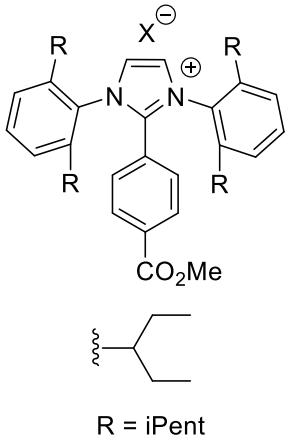

2-(4-Methyl Benzoate)-1,3-bis-(2,6-diisopentylphenyl)imidazolylidinium (**78d**) Following procedure D, the title compound was isolated as a clear oil. ^{1}H NMR (500 MHz, $CDCl_3$) δ 8.35 (s, 2H), 7.83 (d, *J* = 8.7 Hz, 2H), 7.62 (t, *J* = 7.8 Hz, 2H), 7.30 (d, *J* = 7.4 Hz, 4H), 7.19 (d, *J* = 8.7 Hz, 2H), 3.90 (s, 3H), 2.05 (m, 4H), 1.60-1.80 (m, 16H), 0.92 (t, *J* = 7.4 Hz, 12H), 0.63 (t, *J* = 7.4 Hz, 12H); ^{13}C NMR (125 MHz, $CDCl_3$) δ 164.9, 142.8, 142.3, 133.3, 132.3, 131.9, 129.7, 129.6,

128.3, 126.2, 124.8, 52.8, 43.5, 29.3, 26.6, 12.2, 12.1; HRMS (ESI) calculated for $C_{43}H_{59}N_2O_2^+$, 635.4577; found 635.4571.

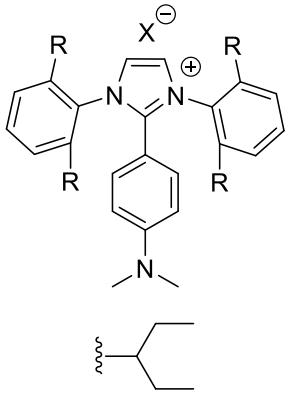

R = iPent

2-(4-*N*,*N*-dimethylaniline)-1,3-bis-(2,6-diisopentylphenyl)imidazolylidinium (**78g**) Following procedure D, the title compound was isolated as a brown oil. ^{1}H NMR (500 MHz, $CDCl_3$) δ 7.81 (s, 2H), 7.66 (t, *J* = 7.8 Hz, 2H), 7.34 (d, *J* = 7.8 Hz, 4H), 6.83 (d, *J* = 9.3 Hz, 2H), 6.30 (d, *J* = 9.3 Hz, 2H), 2.96 (s, 6H), 2.10 (m, 4H), 1.56-1.81 (m, 16H), 0.89 (t, *J* = 7.4 Hz, 12H), 0.67 (t, *J* = 7.4Hz, 12H); ^{13}C NMR (125 MHz, $CDCl_3$) δ 142.8, 142.4, 133.2, 132.7, 131.9, 130.7, 127.5, 126.3, 125.6, 124.8, 51.4, 43.6, 29.2, 27.2, 12.4, 12.3; HRMS (ESI) calculated for $C_{43}H_{62}N_3^+$, 620.4944; found 620.4958.

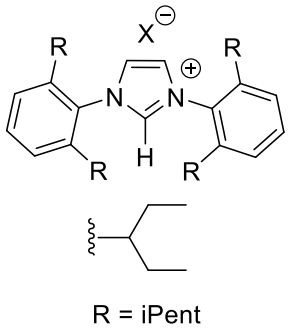

R = iPent

1,3-bis-(2,6-diisopentylphenyl)imidazolylidinium (**77**) Spectra and physical data are in agreement with the literature.[156]

7.4 Supporting info for chapter 4

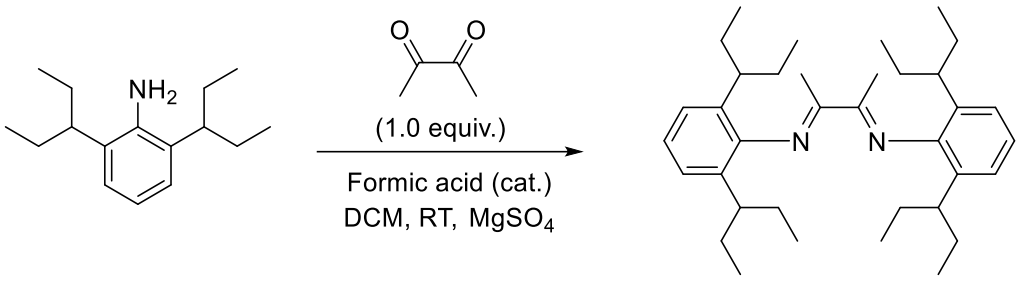

94a
(3.5 equiv.)

95a

A round bottom flask equipped with a stir bar was charged with DCM (10 mL), 2,6-diisopentylaniline (3.277 g, 14.04 mmol, 3.5 equivalent) and 2,3-butanedione (344 mg, 4.0 mmol, 1.0 equivalent). To the stirred solution was added formic acid (~3-4 drops) and a large excess of anhydrous $MgSO_4$ stirred for 24 h, filtered through celite, washed with DCM, concentrated to approximately 10mL, charged with more anhydrous $MgSO_4$ and stirred for 24hr. This process was repeated twice more. The solution was filtered through celite, concentrated under reduced pressure, and purified by column chromatography to separate the bisimine, monoamine and excess aniline. Note, a large ratio of silica to crude product aas required. The bisimine can be eluted with hexanes, the monoamine with 1% EtOAc in hexanes, and the aniline elutes with 2% EtOAc in hexanes. The monoimine and aniline can be recycled using the same procedure.

^{1}H NMR (400 MHz, $CDCl_3$) δ 7.01-7.11 (m, 6H), 2.25 (m, 4H), 2.02 (s, 6H), 1.54-1.69 (m, 12H), 1.34-1.50 (m, 4H), 0.85 (t, J = 7.3 Hz, 12H), 0.76 (t, J = 7.3 Hz, 12H); ^{13}C NMR (100 MHz, $CDCl_3$) δ 167.3, 149.0, 132.4, 123.7, 123.2, 43.1, 29.3, 27.2, 17.0, 12.8, 11.9; HRMS (ESI) calculated for $C_{36}H_{56}N_2H^+$, 517.4522; found 517.4536.

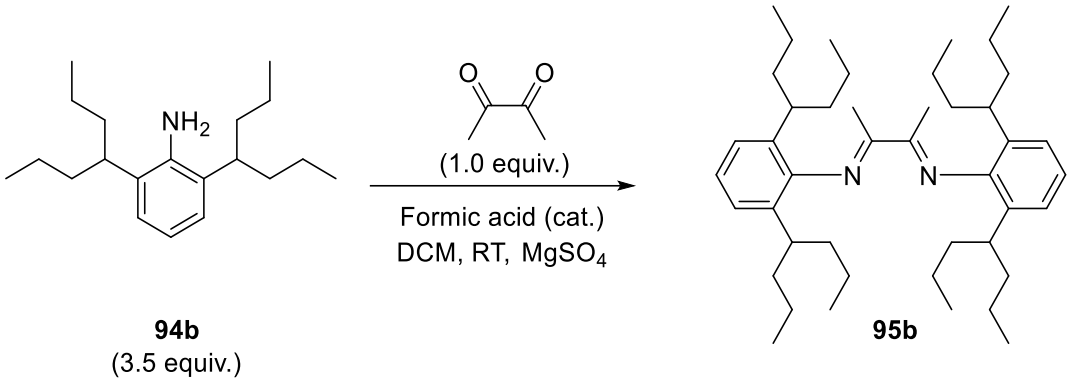

A round bottom flask equipped with a stir bar was charged with DCM (15 mL), 2,6-diisoheptyl aniline (3.500 g, 12.09 mmol, 3.5 equivalent) and 2,3-butanedione (297 mg, 3.454 mmol, 1.0 equivalent). To the stirred solution was added formic acid (~3-4 drops) and a large excess of anhydrous $MgSO_4$. The mixture was stirred for 24 h, filtered through celite, washed with DCM, concentrated to approximately 15mL, charged with more anhydrous $MgSO_4$ and stirred for 24hr. This process was repeated twice more. The solution was filtered through celite, concentrated under reduced pressure and purified by column chromatography to separate the bisimine, monoamine and excess aniline. Yield of bisimine was 0.7883g (1.525 mmol, 38%). Note, a large ratio of silica to crude product was required. The bisimine can be eluted with hexanes, the monoamine with 1% EtOAc in hexanes, and the aniline with 2% EtOAc in hexanes. The monoimine and aniline can be recycled using the same procedure.

^{1}H NMR (400 MHz, $CDCl_3$) δ 7.05 (s, 6H), 2.44 (m, 4H), 2.01 (s, 6H), 1.35-1.61 (m, 16H), 1.10-1.30 (m, 16H), 0.87 (t, J = 7.3 Hz, 12H), 0.80 (t, J = 7.3 Hz, 12H); ^{13}C NMR (100 MHz, $CDCl_3$) δ 167.3, 148.5, 133.1, 123.7, 123.3, 39.2, 38.8, 37.6, 21.2, 20.4, 17.0, 14.4, 14.2; HRMS (ESI) calculated for $C_{44}H_{72}N_2H^+$, 629.5774; found 629.5746.

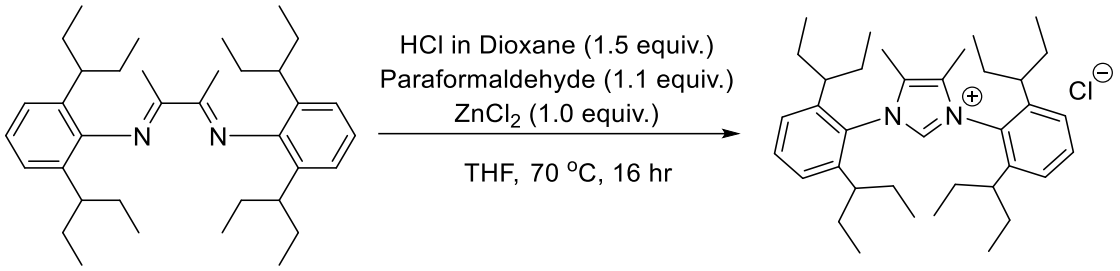

95a
(1.0 equiv.)

97a

Procedure adapted from literature.[47] In a glovebox, a 3-neck round bottom flask equipped with a stir bar, reflux condenser, a Schlenk adapter and a rubber septum was charged with bisimine (1.37 g, 2.65 mmol, 1.0 equivalent), $ZnCl_2$ (361 mg, 2.65 mmol, 1.0 equivalent) and THF (13 mL). The flask was sealed and moved out of the glovebox. Paraformaldehyde (87 mg, 2.9 mmol, 1.1 equivalent) was added against a positive nitrogen pressure followed by a 4M solution of HCl in dioxane (0.99 mL, 3.975 mmol, 1.5 equivalent) using a syringe and long needle. The mixture was stirred and heated at 70 °C overnight. The mixture was concentrated, diluted with EtOAc (ca. 10 mL) and washed with water (3 x 10 mL). The combined aqueous phases were extracted with EtOAc (ca. 10mL), the combined organic phases washed with brine (ca. 10 mL) and dried over anhydrous Na_2SO_4. The organic phase was concentrated using a rotary evaporator until a precipitate begins to form. The flask was removed, stored at −18 °C for 6 h, and the resultant precipitate collected using vacuum filtration. The white precipitate was washed with pentane and dried under high vacuum to yield $IPent^{Me}$ HCl as a white powder (460.8 mg, 0.8608 mmol, 32%). Additional crops of crystals can be obtained by concentrating the filtrate, seeding with crystals from the first crop and storing at−18 °C overnight (270.9 mg, 0.4792 mmol, 18%).

^{1}H NMR (400 MHz, $CDCl_3$) δ 8.45 (s, 1H), 7.62 (t, *J* = 7.8 Hz, 2H), 7.31 (d, *J* = 7.8 Hz, 4H), 2.30 (s, 6H), 1.86-1.98 (m, 4H), 1.48-1.77 (m, 16H), 0.87 (t, *J* = 7.3 Hz, 12H), 0.73 (t, *J* = 7.3 Hz,

12H); ^{13}C NMR (100 MHz, $CDCl_3$) δ 142.9, 133.9, 131.9, 131.2, 130.4, 126.0, 42.7, 28.6, 27.6, 12.5, 11.5, 10.2; HRMS (ESI) calculated for $C_{37}H_{57}N_2^+$, 529.4522; found 529.4501.

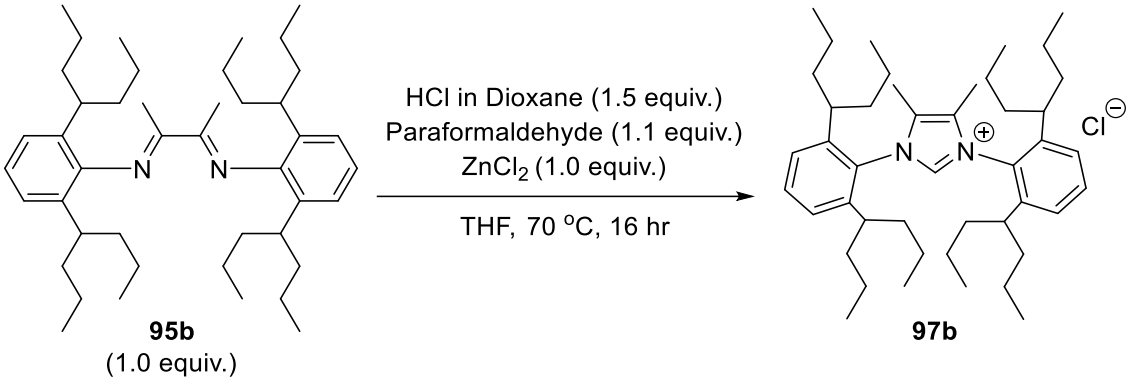

Procedure adapted from literature.[47] In a glovebox, a 3-neck round bottom flask equipped with a stir bar, reflux condenser, a Schlenk adapter and a rubber septum was charged with bisimine (1.90 g, 3.02 mmol, 1.0 equivalent) and $ZnCl_2$ (411 mg, 3.02 mmol, 1.0 equivalent) and THF (15 mL). The flask was sealed and moved out of the glovebox. Paraformaldehyde (99.7 mg, 2.9 mmol, 1.1 equivalent) was added against a positive Nitrogen pressure followed by a 4M solution of HCl in Dioxane (1.15 mL, 3.975 mmol, 1.5 equivalent) using a syringe and long needle. The mixture was stirred and heated at 70 °C overnight. The mixture was then concentrated, diluted with EtOAc (ca. 10mL) and washed with water (3 x 10mL). The combined aqueous phases were extracted with EtOAc (ca. 10mL), the combined organic phases washed with brine (ca. 10mL) and dried over anhydrous Na_2SO_4. The organic phase was concentrated using a rotary evaporator until a precipitate begins to form. The flask was removed, stored at −18 °C for 6 h, and the resultant precipitate collected using vacuum filtration. The white precipitate was washed with pentane and dried under high vacuum to yield IHept^{Me} HCl as a white crystalline powder (814.8 mg, 1.206 mmol, 40%). Additional crops of crystals can be obtained by concentrating the filtrate, seeding with crystals from the first crop and storing at −18 °C overnight (226.3 mg, 0.3340 mmol, 11%).

^{1}H NMR (400 MHz, $CDCl_3$) δ 8.15 (s, 1H), 7.65 (t, *J* = 7.8 Hz, 2H), 7.33 (d, *J* = 7.8 Hz, 4H), 2.23 (s, 6H), 2.07-1.98 (m, 4H), 1.43-1.65 (m, 16H), 1.23-1.38 (m, 4H), 1.09-1.21 (m, 4H), 0.94-1.07 (m, 8H), 0.87 (t, *J* = 7.2 Hz, 12H), 0.82 (t, *J* = 7.2 Hz, 12H); ^{13}C NMR (100 MHz, $CDCl_3$) δ 143.3, 133.6, 132.3, 131.2, 129.5, 126.1, 39.9, 38.5, 38.0, 21.1, 20.4, 14.5, 14.2, 9.9; HRMS (ESI) calculated for $C_{45}H_{73}N_2^+$, 641.5774; found 641.5744.

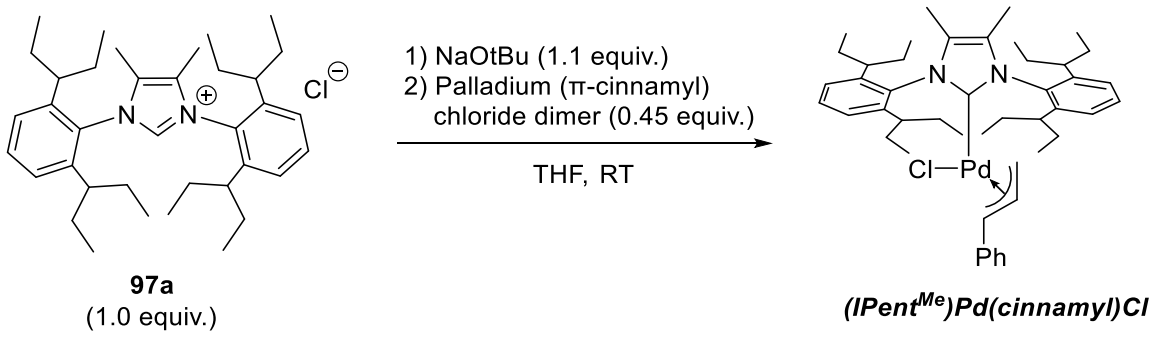

97a
(1.0 equiv.)

(IPent^{Me})Pd(cinnamyl)Cl

In a glovebox, a vial was charged with a stir bar, iPent^{Me} HCl (81.3 mg, 0.1240 mmol, 1.0 equivalent), NaOtBu (13.1 mg, 0.1363 mmol, 1.1 equivalent) and THF (0.83 mL). The mixture was stirred for 5 minutes to produce a light brown solution and ^{1}H NMR of the solution confirmed the absence of the IPent^{Me} HCl. To this solution was added Palladium(π-cinnamyl) Chloride Dimer (28.9 mg, 0.0557 mmol, 0.45 equivalent) to form a yellow solution. The solution was stirred for 20 minutes, at which time ^{1}H NMR of the solution confirms the absence of the Palladium(π-cinnamyl) Chloride Dimer. The reaction mixture was flushed through a plug of neutral alumina, eluting with DCM until the yellow band passes. The filtrate was concentrated under reduced pressure and the resulting yellow oil was dissolved in pentane (ca. 0.5 mL) and concentrated under vacuum to produce a sticky foam. A minimal amount of pentane was added to the foam (ca. 0.5 mL) and the foam was manually broken up to produce a slurry. The solids were sonicated for 5 minutes then collected by filtration, washed with ice cold pentane, and dried under vacuum to produce *(IPent^{Me})Pd(cinnamyl)Cl* as a free flowing, bright yellow powder (32.5 mg, 37%). When

left at room temperature under an inert atmosphere, the complex decomposed over the course of 3-4 months. When stored at -28 °C under an inert atmosphere this complex was stable indefinitely.

^{1}H NMR (400 MHz, $CDCl_3$) δ 7.38 (t, *J* = 7.8 Hz, 2H), 7.10-7.19 (m, 9H), 5.08-5.18 (m, 1H), 4.36 (d, *J* = 13.0 Hz, 1H), 2.55-2.63 (m, 4H), 1.93-2.03 (m, 4H), 1.91 (s, 6H), 1.72-1.82 (m, 4H), 1.47-1.65 (m, 8H), 1.54 (t, 3.7 Hz, 2H), 0.95 (t, *J* = 7.4 Hz, 12H), 0.77 (t, *J* = 7.4 Hz, 12H); ^{13}C NMR (100 MHz, $CDCl_3$) δ 178.0, 143.7, 138.0, 136.6, 128.5, 128.3, 127.7, 127.2, 126.7, 126.3, 125.7, 108.3, 91.7, 77.2, 47.6, 41.2, 40.2, 26.9, 25.7, 12.6, 11.9, 11.5, 11.2, 10.9, 10.6; HRMS (ESI) calculated for $C_{46}H_{65}N_2Pd^+$, 749.4188; found 749.4213.

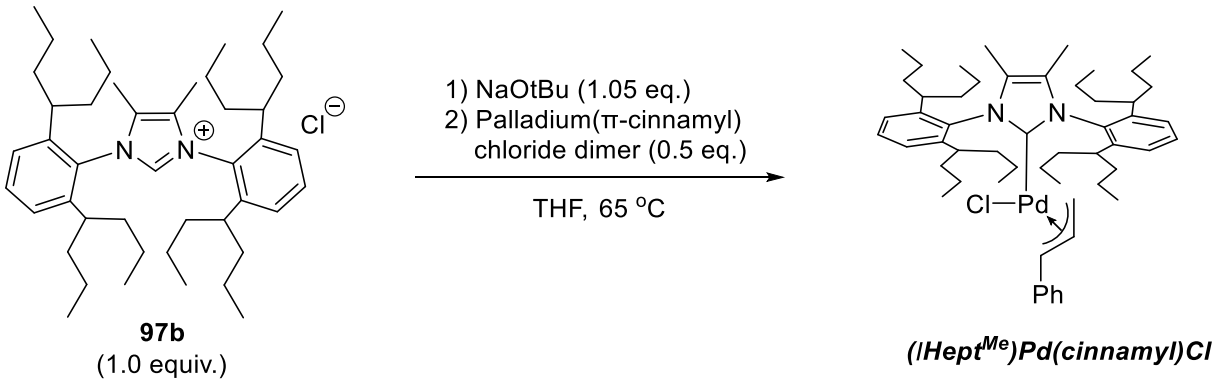

97b
(1.0 equiv.)

(IHept^{Me})Pd(cinnamyl)Cl

In a glovebox, a vial was charged with a stir bar, IHept^{Me} HCl (106.0 mg, 0.1564 mmol, 1.0 equivalent) and NaOtBu (15.8 mg, 0.1642 mmol, 1.05 equivalent) and THF (1.1 mL). The mixture was stirred for 1 hr to produce a light brown solution and ^{1}H NMR of the solution confirmed the absence of the IHept^{Me} HCl. To this solution was added Palladium(π-cinnamyl) Chloride Dimer (40.5 mg, 0.0782 mmol, 0.50 equivalent) to form a yellow solution. The mixture was stirred at room temperature for 9 hr, at which time ^{1}H NMR of the solution shows only the desired complex and no starting materials. The reaction mixture was concentrated under vacuum at room temperature then flushed through a plug of neutral alumina, eluting with DCM until the filtrate was clear. The filtrate was then concentrated under high vacuum to produce a foamy yellow solid.

A minimal amount of pentane was added to the foam (ca. 0.5 mL) and the foam was manually broken up to produce a slurry. The solids were sonicated for 5 minutes then collected by filtration, washed with ice cold pentane, and dried under vacuum to produce *(IHept^{Me})Pd(cinnamyl)Cl* as a free flowing, bright yellow powder (44.2 mg, 31%). When left at room temperature under an inert atmosphere, the complex decomposed over the course of 3-4 months. When stored at -28 °C under an inert atmosphere this complex was stable indefinitely.

^{1}H NMR (600 MHz, $CDCl_3$) δ 7.36 (t, *J* = 7.8 Hz, 2H), 7.10-7.19 (m, 9H), 5.07-5.14 (m, 1H), 4.40 (d, *J* = 12.8 Hz, 1H), 3.75 (t, *J* = 6.5 Hz, 1H), 2.64-2.70 (m, 4H), 1.87 (s, 6H), 1.76-1.84 (m, 4H), 1.67-1.75 (m, 4H), 1.50-1.58 (m, 4H, overlaps with H_2O), 1.30-1.47 (m, 12H), 1.24-1.27 (m, 1H), 1.13-1.23 (m, 8H), 0.81-0.87 (m, 24H); ^{13}C NMR (150 MHz, $CDCl_3$) δ 177.6, 144.2, 137.9, 136.4, 128.5, 128.1, 127.8, 127.1, 126.6, 125.6, 108.1, 92.1, 68.0, 46.8, 38.7, 36.7, 20.3, 20.2, 14.8, 14.5, 10.7; HRMS (ESI) calculated for $C_{54}H_{81}N_2Pd^+$ 861.5440, found 861.5459.

Synthesis of decylzinc bromide (95)

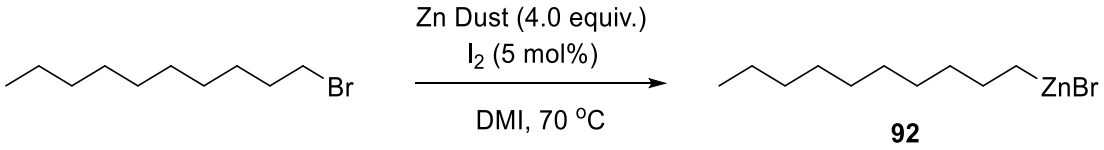

92

Procedure adapted from literature.[24] A 25 mL, round bottom Schlenk flask equipped with a large stir bar was charged with zinc dust (1.255 g, 19.2 mmol, 4.0 equivalent) and flame dried under vacuum for 5 minutes. The flask was allowed to cool then purged with nitrogen three times. DMI (5mL) was added, and the suspension was stirred vigorously to create a uniform slurry. Iodine (60.7 mg, 0.239 mmol, 5 mol%) was added, followed by 1-bromodecane (1 mL, 4.8 mmol, 1.0 equivalent). The flask was heated in an oil bath set to 70 °C overnight, at which time GC-MS

analysis confirmed the full consumption of starting material. The flask was removed from the oil bath, left to cool and let the excess zinc settle for 24hr, after which it was titrated using Knochel's protocol (0.76 M) and used for the general cross-coupling procedure below.

General alkyl-alkyl cross-coupling procedure using *n*-Bu_2Zn (70)

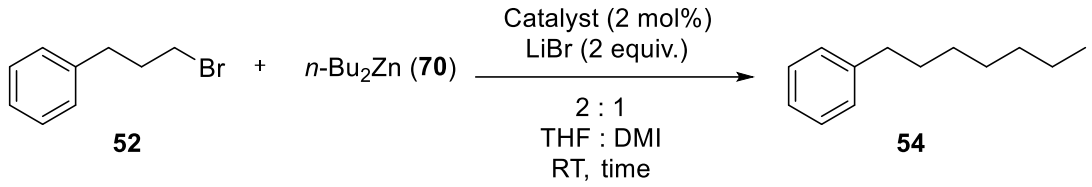

Procedure adapted from literature.[39,97,114] In a glovebox, a 1-dram vial was charged with a stir bar, LiBr (35 mg, 0.4 mmol, 2.0 equivalent), catalyst (0.004 mmol, 2 mol%), THF (0.55 mL) and DMI (0.33 mL). 3-bromo-phenylpropane was added (40 mg, 0.2 mmol, 1.0 equivalent) and a precisely measured amount of internal standard (dodecane, ca. 17 mg). The solution was stirred and *n*-Bu_2Zn (0.12 mL, 0.97M, 0.12 mmol, 0.6 equivalent) was added in one shot. For kinetic trials, 75 µL aliquots were taken at different time intervals and quenched on silica loaded in glass pipettes. These pipettes were then eluted with 5% EtOAc in hexanes and analyzed using GC-FID and calibrated curves for each product (see below). In all other cases, the reactions mixtures were left overnight before 75 µL aliquots were quenched on silica and analyzed using the same method. A example of calculating the GC-FID yield is below.

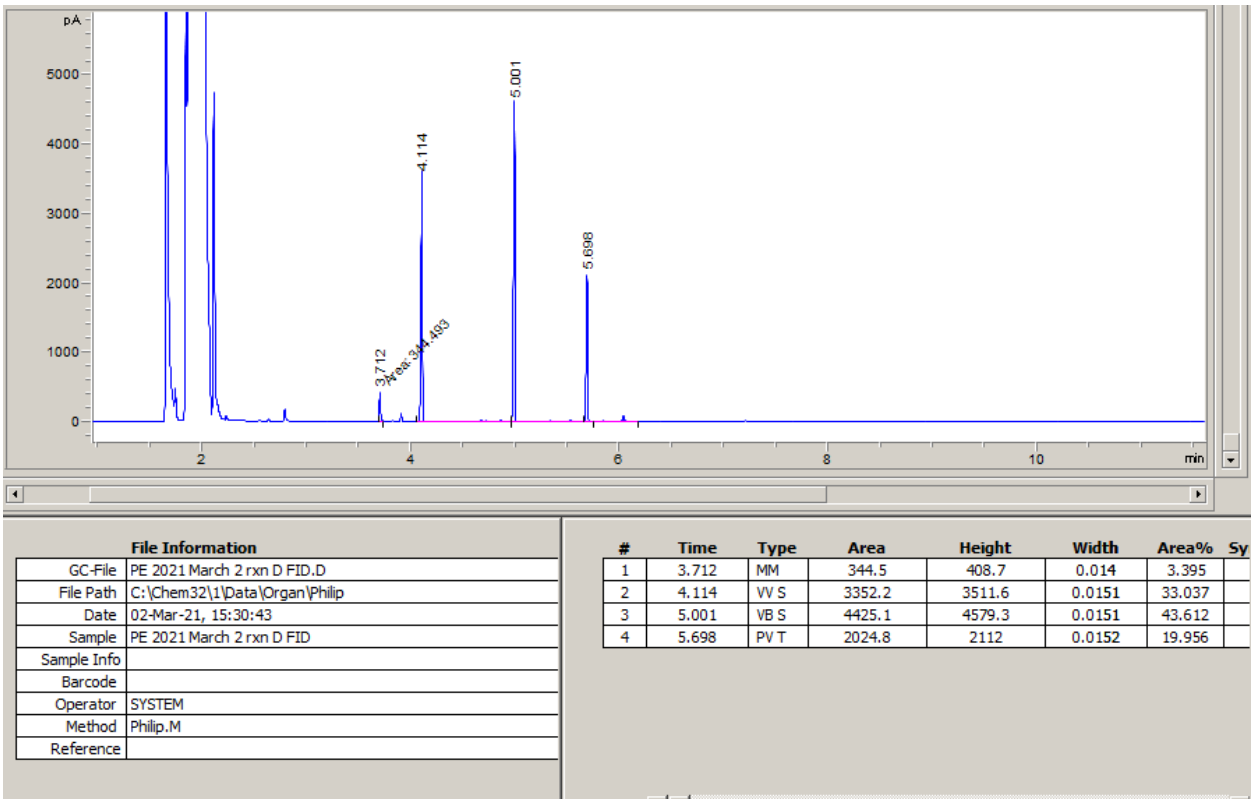

File Information	
GC-File	PE 2021 March 2 rxn D FID.D
File Path	C:\Chem32\1\Data\Organ\Philip
Date	02-Mar-21, 15:30:43
Sample	PE 2021 March 2 rxn D FID
Sample Info	
Barcode	
Operator	SYSTEM
Method	Philip.M
Reference	

#	Time	Type	Area	Height	Width	Area%	Sy
1	3.712	MM	344.5	408.7	0.014	3.395	
2	4.114	VV S	3352.2	3511.6	0.0151	33.037	
3	5.001	VB S	4425.1	4579.3	0.0151	43.612	
4	5.698	PV T	2024.8	2112	0.0152	19.956	

Product	Signal Area	Concentration in diluted aliquot (M)	Amount of product in reaction mixture (mMol)	% Yield
Internal Standard (20.9 mg)	4425.1	0.01561	0.1227	-
trans-1-Phenyl-1-propene (**86**)	3352.2	0.01625	0.1277	64
Propylbenzene (**87**)	344.5	0.00172	0.0135	7
Heptylbenzene (**54**)	2024.8	0.00677	0.0532	27

$$\text{Concentration of IS in diluted aliquot} = \frac{4425.1 + 8.14 * 10^1}{2.886 * 10^5} = 0.01561\ \text{M}$$

$$\text{Concentration of } \mathbf{86} \text{ in diluted aliquot} = \frac{3352.2 + 1.143}{2.063 * 10^5} = 0.01625\ \text{M}$$

$$\text{Amount of } \mathbf{86} \text{ in reaction mixture } = \frac{[\mathbf{86}]}{[\text{IS}]} * \text{mMol IS} = \frac{0.01625\text{M}}{0.01561\ \text{M}} * 0.1227\ \text{mMol} = 0.1277\ \text{mMol}$$

$$\text{Percent yield of } \mathbf{86} = \frac{0.1277\ \text{mMol}}{0.20\ \text{mMol}} * 100 = 64\%\ \text{Yield}$$

Figure 20 Calibration curve for the internal standard (dodecane) using GC-FID.

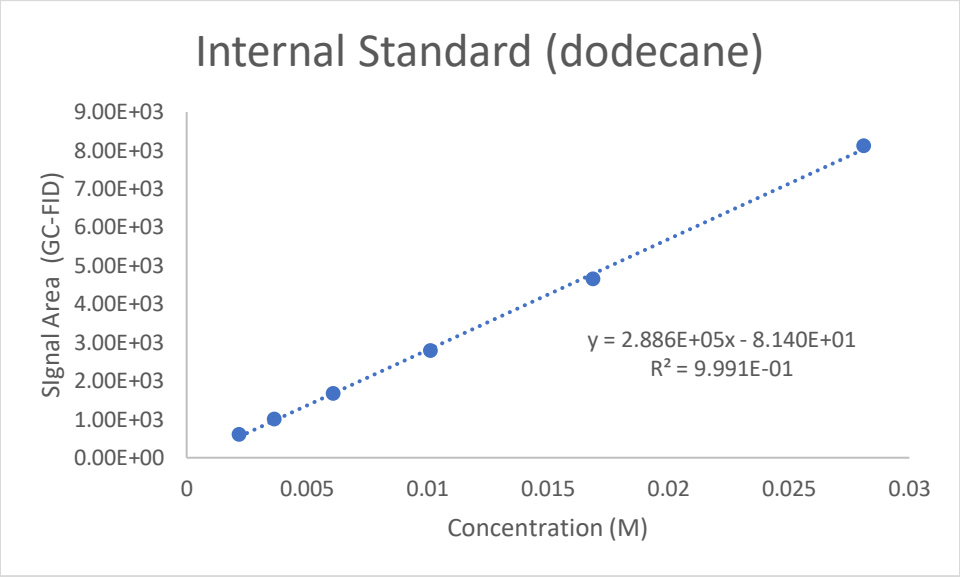

Figure 21 Calibration curve for trans-1-phenyl-1-propene (86) using GC-FID.

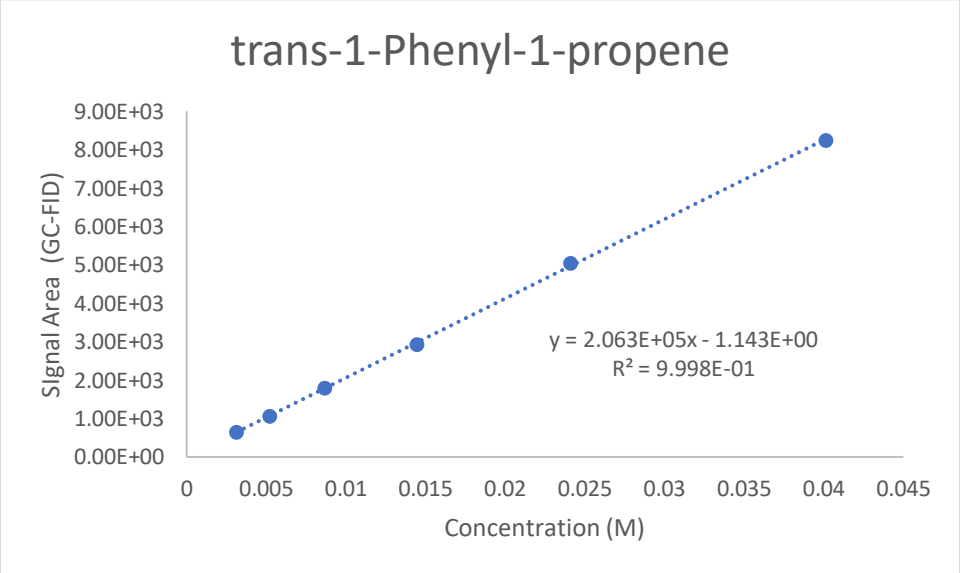

Figure 22 Calibration curve for heptylbenzene (54) using GC-FID.

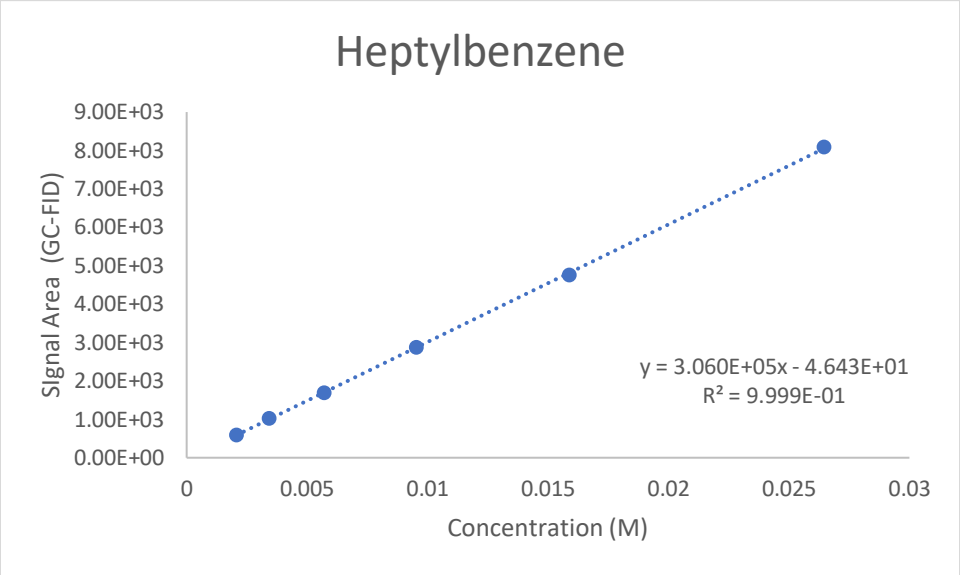

Figure 23 Calibration curve for propylbenzene (87) using GC-FID.

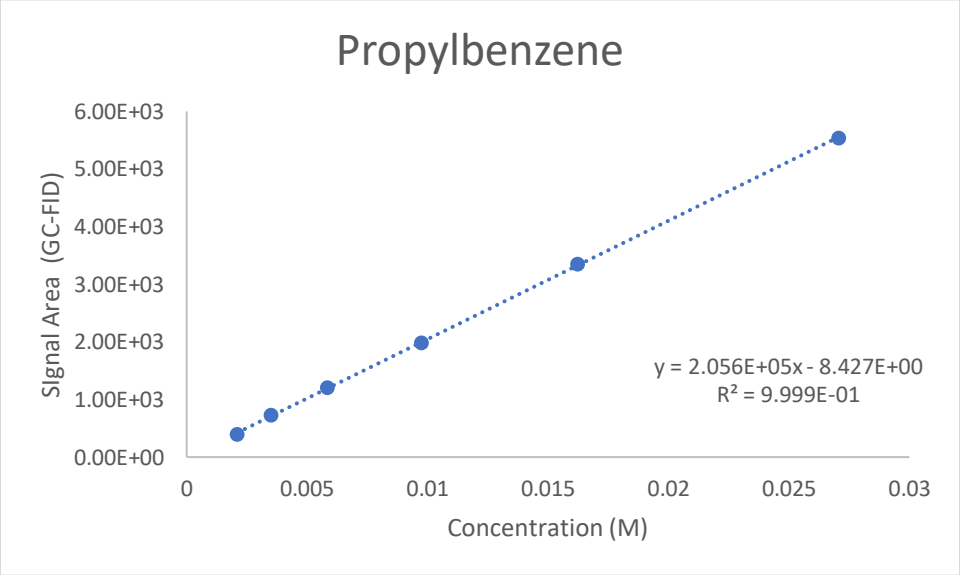

Figure 24 Calibration curve for 1-bromo-3-phenylpropane (52) using GC-FID

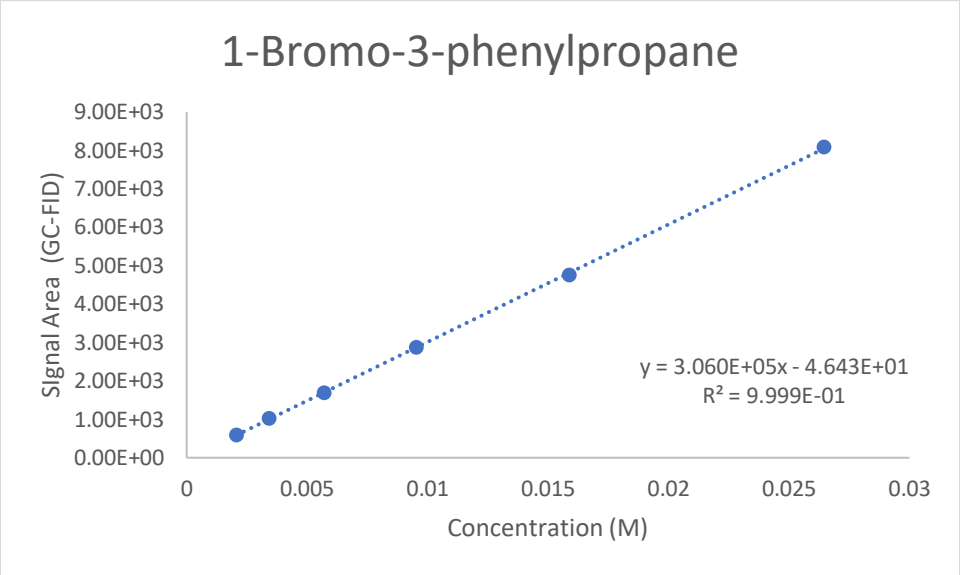

General heteroaryl-alkyl cross-coupling procedure using iPr_2Zn (99)

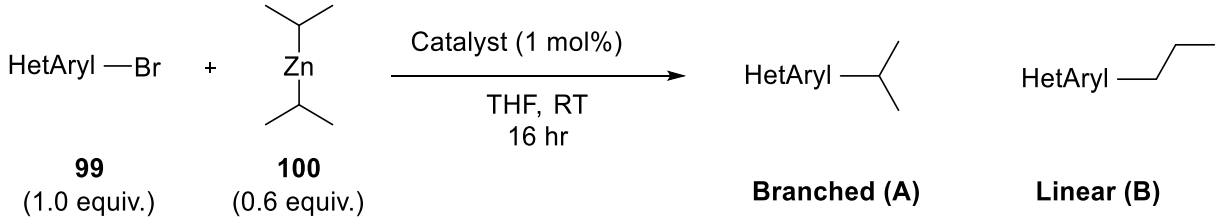

In a glovebox, a 1-dram vial was charged with a stir bar, catalyst (0.001 mmol, 1 mol%), aryl halide (0.1 mmol, 1.0 equivalent) and THF (0.14 mL). The solution was stirred and iPr_2Zn (0.36 mL, 0.16 M, 0.06 mmol, 0.6 equivalent) was added in one shot. The reaction mixture was stirred at room temperature overnight. The reaction mixture was flushed through a plug of silica with 5% EtOAc in hexanes and the filtrate was concentrated to yield the crude product. The mass was recorded, and the crude mixture was analyzed by ^1H NMR to confirm the reaction went to full conversion and measure the ratio between branched and linear using the benzyl signals (see below).

Figure 25 Representative example for the measurement of branched to linear product using ^{1}H NMR analysis.

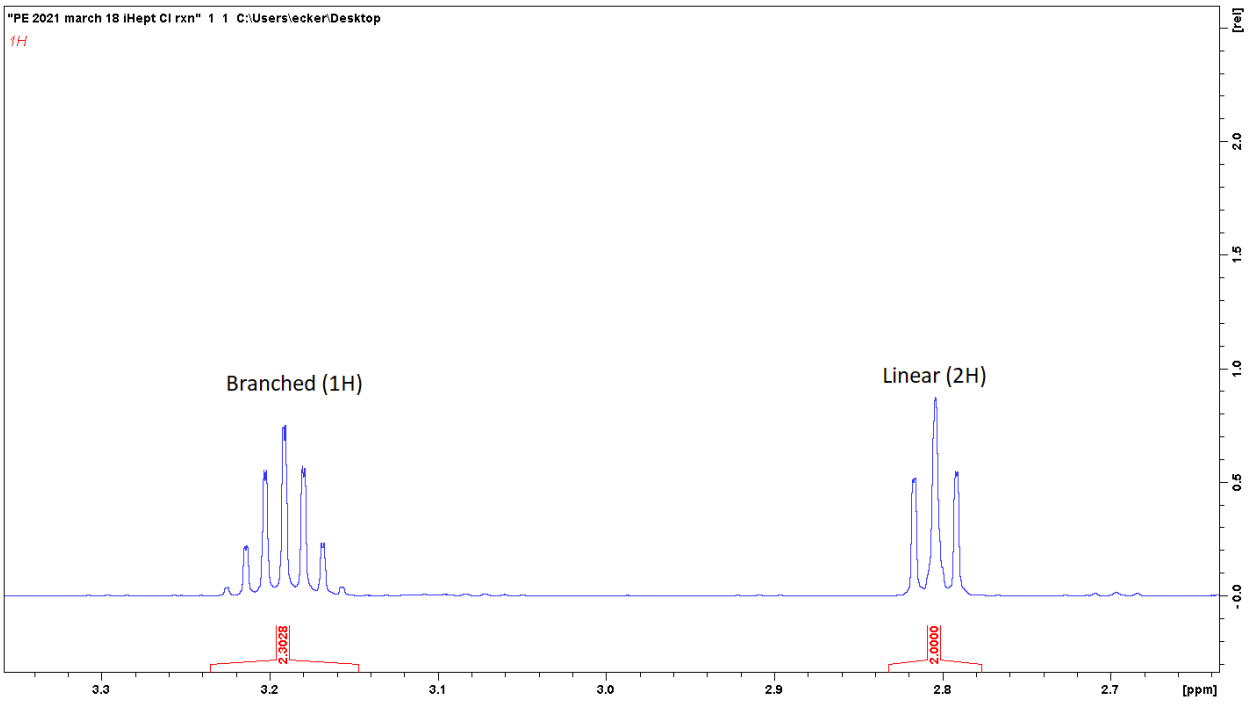

7.5 Supporting info for chapter 5

Synthesis of racemic amino acid 108b

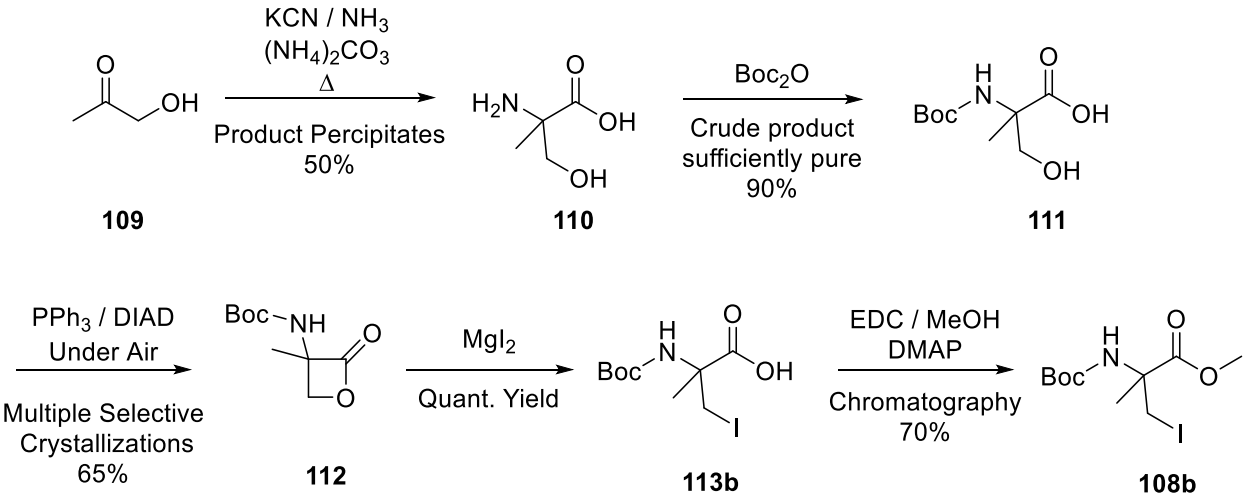

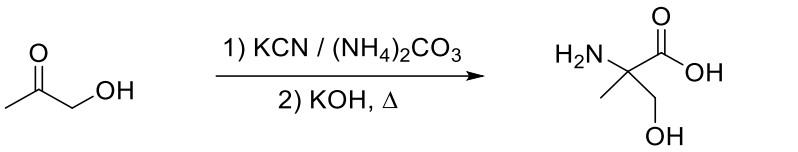

109 **110**
α-Methyl-DL-serine

Procedure adapted from literature.[143] A 1L flask was equipped with a condenser and a large stir bar. Ammonium carbonate (113.7 g, 1184 mmol, 1.5 equivalent), water (150 mL), ammonium hydroxide solution (S.G. 0.88, 59 mL, ~1062 mmol) and potassium cyanide (50.0g, 767.6 mmol, 1.0 equivalent) were added in that order, washing the powder funnel with water. Hydroxyacetone (55.2 mL, 791.6 mmol, 1.03 equivalent) was added dropwise to the stirred solution. The solution was stirred at room temperature for 30 minutes, heated to 60 °C over 2 hours, then to 85 °C over another 4 hr. The reaction was cooled to room temperature and placed in an ice bath. Potassium hydroxide (208.8 g, 85%, 3163 mmol, 4.1 equivalent) was added *slowly* to control the amount of ammonia discharged during the addition. The resulting mixture was heated at 90 °C overnight. The mixture was cooled, and 300 mL of methanol was added to help precipitate the potassium sulfate. The mixture was placed in an ice bath and ***slowly*** neutralized with H_2SO_4 (35 mL of 50% H_2SO_4 : water until pH~13, followed by 100mL of concentrated H_2SO_4, until pH~6). There was significant CO_2 effervescence during the neutralization. Following the neutralization, the potassium sulfate was removed by filtration and washed with a 1:1 mixture of water: methanol. The filtration of potassium sulfate was very slow due to the fine precipitate it forms. The filtrate was placed in an ice bath and stirred gently. Acetone was added in two batches, 240 mL in one shot, followed by another 240 mL slowly added over the course of an hour. The precipitated α-methyl-DL-serine was collected by filtration, washed with acetone, placed in a large round bottom

flask and dried overnight under high vacuum while heating in an oil bath at 65 °C resulting in a dry, free flowing white powder (43.6g, 366 mmol, 48%).

^{1}H NMR (500 MHz, DMSO D_6) δ 7.00 (br s, 3H), 3.54 (d, *J* = 11.1 Hz, 1H), 3.41 (d, *J* = 11.1 Hz, 1H), 1.20 (s, 3H); ^{1}H NMR (400 MHz, D_2O): δ 3.93 (d, *J* = 12.2 Hz, 1H), 3.68 (d, *J* = 12.2 Hz), 1.44 (s, 3H); ^{13}C NMR (100 MHz, D_2O) δ 175.4, 64.7, 62.5, 18.4.

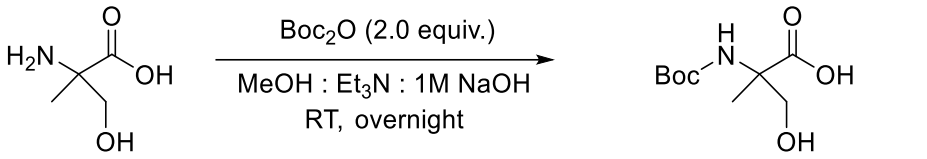

110
(1.0 equiv.)

111
N-Boc-α-Methyl-DL-serine

Procedure adapted from literature.[144] A 1L flask was charged with α-Methyl-DL-serine (37.1 g, 311.5 mmol, 1.0 equivalent) followed by triethylamine (85 mL, 613.5 mmol, 2.0 equivalent), aqueous 1M NaOH solution (84 mL, 84 mmol, 0.25 equivalent) and MeOH (780 mL). Boc anhydride (136.0 g, 623 mmol, 2.0 equivalent) was added in one addition and the suspension was stirred at room temperature overnight. The mixture was concentrated using a rotary evaporator to remove approximately 700-800 mL of solvent. EtOAc (400 mL) and water (100 mL) were added, and the aqueous layer was acidified to pH∼1 using 1M HCl. The organic layer was collected, and the aqueous phase was extracted twice more with EtOAc (2 x 400 mL). The combined organic phases were washed with acidified (pH = 1) brine (200 mL), dried over anhydrous Na_2SO_4, concentrated, and dried under high vacuum over night to yield a viscous, sometimes foamy, yellow oil (67.6 g, 85% purity, 262 mmol, 85%). The purity of the oil was assessed using ^{1}H NMR, the residue often contains small amounts of Boc anhydride and ethyl acetate that can be difficult to remove. These impurities do not interfere with the subsequent cyclization and the oil can be used as is.

^{1}H NMR (400 MHz, $CDCl_3$) δ 6.8 (br s, 2H), 5.5 (br s, 1H), 3.88 (s, 2H), 1.50 (s, 3H), 1.44 (s, 9H).

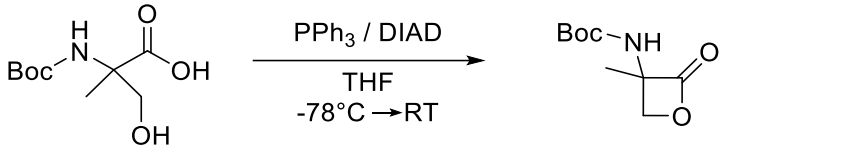

111 **112**

N-Boc-DL-Serine-β-Lactone

Procedure adapted from literature.[142] A 2L round bottom flask was charged with PPh_3 (75.67 g, 288.5 mmol, 1.1 equivalent) and three vacuum/ purge cycles were performed. THF (750 mL, uninhibited) was added to the PPh_3. The crude N-Boc-α-Methyl-DL-serine was dissolved in THF (250 mL, uninhibited). Dissolving the viscous oil can be slow, sonication and gentle heating helped speed up the dissolution. The flask containing the PPh_3 was cooled to -78 °C, DIAD (56.8 mL, 288.5 mmol, 1.1 equivalent) was slowly added using a syringe, and the mixture was stirred for 15 minutes. The solution of N-Boc-α-Methyl-DL-serine was then added dropwise using an addition funnel and left to warm up to room temperature overnight. The solution was concentrated using a rotary evaporator to remove approximately 550 mL of THF. Hexanes (500 mL) was added, and the solution as placed in a freezer for 24 hr. The solution was decanted from the precipitated PPh_3O and concentrated. The resulting residue was flushed through a plug of silica with an excess of DCM. Note, in later experiments it was found that **112** is unstable on silica gel. In the future, silica should be substituted with neutral alumina. The filtrate was concentrated, redissolved in 100 ml of DCM and 80 mL of hexanes, and placed in a freezer for 24 hr. The precipitated Diisopropyl Hydrazine-1,2-dicarboxylate was removed by filtration and the filtrate concentrated, redissolved in 50 ml of DCM and 45 mL of hexanes and placed in a freezer for 24 hr. The white precipitate was collected by filtration and washed with hexanes to yield N-Boc-DL-Serine-β-Lactone as a

white powder which should be stored under nitrogen in a freezer (31.6 g, 157.2 mmol, 60%). Note, all precipitates should be analyzed by ^{1}H NMR to confirm the identity of the precipitate and ensure no product is discarded. The final filtrate still contains some product which can be recovered by column chromatography using neutral alumina. The next ring opening step can tolerate minor to moderate amounts of Diisopropyl Hydrazine-1,2-dicarboxylate and PPh_3O.

^{1}H NMR (400 MHz, DMSO d_6) δ 7.69 (br s, 1H), 4.48 (d, J = 4.5 Hz, 1H), 4.15 (d, J = 4.5 Hz, 1H), 1.59 (s, 3H), 1.44 (s, 9H); ^{13}C NMR (100 MHz, $CDCl_3$) δ 172.9, 154.3, 79.3, 71.2, 65.9, 27.9, 19.4; HRMS (ESI) calculated for $C_9H_{15}NO_4Na^+$, 224.0899; found 224.0903.

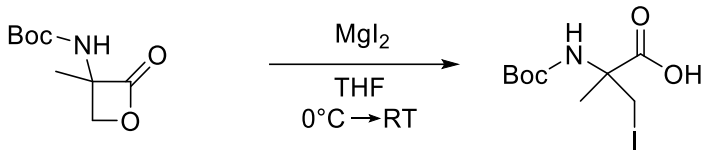

112 **113b**

Procedure adapted from literature.[145] In a glovebox, a round bottom flask was charged with a stir bar and THF (27 mL). This flask was cooled in a freezer. Once fully cooled, the flask was removed and stirred aggressively while MgI_2 (3.754 g, 13.5 mmol, 2.0 equivalent) was added to create a slurry. The N-Boc-DL-Serine-β-Lactone (1.358 g, 6.75 mmol, 1.0 equivalent) was added slowly, and the resulting slurry was left to warm to room temperature while aggressively stirring. After 3hr, most of the THF was removed using a rotary evaporator. The resulting residue was dissolved in 40 mL of EtOAc and 10 mL water. The aqueous phase was acidified to pH∼1 using 1M HCl. The organic layer was collected and washed with 1M aqueous sodium thiosulfate (20 mL) to quench any iodine present. Before draining the sodium thiosulfate aqueous phase, it was acidified to pH ∼ 1 and shaken with the organic layer. The organic layer was washed with acidified brine

(20 mL, pH ~ 1), dried over anhydrous Na_2SO_4, and concentrated under reduce pressure to produce a grey powder (2.22 g, 6.75 mmol, quantitative yield).

^{1}H NMR (400 MHz, $CDCl_3$) δ 5.30 (br s, 1H), 3.88 (s, 2H), 1.66 (s, 3H), 1.44 (s, 9H); ^{13}C NMR (100 MHz, $CDCl_3$) δ 175.8, 154.4, 59.3, 28.4, 23.7, 22.0, 12.8; HRMS (ESI) calculated for $C_9H_{16}NO_4INa^+$, 352.0022, found 352.0001.

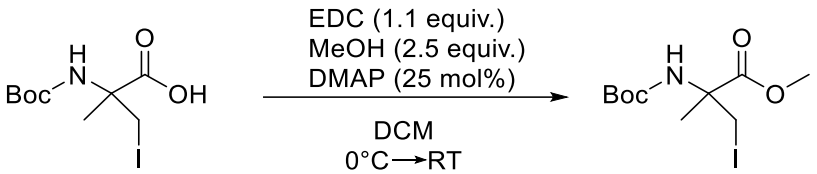

113b **108b**

A round bottom flask equipped with a stir bar was placed in an ice bath and charged with DCM (20 mL), MeOH (2.0 mL, 50.5 mmol, 2.5 equivalent), DMAP (617 mg, 5.05 mmol, 25 mol%) and **116** (6.652 g, 20.2 mmol, 1.0 equivalent). EDC (4.26 g, 22.2 mmol, 1.1 equivalent) was added and the mixture was left stirring in the ice bath, allowed to warm to room temperature overnight. The mixture as diluted with DCM (20 mL) and washed once with water (20 mL), twice with 1M HCl (2 x 20 mL) then once with brine (20 mL). The organic phase was dried over anhydrous Na_2SO_4 and concentrated to produce a brown oil. The crude product was purified using column chromatography (0 → 7% EtOAC in hexanes) to yield a brown oil. This oil should be protected from light to prevent discoloration. The product was dried under high vacuum, then placed in a freezer overnight. The resulting solid can be ground up and further dried under high vacuum at room temperature to produce a free-flowing white powder. (4.844 g, 14.1 mmol, 70%).

^{1}H NMR (600 MHz, $CDCl_3$) δ 5.46 (br s, 1H), 4.03 (br s, 2H), 3.77 (d, J = 10.3 Hz, 1H), 1.66 (s, 3H), 1.45 (s, 9H); ^{13}C NMR (150 MHz, $CDCl_3$) δ 172., 154.1, 106.2, 80.2, 59.7, 53.4, 28.5, 23.5; HRMS (ESI) calculated for $C_{10}H_{18}NO_4INa^+$, 366.0178; found 366.0178.

Synthesis of chiral amino acid 127

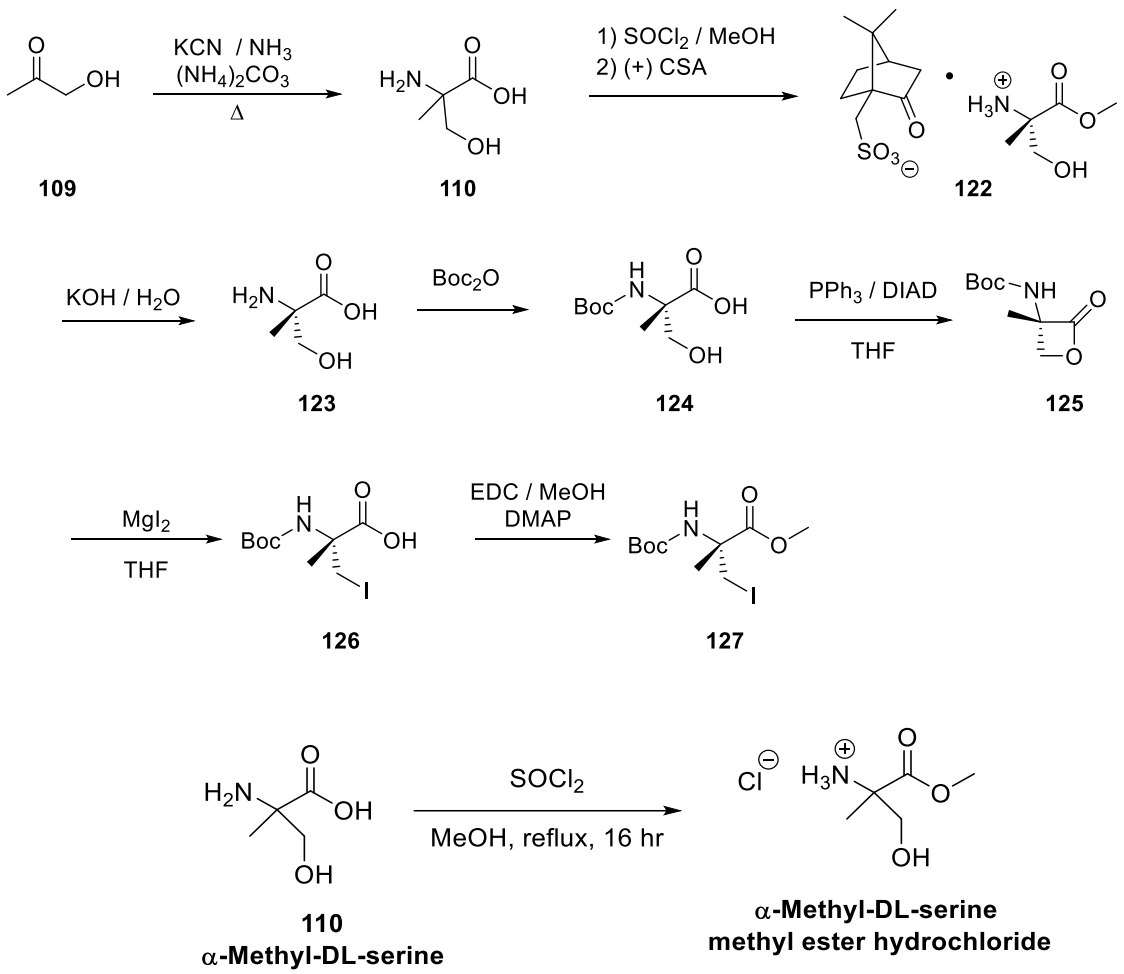

Procedure adapted from literature.[143] A flask was charged with a stir bar and α-Methyl-DL-serine (10.0 g, 83.9 mmol, 1.0 equivalent) then evacuated / purged with Nitrogen 3 times. Methanol (100 mL) was added, and the slurry was stirred in an ice bath. Thionyl chloride (12 mL, 168 mmol, 2.0 equivalent) was added dropwise using an additional funnel. The mixture was stirred at room temperature for 30 mins then heated to 75 °C overnight. A small aliquot was concentrated to produce α-Methyl-DL-serine methyl ester hydrochloride as mildly viscous orange oil containing trace amounts of methanol and HCl.

^{1}H NMR (400 MHz, DMSO D_6) δ 8.61 (br s, 3H), 3.75 (s, 3H), 3.74 (d, *J* = 10.8 Hz, 1H), 3.64 (d, *J* = 10.8 Hz, 1H), 1.39 (s, 3H); ^{13}C NMR (100 MHz, DMSO D_6) δ 170.8, 64.7, 61.1, 53.2, 18.3.

α-Methyl-DL-serine methyl ester hydrochloride

122
α-Methyl-L-serine methyl ester (1S)-(+)-Camphor-10-sulfonate

Procedure adapted from literature.[143] (1S)-(+)-Camphor-10-sulfonic acid (71.0 g, 305.6 mmol, 1.0 equivalent) was added to the solution of α-Methyl-DL-serine methyl ester hydrochloride. The excess HCl was removed by distilling the methanol off with a rotovap, adding methanol (50 mL) and repeating with two more additions of DME (2 x 75 mL). DME (75 mL) was added once more, and a suspension slowly formed. This suspension was left stirring at room temperature for 3 days. The suspension was filtered, washed with fresh DME (2 x 75 mL) and then dried to give the crude salt **122** a free-flowing white powder (32.2 g). The crude salt, acetone (76 mL), and methanol (13.6 mL) were heated at 58 °C for 2 hr, slowly cooled to room temperature, and then filtered. The solid was washed with acetone (2 x 75 mL) and dried to give the salt **125** as a free-flowing white powder (28.8 g, 78.8 mmol, 26%). The diastereomeric excess (94%) was measured using the protocols for measuring diastereomeric excess of **122** described below.

^{1}H NMR (400 MHz, DMSO D_6) δ 8.4 (br s, 3 H), 5.82 (t, *J* = 5.0 Hz, 1 H), 3.73-3.79 (m, 1H), 3.76 (s, 3 H), 3.56 (dd, *J* = 11.3, 5.0 Hz, 1H), 2.90 (d, *J* = 14.7 Hz, 1H), 2.62-2.73 (m, 1H), 2.40 (d, *J* = 14.7 Hz, 1H), 2.25 (dt, J = 18.1, 3.9 Hz, 1H), 1.95 (t, *J* = 4.5 Hz, 1H), 1.81-1.92 (m, 1H), 1.81 (d, *J* = 18.1 Hz, 1H), 1.37 (s, 3 H), 1.24-1.34 (m, 2H), 1.05 (s, 3H), and 0.75 (s, 3H); ^{13}C

NMR (100 MHz, DMSO D_6) δ 216.8, 170.6, 64.5, 60.8, 58.1, 53.0, 47.0, 46.5, 42.1, 42.0, 26.3, 24.0, 20.0, 19.4, 18.1.

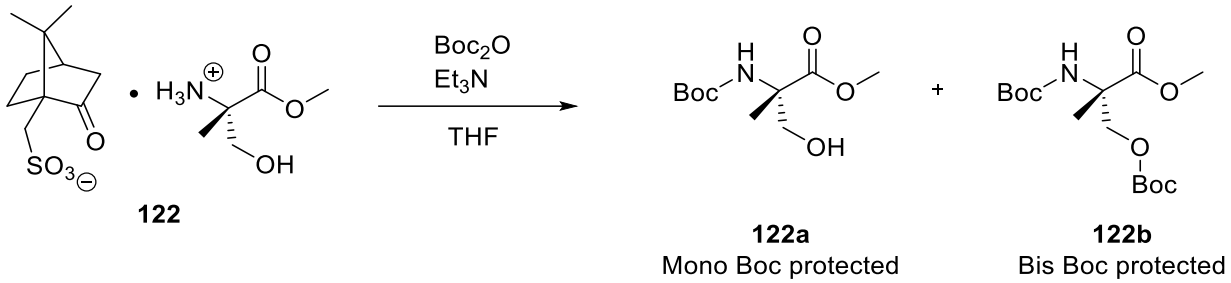

122

122a
Mono Boc protected

122b
Bis Boc protected

Protocols for measuring diastereomeric excess of 122

Procedure adapted from literature.[143] A 1-dram vial was charged with camphor sulfonate salt **122** (10 mg, 0.027 mmols, 1.0 equivalent), Boc anhydride (20 mg, 0.092 mmols, 3.4 equivalent), triethylamine (40 μL, 0.29 mmols, 10 equivalent) and THF (0.2 mL). The suspension was stirred at room temperature for 4 hr, flushed through a plug of silica eluting with MTBE, and analyzed using chiral GC. The mono boc protected derivative (**122a**) could be analyzed using method 1 and the bis boc protected derivative (**122b**) analyzed with method 2.

Method 1 for chiral analysis of **122a**

Instrument: Agilent 6850 Series II Network GC system.
OVEN
Equilibration time: 0.25 min
Maximum temp: 200 C
Initial temp: 150 C (On)
Initial time: 15.00 min
Ramps:
Rate Final temp Final time
1 20.00 175 10.00
2 0 (Off)
Post temp: 0 C
Post time: 0.00 min

Run time: 26.25 min

INLET (SPLIT/SPLITLESS)
Mode: Split
Initial temp: 250 C (On)
Pressure: 19.32 psi (On)
Split ratio: 50:1
Split flow: 59.9 mL/min
Total flow: 64.0 mL/min
Gas saver: Off
Gas type: Helium

COLUMN
Capillary Column
Manufacturer: Agilent
Model Number: 19091G-B133E
Description: HP Chiral ß
Max temperature: 240 C
Nominal length: 30.0 m
Nominal diameter: 250.00 um
Nominal film thickness: 0.25 um
Mode: constant flow
Initial flow: 1.2 mL/min
Nominal init pressure: 19.32 psi
Average velocity: 33 cm/sec
Source: Inlet
Outlet: Detector
Outlet pressure: ambient

DETECTOR (FID)
Temperature: 250 C (On)
Hydrogen flow: 40.0 mL/min (On)
Air flow: 450.0 mL/min (On)
Mode: Constant makeup flow
Makeup flow: 45.0 mL/min (On)
Makeup Gas Type: Nitrogen
Flame: On
Electrometer: On
Lit offset: 2.0 pA

SIGNAL
Data rate: 20 Hz
Type: detector
Save Data: On
Retention Times:
(S): 7.50 minutes.

(R): 7.69 minutes.

Method 2 for chiral analysis of **122b**

Instrument: Agilent 6850 Series II Network GC system.
OVEN
Equilibration time: 0.25 min
Maximum temp: 200 C
Initial temp: 50 C (On)
Initial time: 3.00 min
Ramps:

#	Rate	Final temp	Final time
1	20.00	100	10.00
2	20.00	150	10.00
3	20.00	175	5.00
4	0 (Off)		

Post temp: 0 C
Post time: 0.00 min
Run time: 34.25 min

INLET (SPLIT/SPLITLESS)
Mode: Split
Initial temp: 250 C (On)
Pressure: 13.84 psi (On)
Split ratio: 50:1
Split flow: 59.9 mL/min
Total flow: 64.0 mL/min
Gas saver: Off
Gas type: Helium

COLUMN
Capillary Column
Manufacturer: Agilent
Model Number: 19091G-B133E
Description: HP Chiral ß
Max temperature: 240 C
Nominal length: 30.0 m
Nominal diameter: 250.00 um
Nominal film thickness: 0.25 um
Mode: constant flow
Initial flow: 1.2 mL/min
Nominal init pressure: 13.84 psi
Average velocity: 29 cm/sec
Source: Inlet
Outlet: Detector
Outlet pressure: ambient

DETECTOR (FID)
Temperature: 250 C (On)
Hydrogen flow: 40.0 mL/min (On)
Air flow: 450.0 mL/min (On)
Mode: Constant makeup flow
Makeup flow: 45.0 mL/min (On)
Makeup Gas Type: Nitrogen
Flame: On
Electrometer: On
Lit offset: 2.0 pA

SIGNAL
Data rate: 20 Hz
Type: detector
Save Data: On
Retention Times:
(S): 23.5 minutes.
(R): 23.82 minutes.

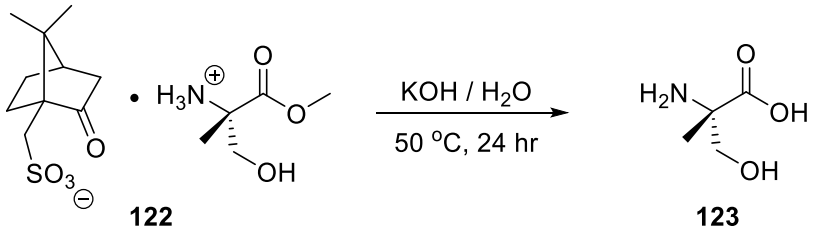

122 **123**

A round bottom flask was charged with camphor sulfonate salt **122** (3.600 g, 9.87 mmol, 1.0 equivalent) and water (15 mL). KOH pellets (85% purity, 78.9 mmol, 8.0 equivalent) were added and the slurry was heated at 50 °C to produce an opaque, homogenous solution. The solution was heated at 50 °C for 24 hr after which it was cooled to room temperature and left standing for 30 minutes during which time a precipitate formed. Sometimes crystallization was slow and must be seeded with potassium camphorsulfonate from previous batches. The resulting potassium camphorsulfonate precipitate was removed by filtration and washed with a minimal amount of acetonitrile. The filtrate was seeded with the filtered crystals and placed in an ice bath for an hour. The resulting potassium camphorsulfonate was removed by filtration and washed with a minimal

amount of acetonitrile. Methanol (5 mL) was added to the filtrate and the flask was cooled in an ice bath while it was neutralized with concentrated H_2SO_4 (until pH=6). CAUTION, the addition of H_2SO_4 was extremely exothermic and releases fumes if added to fast. The H_2SO_4 should be added *slowly* using a suitable addition funnel. Following neutralization, the flask was left in the ice bath for 30 minutes before the potassium sulfate was removed by filtration and washed with a 1:1 mixture of water: methanol (10 mL). The filtrate was concentrated to approximately 3/4 the initial volume using a rotovap with the water bath set to 60 °C. The solution was placed in an ice bath and stirred gently while acetone (30 mL) was added dropwise. The precipitated α-methyl-L-serine (**123**) was collected by filtration and washed with acetone (30 mL). A second batch of crystals were obtained by seeding the filtrate and adding more acetone (20 mL) to provide a total yield of 914 mg, 7.68 mmol, 86%. NMR characterization was identical to the racemic material. The measured optical rotation was inconsistent, presumably due to potassium sulfate contamination.

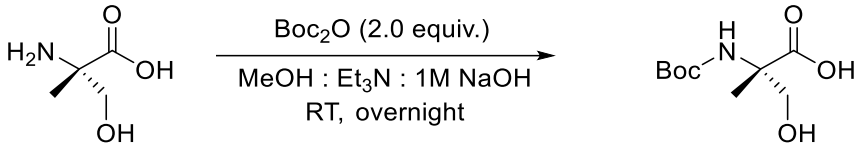

123 **124**

The same procedure as previously described was used. NMR spectral data and physical properties were identical to the racemic material.

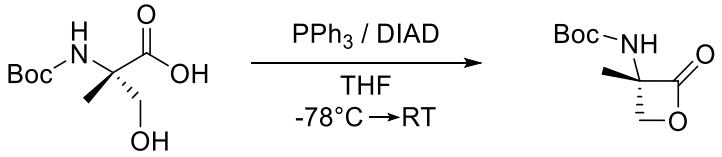

124 **125**

The same synthetic procedure as previously described was used. The reaction mixture was concentrated and purified using column chromatography to produce the title compound in a low yield (168.5 mg, 0.837 mmol, 18%). The low yield is believed to be caused by the instability of **125** on silica gel, future procedures should either perform multiple crystallizations or use other stationary phases such as neutral alumina. NMR spectral data and physical properties were identical to the racemic material.

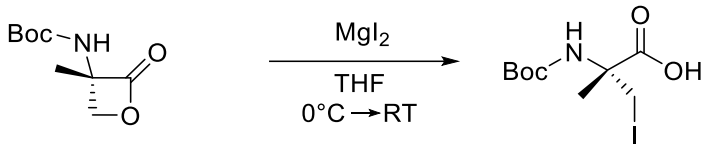

125 **126**

The same procedure as previously described was used. NMR spectral data and physical properties were identical to the racemic material.

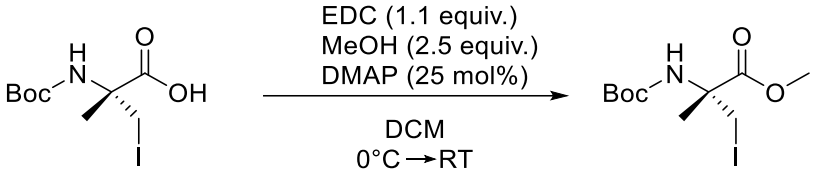

126 **127**

The same procedure as previously described was used, resulting in a colorless oil while the racemic material was a solid. NMR spectral data were identical. The enantiomeric excess could be analyzed using Method 3 below.

Method 3 for chiral analysis of **127**

Instrument: Agilent 6850 Series II Network GC system.
OVEN
Equilibration time: 0.25 min
Maximum temp: 200 C
Initial temp: 100 C (On)

Initial time: 50.00 min
Ramps:
Rate Final temp Final time
1 10.00 165 10.00
2 0 (Off)
Post temp: 0 C
Post time: 0.00 min
Run time: 66.50 min

INLET (SPLIT/SPLITLESS)
Mode: Split
Initial temp: 250 C (On)
Pressure: 16.58 psi (On)
Split ratio: 50:1
Split flow: 59.9 mL/min
Total flow: 64.0 mL/min
Gas saver: Off
Gas type: Helium

COLUMN
Capillary Column
Manufacturer: Agilent
Model Number: 19091G-B133E
Description: HP Chiral ß
Max temperature: 240 C
Nominal length: 30.0 m
Nominal diameter: 250.00 um
Nominal film thickness: 0.25 um
Mode: constant flow
Initial flow: 1.2 mL/min
Nominal init pressure: 19.32 psi
Average velocity: 33 cm/sec
Source: Inlet
Outlet: Detector
Outlet pressure: ambient

DETECTOR (FID)
Temperature: 250 C (On)
Hydrogen flow: 40.0 mL/min (On)
Air flow: 450.0 mL/min (On)
Mode: Constant makeup flow
Makeup flow: 45.0 mL/min (On)
Makeup Gas Type: Nitrogen
Flame: On
Electrometer: On
Lit offset: 2.0 pA

SIGNAL
Data rate: 20 Hz
Type: detector
Save Data: On
Retention Times:
(R): 57.05 minutes.
(S): 57.19 minutes.

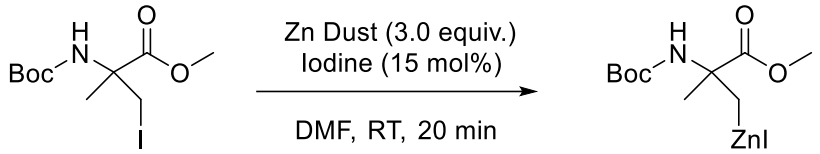

108b **115**

In a glovebox, a 1-dram vial was charged with a stir bar, Zn dust (47 mg, 0.75mmol, 3.0 equivalent), **108b** (86 mg, 0.25 mmol, 1.0 equivalent) and any additives (such as LiCl, 21 mg, 0.5 mmol, 2.0 equivalent). DMF (0.2 mL) was added, and the mixture was stirred aggressively to suspend the zinc dust. Iodine (10 mg, 0.039 mmol, 15 mol%) was added and the mixture was stirred for 20 minutes. After 20 minutes, a precisely measured amount of 1,3,5-trimethoxybenzene (~13-15 mg, 0.33 equivalent) was added and stirring was halted so the zinc can settle to the bottom (approximately 5-10 minutes). The mixture was then carefully to an NMR tube using a syringe. ^{1}H NMR analysis was used to determine the yield of the organozinc using a proton gradient shim for non-deuterated DMF mixtures, and calibrating the axis to the solvent peaks.

115 (salt-free) ^{1}H NMR (500 MHz, DMF) δ 6.07 (br s, 1H), 3.55 (s, 3H), 1.48 (s, 3H), 1.34 (s, 9H), 0.63 (d, J = 12.6 Hz, 1H), 0.51 (d, J = 12.6 Hz, 1H).

Figure 26 ^{1}H NMR of organozinc 115 with an internal standard.

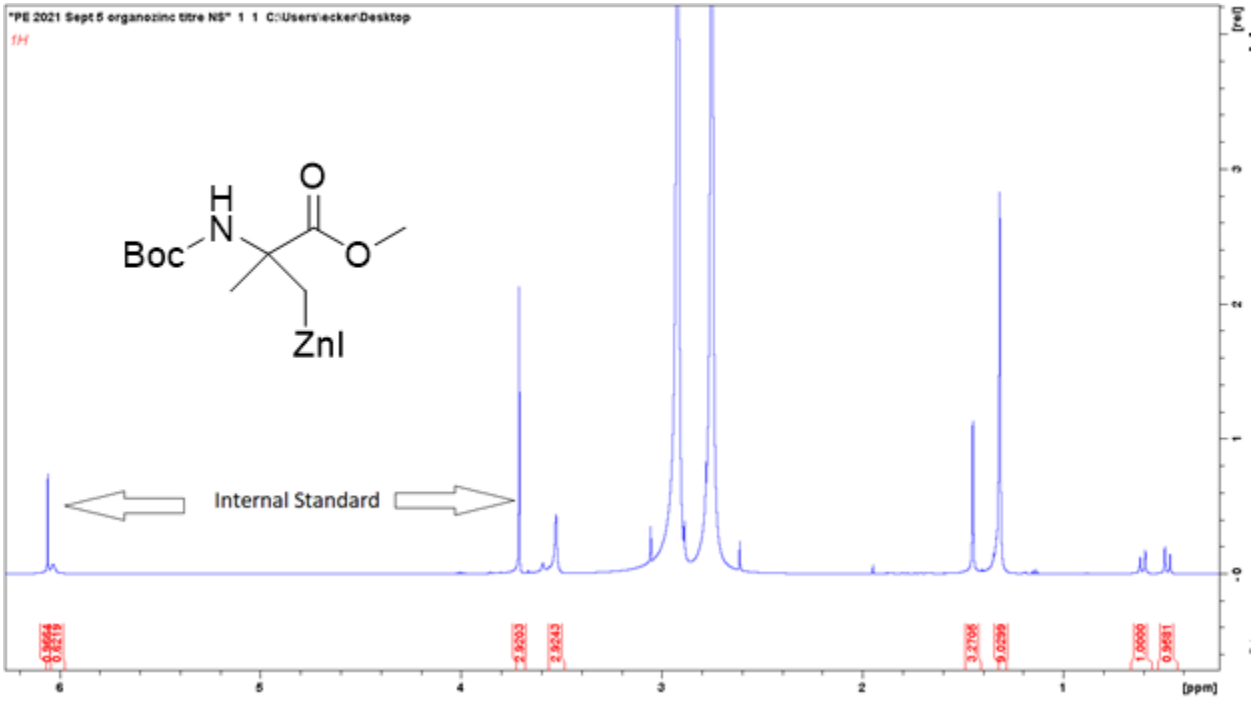

Figure 27 ^{1}H NMR of organozinc 115 with and without TMEDA (1 equivalent).

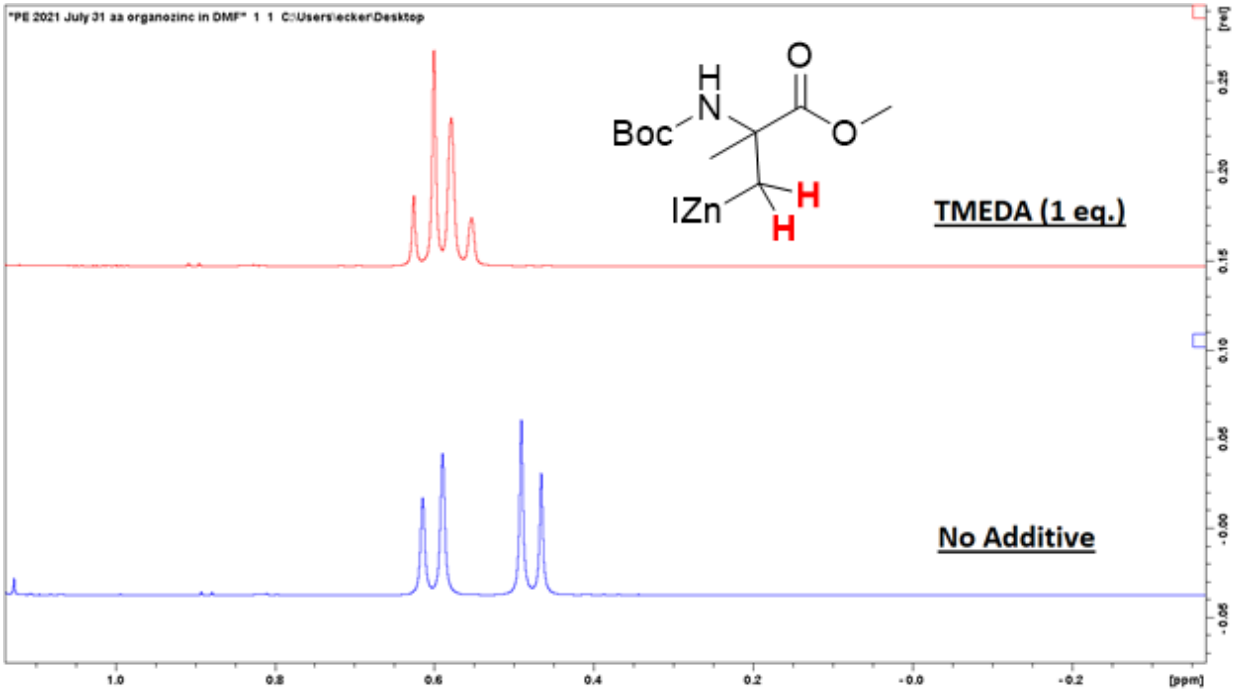

General cross-coupling procedure for 108b

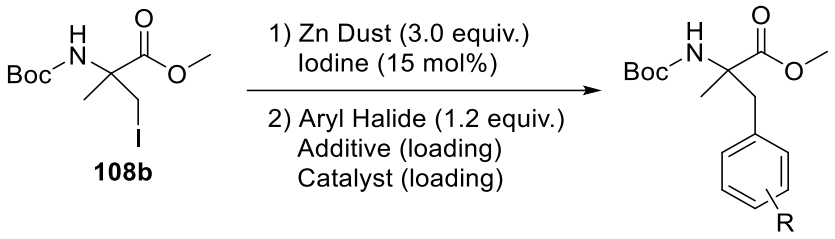

In a glovebox, a 1-dram vial was charged with a stir bar, Zn dust (47 mg, 0.75 mmol, 3.0 equivalent) and **108b** (86 mg, 0.25 mmol, 1.0 equivalent). DMF (0.2 mL) was added, and the mixture stirred aggressively to suspend the zinc dust. Iodine (10 mg, 0.039 mmol, 15 mol%) was added and stirred for 20 minutes. A second vial was charged with a stir bar, the aryl halide (0.3 mmol, 1.2 equivalent), additive (e.g. LiCl 21mg, 0.5 mmol, 2.0 equivalent) and catalyst (e.g. *Pd-PEPPSI-Pr*^{Cl}, 9.8 mg, 0.0125 mmol, 5 mol%). Stirring was halted to allow the zinc to settle (approximately 5-10 minutes). DMF (0.1 mL) was added to the second vial and stirred to create a slurry. The organozinc solution was carefully collected using a syringe and added to the second vial. In trials where the catalyst was preactivated, approximately 0.05mL of 1M *n*-Bu_2Zn in THF was added to the solution of catalyst, aryl bromide and LiCl. A strong color change was usually observed, creating a bright yellow solution in 1-2 minutes. The freshly prepared organozinc was then transferred to the solution of active catalyst. The vial was capped, sealed with parafilm, moved out of the glovebox, and stirred for 72 hr at room temperature. The reaction mixture was analyzed by ^{1}H NMR to test for the presence of organozinc and purified directly by column chromatography (6→ 20% EtOAc in hexanes).

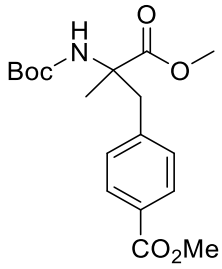

116

Following the general coupling procedure, the title compound was isolated as a clear oil. **116** ^{1}H NMR (600 MHz, $CDCl_3$) δ 7.93 (d, *J* = 8.4 Hz, 2H), 7.14 (d, *J* = 8.4 Hz, 2H), 5.15 (br s, 1H), 3.90 (s, 3H), 3.76 (s, 3H), 3.49 (br s, 1H), 3.27 (d, *J* = 13.4 Hz, 1H), 1.57 (s, 3H), 1.47 (s, 9H); ^{13}C NMR (150 MHz, $CDCl_3$) δ 174.1, 167.0, 154.3, 142.1, 130.1, 129.4, 128.8, 79.6, 60.32, 52.6, 52.1, 41.3, 28.4, 23.8; HRMS (ESI) calculated for $C_{18}H_{25}NO_6Na^+$, 374.1580; found 374.1608.

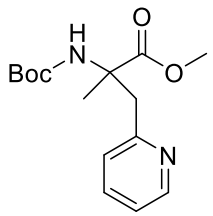

117

Following the general coupling procedure, the title compound was isolated as a pale-yellow oil. **117** ^{1}H NMR (500 MHz, $CDCl_3$) δ 8.52 (d, *J* = 4.7 Hz, 1H), 7.62 (t, *J* = 7.4 Hz, 1H), 7.05-7.20 (m, 2H), 6.08 (s, 1H), 3.73 (s, 3H), 3.34 (s, 2H), 1.60 (s, 3H), 1.41 (s, 9H); ^{13}C NMR (125 MHz, $CDCl_3$) δ 174.5, 157.1, 154.6, 149.1, 136.4, 124.6, 121.9, 79.2, 59.6, 52.4, 44.6, 28.4, 23.3; HRMS (ESI) calculated for $C_{15}H_{22}N_2O_4Na^+$, 317.1477; found 317.1490.

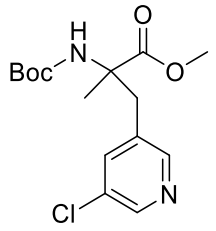

118

Following the general coupling procedure, the title compound was isolated as a bright yellow oil. **118** ^{1}H NMR (500 MHz, $CDCl_3$) δ 8.46 (s, 1H), 8.21 (s, 1H), 7.47 (s, 1H), 5.20 (br s, 1H), 3.79 (s, 3H), 3.49 (d, J = 13.8 Hz, 1H), 3.29 (d, J = 13.8 Hz, 1H), 1.56 (s, 3H), 1.48 (s, 9H); ^{13}C NMR (125 MHz, $CDCl_3$) δ 174.5, 157.1, 154.6, 149.1, 136.4, 124.6, 121.9, 79.2, 59.6, 52.4, 44.6, 28.4, 23.3; HRMS (ESI) calculated for $C_{15}H_{21}N_2O_4ClH^+$, 329.1268; found 329.1243.

Chapter 8: References

(1) Corbet, J. P.; Mignani, G. Selected Patented Cross-Coupling Reaction Technologies. *Chem. Rev.* **2006**, *106* (7), 2651–2710. https://doi.org/10.1021/cr0505268.

(2) Ruiz-Castillo, P.; Buchwald, S. L. Applications of Palladium-Catalyzed C-N Cross-Coupling Reactions. *Chem. Rev.* **2016**, *116* (19), 12564–12649. https://doi.org/10.1021/acs.chemrev.6b00512.

(3) Hooshmand, S. E.; Heidari, B.; Sedghi, R.; Varma, R. S. Recent Advances in the Suzuki-Miyaura Cross-Coupling Reaction Using Efficient Catalysts in Eco-Friendly Media. *Green Chem.* **2019**, *21* (3), 381–405. https://doi.org/10.1039/c8gc02860e.

(4) Beletskaya, I. P.; Cheprakov, A. V. Heck Reaction as a Sharpening Stone of Palladium Catalysis. *Chem. Rev.* **2000**, *100* (8), 3009–3066. https://doi.org/10.1021/cr9903048.

(5) Oxtoby, L. J.; Gurak, J. A.; Wisniewski, S. R.; Eastgate, M. D.; Engle, K. M. Palladium-Catalyzed Reductive Heck Coupling of Alkenes. *Trends Chem.* **2019**, *1* (6), 572–587. https://doi.org/10.1016/j.trechm.2019.05.007.

(6) Haas, D.; Hammann, J. M.; Greiner, R.; Knochel, P. Recent Developments in Negishi Cross-Coupling Reactions. *ACS Catal.* **2016**, *6* (3), 1540–1552. https://doi.org/10.1021/acscatal.5b02718.

(7) Shaughnessy, K. H. Development of Palladium Precatalysts That Efficiently Generate LPd(0) Active Species. *Isr. J. Chem.* **2020**, *60* (3–4), 180–194. https://doi.org/10.1002/ijch.201900067.

(8) Ahmadvand, Z.; Bayat, M.; Zolfigol, M. A. Toward Prediction of the Precatalyst Activation Mechanism through the Cross-Coupling Reactions: Reduction of Pd(II) to Pd(0) in Precatalyst of the Type Pd-PEPPSI. *J. Comput. Chem.* **2020**, *41* (26), 2296–2309. https://doi.org/10.1002/jcc.26393.

(9) Melvin, P. R.; Balcells, D.; Hazari, N.; Nova, A. Understanding Precatalyst Activation in Cross-Coupling Reactions: Alcohol Facilitated Reduction from Pd(II) to Pd(0) in Precatalysts of the Type (η^3-Allyl)Pd(L)(Cl) and (η^3-Indenyl)Pd(L)(Cl). *ACS Catal.* **2015**, *5* (9), 5596–5606.

https://doi.org/10.1021/acscatal.5b01291.

(10) Hazari, N.; Melvin, P. R.; Beromi, M. M. Well-Defined Nickel and Palladium Precatalysts for Cross-Coupling. *Nat. Rev. Chem.* **2017**, *1* (3). https://doi.org/10.1038/s41570-017-0025.

(11) Dardir, A. H.; Melvin, P. R.; Davis, R. M.; Hazari, N.; Mohadjer Beromi, M. Rapidly Activating Pd-Precatalyst for Suzuki-Miyaura and Buchwald-Hartwig Couplings of Aryl Esters. *J. Org. Chem.* **2018**, *83* (1), 469–477. https://doi.org/10.1021/acs.joc.7b02588.

(12) Cao, Q.; Nicholson, W. I.; Jones, A. C.; Browne, D. L. Robust Buchwald-Hartwig Amination Enabled by Ball-Milling. *Org. Biomol. Chem.* **2019**, *17* (7), 1722–1726. https://doi.org/10.1039/c8ob01781f.

(13) Farmer, J. L.; Pompeo, M.; Lough, A. J.; Organ, M. G. (IPent)PdCl$_2$(Morpholine)]: A Readily Activated Precatalyst for Room-Temperature, Additive-Free Carbon-Sulfur Coupling. *Chem. Eur. J.* **2014**, *20* (48), 15790–15798. https://doi.org/10.1002/chem.201404705.

(14) Sayah, M.; Organ, M. G. Potassium Isopropoxide: For Sulfination It Is the Only Base You Need! *Chem. Eur. J.* **2013**, *19* (48), 16196–16199. https://doi.org/10.1002/chem.201303756.

(15) Roy, A. H.; Hartwig, J. F. Oxidative Addition of Aryl Sulfonates to Palladium (0) Complexes of Mono- and Bidentate Phosphines. Mild Addition of Aryl Tosylates and the Effects of Anions on Rate and Mechanism. *Organometallics* **2004**, *23* (2), 194–202. https://doi.org/10.1021/om034187p.

(16) Barrios-Landeros, F.; Carrow, B. P.; Hartwig, J. F. Effect of Ligand Steric Properties and Halide Identity on the Mechanism for Oxidative Addition of Haloarenes to Trialkylphosphine Pd(0) Complexes. *J. Am. Chem. Soc.* **2009**, *131* (23), 8141–8154. https://doi.org/10.1021/ja900798s.

(17) Rheingold, A. L.; Fultz, W. C. Crystal and Molecular Structure of Bis(μ-Iodo)Bis[o-(Di-o-Tolylphosphino)Benzyl]Dlpalladium(II), a Product of the Cyclopalladation for Frans-[(o-Tol)$_3$P]$_2$PdI$_2$. *Organometallics* **1984**, *3* (9), 1414–1417. https://doi.org/10.1021/om00087a017.

(18) Stille, J. K.; Lau, K. S. Y. Mechanisms of Oxidative Addition of Organic Halides to Group 8 Transition-Metal Complexes. *Acc. Chem. Res.* **1977**, *10* (12), 434–442. https://doi.org/10.1021/ar50120a002.

(19) Maes, B. U. W.; Verbeeck, S.; Verhelst, T.; Ekomié, A.; Von Wolff, N.; Lefèvre, G.; Mitchell, E. A.; Jutand, A. Oxidative Addition of Haloheteroarenes to Palladium(0): Concerted versus S_NAr-Type Mechanism. *Chem. Eur. J.* **2015**, *21* (21), 7858–7865. https://doi.org/10.1002/chem.201406210.

(20) Li, Z.; Fu, Y.; Guo, Q. X.; Liu, L. Theoretical Study on Monoligated Pd-Catalyzed Cross-Coupling Reactions of Aryl Chlorides and Bromides. *Organometallics* **2008**, *27* (16), 4043–4049. https://doi.org/10.1021/om701065f.

(21) Sinha, N.; Champagne, P. A.; Rodriguez, M. J.; Lu, Y.; Kopach, M. E.; Mitchell, D.; Organ, M. G. One-Pot Sequential Kumada–Tamao–Corriu Couplings of (Hetero)Aryl Polyhalides in the Presence of Grignard-Sensitive Functional Groups Using Pd-PEPPSI-IPent^{Cl}. *Chem. Eur. J.* **2019**, *25* (26), 6508–6512. https://doi.org/10.1002/chem.201901150.

(22) Ariafard, A.; Lin, Z. Understanding the Relative Easiness of Oxidative Addition of Aryl and Alkyl Halides to Palladium(0). *Organometallics* **2006**, *25* (16), 4030–4033. https://doi.org/10.1021/om060236x.

(23) Chass, G. A.; O'Brien, C. J.; Hadei, N.; Kantchev, E. A. B.; Mu, W. H.; Fang, D. C.; Hopkinson, A. C.; Csizmadia, I. G.; Organ, M. G. Density Functional Theory Investigation of the Alkyl-Aikyl Negishi Cross-Coupling Reaction Catalyzed by N-Heterocyclic Carbene (NHC)-Pd Complexes. *Chem. Eur. J.* **2009**, *15* (17), 4281–4288. https://doi.org/10.1002/chem.200900042.

(24) Huo, S. Highly Efficient, General Procedure for the Preparation of Alkylzinc Reagents from Unactivated Alkyl Bromides and Chlorides. *Org. Lett.* **2003**, *5* (4), 423–425. https://doi.org/10.1021/ol0272693.

(25) Hadei, N.; Achonduh, G. T.; Valente, C.; O'Brien, C. J.; Organ, M. G. Differentiating C-Br and C-Cl Bond Activation by Using Solvent Polarity: Applications to Orthogonal Alkyl-Alkyl Negishi Reactions. *Angew. Chem. Int. Ed.* **2011**, *50* (17), 3896–3899. https://doi.org/10.1002/anie.201100705.

(26) Casares, J. A.; Espinet, P.; Fuentes, B.; Salas, G. Insights into the Mechanism of the Negishi Reaction: ZnRX versus ZnR_2 Reagents. *J. Am. Chem. Soc.* **2007**, *129* (12), 3508–3509. https://doi.org/10.1021/ja070235b.

(27) García-Melchor, M.; Fuentes, B.; Lledós, A.; Casares, J. A.; Ujaque, G.; Espinet, P. Cationic Intermediates in the Pd-Catalyzed Negishi Coupling. Kinetic and Density Functional Theory Study of Alternative Transmetalation Pathways in the Me-Me Coupling of $ZnMe_2$ and Trans - [$PdMeCl(PMePh_2)_2$]. *J. Am. Chem. Soc.* **2011**, *133* (34), 13519–13526. https://doi.org/10.1021/ja204256x.

(28) Liu, Q.; Lan, Y.; Liu, J.; Li, G.; Wu, Y. D.; Lei, A. Revealing a Second Transmetalation Step in the Negishi Coupling and Its Competition with Reductive Elimination: Improvement in the Interpretation of the Mechanism of Biaryl Syntheses. *J. Am. Chem. Soc.* **2009**, *131* (29), 10201–10210. https://doi.org/10.1021/ja903277d.

(29) Fuentes, B.; García-Melchor, M.; Lledós, A.; Maseras, F.; Casares, J. A.; Ujaque, G.; Espinet, P. Palladium Round Trip in the Negishi Coupling of Trans- [$PdMeCl(PMePh_2)_2$] with ZnMeCl: An Experimental and DFT Study of the Transmetalation Step. *Chem. Eur. J.* **2010**, *16* (29), 8596–8599. https://doi.org/10.1002/chem.201001332.

(30) González-Pérez, A. B.; Álvarez, R.; Faza, O. N.; De Lera, Á. R.; Aurrecoechea, J. M. DFT-Based Insights into Pd-Zn Cooperative Effects in Oxidative Addition and Reductive Elimination Processes Relevant to Negishi Cross-Couplings. *Organometallics* **2012**, *31* (5), 2053–2058. https://doi.org/10.1021/om300024p.

(31) Del Pozo, J.; Salas, G.; Álvarez, R.; Casares, J. A.; Espinet, P. The Negishi Catalysis: Full Study of the Complications in the Transmetalation Step and Consequences for the Coupling Products. *Organometallics* **2016**, *35* (20), 3604–3611. https://doi.org/10.1021/acs.organomet.6b00660.

(32) Gillie, A.; Stille, J. K. Mechanisms of 1,1-Reductive Elimination from Palladium. *J. Am. Chem. Soc.* **1980**, *102* (15), 4933–4941. https://doi.org/10.1021/ja00535a018.

(33) Zhang, H.; Luo, X.; Wongkhan, K.; Duan, H.; Li, Q.; Zhu, L.; Wang, J.; Batsanov, A. S.; Howard, J. A. K.; Marder, T. B.; Lei, A. Acceleration of Reductive Elimination of [Ar-Pd-C_{sp3}] by a Phosphine/Electron-Deficient Olefin Ligand: A Kinetic Investigation. *Chem. Eur. J.* **2009**, *15* (15), 3823–3829. https://doi.org/10.1002/chem.200802209.

(34) Mueller, J. A.; Goller, C. P.; Sigman, M. S. Elucidating the Significance of β-Hydride Elimination and the Dynamic Role of Acid/Base Chemistry in a Palladium-Catalyzed Aerobic Oxidation of Alcohols. *J. Am. Chem. Soc.* **2004**, *126* (31), 9724–9734. https://doi.org/10.1021/ja047794s.

(35) Alibrandi, G.; Scolaro, L. M.; Minniti, D.; Romeo, R. Kinetic Study of β-Hydride Elimination of Monoalkyl Complexes of Platinum(II): Effects of Varying the Alkyl Chain Length or the Cis Group in the Reaction of Cis-Bis(Triethylphosphine) (Alkyl)(Halo or Pseudohalo)Platinum(II) Complexes. *Inorg. Chem.* **1990**, *29* (18), 3467–3472. https://doi.org/10.1021/ic00343a037.

(36) Lu, X. Control of the β-Hydride Elimination Making Palladium-Catalyzed Coupling Reactions More Diversified. *Top. Catal.* **2005**, *35* (1–2), 73–86. https://doi.org/10.1007/s11244-005-3814-4.

(37) Biemolt, J.; Ruijter, E. Advances in Palladium-Catalyzed Cascade Cyclizations. *Adv. Synth. Catal.* **2018**, *360* (20), 3821–3871. https://doi.org/10.1002/adsc.201800526.

(38) Valente, C.; Baglione, S.; Candito, D.; O'Brien, C. J.; Organ, M. G. High Yielding Alkylations of Unactivated Sp^3 and Sp^2 Centres with Alkyl-9-BBN Reagents Using an NHC-Based Catalyst: Pd-

PEPPSI-IPr. *Chem. Commun.* **2008**, No. 6, 735–737. https://doi.org/10.1039/b715081d.

(39) Hadei, N.; Kantchev, E. A. B.; O'Brien, C. J.; Organ, M. G. The First Negishi Cross-Coupling Reaction of Two Alkyl Centers Utilizing a Pd-N-Heterocyclic Carbene (NHC) Catalyst. *Org. Lett.* **2005**, *7* (17), 3805–3807. https://doi.org/10.1021/ol0514909.

(40) Atwater, B.; Chandrasoma, N.; Mitchell, D.; Rodriguez, M. J.; Organ, M. G. Pd-PEPPSI-IHept^{Cl}: A General-Purpose, Highly Reactive Catalyst for the Selective Coupling of Secondary Alkyl Organozincs. *Chem. Eur. J.* **2016**, *22* (41), 14531–14534. https://doi.org/10.1002/chem.201603603.

(41) Alexanian, E. J.; Hartwig, J. F. Mechanistic Study of β-Hydrogen Elimination from Organoplatinum(II) Enolate Complexes. *J. Am. Chem. Soc.* **2008**, *130* (46), 15627–15635. https://doi.org/10.1021/ja8056908.

(42) Vikse, K.; Naka, T.; McIndoe, J. S.; Besora, M.; Maseras, F. Oxidative Additions of Aryl Halides to Palladium Proceed through the Monoligated Complex. *ChemCatChem* **2013**, *5* (12), 3604–3609. https://doi.org/10.1002/cctc.201300723.

(43) Christmann, U.; Vilar, R. Monoligated Palladium Species as Catalysts in Cross-Coupling Reactions. *Angew. Chem. Int. Ed.* **2005**, *44* (3), 366–374. https://doi.org/10.1002/anie.200461189.

(44) Zheng, Q.; Liu, Y.; Chen, Q.; Hu, M.; Helmy, R.; Sherer, E. C.; Welch, C. J.; Chen, H. Capture of Reactive Monophosphine-Ligated Palladium(0) Intermediates by Mass Spectrometry. *J. Am. Chem. Soc.* **2015**, *137* (44), 14035–14038. https://doi.org/10.1021/jacs.5b08905.

(45) Çalimsiz, S.; Organ, M. G. Negishi Cross-Coupling of Secondary Alkylzinc Halides with Aryl/Heteroaryl Halides Using Pd–PEPPSI–IPent. *Chem. Commun.* **2011**, *47* (18), 5181–5183. https://doi.org/10.1039/c0cc04835f.

(46) Pompeo, M.; Froese, R. D. J.; Hadei, N.; Organ, M. G. Pd-PEPPSI-IPent^{Cl}: A Highly Effective Catalyst for the Selective Cross-Coupling of Secondary Organozinc Reagents. *Angew. Chem. Int. Ed.* **2012**, *51* (45), 11354–11357. https://doi.org/10.1002/anie.201205747.

(47) Atwater, B.; Chandrasoma, N.; Mitchell, D.; Rodriguez, M. J.; Pompeo, M.; Froese, R. D. J.; Organ, M. G. The Selective Cross-Coupling of Secondary Alkyl Zinc Reagents to Five-Membered-Ring Heterocycles Using Pd-PEPPSI-IHept^{Cl}. *Angew. Chem. Int. Ed.* **2015**, *54* (33), 9502–9506. https://doi.org/10.1002/anie.201503941.

(48) Yang, Y.; Niedermann, K.; Han, C.; Buchwald, S. L. Highly Selective Palladium-Catalyzed Cross-Coupling of Secondary Alkylzinc Reagents with Heteroaryl Halides. *Org. Lett.* **2014**, *16* (17), 4638–4641. https://doi.org/10.1021/ol502230p.

(49) Han, C.; Buchwald, S. L. Negishi Coupling of Secondary Alkylzinc Halides with Aryl Bromides and Chlorides. *J. Am. Chem. Soc.* **2009**, *131* (22), 7532–7533. https://doi.org/10.1021/ja902046m.

(50) Noyori, R.; Takaya, H. BINAP: An Efficient Chiral Element for Asymmetric Catalysis. *Acc. Chem. Res.* **1990**, *23* (10), 345–350. https://doi.org/10.1021/ar00178a005.

(51) Littke, A. F.; Dai, C.; Fu, G. C. Versatile Catalysts for the Suzuki Cross-Coupling of Arylboronic Acids with Aryl and Vinyl Halides and Triflates under Mild Conditions. *J. Am. Chem. Soc.* **2000**, *122* (17), 4020–4028. https://doi.org/10.1021/ja0002058.

(52) Ingoglia, B. T.; Wagen, C. C.; Buchwald, S. L. Biaryl Monophosphine Ligands in Palladium-Catalyzed C–N Coupling: An Updated User's Guide. *Tetrahedron* **2019**, *75* (32), 4199–4211. https://doi.org/10.1016/j.tet.2019.05.003.

(53) McCann, S. D.; Reichert, E. C.; Arrechea, P. L.; Buchwald, S. L. Development of an Aryl Amination Catalyst with Broad Scope Guided by Consideration of Catalyst Stability. *J. Am. Chem. Soc.* **2020**,

142 (35), 15027–15037. https://doi.org/10.1021/jacs.0c06139.

(54) Tolman, C. A. Steric Effects of Phosphorus Ligands in Organometallic Chemistry and Homogeneous Catalysis. *Chem. Rev.* **1977**, *77* (3), 313–348. https://doi.org/10.1021/cr60307a002.

(55) Tolman, C. A. Phosphorus Ligand Exchange Equilibria on Zerovalent Nickel. A Dominant Role for Steric Effects. *J. Am. Chem. Soc.* **1970**, *92* (10), 2956–2965. https://doi.org/10.1021/ja00713a007.

(56) Tolman, C. A. Electron Donor-Acceptor Properties of Phosphorus Ligands. Substituent Additivity. *J. Am. Chem. Soc.* **1970**, *92* (10), 2953–2956. https://doi.org/10.1021/ja00713a006.

(57) Hopkinson, M. N.; Richter, C.; Schedler, M.; Glorius, F. An Overview of N-Heterocyclic Carbenes. *Nature* **2014**, *510* (7506), 485–496. https://doi.org/10.1038/nature13384.

(58) Wanzlick, H. W. Aspects of Nucleophilic Carbene Chemistry. *Angew. Chem. Int. Ed.* **1962**, *1* (2), 75–80. https://doi.org/10.1002/anie.196200751.

(59) Arduengo, A. J.; Harlow, R. L.; Kline, M. A Stable Crystalline Carbene. *J. Am. Chem. Soc.* **1991**, *113* (1), 361–363. https://doi.org/10.1021/ja00001a054.

(60) Herrmann, W. A.; Elison, M.; Fischer, J.; Köcher, C.; Artus, G. R. J. Metal Complexes of N-Heterocyclic Carbenes—A New Structural Principle for Catalysts in Homogeneous Catalysis. *Angew. Chem. Int. Ed.* **1995**, *34* (21), 2371–2374. https://doi.org/10.1002/anie.199523711.

(61) Sharif, S.; Day, J.; Hunter, H. N.; Lu, Y.; Mitchell, D.; Rodriguez, M. J.; Organ, M. G. Cross-Coupling of Primary Amides to Aryl and Heteroaryl Partners Using (DiMeIHept^{Cl})Pd Promoted by Trialkylboranes or $B(C_6F_5)_3$. *J. Am. Chem. Soc.* **2017**, *139* (51), 18436–18439. https://doi.org/10.1021/jacs.7b09488.

(62) Çalimsiz, S.; Sayah, M.; Mallik, D.; Organ, M. G. Pd-PEPPSI-IPent: Low-Temperature Negishi Cross-

Coupling for the Preparation of Highly Functionalized, Tetra-Ortho-Substituted Biaryls. *Angew. Chem. Int. Ed.* **2010**, *49* (11), 2014–2017. https://doi.org/10.1002/anie.200906811.

(63) Chartoire, A.; Lesieur, M.; Falivene, L.; Slawin, A. M. Z.; Cavallo, L.; Cazin, C. S. J.; Nolan, S. P. [PdA (IPr*) (Cinnamyl)^{Cl}]: An Efficient Pre-Catalyst for the Preparation of Tetra-Ortho-Substituted Biaryls by Suzuki-Miyaura Cross-Coupling. *Chem. Eur. J.* **2012**, *18* (15), 4517–4521. https://doi.org/10.1002/chem.201104009.

(64) Chartoire, A.; Frogneux, X.; Boreux, A.; Slawin, A. M. Z.; Nolan, S. P. A Novel and Efficient PEPPSI Precatalyst. *Organometallics* **2012**, *31* (19), 6947–6951. https://doi.org/10.1021/om300725f.

(65) Meiries, S.; Chartoire, A.; Slawin, A. M. Z.; Nolan, S. P. [Pd(IPr*)(Acac)^{Cl}]: An Easily Synthesized, Bulky Precatalyst for C-N Bond Formation. *Organometallics* **2012**, *31* (8), 3402–3409. https://doi.org/10.1021/om300205c.

(66) Luan, X.; Mariz, R.; Gatti, M.; Costabile, C.; Poater, A.; Cavallo, L.; Linden, A.; Dorta, R. Identification and Characterization of a New Family of Catalytically Highly Active Imidazolin-2-Ylidenes. *J. Am. Chem. Soc.* **2008**, *130* (21), 6848–6858. https://doi.org/10.1021/ja800861p.

(67) Wu, L.; Drinkel, E.; Gaggia, F.; Capolicchio, S.; Linden, A.; Falivene, L.; Cavallo, L.; Dorta, R. Room-Temperature Synthesis of Tetra-Ortho-Substituted Biaryls by NHC-Catalyzed Suzuki-Miyaura Couplings. *Chem. Eur. J.* **2011**, *17* (46), 12886–12890. https://doi.org/10.1002/chem.201102442.

(68) Arduengo, A. J.; Krafczyk, R.; Schmutzler, R.; Craig, H. A.; Goerlich, J. R.; Marshall, W. J.; Unverzagt, M. Imidazolylidenes, Imidazolinylidenes and Imidazolidines. *Tetrahedron* **1999**, *55* (51), 14523–14534. https://doi.org/10.1016/S0040-4020(99)00927-8.

(69) Seiders, T. J.; Ward, D. W.; Grubbs, R. H. Enantioselective Ruthenium-Catalyzed Ring-Closing Metathesis. *Org. Lett.* **2001**, *3* (20), 3225–3228. https://doi.org/10.1021/ol0165692.

(70) Herrmann, W. A.; Goossen, L. J.; Köcher, C.; Artus, G. R. J. Chiral Heterocylic Carbenes in Asymmetric Homogeneous Catalysis. *Angew. Chem. Int. Ed.* **1996**, *35* (2324), 2805–2807. https://doi.org/10.1002/anie.199628051.

(71) Kelly, R. A.; Clavier, H.; Giudice, S.; Scott, N. M.; Stevens, E. D.; Bordner, J.; Samardjiev, I.; Hoff, C. D.; Cavallo, L.; Nolan, S. P. Determination of N-Heterocyclic Carbene (NHC) Steric and Electronic Parameters Using the [(NHC)Ir$(CO)_2$Cl] System. *Organometallics* **2008**, *27* (2), 202–210. https://doi.org/10.1021/om701001g.

(72) Chianese, A. R.; Kovacevic, A.; Zeglis, B. M.; Faller, J. W.; Crabtree, R. H. Abnormal C_5-Bound N-Heterocyclic Carbenes: Extremely Strong Electron Donor Ligands and Their Iridium(I) and Iridium(III) Complexes. *Organometallics* **2004**, *23* (10), 2461–2468. https://doi.org/10.1021/om049903h.

(73) Voutchkova, A. M.; Appelhans, L. N.; Chianese, A. R.; Crabtree, R. H. Disubstituted Imidazolium-2-Carboxylates as Efficient Precursors to N-Heterocyclic Carbene Complexes of Rh, Ru, Ir, and Pd. *J. Am. Chem. Soc.* **2005**, *127* (50), 17624–17625. https://doi.org/10.1021/ja056625k.

(74) Organ, M. G.; Çalimsiz, S.; Sayah, M.; Hoi, K. H.; Lough, A. J. Pd-PEPPSI-IPent: An Active, Sterically Demanding Cross-Coupling Catalystand Its Application in the Synthesis of Tetra-Ortho-Substituted Biaryls. *Angew. Chem. Int. Ed.* **2009**, *48* (13), 2383–2387. https://doi.org/10.1002/anie.200805661.

(75) Hillier, A. C.; Sommer, W. J.; Yong, B. S.; Petersen, J. L.; Cavallo, L.; Nolan, S. P. A Combined Experimental and Theoretical Study Examining the Binding of N-Heterocyclic Carbenes (NHC) to the Cp*RuCl (Cp* = η^5-C_5Me_5) Moiety: Insight into Stereoelectronic Differences between Unsaturated and Saturated NHC Ligands. *Organometallics* **2003**, *22* (21), 4322–4326. https://doi.org/10.1021/om034016k.

(76) Hoshimoto, Y.; Ogoshi, S. Development of Metal Complexes Equipped with Structurally Flexible Carbenes. *Bull. Chem. Soc. Jpn.* **2021**, *94* (1), 327–338. https://doi.org/10.1246/BCSJ.20200293.

(77) Zhou, G.; Ting, P.; Aslanian, R.; Piwinski, J. J. A Useful Pd-Catalyzed Negishi Coupling Approach to Benzylic Sulfonamide Derivatives. *Org. Lett.* **2008**, *10* (12), 2517–2520. https://doi.org/10.1021/ol800785g.

(78) Zhou, J.; Fu, G. C. Palladium-Catalyzed Negishi Cross-Coupling Reactions of Unactivated Alkyl Iodides, Bromides, Chlorides, and Tosylates. *J. Am. Chem. Soc.* **2003**, *125* (41), 12527–12530. https://doi.org/10.1021/ja0363258.

(79) Semeniuchenko, V.; Sharif, S.; Day, J.; Chandrasoma, N.; Pietro, W. J.; Manthorpe, J.; Braje, W. M.; Organ, M. G. (DiMeIHept^{Cl})Pd: A Low-Load Catalyst for Solvent-Free (Melt) Amination. *J. Org. Chem.* **2021**, *86* (15), 10343–10359. https://doi.org/10.1021/acs.joc.1c01057.

(80) Khadra, A.; Mayer, S.; Organ, M. G. Pd-PEPPSI-IPent^{Cl}: A Useful Catalyst for the Coupling of 2-Aminopyridine Derivatives. *Chem. Eur. J.* **2017**, *23* (13), 3206–3212. https://doi.org/10.1002/chem.201605490.

(81) Organ, M. G.; Chass, G. A.; Fang, D. C.; Hopkinson, A. C.; Valente, C. Pd-NHC (PEPPSI) Complexes: Synthetic Utility and Computational Studies into Their Reactivity. *Synthesis* **2008**, No. 17, 2776–2797. https://doi.org/10.1055/s-2008-1067225.

(82) Organ, M. G.; Avola, S.; Dubovyk, I.; Hadei, N.; Kantchev, E. A. B.; O'Brien, C. J.; Valente, G. A User-Friendly, All-Purpose Pd-NHC (NHC = N-Heterocyclic Carbene) Precatalyst for the Negishi Reaction: A Step towards a Universal Cross-Coupling Catalyst. *Chem. Eur. J.* **2006**, *12* (18), 4749–4755. https://doi.org/10.1002/chem.200600206.

(83) Price, G. A.; Bogdan, A. R.; Aguirre, A. L.; Iwai, T.; Djuric, S. W.; Organ, M. G. Continuous Flow

Negishi Cross-Couplings Employing Silica-Supported: Pd-PEPPSI - IPr Precatalyst. *Catal. Sci. Technol.* **2016**, *6* (13), 4733–4742. https://doi.org/10.1039/c6cy00331a.

(84) Sharif, S.; Rucker, R. P.; Chandrasoma, N.; Mitchell, D.; Rodriguez, M. J.; Froese, R. D. J.; Organ, M. G. Selective Monoarylation of Primary Amines Using the Pd-PEPPSI-IPent^{Cl} Precatalyst. *Angew. Chem. Int. Ed.* **2015**, *54* (33), 9507–9511. https://doi.org/10.1002/anie.201502822.

(85) Hoi, K. H.; Coggan, J. A.; Organ, M. G. Pd-PEPPSI-IPent^{Cl}: An Effective Catalyst for the Preparation of Triarylamines. *Chem. Eur. J.* **2013**, *19* (3), 843–845. https://doi.org/10.1002/chem.201203379.

(86) Organ, M. G.; Abdel-Hadi, M.; Avola, S.; Dubovyk, I.; Hadei, N.; Kantchev, E. A. B.; O'Brien, C. J.; Sayah, M.; Valente, C. Pd-Catalyzed Aryl Amination Mediated by Well Defined, N-Heterocyclic Carbene (NHC)-Pd Precatalysts, PEPPSI. *Chem. Eur. J.* **2008**, *14* (8), 2443–2452. https://doi.org/10.1002/chem.200701621.

(87) Sayah, M.; Organ, M. G. Carbon-Sulfur Bond Formation of Challenging Substrates at Low Temperature by Using Pd-PEPPSI-IPent. *Chem. Eur. J.* **2011**, *17* (42), 11719–11722. https://doi.org/10.1002/chem.201102158.

(88) Farmer, J. L.; Hunter, H. N.; Organ, M. G. Regioselective Cross-Coupling of Allylboronic Acid Pinacol Ester Derivatives with Aryl Halides via Pd-PEPPSI-IPent. *J. Am. Chem. Soc.* **2012**, *134* (42), 17470–17473. https://doi.org/10.1021/ja308613b.

(89) Hevia, E.; Chua, J. Z.; García-Álvarez, P.; Kennedy, A. R.; McCall, M. D. Exposing the Hidden Complexity of Stoichiometric and Catalytic Metathesis Reactions by Elucidation of Mg-Zn Hybrids. *Proc. Natl. Acad. Sci. U. S. A.* **2010**, *107* (12), 5294–5299. https://doi.org/10.1073/pnas.0913307107.

(90) Kim, J. G.; Walsh, P. J. From Aryl Bromides to Enantioenriched Benzylic Alcohols in a Single Flask:

Catalytic Asymmetric Arylation of Aldehydes. *Angew. Chem. Int. Ed.* **2006**, *45* (25), 4175–4178. https://doi.org/10.1002/anie.200600741.

(91) Campos, K. R.; Klapars, A.; Waldman, J. H.; Dormer, P. G.; Chen, C. Y. Enantioselective, Palladium-Catalyzed α-Arylation of N-Boc-Pyrrolidine. *J. Am. Chem. Soc.* **2006**, *128* (11), 3538–3539. https://doi.org/10.1021/ja0605265.

(92) Berman, A. M.; Johnson, J. S. Copper-Catalyzed Electrophilic Amination of Functionalized Diarylzinc Reagents. *J. Org. Chem.* **2005**, *70* (1), 364–366. https://doi.org/10.1021/jo048168g.

(93) Tucker, C. E.; Majid, T. N.; Knochel, P. Preparation of Highly Functionalized Magnesium, Zinc, and Copper Aryl and Alkenyl Organometallics via the Corresponding Organolithiums. *J. Am. Chem. Soc.* **1992**, *114* (10), 3983–3985. https://doi.org/10.1021/ja00036a060.

(94) Rieke, R. D.; Uhm, S. J.; Hudnall, P. M. Activated Metals. Preparation of Highly Reactive Zinc. *J. Chem. Soc. Chem. Commun.* **1973**, No. 8, 269b--270. https://doi.org/10.1039/C3973000269b.

(95) Krasovskiy, A.; Malakhov, V.; Gavryushin, A.; Knochel, P. Efficient Synthesis of Functionalized Organozinc Compounds by the Direct Insertion of Zinc into Organic Iodides and Bromides. *Angew. Chem. Int. Ed.* **2006**, *45* (36), 6040–6044. https://doi.org/10.1002/anie.200601450.

(96) Scott, W. J.; Stille, J. K. Palladium-Catalyzed Coupling of Vinyl Triflates with Organostannanes. Synthetic and Mechanistic Studies. *J. Am. Chem. Soc.* **1986**, *108* (11), 3033–3040. https://doi.org/10.1021/ja00271a037.

(97) Achonduh, G. T.; Hadei, N.; Valente, C.; Avola, S.; O'Brien, C. J.; Organ, M. G. On the Role of Additives in Alkyl-Alkyl Negishi Cross-Couplings. *Chem. Commun.* **2010**, *46* (23), 4109–4111. https://doi.org/10.1039/c002759f.

(98) Koszinowski, K.; Böhrer, P. Formation of Organozincate Anions in LiCl-Mediated Zinc Insertion

Reactions. *Organometallics* **2009**, *28* (3), 771–779. https://doi.org/10.1021/om800947t.

(99) Koszinowski, K.; Böhrer, P. Aggregation and Reactivity of Organozincate Anions Probed by Electrospray Mass Spectrometry. *Organometallics* **2009**, *28* (1), 100–110. https://doi.org/10.1021/om8007037.

(100) Hunter, H. N.; Hadei, N.; Blagojevic, V.; Patschinski, P.; Achonduh, G. T.; Avola, S.; Bohme, D. K.; Organ, M. G. Identification of a Higher-Order Organozincate Intermediate Involved in Negishi Cross-Coupling Reactions by Mass Spectrometry and NMR Spectroscopy. *Chem. Eur. J.* **2011**, *17* (28), 7845–7851. https://doi.org/10.1002/chem.201101029.

(101) Matos, K.; Soderquist, J. A. Alkylboranes in the Suzuki-Miyaura Coupling: Stereochemical and Mechanistic Studies. *J. Org. Chem.* **1998**, *63* (3), 461–470. https://doi.org/10.1021/jo971681s.

(102) Miyaura, N.; Yamada, K.; Suzuki, A. A New Stereospecific Cross-Coupling by the Palladium-Catalyzed Reaction of 1-Alkenylboranes with 1-Alkenyl or 1-Alkynyl Halides. *Tetrahedron Lett.* **1979**, *20* (36), 3437–3440. https://doi.org/10.1016/S0040-4039(01)95429-2.

(103) MacIntosh, I. S.; Sherren, C. N.; Robertson, K. N.; Masuda, J. D.; Pye, C. C.; Clyburne, J. A. C. C. Isolation and Structures of Two New Organozinc Anions from Solutions Rich in Halide Ions. *Organometallics* **2010**, *29* (9), 2063–2068. https://doi.org/10.1021/om901097r.

(104) McCann, L. C.; Hunter, H. N.; Clyburne, J. A. C.; Organ, M. G. Higher-Order Zincates as Transmetalators in Alkyl-Alkyl Negishi Cross-Coupling. *Angew. Chem. Int. Ed.* **2012**, *51* (28), 7024–7027. https://doi.org/10.1002/anie.201203547.

(105) Arp, F. O.; Fu, G. C. Catalytic Enantioselective Negishi Reactions of Racemic Secondary Benzylic Halides. *J. Am. Chem. Soc.* **2005**, *127* (30), 10482–10483. https://doi.org/10.1021/ja053751f.

(106) Tungen, J. E.; Aursnes, M.; Dalli, J.; Arnardottir, H.; Serhan, C. N.; Hansen, T. V. Total Synthesis of

the Anti-Inflammatory and pro-Resolving Lipid Mediator MaR1n-3 DPAutilizing an Sp^3-Sp^3 Negishi Cross-Coupling Reaction. *Chem. Eur. J.* **2014**, *20* (45), 14575–14578. https://doi.org/10.1002/chem.201404721.

(107) McCann, L. C.; Organ, M. G. On the Remarkably Different Role of Salt in the Cross-Coupling of Arylzincs from That Seen with Alkylzincs. *Angew. Chem. Int. Ed.* **2014**, *53* (17), 4386–4389. https://doi.org/10.1002/anie.201400459.

(108) Jin, L.; Liu, C.; Liu, J.; Hu, F.; Lan, Y.; Batsanov, A. S.; Howard, J. A. K.; Marder, T. B.; Lei, A. Revelation of the Difference between Arylzinc Reagents Prepared from Aryl Grignard and Aryllithium Reagents Respectively: Kinetic and Structural Features. *J. Am. Chem. Soc.* **2009**, *131* (46), 16656–16657. https://doi.org/10.1021/ja908198d.

(109) Böck, K.; Feil, J. E.; Karaghiosoff, K.; Koszinowski, K. Catalyst Activation, Deactivation, and Degradation in Palladium-Mediated Negishi Cross-Coupling Reactions. *Chem. Eur. J.* **2015**, *21* (14), 5548–5560. https://doi.org/10.1002/chem.201406408.

(110) Bej, A.; Ghosh, K.; Sarkar, A.; Knight, D. W. Palladium Nanoparticles in the Catalysis of Coupling Reactions. *RSC Adv.* **2016**, *6* (14), 11446–11453. https://doi.org/10.1039/c5ra26304b.

(111) Álvarez, R.; De Lera, A. R.; Aurrecoechea, J. M.; Durana, A. Bimetallic Intermediates in the Formation of Nucleophilic Allenylzincs from Allenylpalladiums: A DFT Study. *Organometallics* **2007**, *26* (11), 2799–2802. https://doi.org/10.1021/om061148f.

(112) Allen, L. C. Electronegativity Is the Average One-Electron Energy of the Valence-Shell Electrons in Ground-State Free Atoms. *J. Am. Chem. Soc.* **1989**, *111* (25), 9003–9014. https://doi.org/10.1021/ja00207a003.

(113) Pompeo, M.; Farmer, J. L.; Froese, R. D. J.; Organ, M. G. Room-Temperature Amination of

Deactivated Aniline and Aryl Halide Partners with Carbonate Base Using a Pd-PEPPSI-IPent^{Cl}-o-Picoline Catalyst. *Angew. Chem. Int. Ed.* **2014**, *53* (12), 3223–3226. https://doi.org/10.1002/anie.201310457.

(114) McCann, L. C.; Hunter, H. N.; Clyburne, J. A. C.; Organ, M. G. Higher-Order Zincates as Transmetalators in Alkyl–Alkyl Negishi Cross-Coupling. *Angew. Chem. Int. Ed.* **2012**, *51* (28), 7024–7027. https://doi.org/10.1002/anie.201203547.

(115) Eckert, P.; Organ, M. G. The Role of LiBr and $ZnBr_2$ on the Cross-Coupling of Aryl Bromides with Bu2Zn or BuZnBr. *Chem. Eur. J.* **2019**, *25* (69), 15751–15754. https://doi.org/10.1002/chem.201903931.

(116) Polynski, M. V.; Pidko, E. A. Intermetallic Species in the Negishi Coupling and Their Involvement in Inhibition Pathways. *Catal. Sci. Technol.* **2019**, *9* (17), 4561–4572. https://doi.org/10.1039/c9cy00752k.

(117) Astakhov, A. V.; Khazipov, O. V.; Chernenko, A. Y.; Pasyukov, D. V.; Kashin, A. S.; Gordeev, E. G.; Khrustalev, V. N.; Chernyshev, V. M.; Ananikov, V. P. A New Mode of Operation of Pd-NHC Systems Studied in a Catalytic Mizoroki-Heck Reaction. *Organometallics* **2017**, *36* (10), 1981–1992. https://doi.org/10.1021/acs.organomet.7b00184.

(118) Graham, D. C.; Cavell, K. J.; Yates, B. F. The Influence of N-Substitution on the Reductive Elimination Behaviour of Hydrocarbyl–Palladium–Carbene Complexes—a DFT Study. *J. Chem. Soc. Dalt. Trans.* **2006**, *60* (1414), 17681768–17751775. https://doi.org/10.1039/b512681a.

(119) Comer, E.; Organ, M. G.; Hynes, S. J. Allylic Ionization versus Oxidative Addition into Vinyl C-X Bonds by Pd with Polyfunctional Olefin Templates. *J. Am. Chem. Soc.* **2004**, *126* (49), 16087–16092. https://doi.org/10.1021/ja045416h.

(120) Nasielski, J.; Hadei, N.; Achonduh, G.; Kantchev, E. A. B.; O'Brien, C. J.; Lough, A.; Organ, M. G. Structure-Activity Relationship Analysis of Pd-PEPPSI Complexes in Cross-Couplings: A Close Inspection of the Catalytic Cycle and the Precatalyst Activation Model. *Chem. Eur. J.* **2010**, *16* (35), 10844–10853. https://doi.org/10.1002/chem.201000138.

(121) Hruszkewycz, D. P.; Balcells, D.; Guard, L. M.; Hazari, N.; Tilset, M. Insight into the Efficiency of Cinnamyl-Supported Precatalysts for the Suzuki-Miyaura Reaction: Observation of Pd(I) Dimers with Bridging Allyl Ligands during Catalysis. *J. Am. Chem. Soc.* **2014**, *136* (20), 7300–7316. https://doi.org/10.1021/ja412565c.

(122) Li, G.; Lei, P.; Szostak, M.; Casals-Cruañas, E.; Poater, A.; Cavallo, L.; Nolan, S. P. Mechanistic Study of Suzuki–Miyaura Cross-Coupling Reactions of Amides Mediated by [Pd(NHC)(Allyl)Cl] Precatalysts. *ChemCatChem* **2018**, *10* (14), 3096–3106. https://doi.org/10.1002/cctc.201800511.

(123) Bruno, B. J.; Miller, G. D.; Lim, C. S. Basics and Recent Advances in Peptide and Protein Drug Delivery. *Ther. Deliv.* **2013**, *4* (11), 1443–1467. https://doi.org/10.4155/tde.13.104.

(124) Mathur, D.; Prakash, S.; Anand, P.; Kaur, H.; Agrawal, P.; Mehta, A.; Kumar, R.; Singh, S.; Raghava, G. P. S. PEPlife: A Repository of the Half-Life of Peptides. *Sci. Rep.* **2016**, *6*. https://doi.org/10.1038/srep36617.

(125) Martin, V.; Egelund, P. H. G.; Johansson, H.; Thordal Le Quement, S.; Wojcik, F.; Sejer Pedersen, D. Greening the Synthesis of Peptide Therapeutics: An Industrial Perspective. *RSC Adv.* **2020**, *10* (69), 42457–42492. https://doi.org/10.1039/d0ra07204d.

(126) López-Otín, C.; Bond, J. S. Proteases: Multifunctional Enzymes in Life and Disease. *J. Biol. Chem.* **2008**, *283* (45), 30433–30437. https://doi.org/10.1074/jbc.R800035200.

(127) Palomo, J. M. Solid-Phase Peptide Synthesis: An Overview Focused on the Preparation of

Biologically Relevant Peptides. *RSC Adv.* **2014**, *4* (62), 32658–32672. https://doi.org/10.1039/c4ra02458c.

(128) Torbeev, V. Y.; Kent, S. B. H. Convergent Chemical Synthesis and Crystal Structure of a 203 Amino Acid "Covalent Dimer" HIV-1 Protease Enzyme Molecule. *Angew. Chem. Int. Ed.* **2007**, *46* (10), 1667–1670. https://doi.org/10.1002/anie.200604087.

(129) Werner, H. M.; Cabalteja, C. C.; Horne, W. S. Peptide Backbone Composition and Protease Susceptibility: Impact of Modification Type, Position, and Tandem Substitution. *ChemBioChem* **2016**, *17* (8), 712–718. https://doi.org/10.1002/cbic.201500312.

(130) Kedrowski, B. L.; Heathcock, C. H. Thiazoline Ring Formation from 2-Methylcysteines and 2-Halomethylalanines. *Heterocycles* **2002**, *58*, 601–634. https://doi.org/10.3987/com-02-s(m)60.

(131) Di Giacomo, M.; Vinci, V.; Serra, M.; Colombo, L. New Fast and Practical Method for the Enantioselective Synthesis of α-Vinyl, α-Alkyl Quaternary α-Amino Acids. *Tetrahedron Asymmetry* **2008**, *19* (2), 247–257. https://doi.org/10.1016/j.tetasy.2007.12.012.

(132) Wang, H. F.; Ma, G. H.; Yang, S. B.; Han, R. G.; Xu, P. F. A Concise Synthesis of (+)-Conagenin and Its Isomer Using Chiral Tricyclic Iminolactones. *Tetrahedron Asymmetry* **2008**, *19* (13), 1630–1635. https://doi.org/10.1016/j.tetasy.2008.06.033.

(133) Jackson, R. F. W.; Moore, R. J.; Dexter, C. S.; Elliott, J.; Mowbray, C. E. Concise Synthesis of Enantiomerically Pure Phenylalanine, Homophenylalanine, and Bishomophenylalanine Derivatives Using Organozinc Chemistry: NMR Studies of Amino Acid-Derived Organozinc Reagents. *J. Org. Chem.* **1998**, *63* (22), 7875–7884. https://doi.org/10.1021/jo981133u.

(134) Sköld, N.; Nielsen, B.; Olsen, J.; Han, L.; Olsen, L.; Madsen, U.; Kristensen, J. L.; Pickering, D. S.; Johansen, T. N. Design, Synthesis and in Vitro Pharmacology of GluK1 and GluK3 Antagonists.

Studies towards the Design of Subtype-Selective Antagonists through 2-Carboxyethyl-Phenylalanines with Substituents Interacting with Non-Conserved Residues in the GluK Binding Sit. *Bioorg. Med. Chem.* **2014**, *22* (19), 5368–5377. https://doi.org/10.1016/j.bmc.2014.07.045.

(135) Ross, A. J.; Lang, H. L.; Jackson, R. F. W. Much Improved Conditions for the Negishi Cross-Coupling of Iodoalanine Derived Zinc Reagents with Aryl Halides. *J. Org. Chem.* **2010**, *75* (1), 245–248. https://doi.org/10.1021/jo902238n.

(136) Brittain, W. D. G.; Cobb, S. L. Negishi Cross-Couplings in the Synthesis of Amino Acids. *Org. Biomol. Chem.* **2017**, *16* (1), 10–20. https://doi.org/10.1039/c7ob02682j.

(137) Ogawa, K.; Hayashi, T.; Lin, Y. Y.; Usuki, T. Synthesis of Desmosine-Containing Cyclic Peptide for the Possible Elucidation of Elastin Crosslinking Structure. *Tetrahedron* **2017**, *73* (27–28), 3838–3847. https://doi.org/10.1016/j.tet.2017.05.045.

(138) Ross, A. J.; Dreiocker, F.; Schä Fer, M.; Oomens, J.; Meijer, A. J. H. M.; Pickup, B. T.; Jackson, R. F. W. Evidence for the Role of Tetramethylethylenediamine in Aqueous Negishi Cross-Coupling: Synthesis of Nonproteinogenic Phenylalanine Derivatives on Water. *J. Org. Chem.* **2011**, *76* (6), 1727–1734. https://doi.org/10.1021/jo102334c.

(139) Chien, H. C.; Colas, C.; Finke, K.; Springer, S.; Stoner, L.; Zur, A. A.; Venteicher, B.; Campbell, J.; Hall, C.; Flint, A.; Augustyn, E.; Hernandez, C.; Heeren, N.; Hansen, L.; Anthony, A.; Bauer, J.; Fotiadis, D.; Schlessinger, A.; Giacomini, K. M.; Thomas, A. A. Reevaluating the Substrate Specificity of the L-Type Amino Acid Transporter (LAT1). *J. Med. Chem.* **2018**, *61* (16), 7358–7373. https://doi.org/10.1021/acs.jmedchem.8b01007.

(140) Dexter, C. S.; Hunter, C.; Jackson, R. F. W.; Elliott, J. NMR Kinetic Studies on the Decomposition of β-Amidozinc Reagents: Optimization of Palladium-Catalyzed Cross-Coupling with Acid Chlorides. *J.*

Org. Chem. **2000**, *65* (22), 7417–7421. https://doi.org/10.1021/jo000558p.

(141) Jackson, R. F. W.; Rilatt, I.; Murray, P. J. The Rate of Elimination of a β-Amino Zinc Reagent Is Reduced by Using a Better Leaving Group. *Chem. Commun.* **2003**, *3* (11), 1242–1243. https://doi.org/10.1039/b302564k.

(142) Smith, N. D.; Goodman, M. Enantioselective Synthesis of α-Methyl-D-Cysteine and Lanthionine Building Blocks via α-Methyl-d-Serine-β-Lactone. *Org. Lett.* **2003**, *5* (7), 1035–1037. https://doi.org/10.1021/ol034025p.

(143) Anson, M. S.; Clark, H. F.; Evans, P.; Fox, M. E.; Graham, J. P.; Griffiths, N. N.; Meek, G.; Ramsden, J. A.; Roberts, A. J.; Simmonds, S.; Walker, M. D.; Willets, M. Complementary Syntheses of N,O-Protected-(S)-2-Methylserine on a Multikilogram Scale. *Org. Process Res. Dev.* **2011**, *15* (2), 389–397. https://doi.org/10.1021/op100299d.

(144) Yu, W.; McConathy, J.; Williams, L.; Camp, V. M.; Malveaux, E. J.; Zhang, Z.; Olson, J. J.; Goodman, M. M. Synthesis, Radiolabeling, and Biological Evaluation of (R)- and (S)-2-Amino-3-[^{18}F]Fluoro-2-Methylpropanoic Acid (FAMP) and (R)- and (S)-3-[^{18}F]Fluoro-2-Methyl-2-n-(Methylamino)Propanoic Acid (NMeFAMP) as Potential PET Radioligands for Imaging Brain Tumor. *J. Med. Chem.* **2010**, *53* (2), 876–886. https://doi.org/10.1021/jm900556s.

(145) Kudaj, A.; Olma, A. A Convenient Transformation of α-Alkylserines into α-Halogenomethyl-α-Alkylglycines. *Tetrahedron Lett.* **2008**, *49* (45), 6445–6447. https://doi.org/10.1016/j.tetlet.2008.08.098.

(146) Usuki, T.; Yanuma, H.; Hayashi, T.; Yamada, H.; Suzuki, N.; Masuyama, Y. Improved Negishi Cross-Coupling Reactions of an Organozinc Reagent Derived from l -Aspartic Acid with Monohalopyridines. *J. Heterocycl. Chem.* **2014**, *51* (1), 269–273.

https://doi.org/10.1002/jhet.1807.

(147) Behrendt, R.; White, P.; Offer, J. Advances in Fmoc Solid-Phase Peptide Synthesis. *J. Pept. Sci.* **2016**, *22* (1), 4–27. https://doi.org/10.1002/psc.2836.

(148) Krasovskiy, A.; Knochel, P. Convenient Titration Method for Organometallic Zinc, Magnesium, and Lanthanide Reagents. *Synthesis* **2006**, No. 5, 890–891. https://doi.org/10.1055/s-2006-926345.

(149) Green, M. L. H.; Conway, S. L. J.; Doerrer, L. H. Hydrogen/Deuterium Exchange in Alkyl-Hydride Derivatives of Ansa-Tungstenocene Compounds. *Polyhedron* **2005**, *24* (11), 1388–1403. https://doi.org/10.1016/j.poly.2005.05.004.

(150) Fors, B. P.; Buchwald, S. L. Pd-Catalyzed Conversion of Aryl Chlorides, Triflates, and Nonaflates to Nitroaromatics. *J. Am. Chem. Soc.* **2009**, *131* (36), 12898–12899. https://doi.org/10.1021/ja905768k.

(151) Zhou, W. J.; Wang, K. H.; Wang, J. X. Pd(PPh3)4-PEG 400 Catalyzed Protocol for the Atom-Efficient Stille Cross-Coupling Reaction of Organotin with Aryl Bromides. *J. Org. Chem.* **2009**, *74* (15), 5599–5602. https://doi.org/10.1021/jo9005206.

(152) Kondolff, I.; Doucet, H.; Santelli, M. Palladium-Tetraphosphine as Catalyst Precursor for High-Turnover-Number Negishi Cross-Coupling of Alkyl- or Phenylzinc Derivatives with Aryl Bromides. *Organometallics* **2006**, *25* (22), 5219–5222. https://doi.org/10.1021/om060605p.

(153) Ackermann, L.; Kapdi, A. R.; Schulzke, C. Air-Stable Secondary Phosphine Oxide or Chloride (Pre)Ligands for Cross-Couplings of Unactivated Alkyl Chlorides. *Org. Lett.* **2010**, *12* (10), 2298–2301. https://doi.org/10.1021/ol100658y.

(154) Moorhouse, S.; Wilkinson, G. Bis[(Trimethylsilyl)Methyl]- and Bis(Neopentyl)-Zinc, and Tris[(Trimethylsilyl)Methyl]Aluminium-Diethyl Ether (1/1); Their Use as Alkylating Agents in

Forming Niobium and Tantalum Alkyls. *J. Chem. Soc. Dalt. Trans.* **1974**, No. 20, 2187–2190. https://doi.org/10.1039/DT9740002187.

(155) Zhang, P.; Le, C. C.; MacMillan, D. W. C. Silyl Radical Activation of Alkyl Halides in Metallaphotoredox Catalysis: A Unique Pathway for Cross-Electrophile Coupling. *J. Am. Chem. Soc.* **2016**, *138* (26), 8084–8087. https://doi.org/10.1021/jacs.6b04818.

(156) Meiries, S.; Le Duc, G.; Chartoire, A.; Collado, A.; Speck, K.; Arachchige, K. S. A.; Slawin, A. M. Z.; Nolan, S. P. Large yet Flexible N-Heterocyclic Carbene Ligands for Palladium Catalysis. *Chem. Eur. J.* **2013**, *19* (51), 17358–17368. https://doi.org/10.1002/chem.201302471.

Appendix

NMR spectra for chapter 2

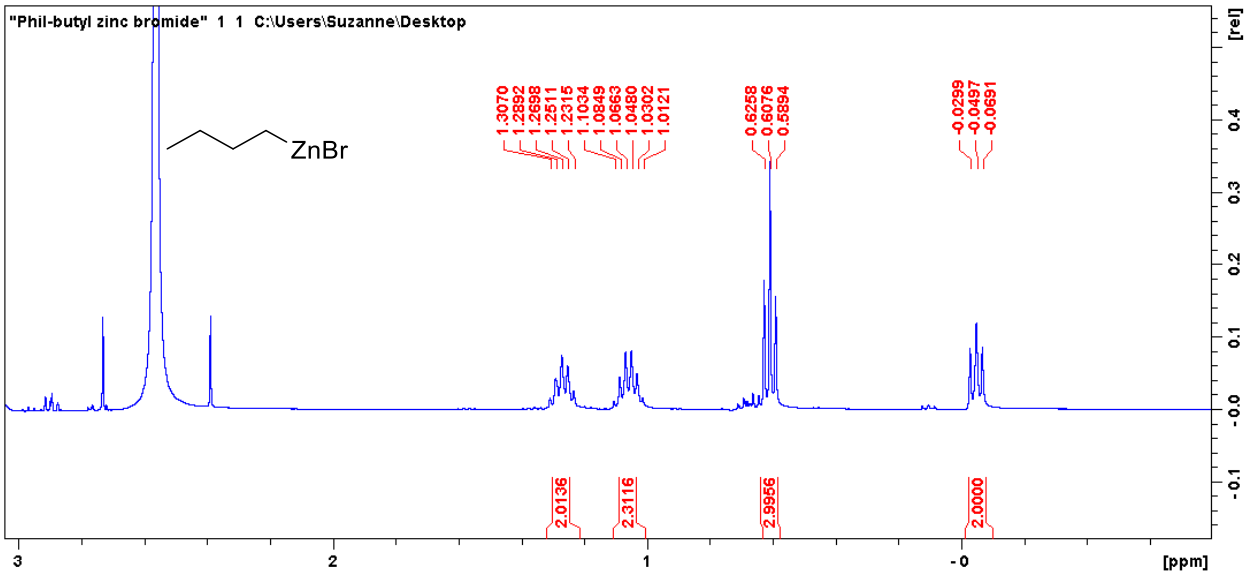

^{1}H NMR spectrum of BuZnBr (**53**) (300 MHz, DMI)

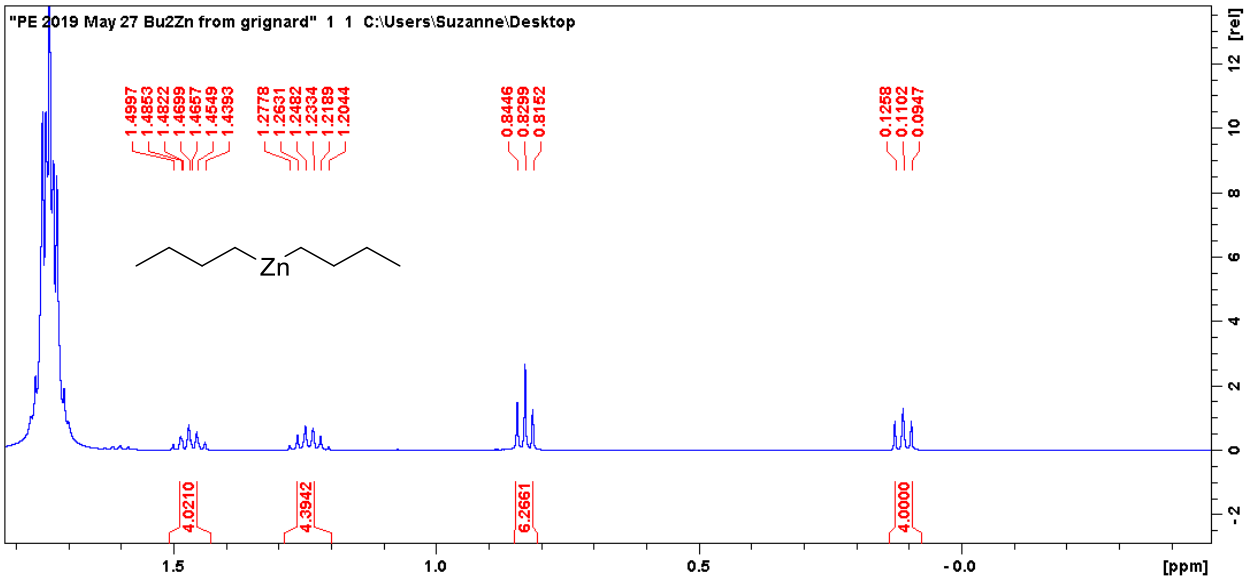

^{1}H Spectrum of Bu_2Zn (**70**) (500 MHz, THF)

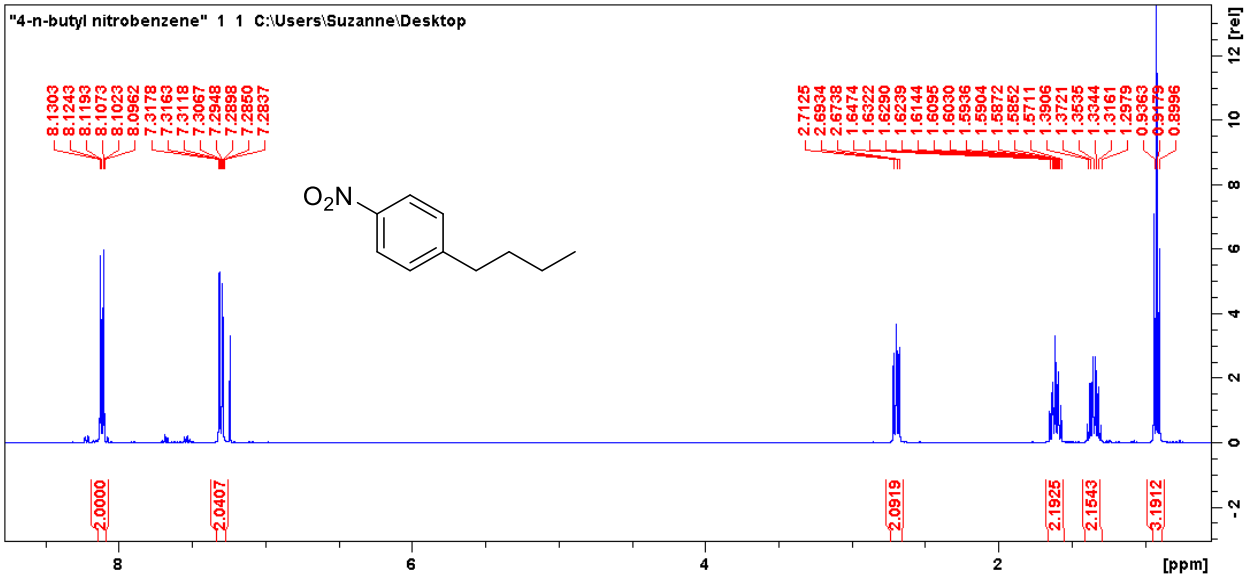

^{1}H NMR spectrum of **69a** (500 MHz, $CDCl_3$)

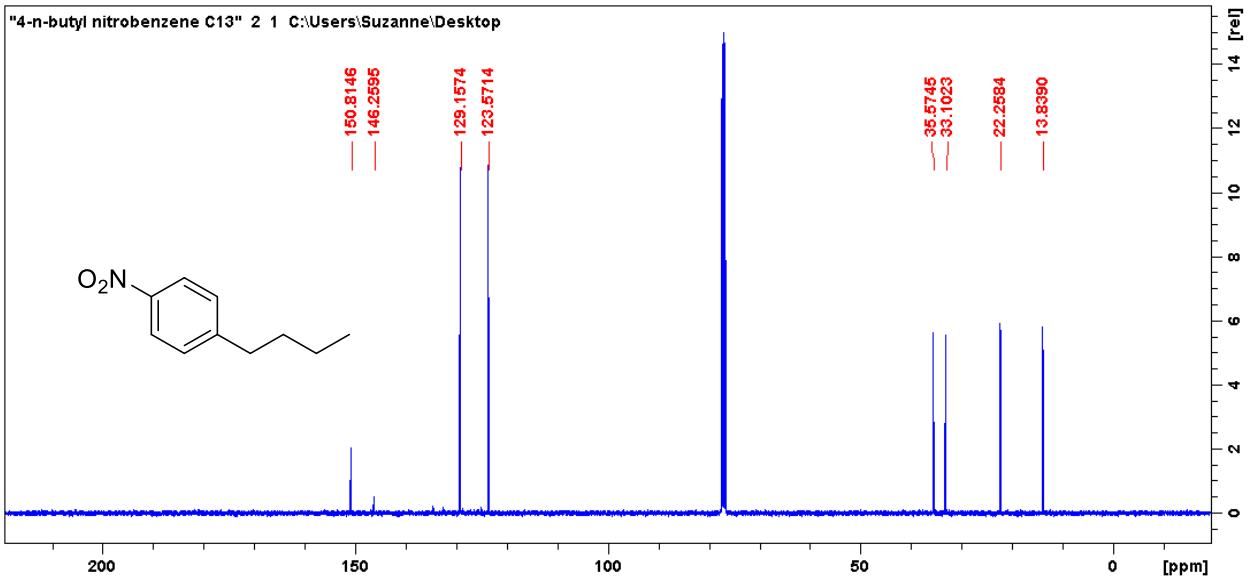

^{13}C NMR spectrum of **69a** (125 MHz, $CDCl_3$)

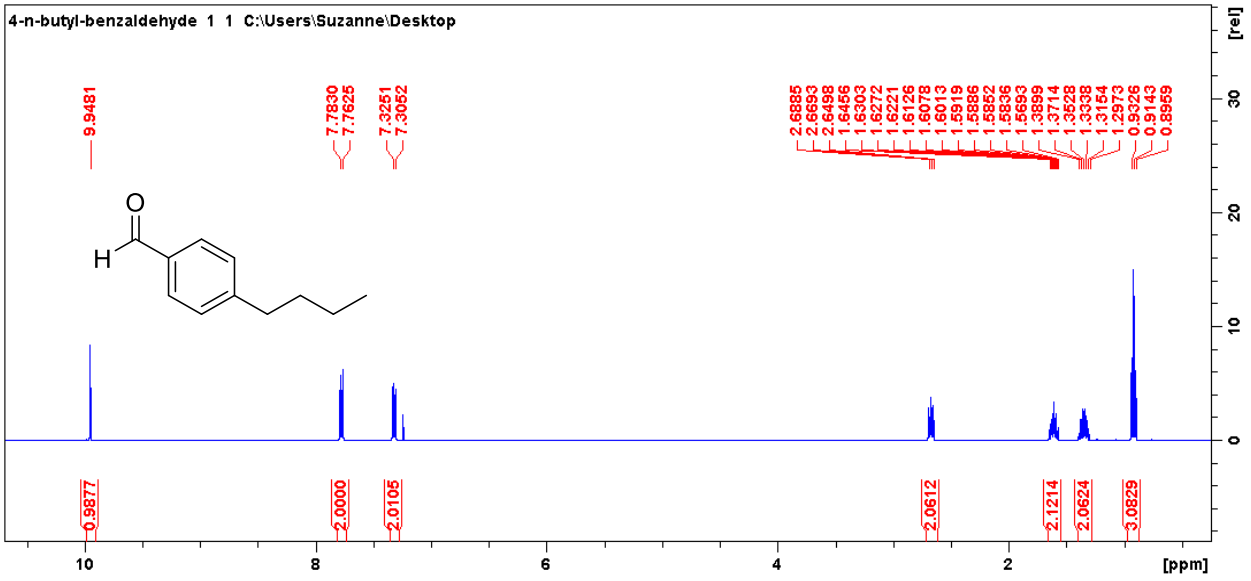

^{1}H NMR spectrum of **69b** (400 MHz, $CDCl_3$)

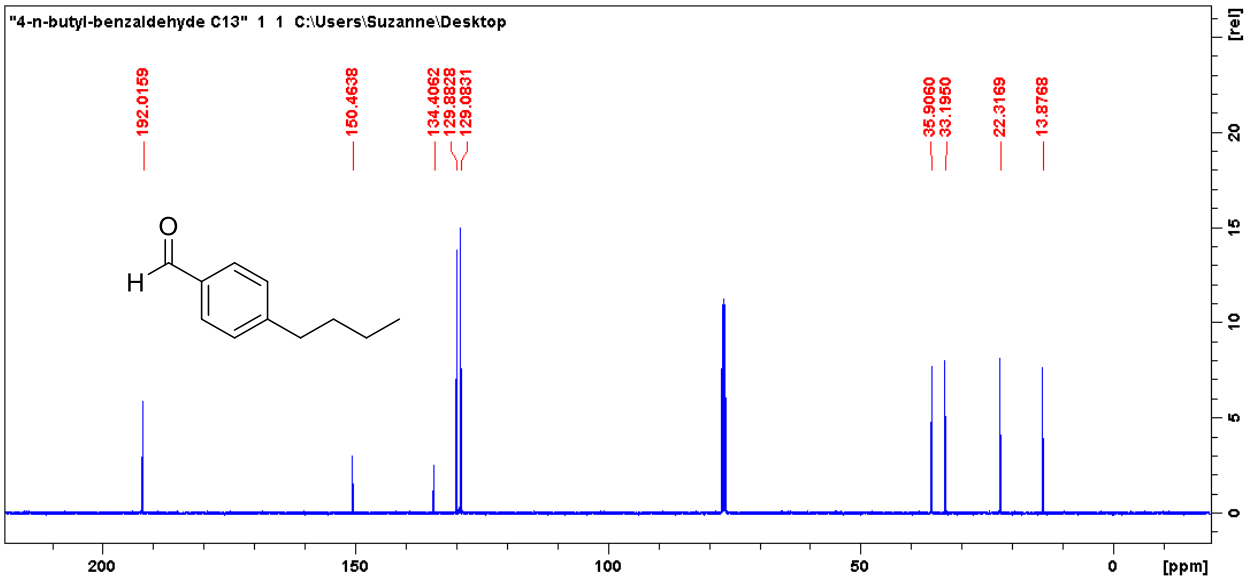

^{13}C NMR spectrum of **69b** (100 MHz, $CDCl_3$)

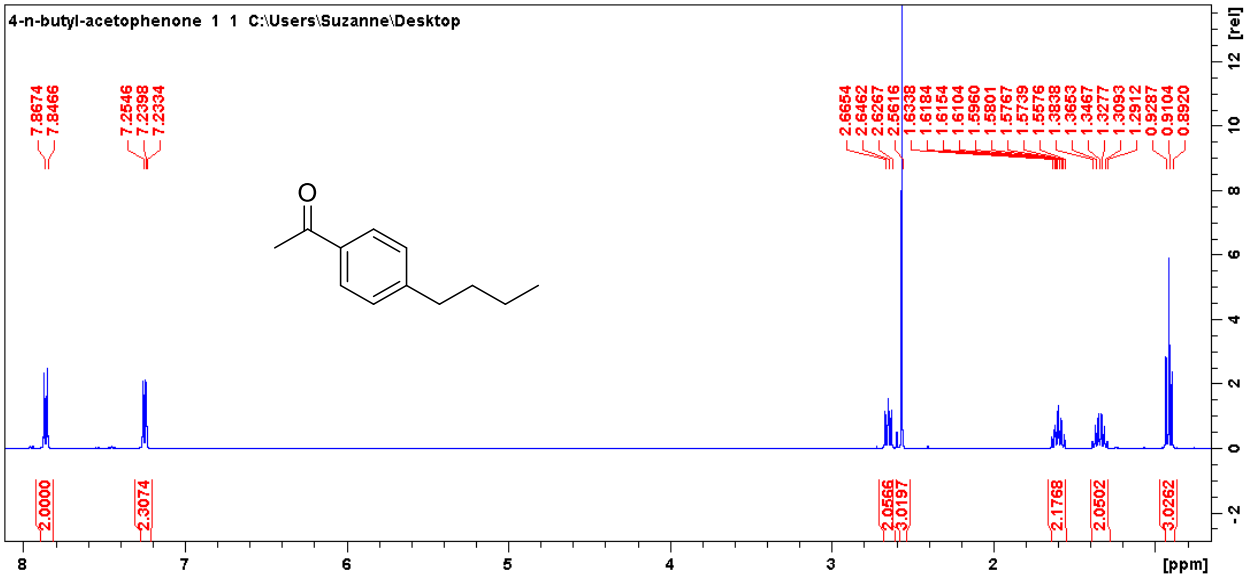

^{1}H NMR spectrum of **69c** (500 MHz, $CDCl_3$)

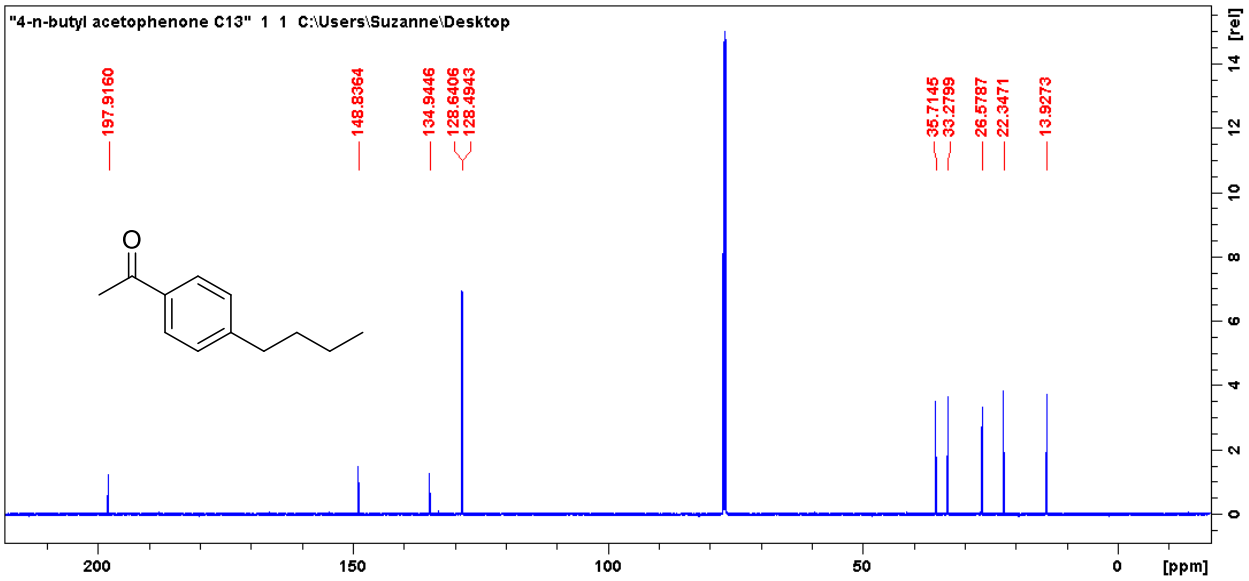

^{13}C NMR spectrum of **69c** (125 MHz, $CDCl_3$)

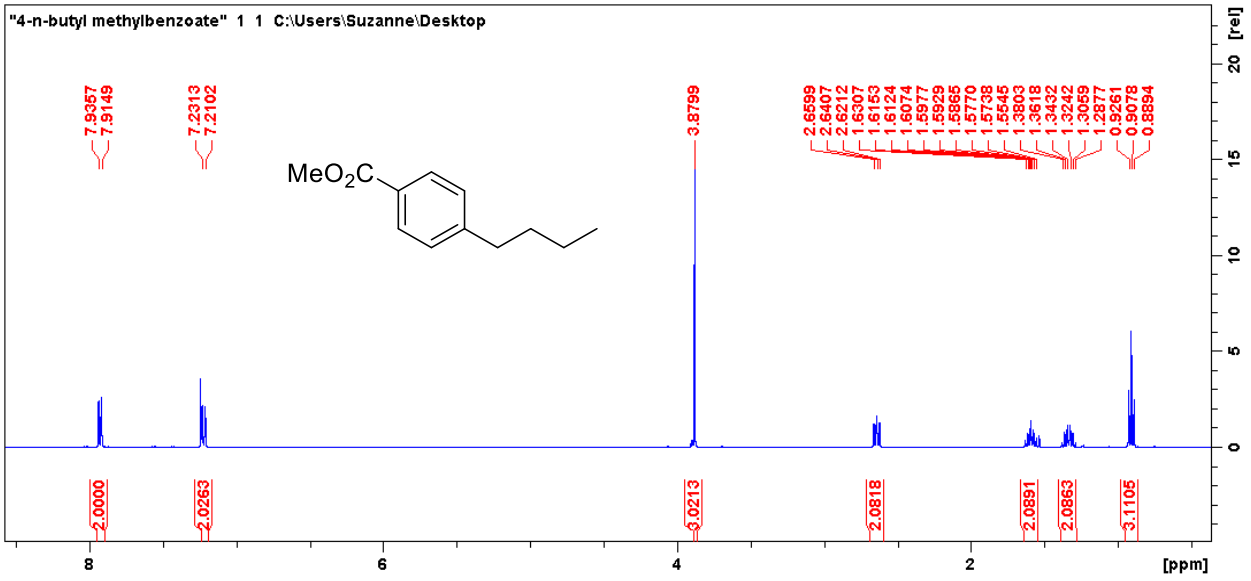

^{1}H NMR spectrum of **69d** (400 MHz, $CDCl_3$)

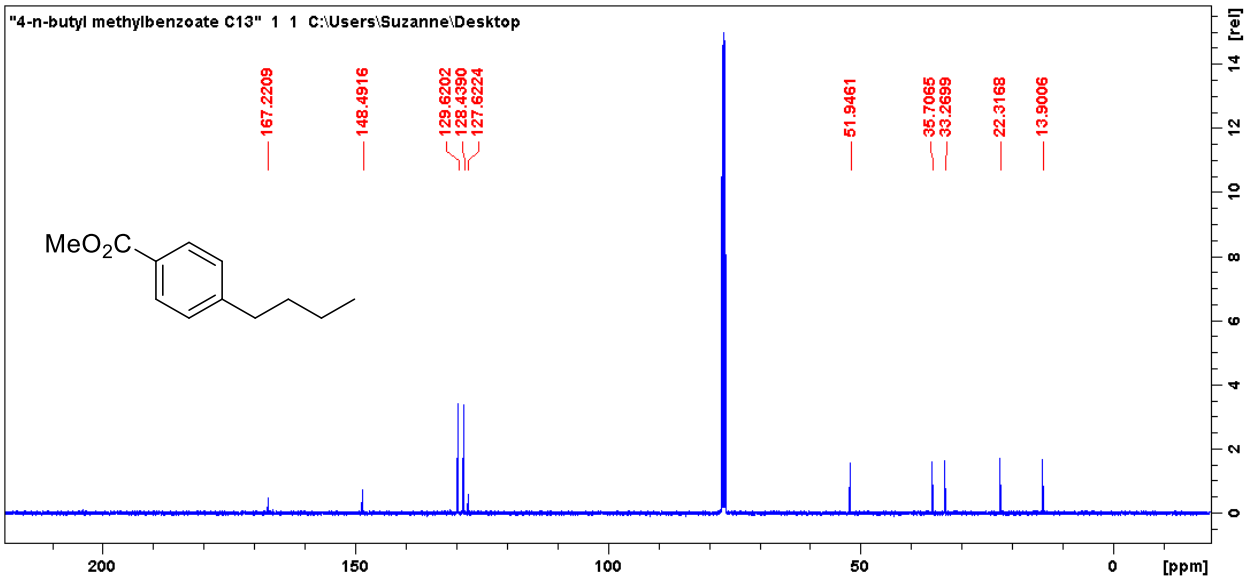

^{13}C NMR spectrum of **69d** (100 MHz, $CDCl_3$)

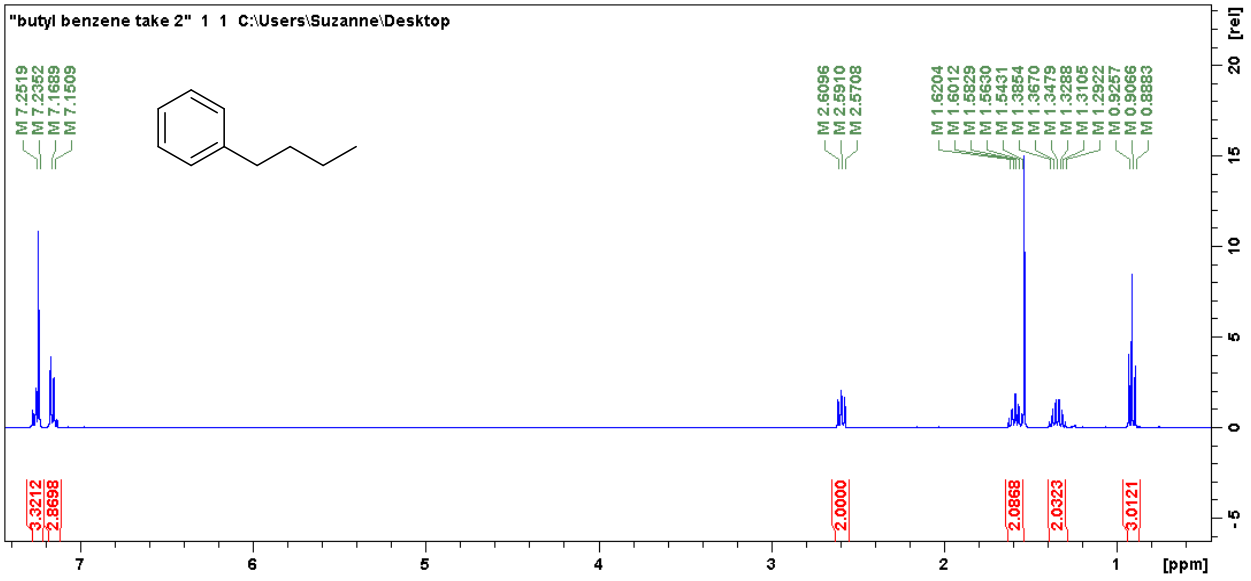

^{1}H NMR spectrum of **69e** (400 MHz, $CDCl_3$)

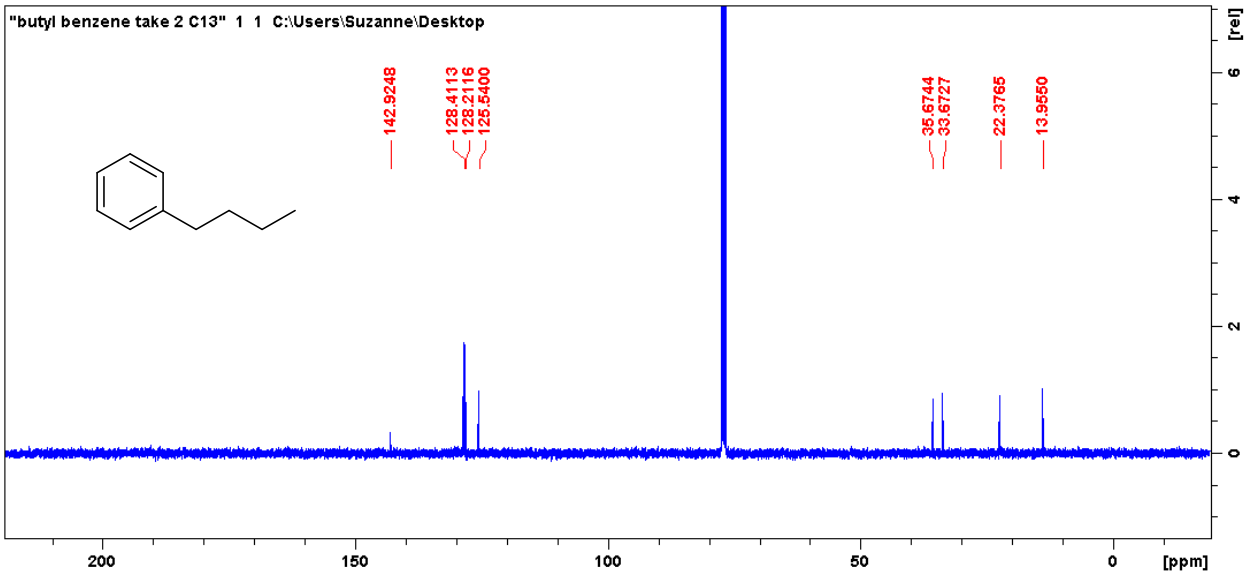

^{13}C NMR spectrum of **69e** (100 MHz, $CDCl_3$)

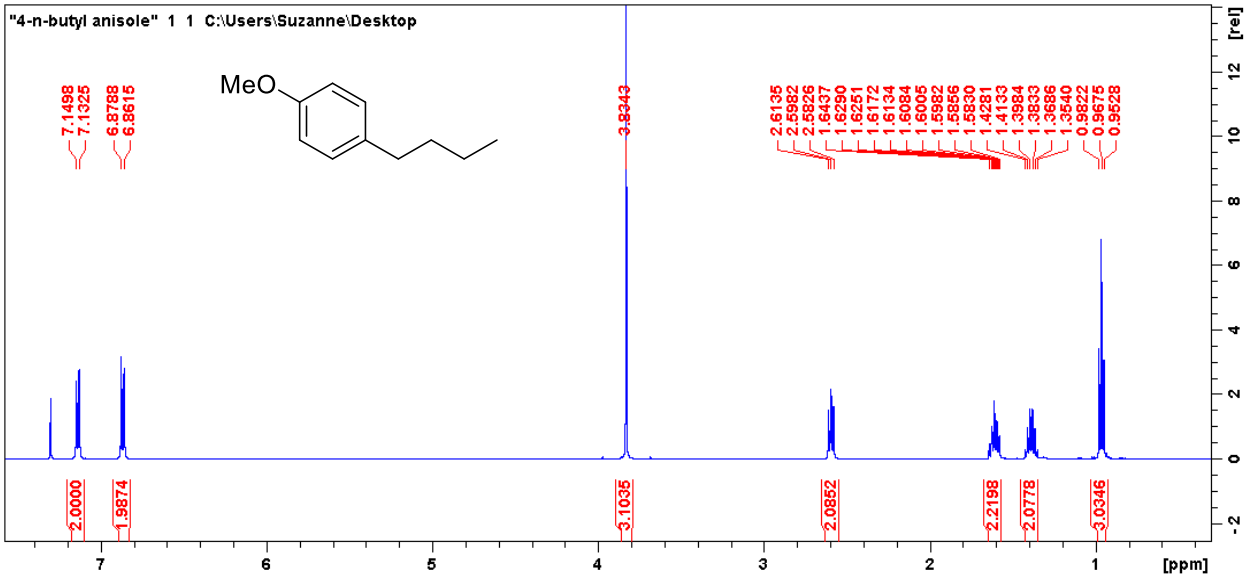

^{1}H NMR spectrum of **69f** (500 MHz, $CDCl_3$)

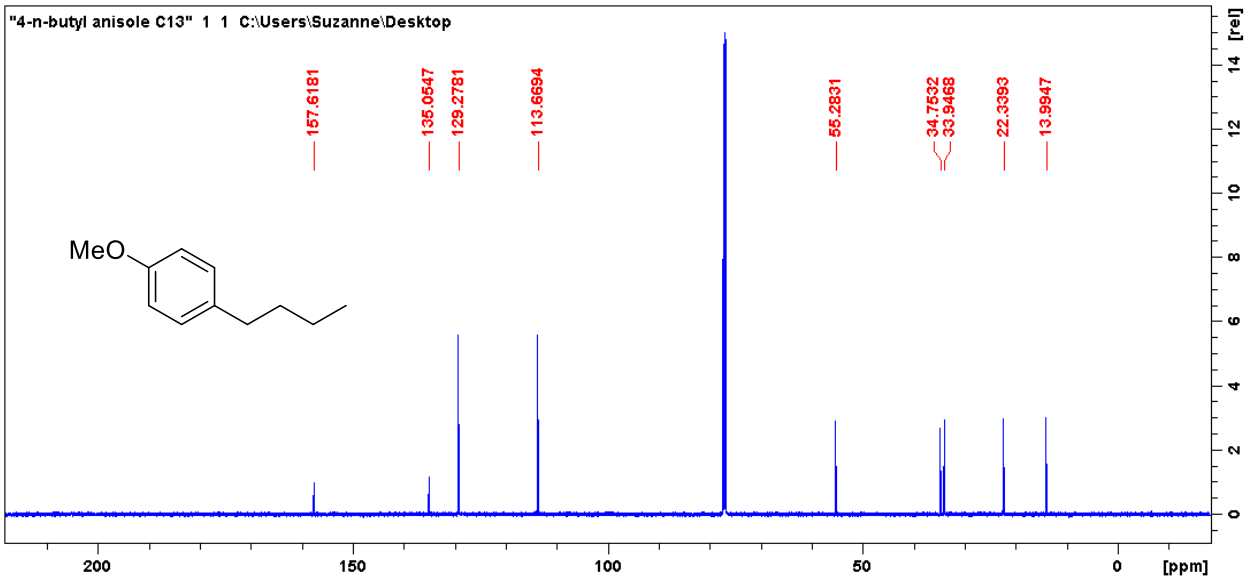

^{13}C NMR spectrum of **69f** (125 MHz, $CDCl_3$)

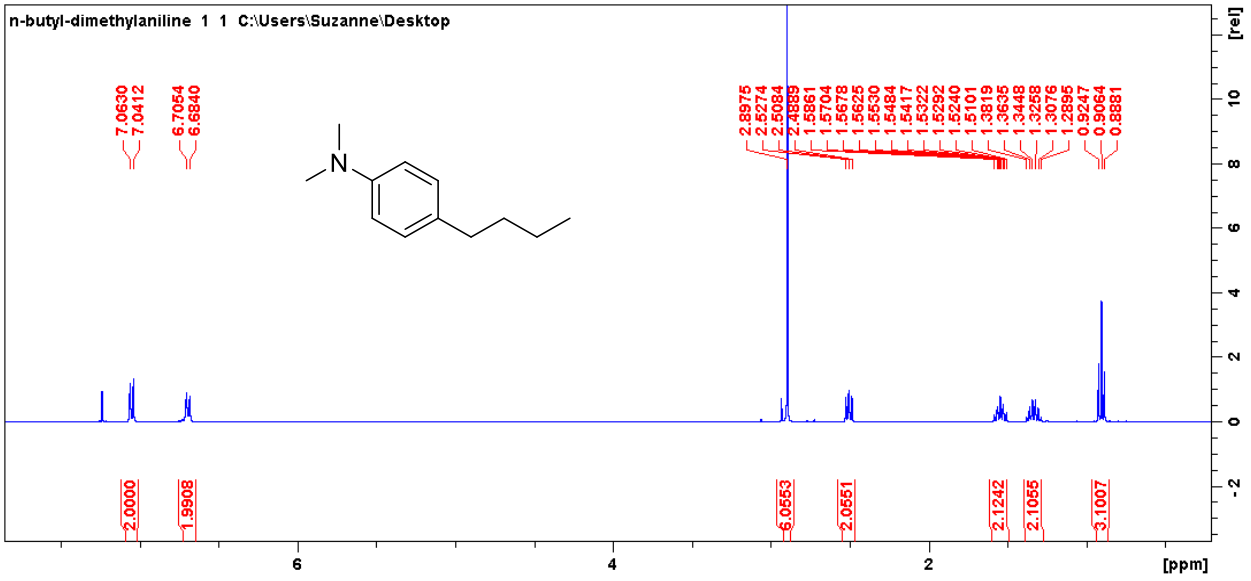

^{1}H NMR spectrum of **69g** (400 MHz, $CDCl_3$)

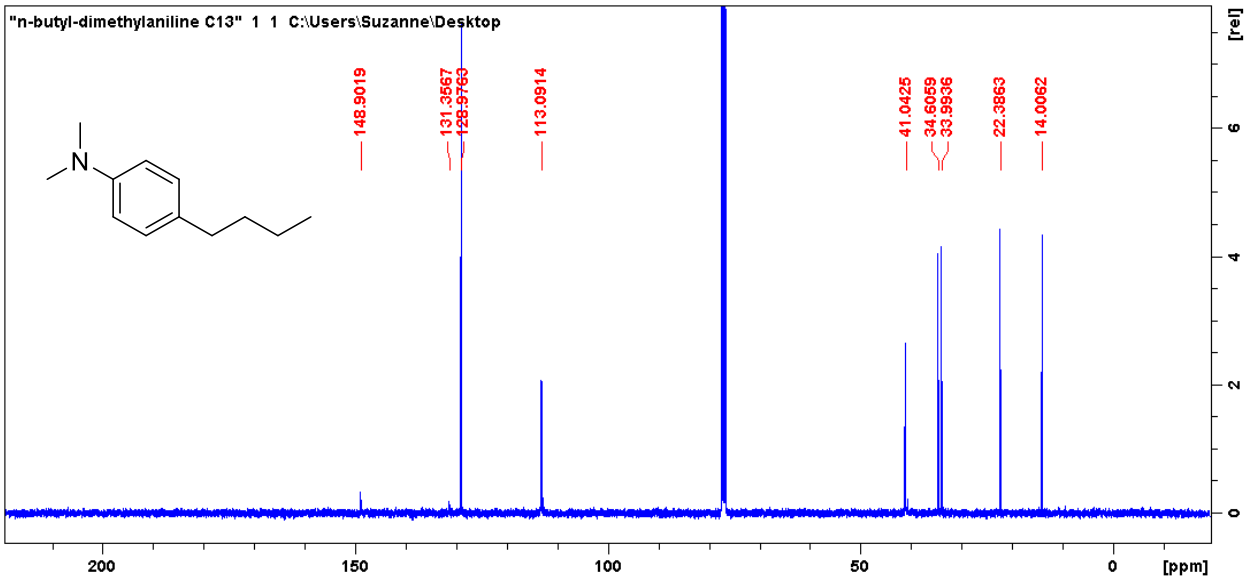

^{13}C NMR spectrum of **69g** (100 MHz, $CDCl_3$)

NMR spectra for chapter 3

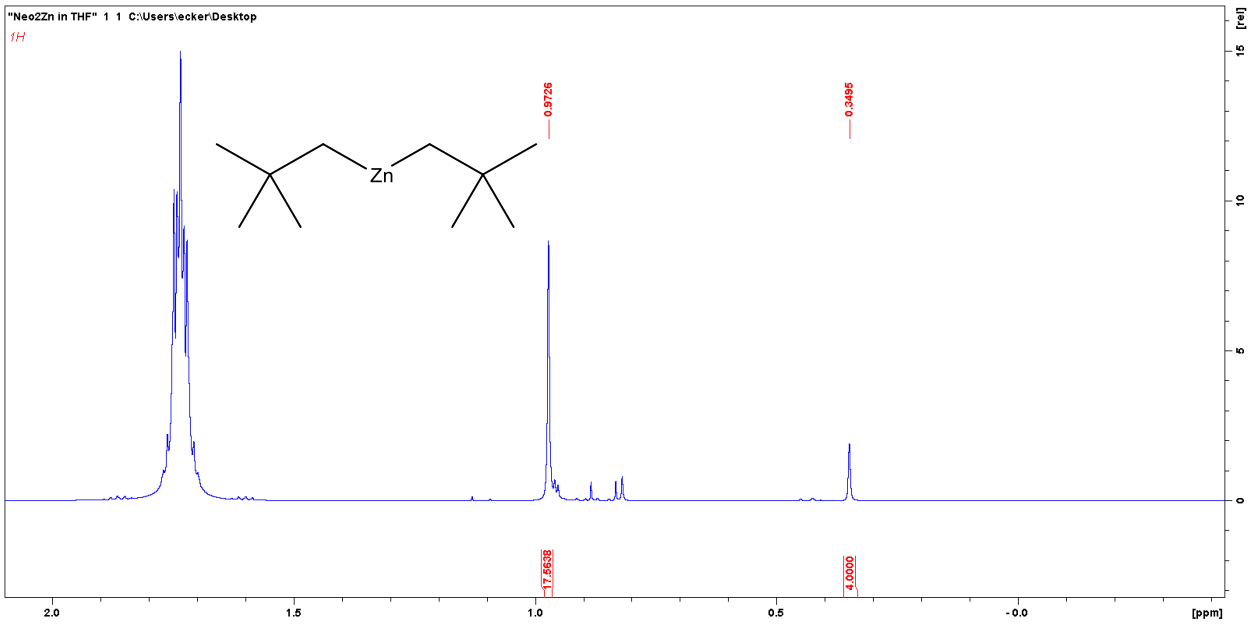

^{1}H Spectrum of Bis-*neo*-Pentyl Zinc (**84**) (500 MHz, THF)

^{1}H NMR spectrum of **85** (500 MHz, $CDCl_3$)

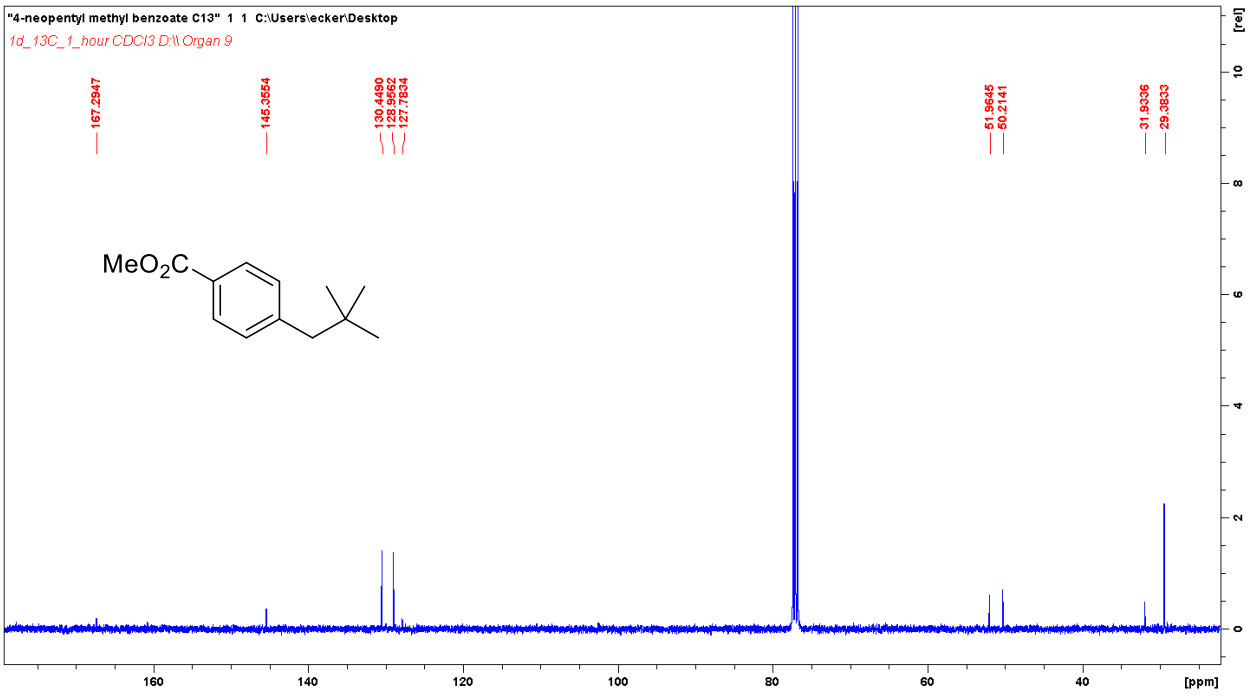

^{13}C NMR spectrum of **85** (125 MHz, $CDCl_3$)

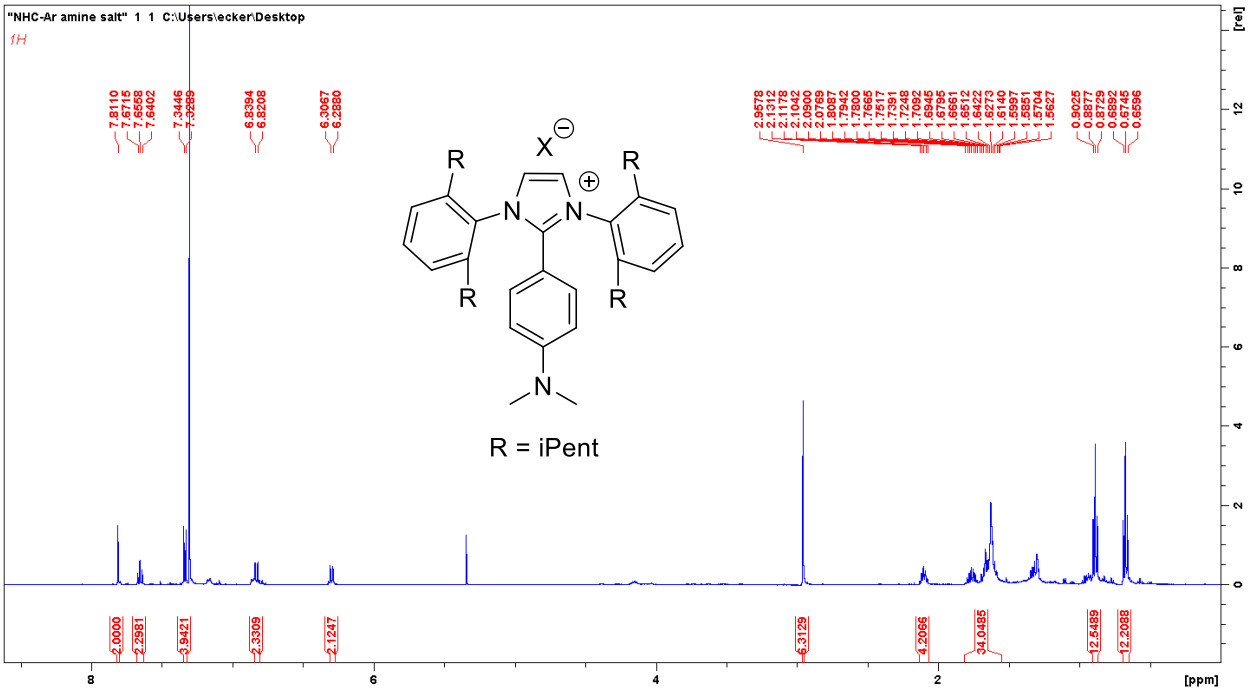

^{1}H NMR spectrum of **78g** (500 MHz, $CDCl_3$)

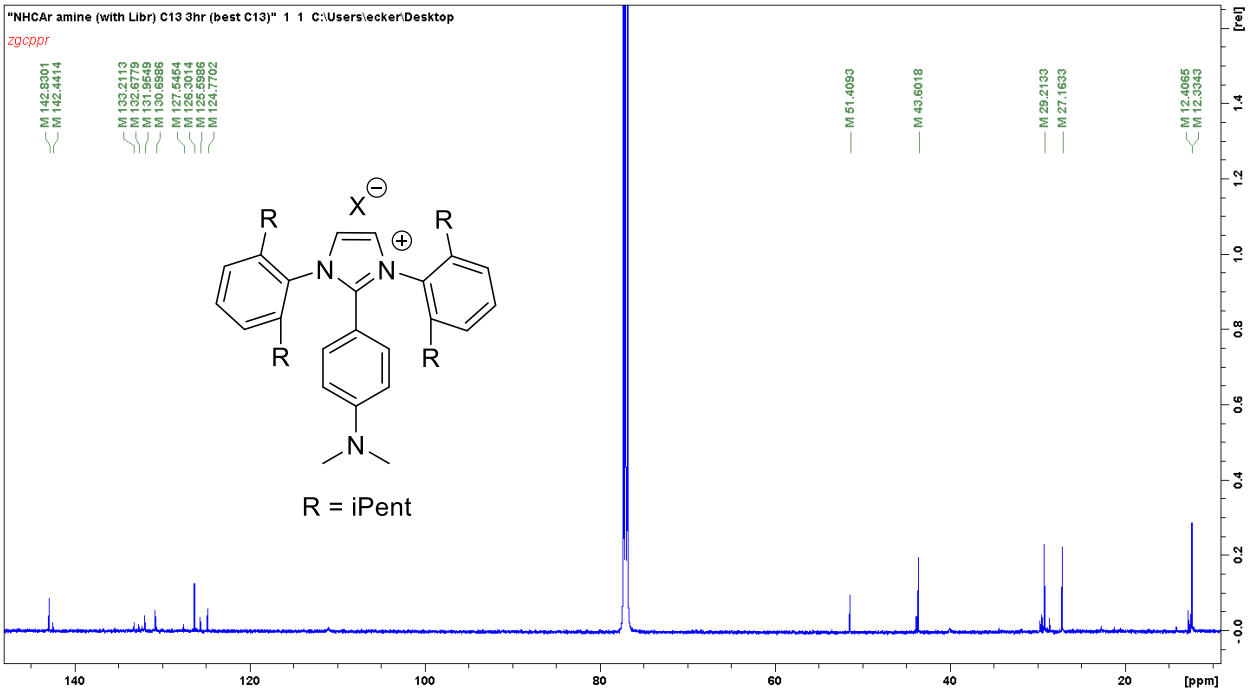

^{13}C NMR spectrum of **78g** (125 MHz, $CDCl_3$)

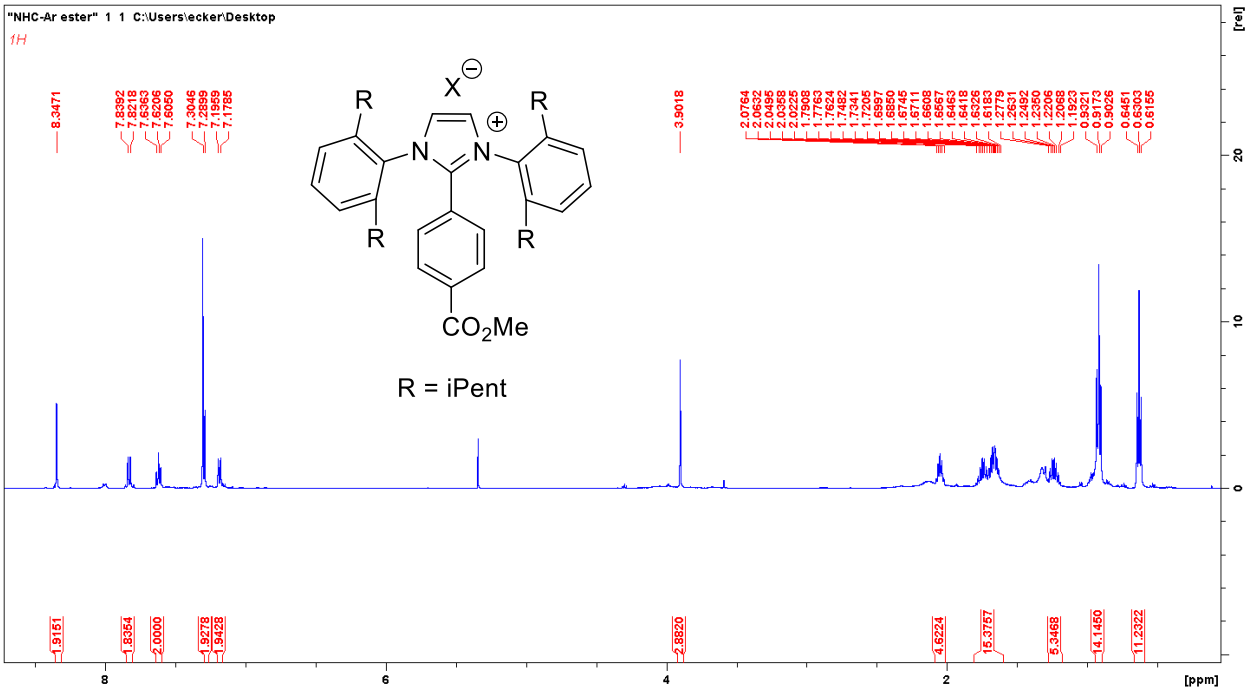

^{1}H NMR spectrum of **78d** (500 MHz, $CDCl_3$)

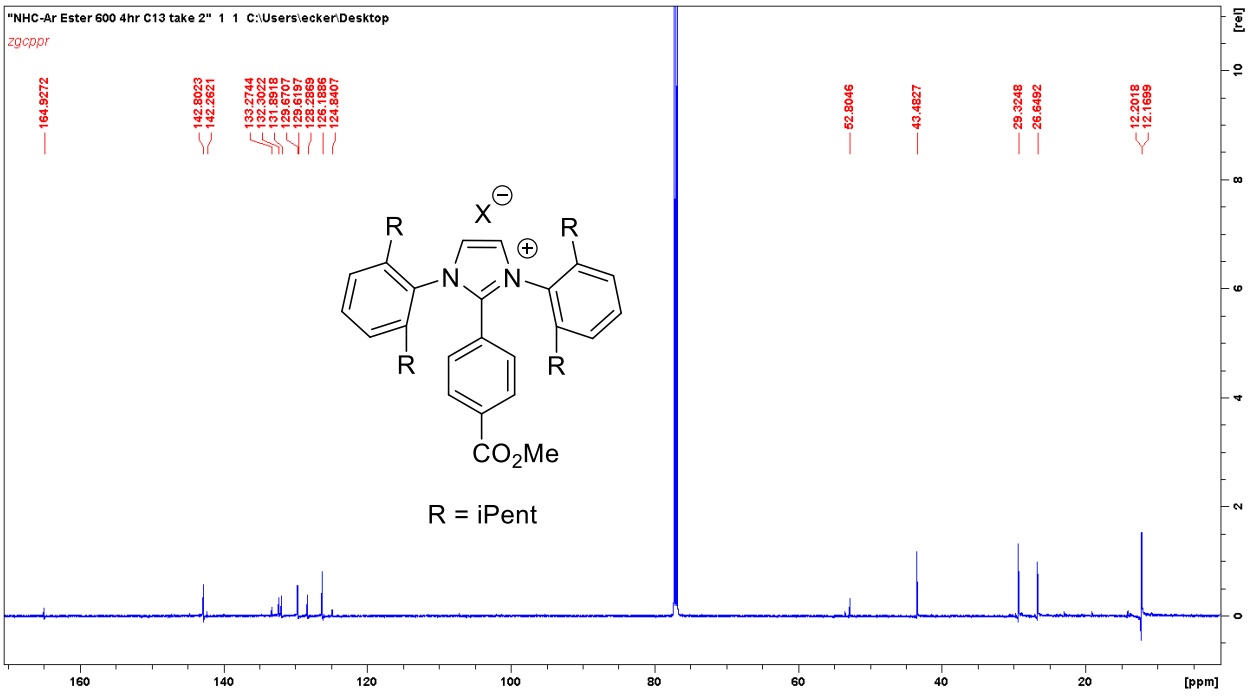

^{13}C NMR spectrum of **78d** (125 MHz, $CDCl_3$)

NMR spectra for chapter 4

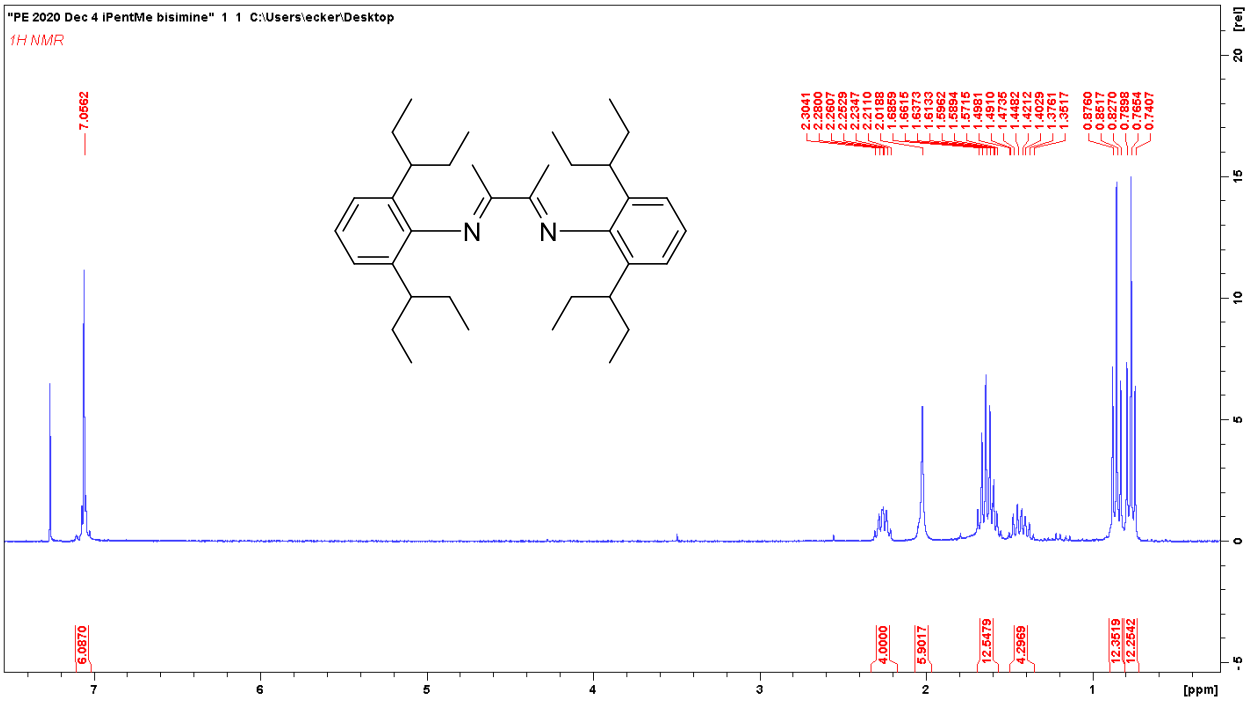

^{1}H NMR spectrum of **95a** (400 MHz, $CDCl_3$)

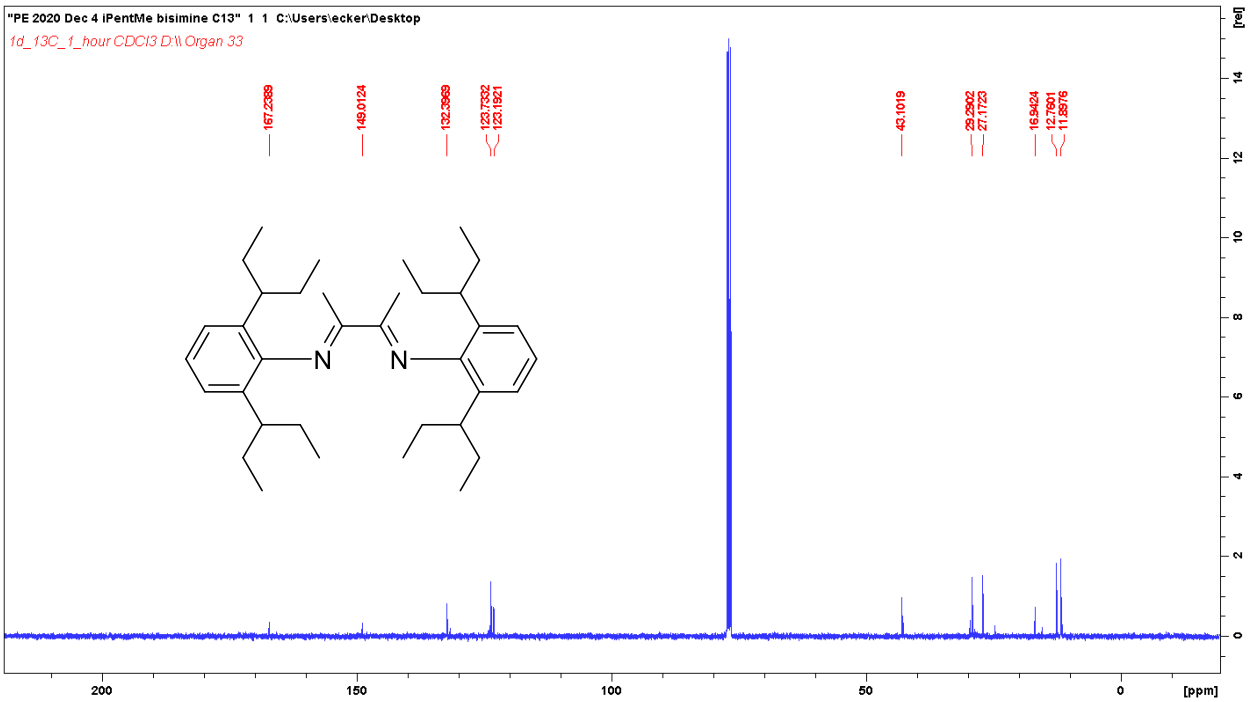

^{13}C NMR spectrum of **95a** (100 MHz, $CDCl_3$)

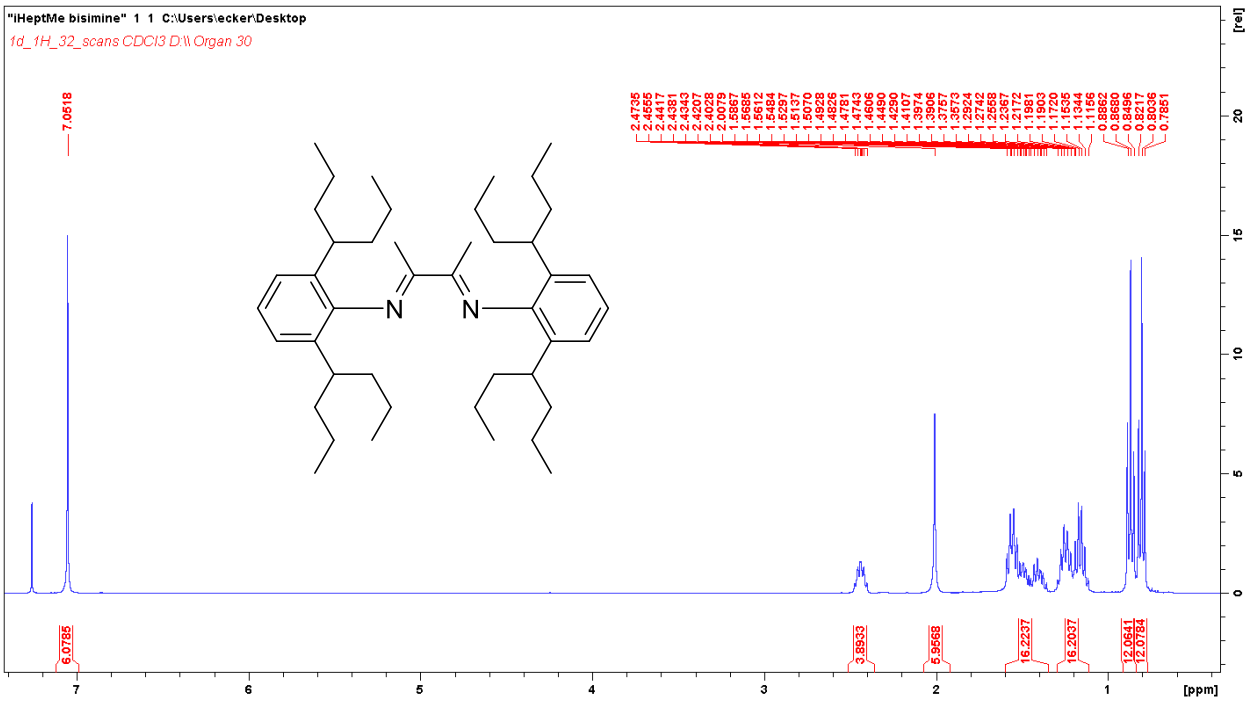

^{1}H NMR spectrum of **95b** (400 MHz, $CDCl_3$)

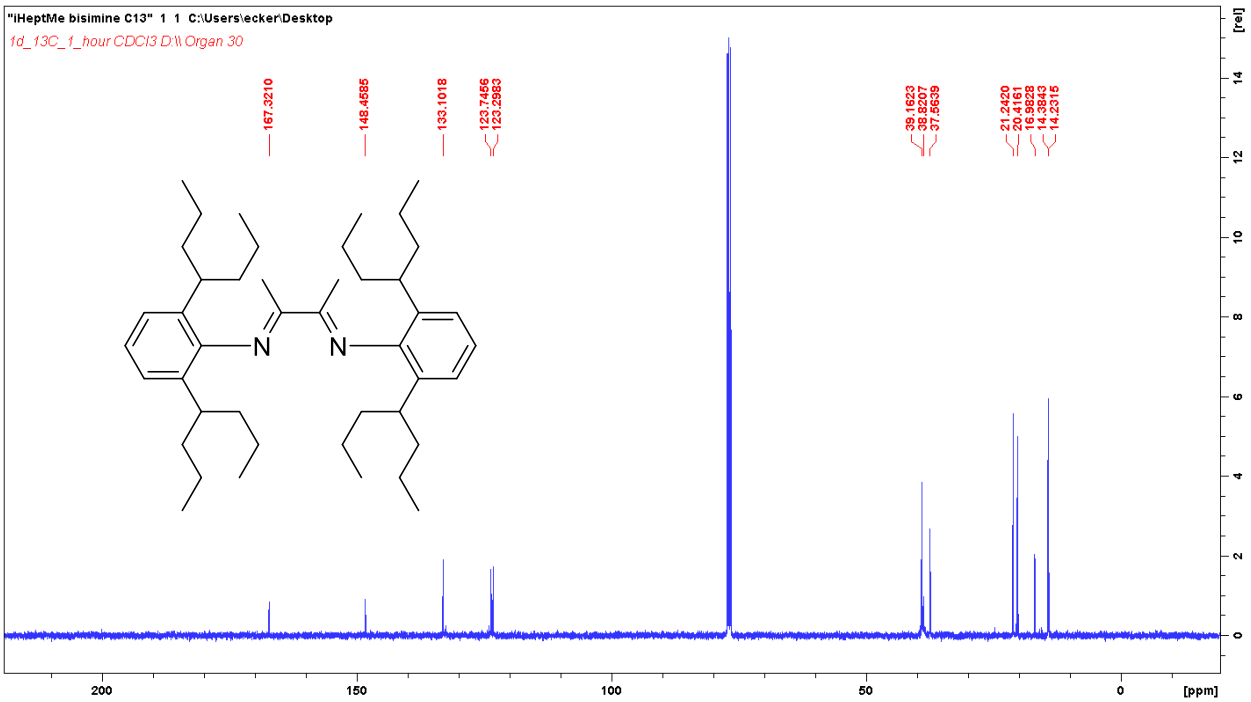

^{13}C NMR spectrum of **95b** (100 MHz, $CDCl_3$)

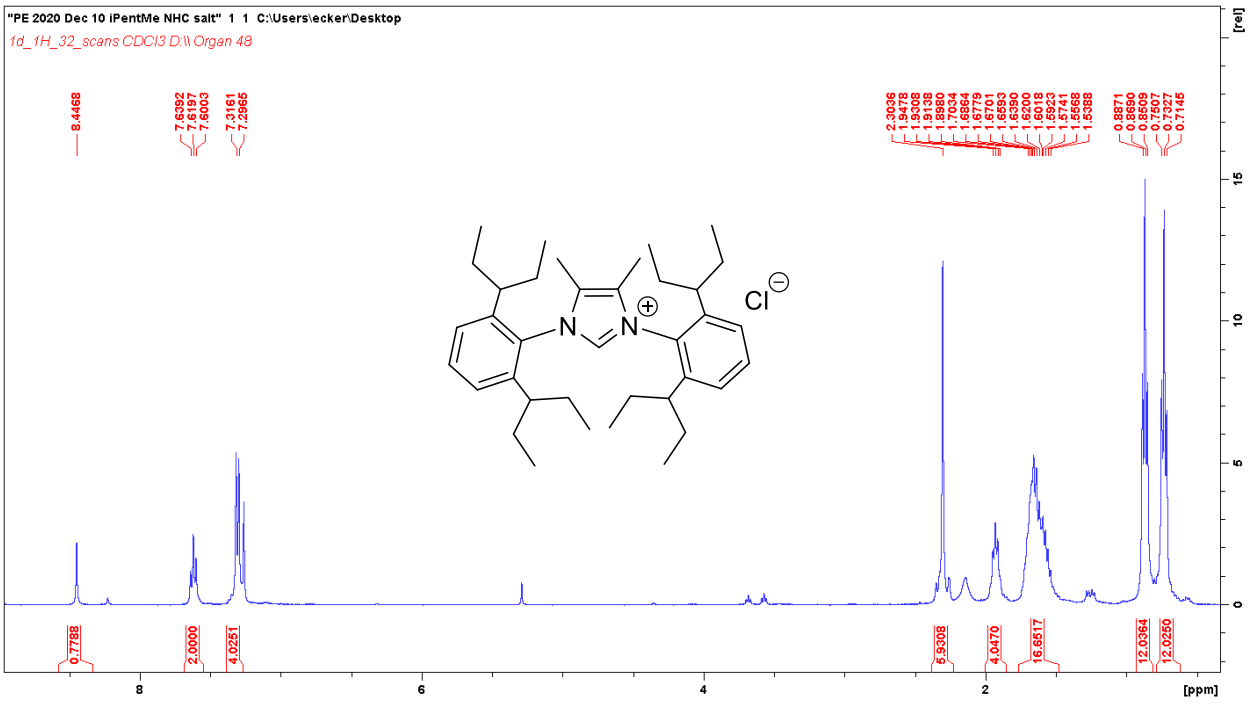

^{1}H NMR spectrum of **97a** (IPent^{Me}·HCl) (400 MHz, $CDCl_3$)

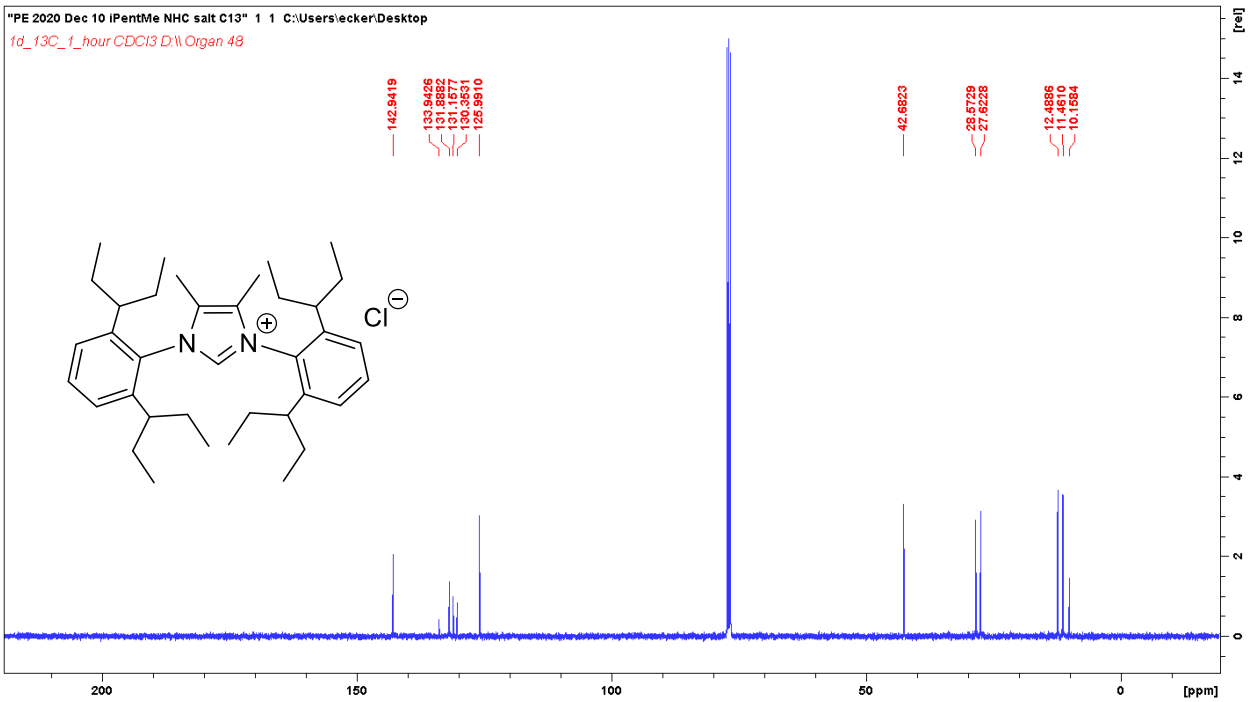

^{13}C NMR spectrum of **97b** (IPent^{Me}·HCl) (100 MHz, $CDCl_3$)

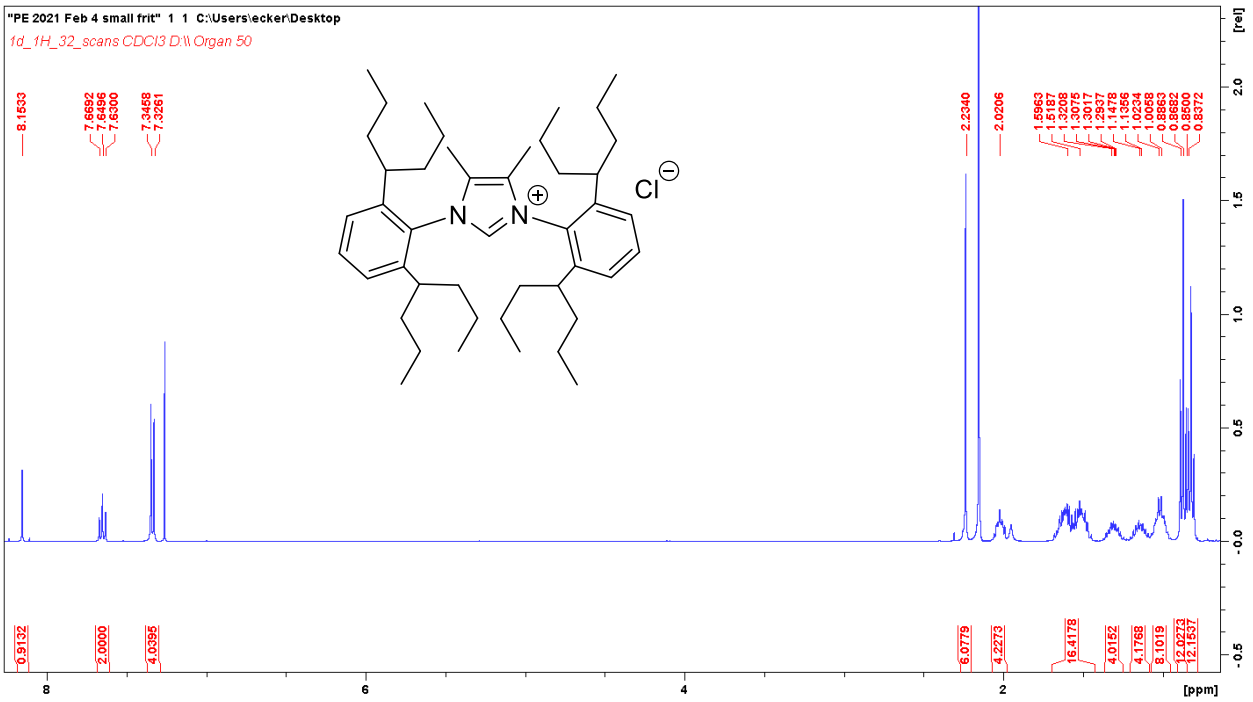

^{1}H NMR spectrum of **97b** (IHept^{Me}·HCl) (400 MHz, $CDCl_3$)

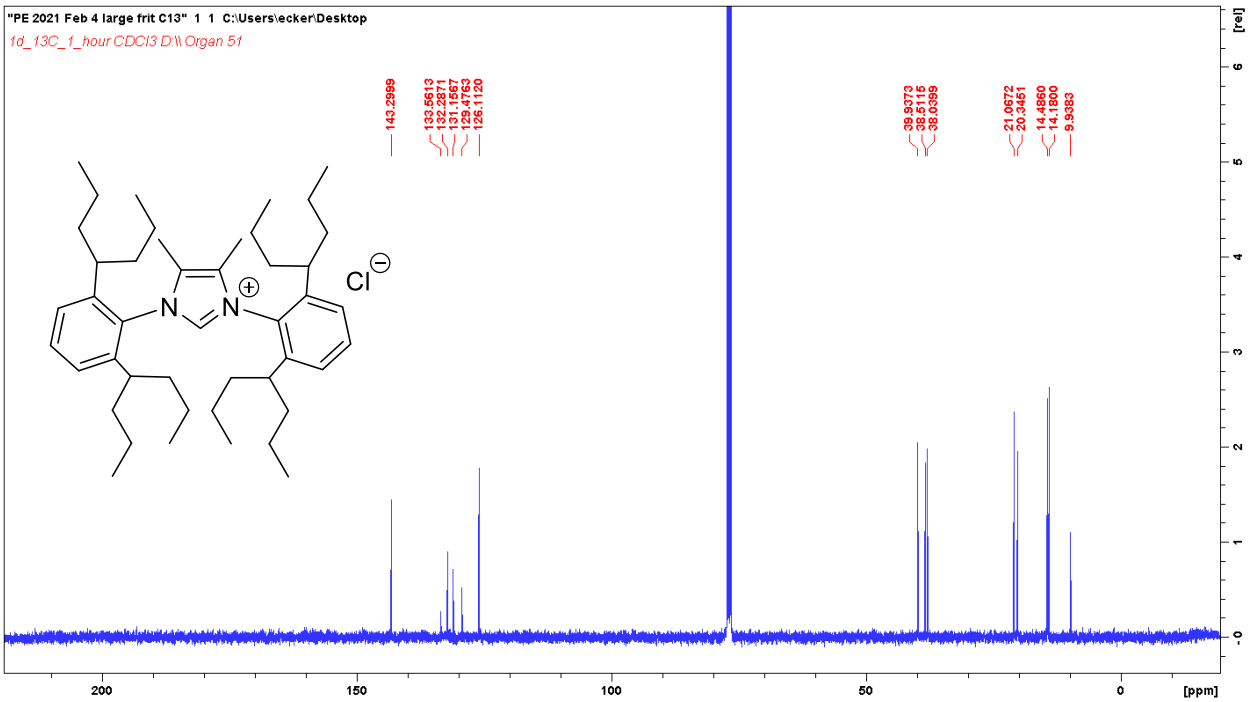

^{13}C NMR spectrum of **97b** (IHept^{Me}·HCl) (100 MHz, $CDCl_3$)

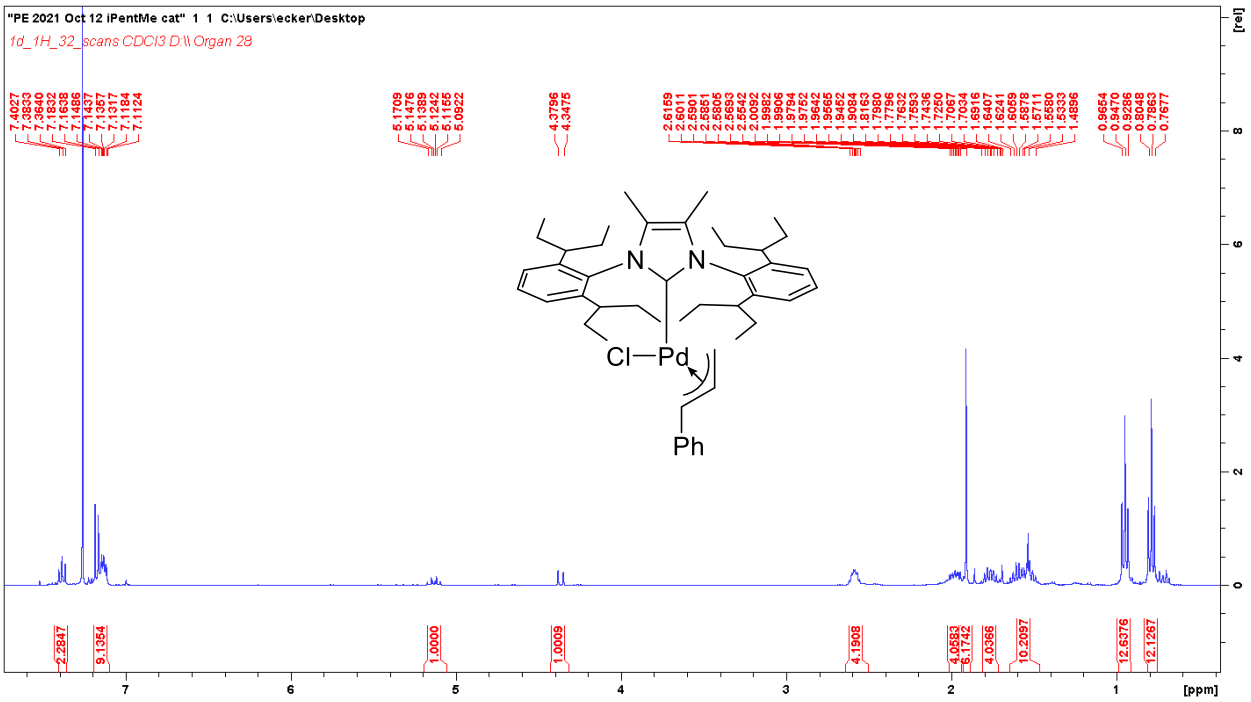

^{1}H NMR spectrum of **(IPent^{Me})Pd(cinnamyl)Cl** (400 MHz, $CDCl_3$)

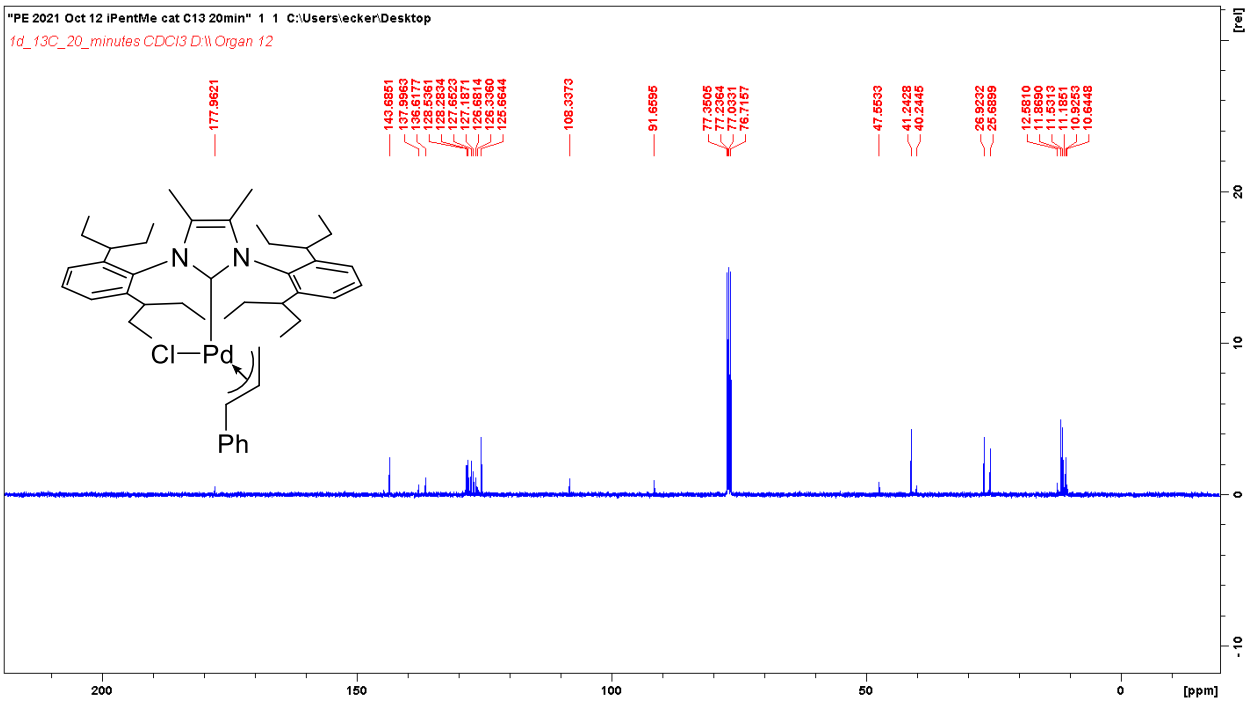

^{13}C NMR spectrum of **(IPent^{Me})Pd(cinnamyl)Cl** (100 MHz, $CDCl_3$)

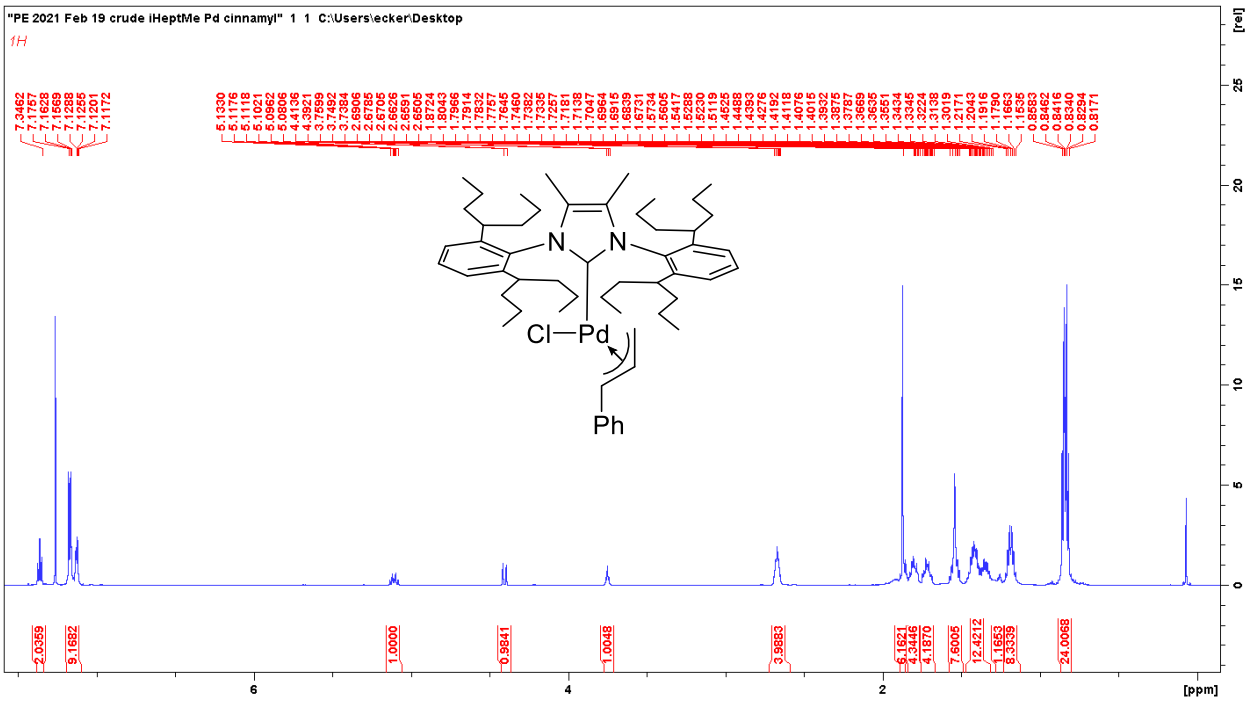

^{1}H NMR spectrum of **(IHept^{Me})Pd(cinnamyl)Cl** (600 MHz, $CDCl_3$)

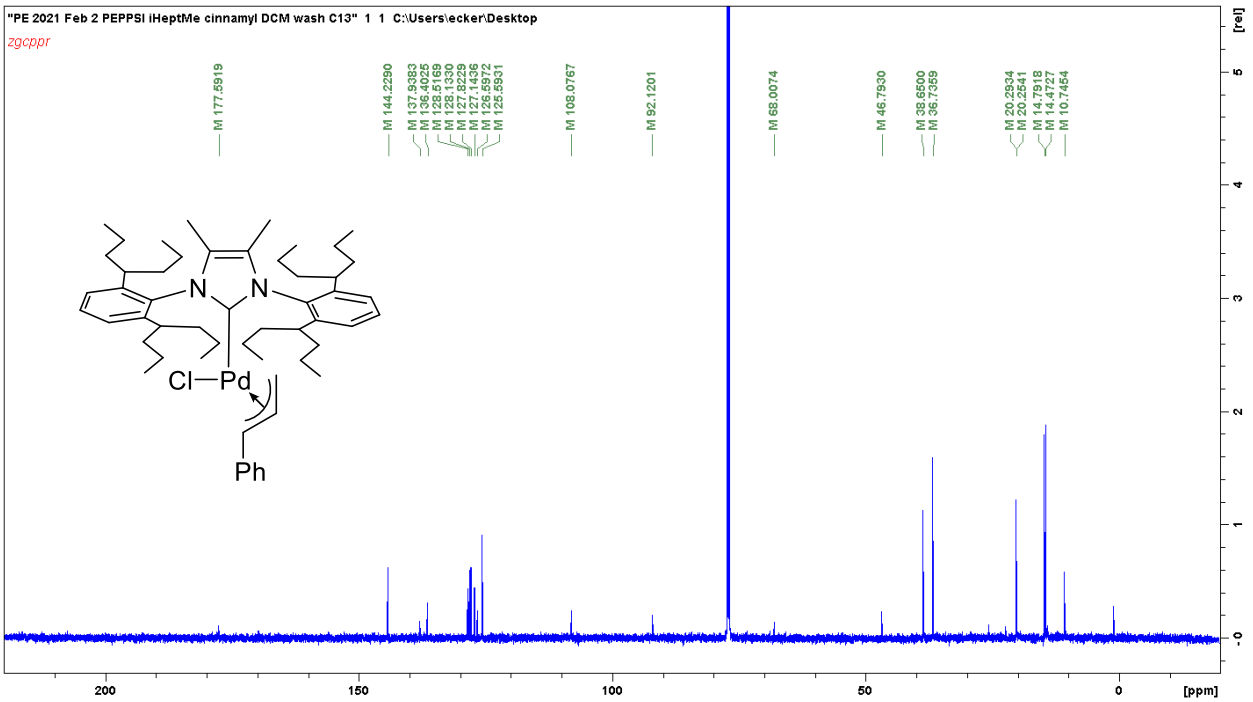

^{13}C NMR spectrum of **(IHept^{Me})Pd(cinnamyl)Cl** (150 MHz, $CDCl_3$)

NMR spectra and chromatograms for chapter 5

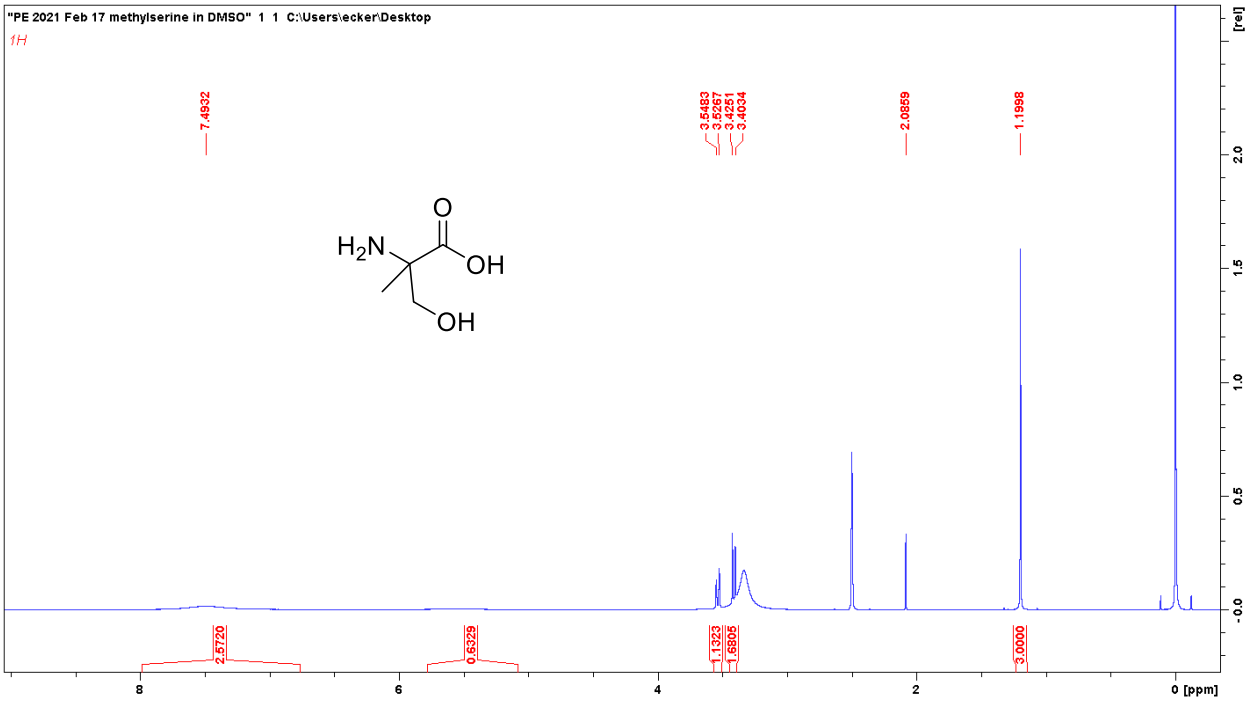

^{1}H NMR spectrum of **110** (500 MHz, DMSO d_6)

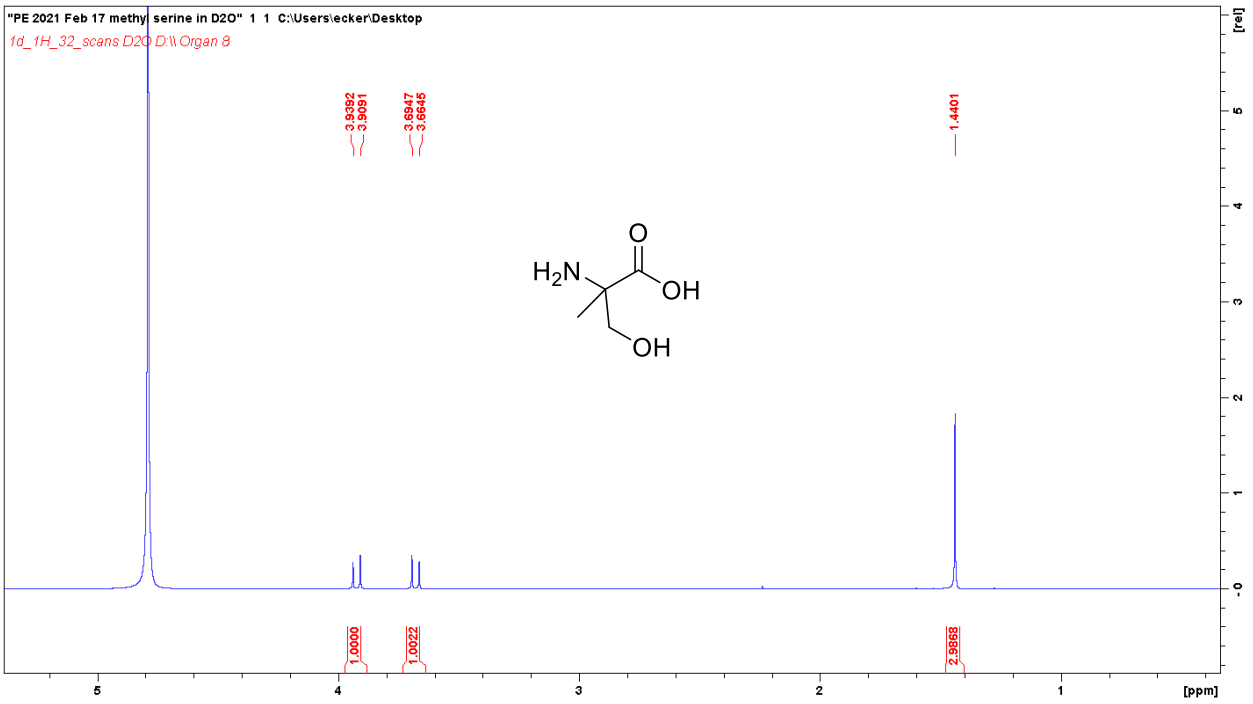

^{1}H NMR spectrum of **110** (400 MHz, D_2O).

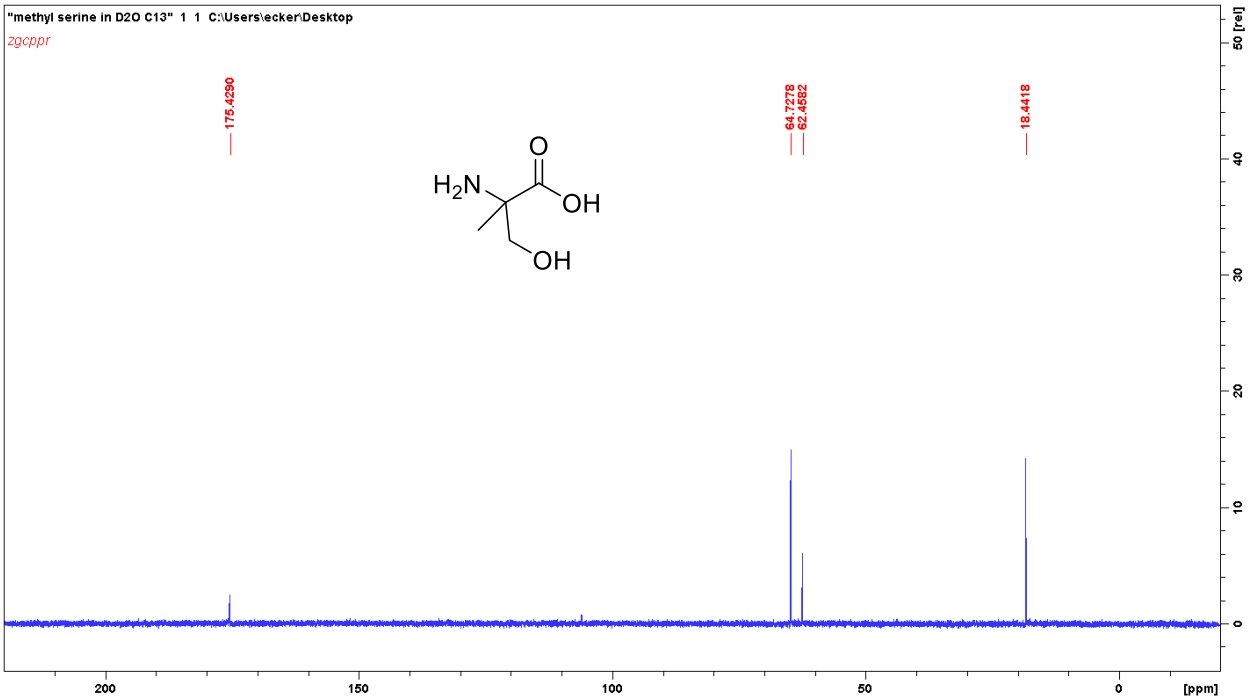

^{13}C NMR spectrum of **110** (100 MHz, D_2O).

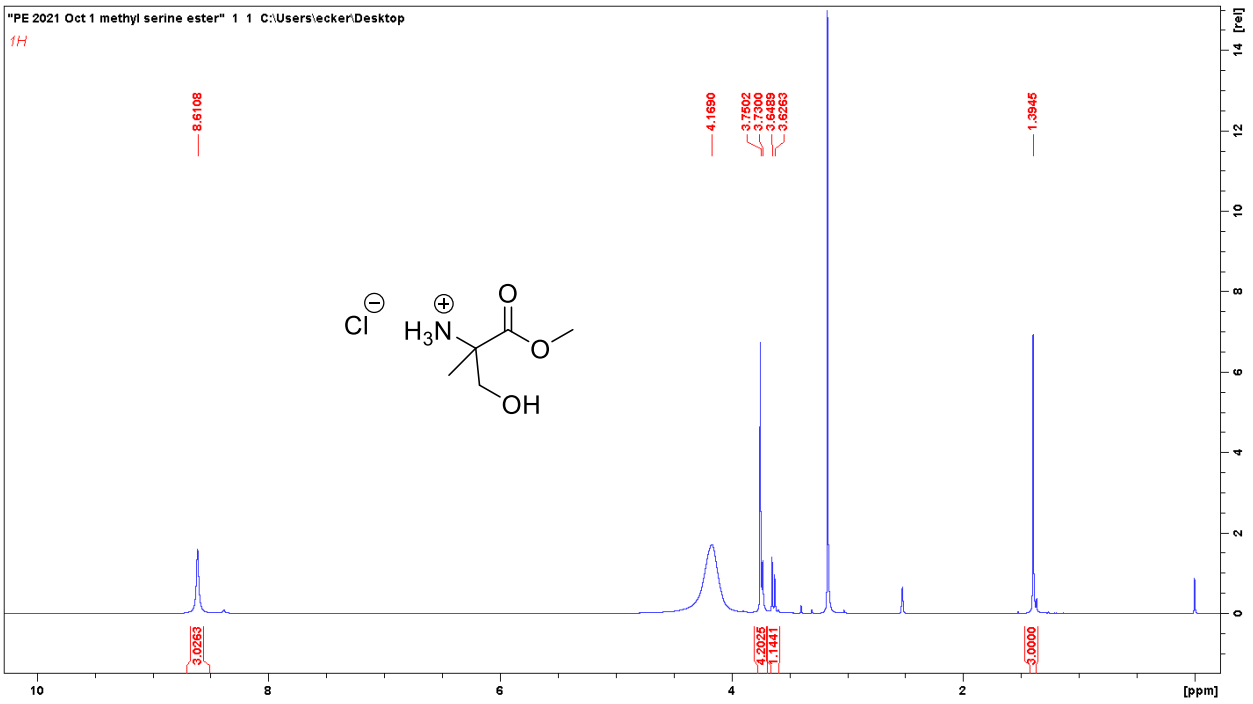

^{1}H NMR spectrum of 2-Methylserine Methyl Ester Hydrochloride (400 MHz, DMSO d_6).

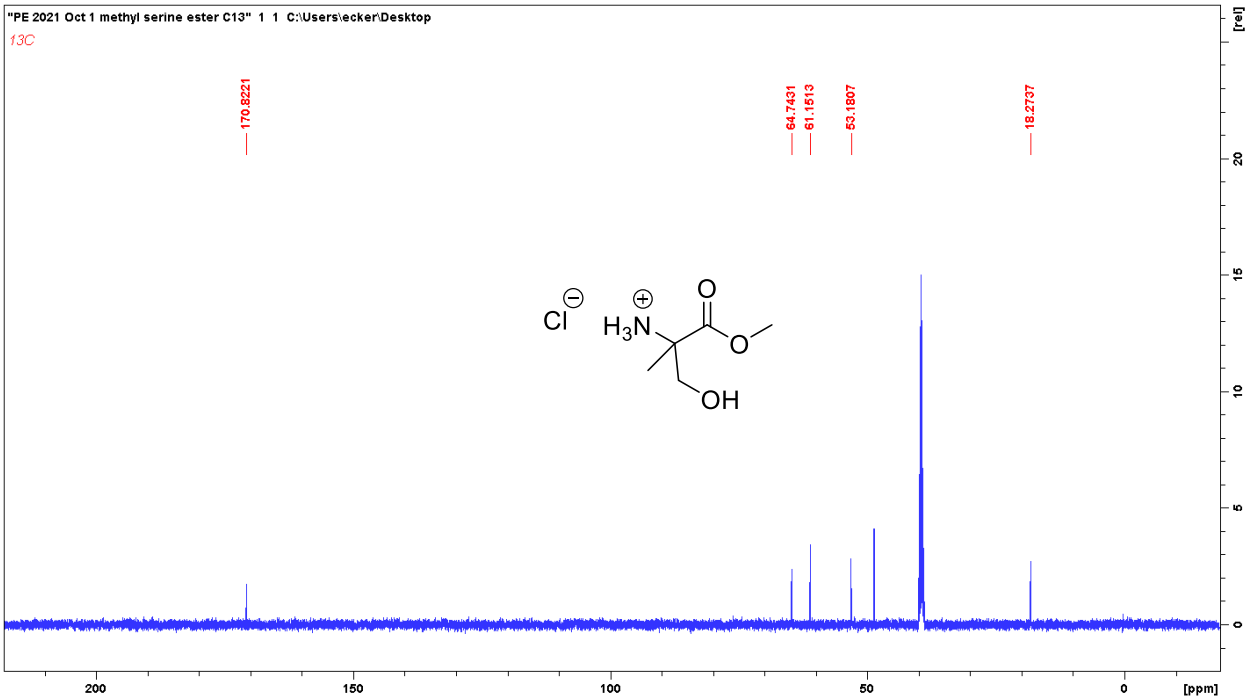

^{13}C NMR spectrum of 2-Methylserine Methyl Ester Hydrochloride (100 MHz, DMSO d_6).

.

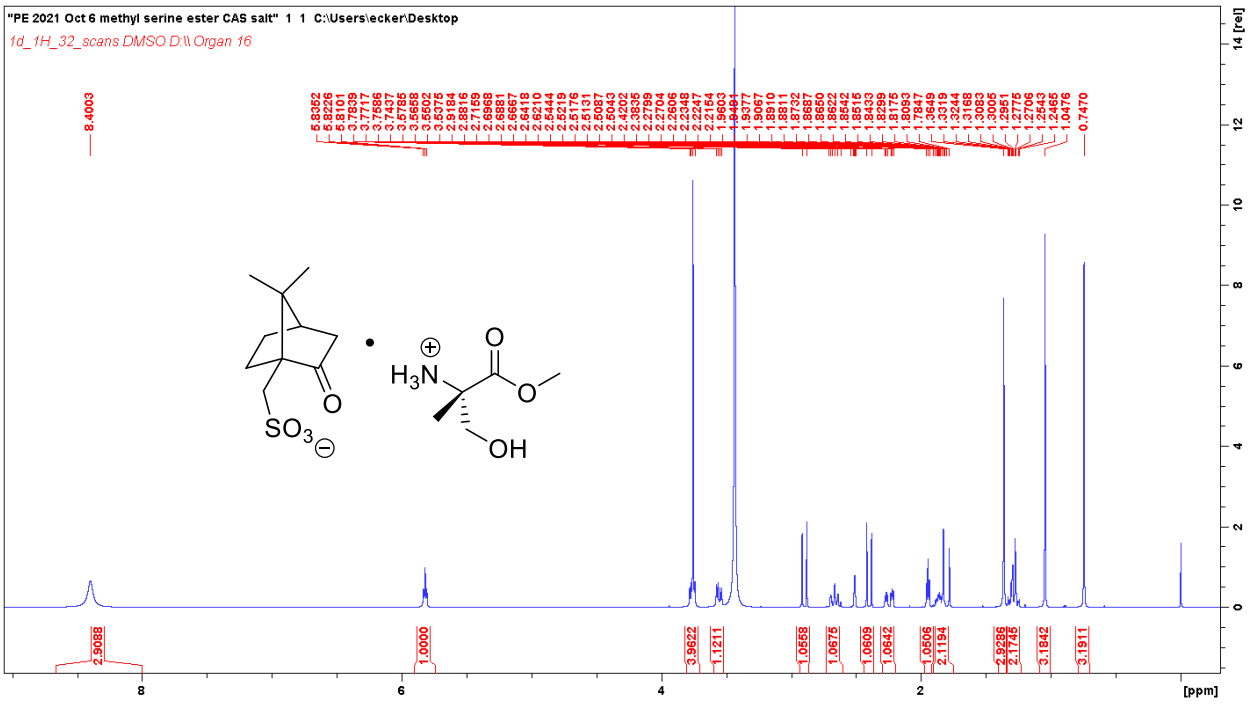

^{1}H NMR spectrum of **122** (400 MHz, DMSO d_6)

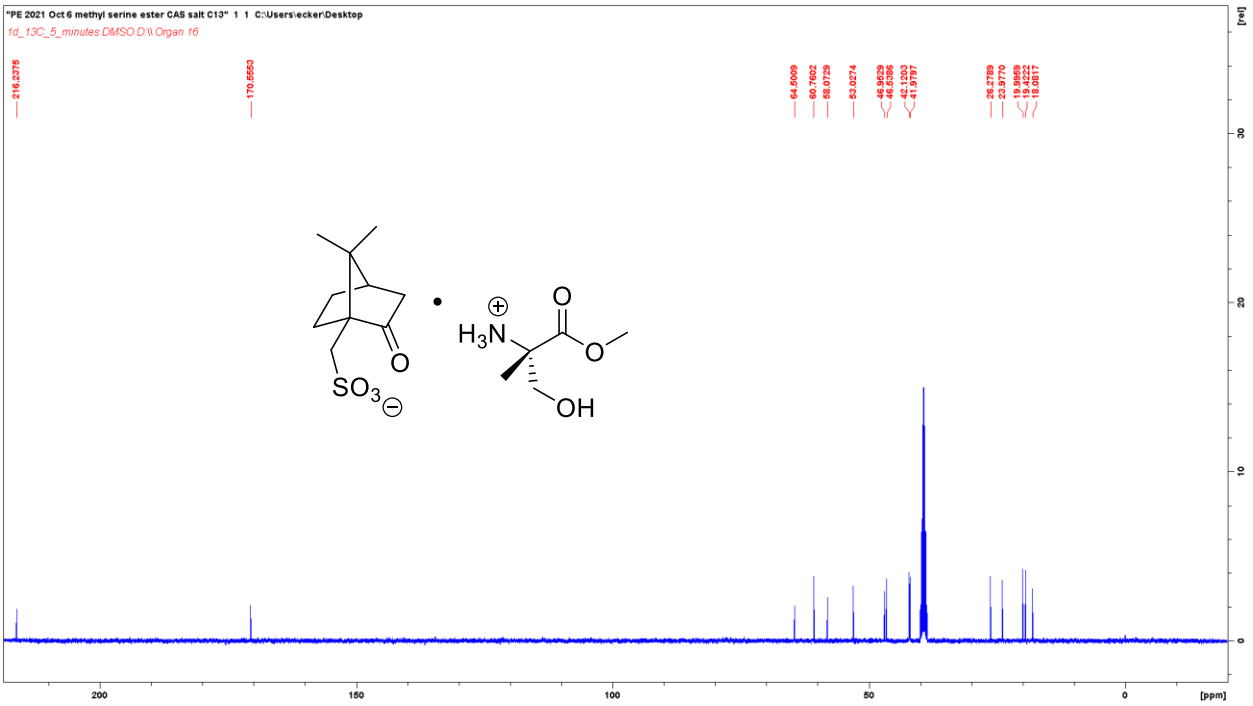

^{13}C NMR spectrum of **122** (100 MHz, DMSO d_6)

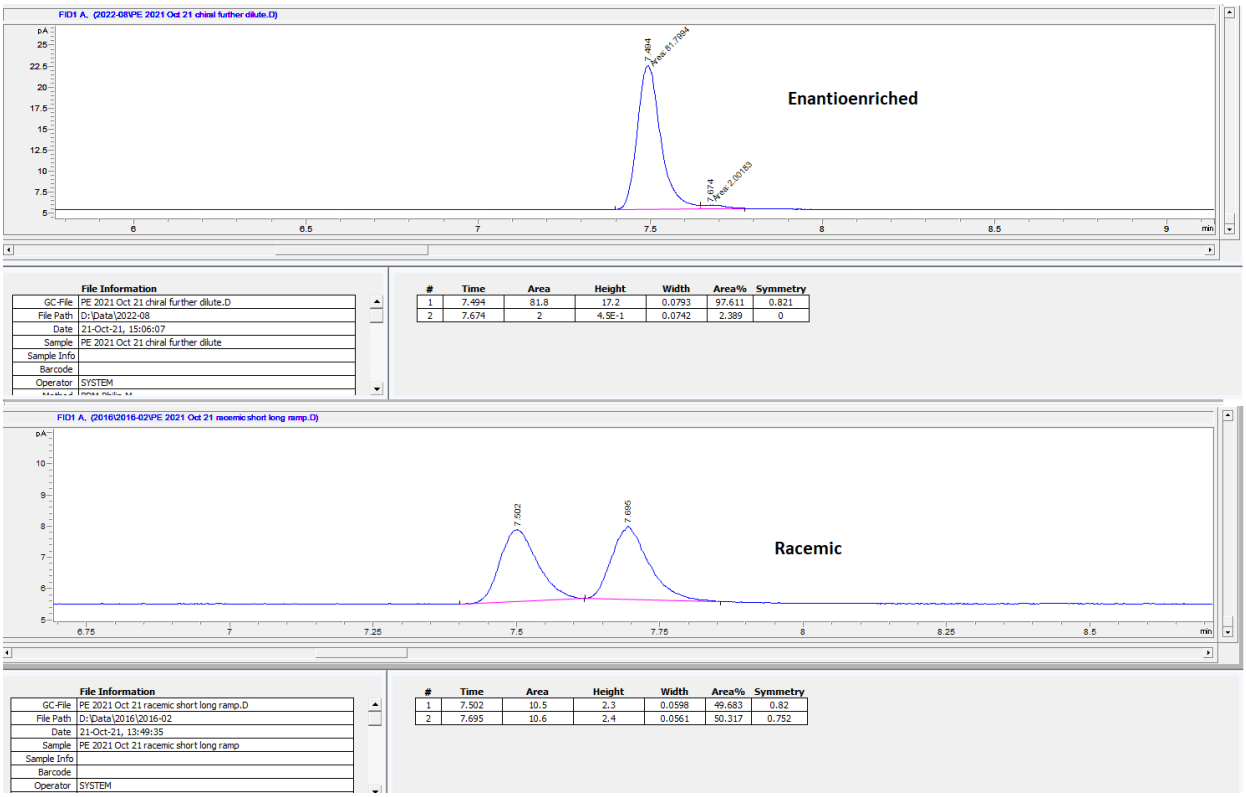

Chiral GC chromatogram of **122a** using method 1.

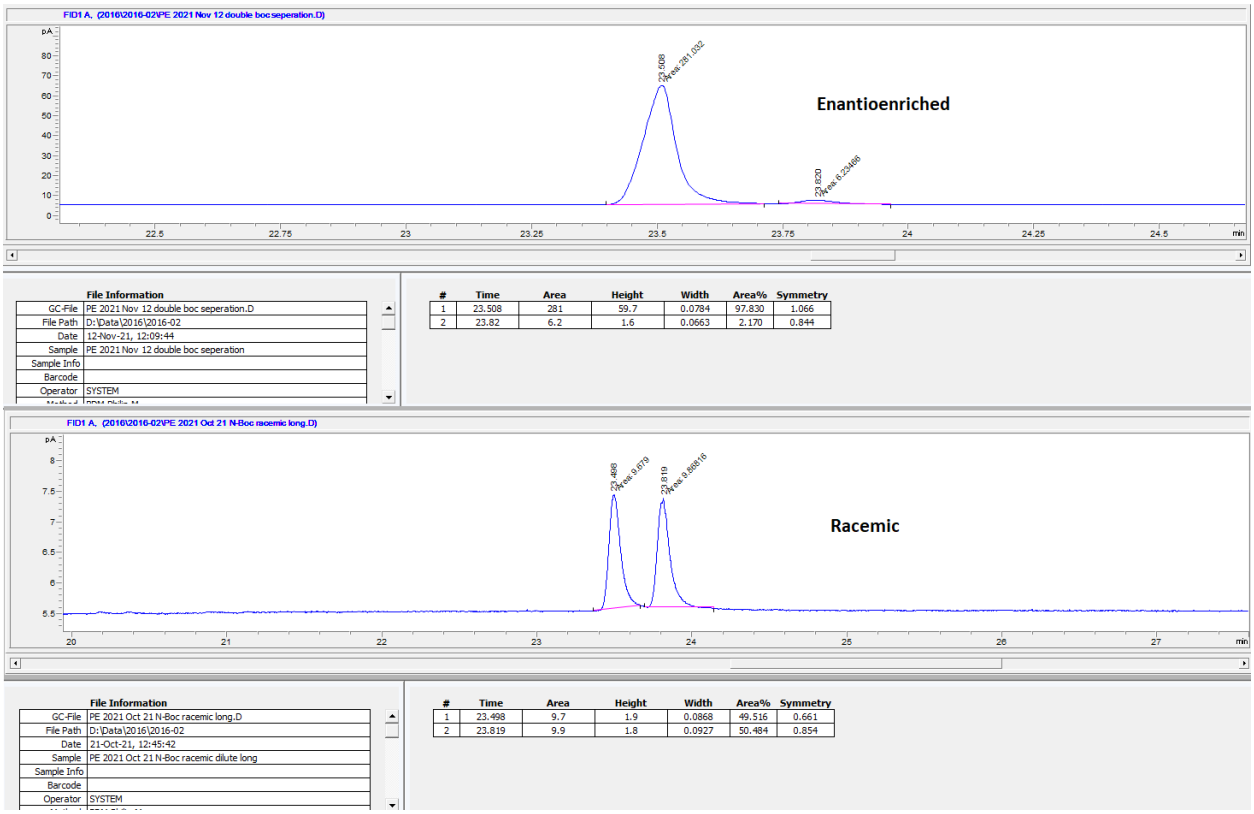

Chiral GC chromatogram of **122b** using method 2.

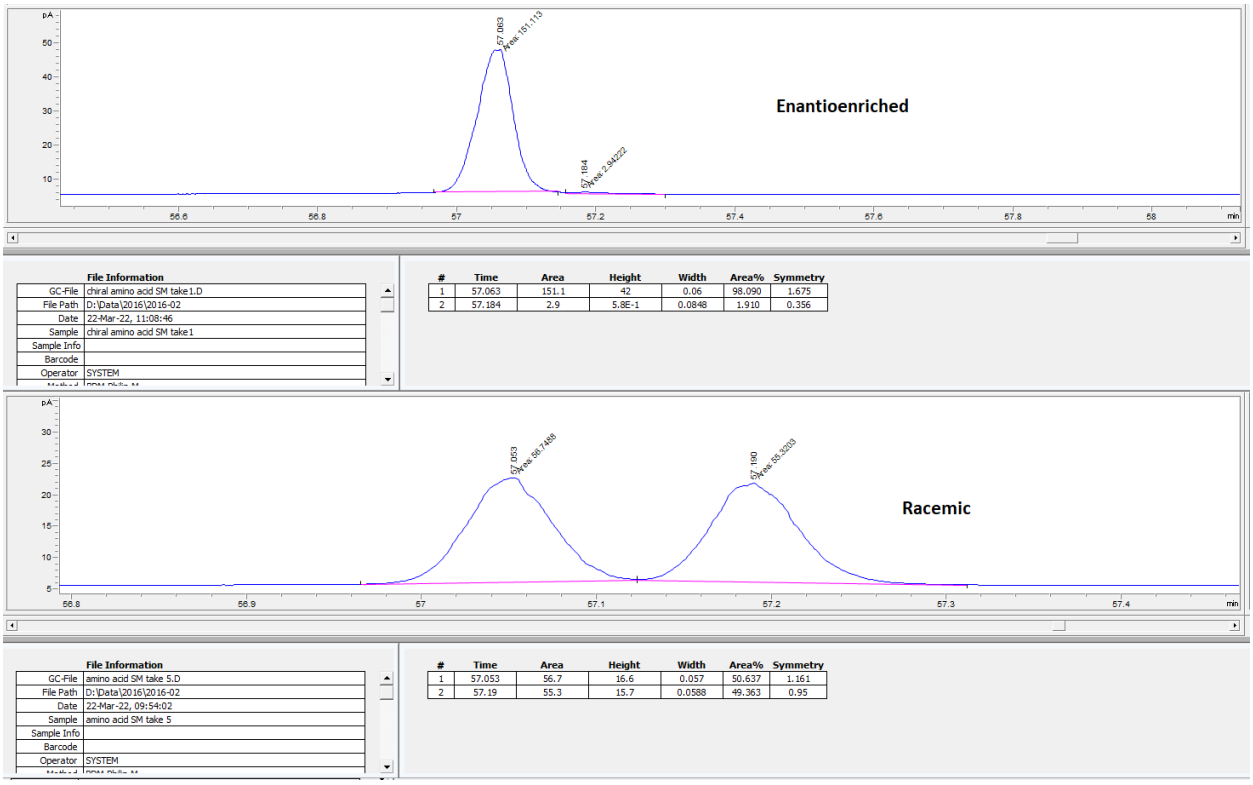

Chiral GC chromatogram of **127** using method 3.

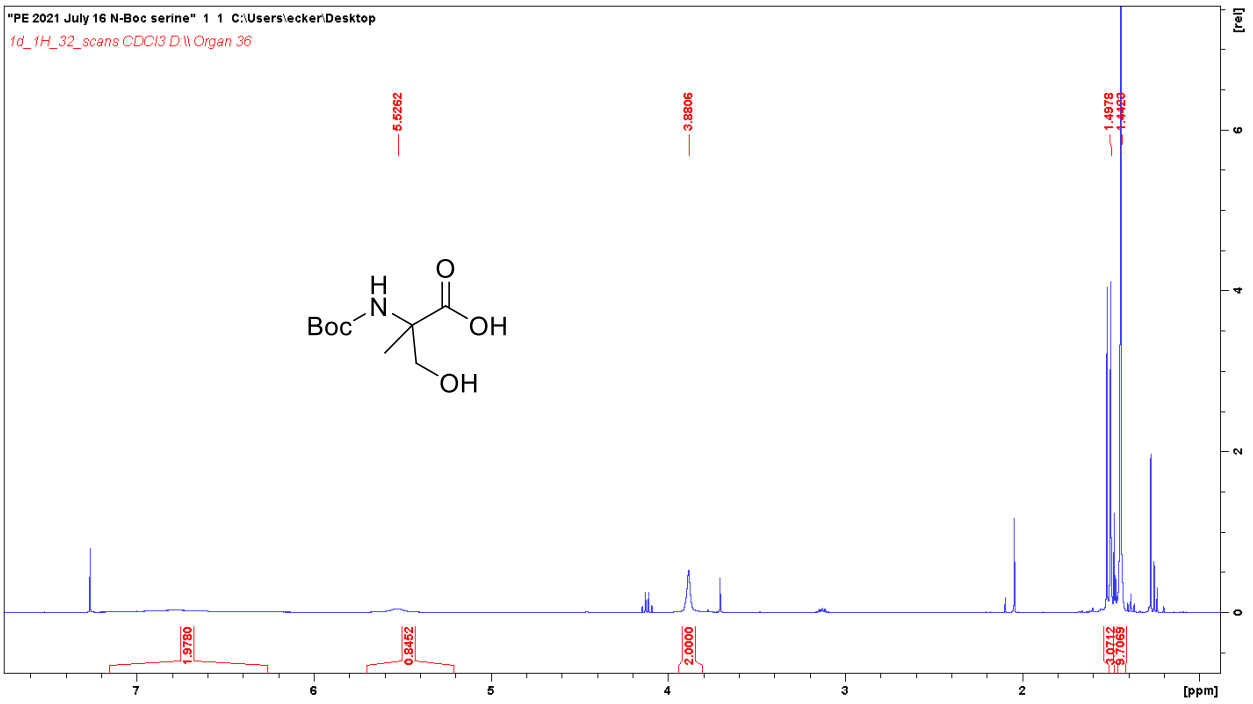

^{1}H NMR spectrum of crude 111 (400 MHz, $CDCl_3$)

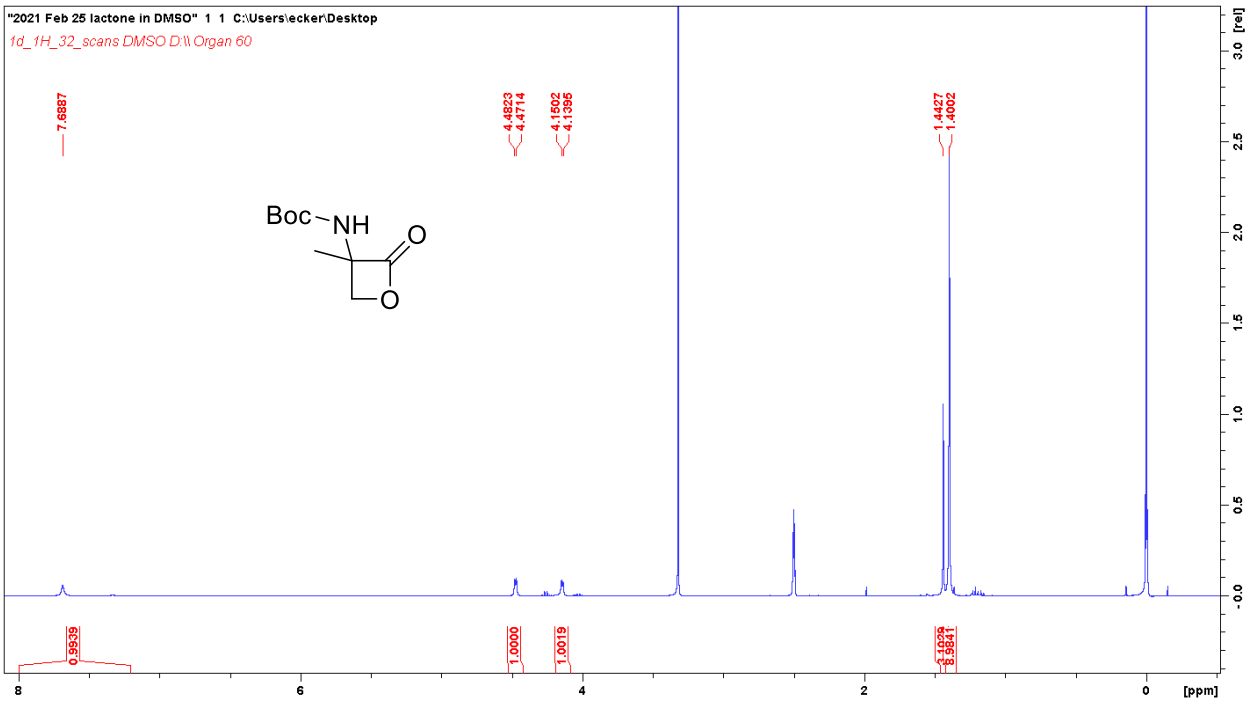

^{1}H NMR spectrum of **112** (400 MHz, DMSO D_6)

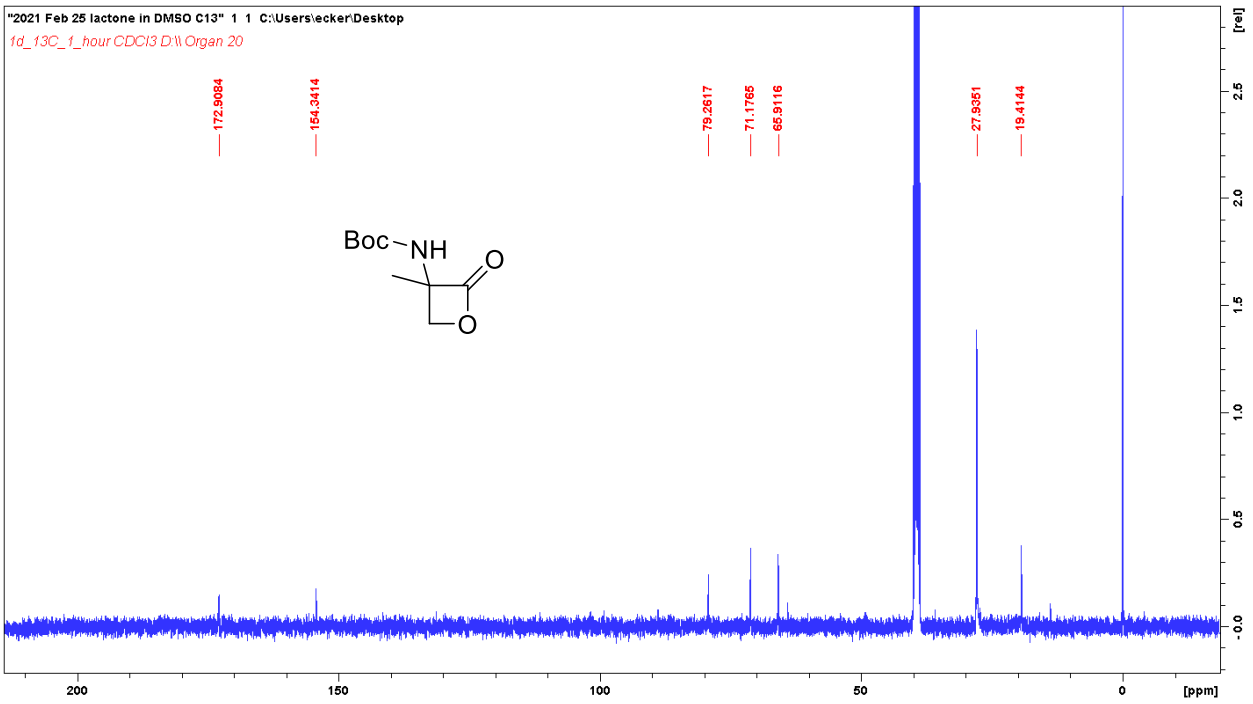

^{13}C NMR spectrum of **112** (100 MHz, DMSO d_6)

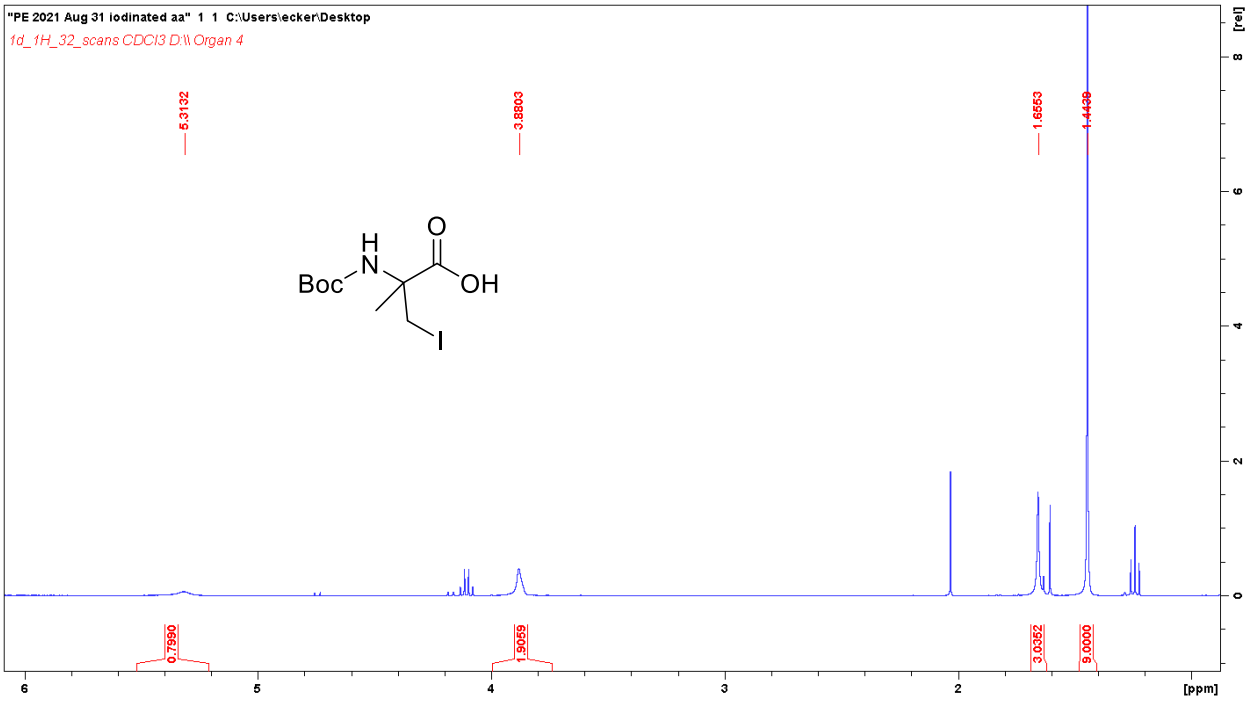

^{1}H NMR spectrum of **113b** (400 MHz, $CDCl_3$)

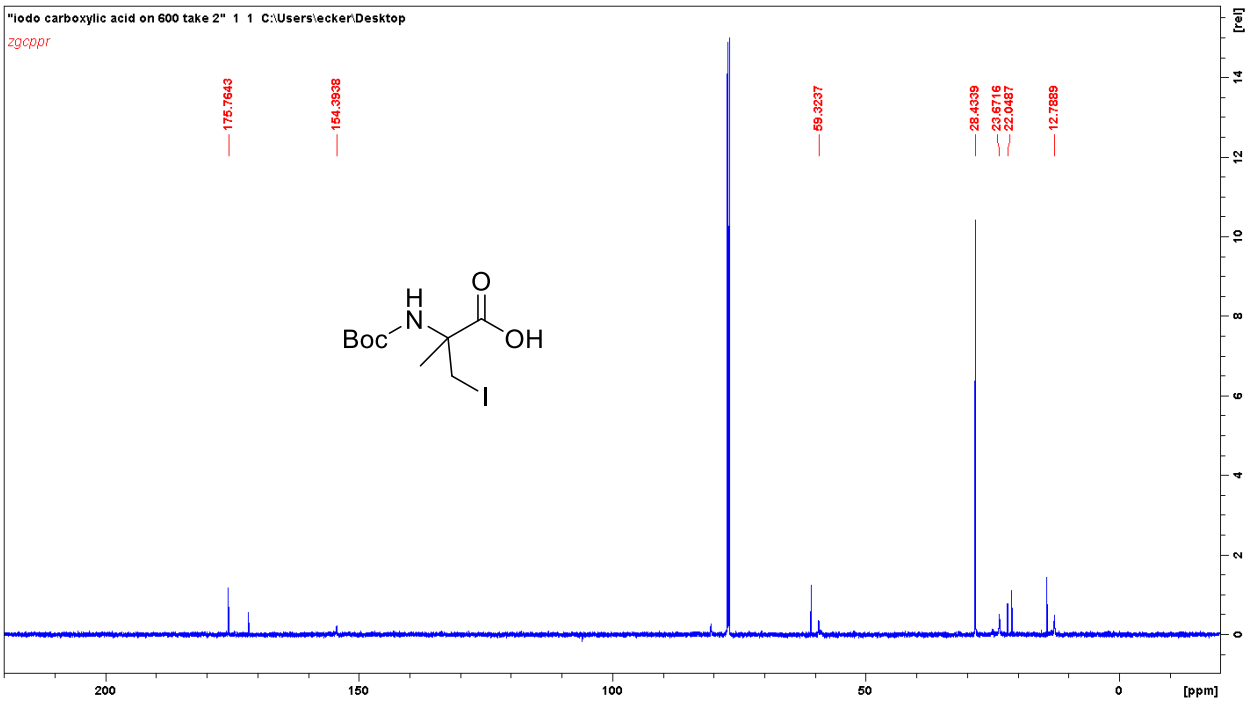

^{13}C NMR spectrum of **113b** (100 MHz, $CDCl_3$)

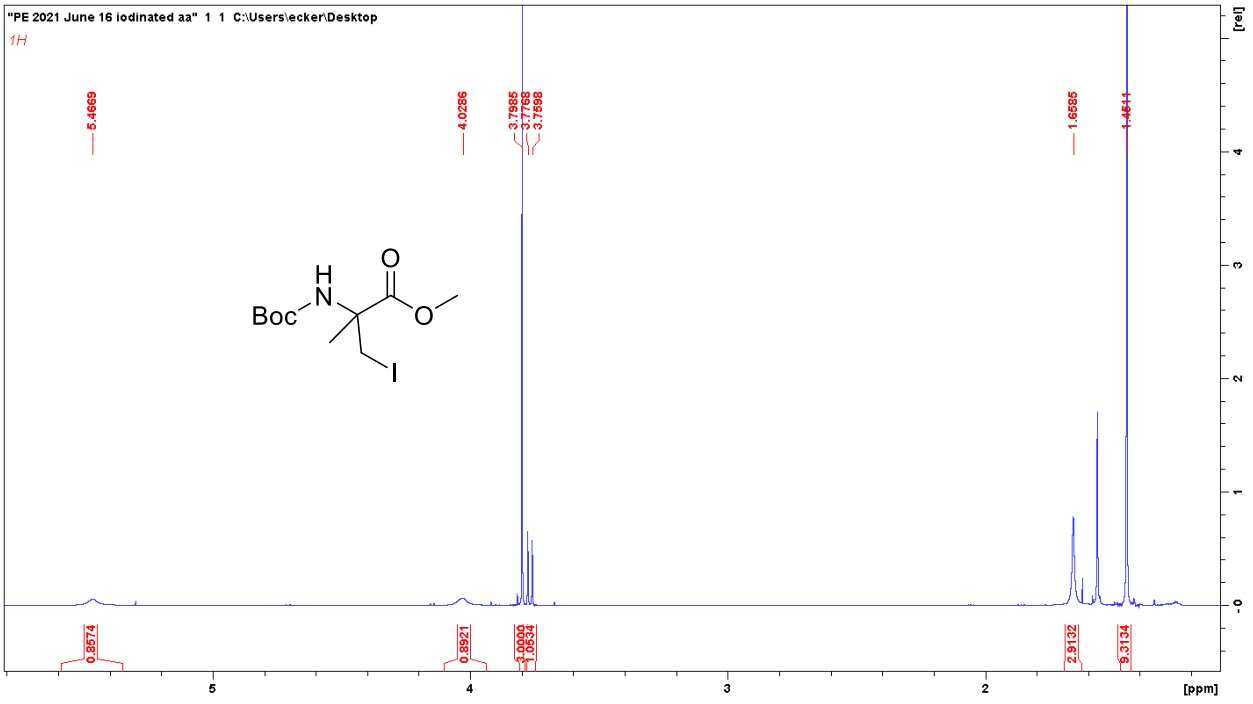

^{1}H NMR spectrum of **108b** (600 MHz, $CDCl_3$)

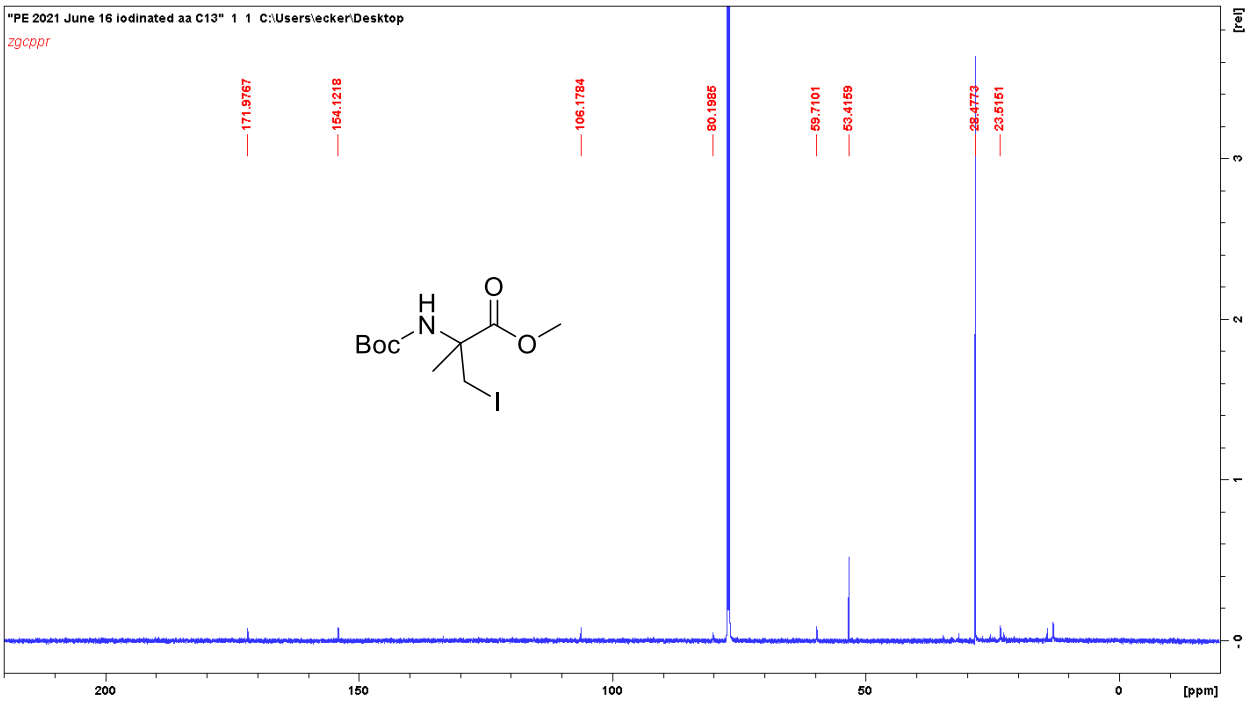

^{13}C NMR spectrum of **108b** (150 MHz, $CDCl_3$)

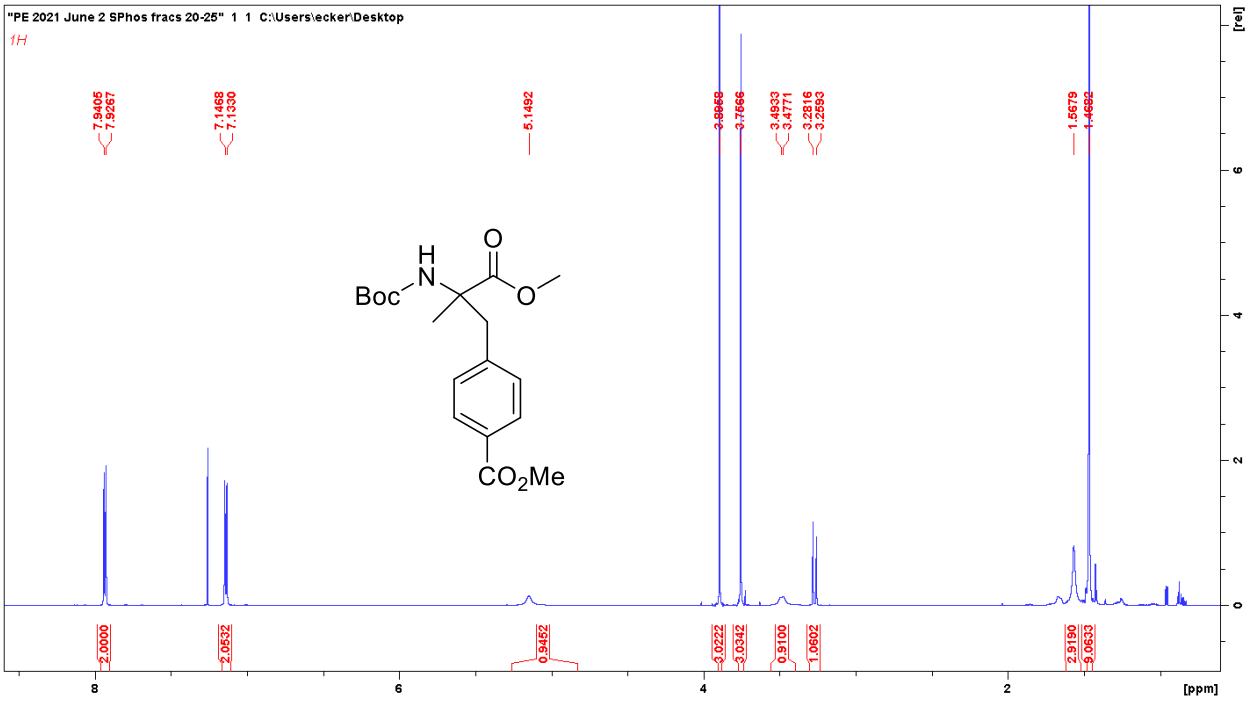

^{1}H NMR spectrum of **116** (600 MHz, $CDCl_3$)

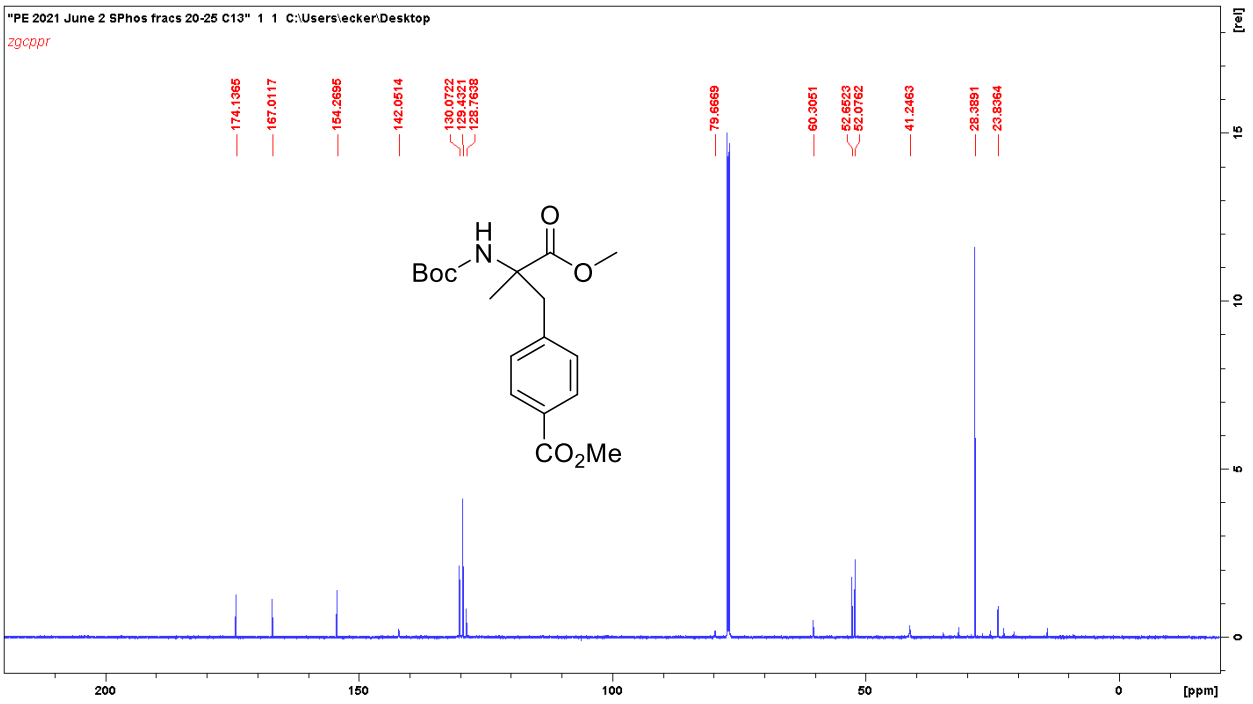

^{13}C NMR spectrum of **116** (150 MHz, $CDCl_3$)

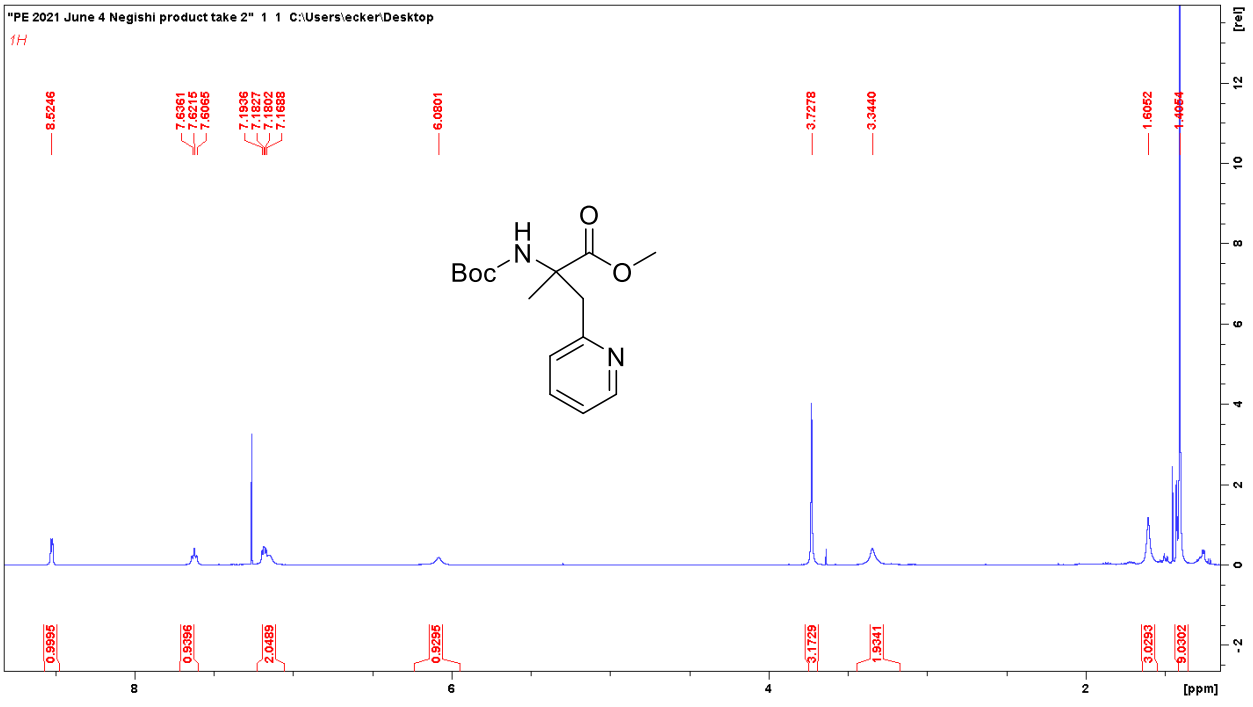

^{1}H NMR spectrum of **117** (500 MHz, $CDCl_3$)

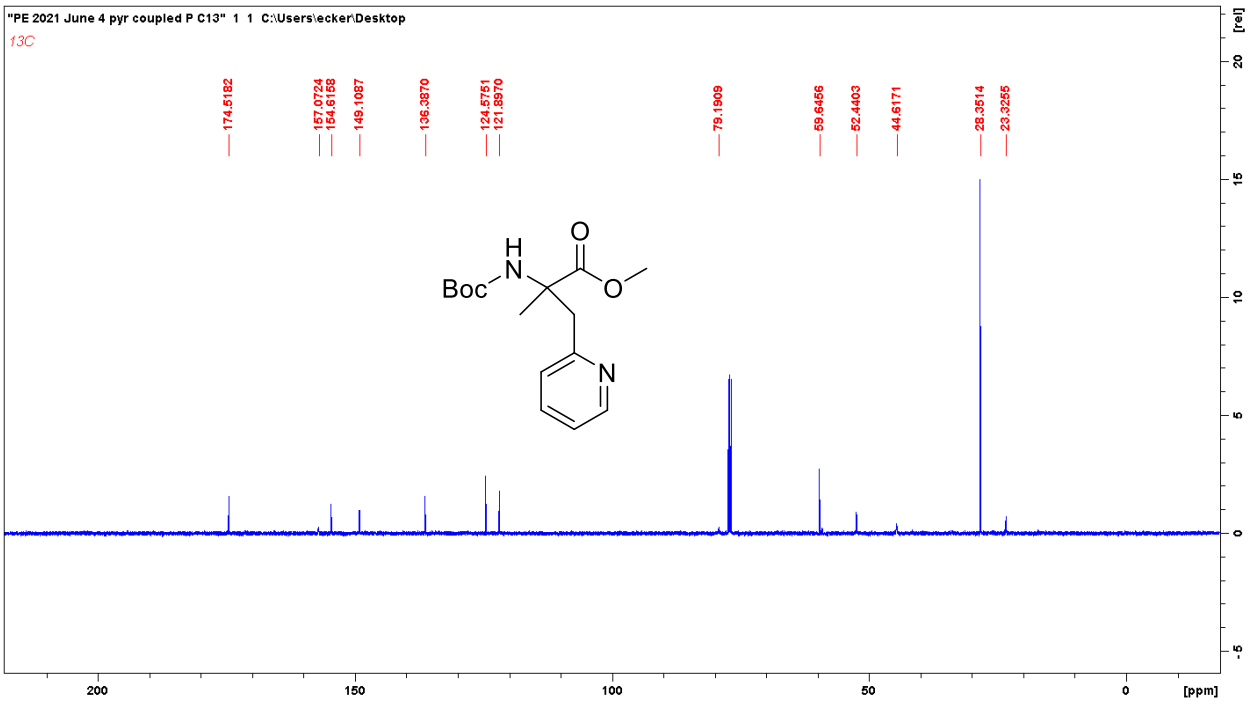

^{13}C NMR spectrum of **117** (125 MHz, $CDCl_3$)

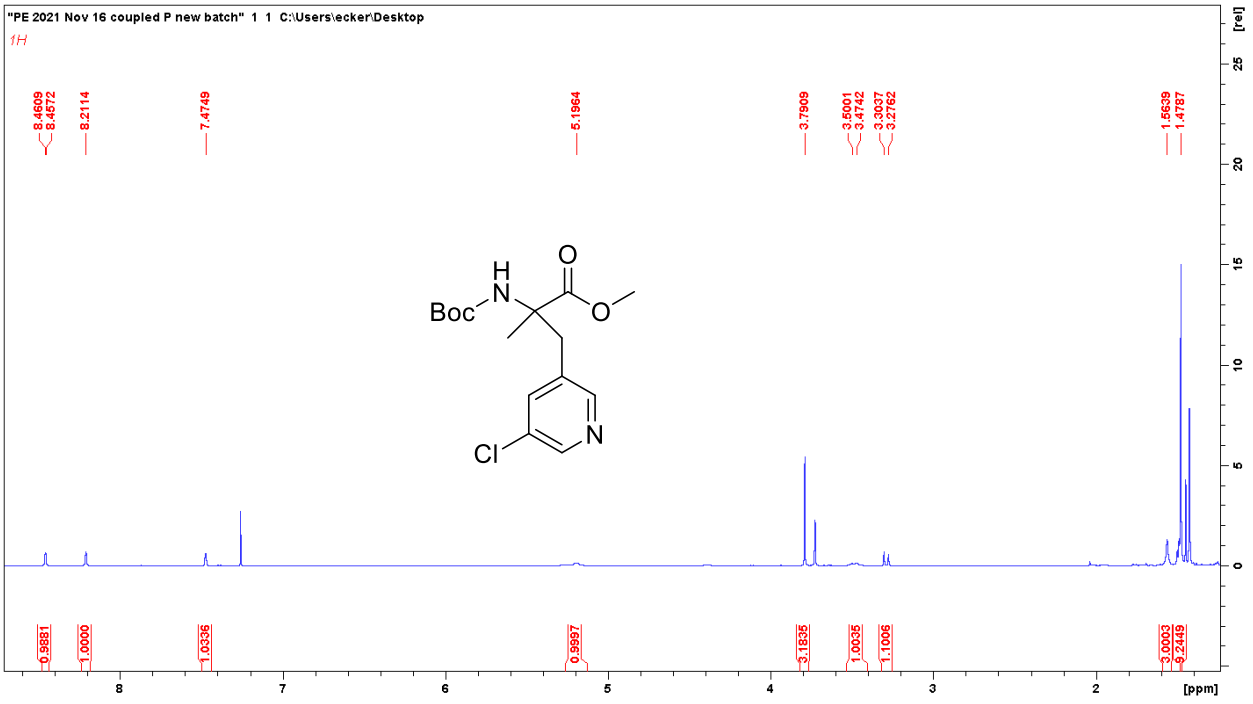

^{1}H NMR spectrum of **118** (500 MHz, $CDCl_3$)

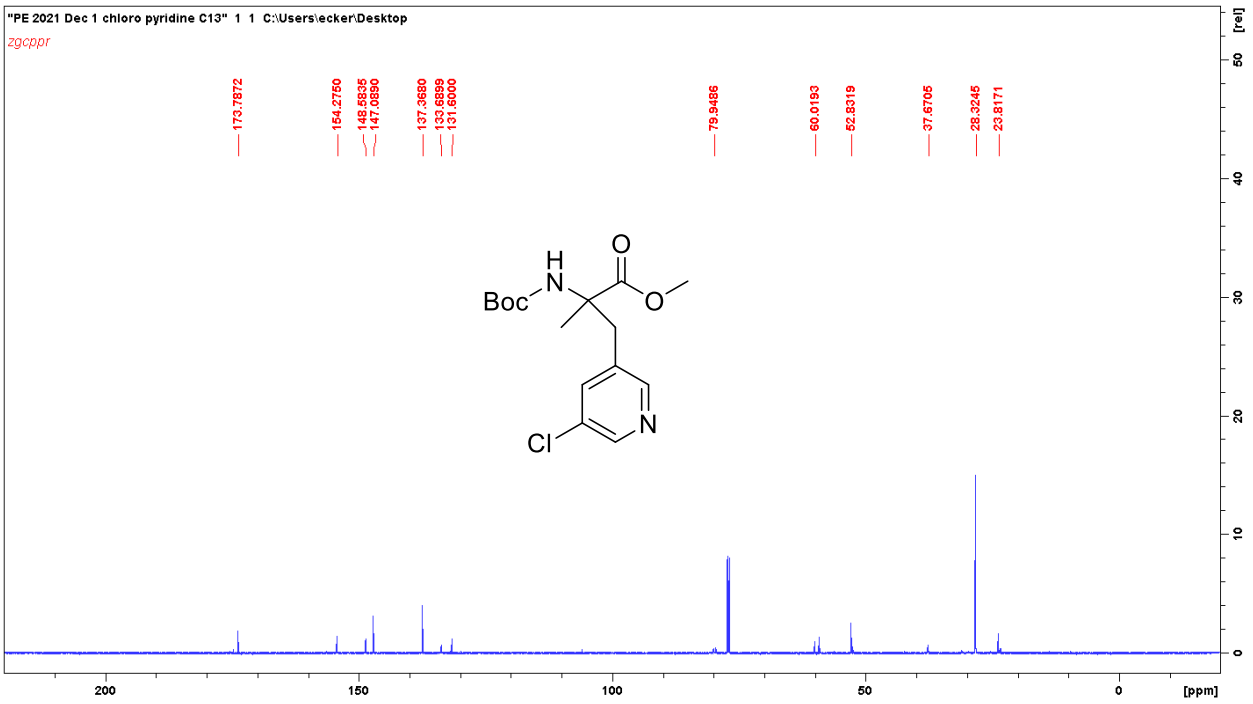

^{13}C NMR spectrum of **118** (125 MHz, $CDCl_3$)